
5-2012

Regulation Of Protein Degradation In The Heart By Amp-Activated Protein Kinase

Kedryn K. Baskin

Kedryn K. Baskin

Follow this and additional works at: https://digitalcommons.library.tmc.edu/utgsbs_dissertations



Part of the [Cardiovascular System Commons](#), [Cell Biology Commons](#), [Cellular and Molecular Physiology Commons](#), and the [Molecular Biology Commons](#)

Recommended Citation

Baskin, Kedryn K. and Baskin, Kedryn K., "Regulation Of Protein Degradation In The Heart By Amp-Activated Protein Kinase" (2012). *Dissertations and Theses (Open Access)*. 252.
https://digitalcommons.library.tmc.edu/utgsbs_dissertations/252


This Dissertation (PhD) is brought to you for free and open access by the MD Anderson UTHealth Houston Graduate School at DigitalCommons@TMC. It has been accepted for inclusion in Dissertations and Theses (Open Access) by an authorized administrator of DigitalCommons@TMC. For more information, please contact digcommons@library.tmc.edu.

REGULATION OF PROTEIN DEGRADATION IN THE HEART BY AMP-ACTIVATED
PROTEIN KINASE


by

Kedryn Kjestine Baskin, BA

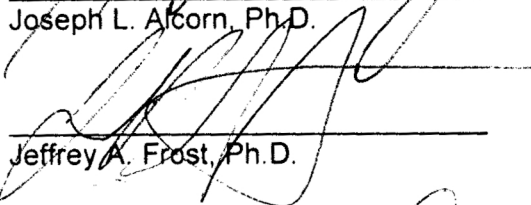
APPROVED:



Heinrich Taegtmeier, M.D., D.Phil.
Supervisory Professor



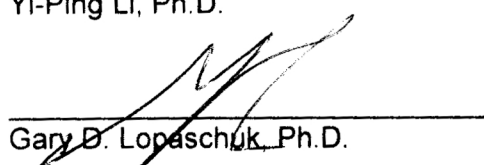
Joseph L. Alcorn, Ph.D.



Jeffrey A. Frost, Ph.D.



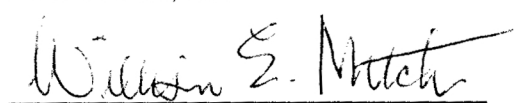
Yi-Ping Li, Ph.D.



Gary D. Lopaschuk, Ph.D.



Ali J. Marian, M.D.



William E. Mitch, M.D.

APPROVED:

George M. Stancel, Ph.D.
Dean, The University of Texas
Health Science Center at Houston
Graduate School of Biomedical Sciences

REGULATION OF PROTEIN DEGRADATION IN THE HEART BY AMP-ACTIVATED
PROTEIN KINASE

A
DISSERTATION

Presented to the Faculty of
The University of Texas
Health Science Center at Houston
and
The University of Texas
M. D. Anderson Cancer Center
Graduate School of Biomedical Sciences

in Partial Fulfillment
of the Requirements
for the Degree of

DOCTOR OF PHILOSOPHY

by
Kedryn Kjestine Baskin, BA
Houston, Texas

May 2012

DEDICATION

To my parents, who encouraged learning at an early age, instilled in me a passion for knowledge, and provided me with a strong Christian foundation on which to stand firm. Thank you for the many words of encouragement and help along my educational journey. Thank you for teaching me diligence and perseverance, and to stand strong in the face of adversity. I love you; this work is dedicated to you.

ACKNOWLEDGEMENTS

I have had much support throughout my journey thus far, and although it will not be possible to thank everyone who has impacted my life, I would like to thank those who have contributed greatly to my personal and professional development. First and foremost, I thank Dr. Taegtmeier for giving me the opportunity to work in his lab on several very exciting projects. He has taught me many things over the years and I thank him for his guidance. He has truly been an inspiration to me and has encouraged my scientific development. Dr. T, thank you for sharing every aspect of science with me, I have learned so much from you. Thank you for the opportunities you provided for me to review manuscripts, attend meetings, and present our work. Thank you for the many Saturdays you spent with me working on manuscripts and discussing results. And thank you for encouraging me to apply for fellowships at every opportunity. You have been a great mentor and I look forward to many more years of discussions with you.

I also would like to thank the faculty members that served on various committees during my graduate work. To the early members (Dr. Molly Bray, now at the University of Alabama at Birmingham; Dr. Bob Schwartz, now at the University of Houston), thank you for the encouragement and help in shaping my thesis project. I thank Dr. Carmen Dessauer for chairing my exam committee, for her experimental help during the later stages of my project, and for the example she set during her time as the graduate program director. I also thank Dr. David Loose for his commitment and leadership as the current graduate program director. Dr. Alcorn, thank you for your experimental help throughout the years, especially during my first year rotation. Dr. Frost, thank you for your continuous encouragement and experimental suggestions. Dr. Li, thank you for your support and helpful discussions. Dr. Marian, thank you for critically evaluating the data and for your perceptive comments. Dr. Mitch, thank you for your suggestions and insight. Thank you all for taking the time to mentor me throughout the years.

Other faculty members have also helped me at critical stages in my project. I thank Dr. Diane Bick for allowing us to use her tissue culture room for some experiments. I also thank Dr. Aarif Khakoo for collaborating on the TAC study and Dr. Vishnu Chintalgattu for performing the surgeries (both currently at Amgen, San Francisco, CA). I especially want to thank Dr. Rebecca Berdeaux for her assistance with the ChIP assay protocol and troubleshooting. I also want to thank all the faculty members of the CRB program and

Integrative Biology and Pharmacology (IBP) department for their helpful comments and suggestions throughout my graduate career.

To those who have helped me on a daily basis: Roxy, thank you for keeping the lab in working order and for the friendly email reminders. I greatly appreciate your support and assistance throughout the years. Patrick, I miss your presence in the lab! (Mostly I miss playing practical jokes on you!) Thanks for your willingness to help with anything and everything! Romain, thanks for keeping me sane in the lab. Although two workaholics may not be the best combination, we completed many experiments! Becky thanks for helping me with the isolations and perfusions. Also, thank you for taking care of the mice. I would not have been able to complete the experiments without you; thanks for providing funny David stories! Truong, thanks for always being prepared with a joke. Meredith, thank you for helping out with the echos and teaching me how to analyze the data. It has been fun having you in the lab and I wish you the best of luck in your scientific career. Hernan, welcome to the girls room! Brother Shiraj, working on the grant was fun while it lasted; I wish you the best in the future. To all those who have come and gone in the lab, thanks for your support and friendship: Mitra, Seema, Genna, Moritz, KK, Peter, and many others.

I would also like to thank my friends and fellow classmates. Susan, my biochem study buddy and coffee break partner, thanks for spending countless hours in the medical school trying to understand crazy methodologies! Sharat, Christina, and Prasad, thanks for the hard core study group for MOHAST. That was the most fun I ever had preparing for exams! Thanks to all the students in the Cell and Regulatory Biology graduate program, both past and present, for drilling me on my project and teaching me to think on my feet.

I would not have begun this scientific journey if I had not been entertained by Mrs. Leibl's "ATP" song as a freshman in high school. Her enthusiasm about science in general, but biochemistry in particular could not be masked. She was one of my most influential teachers. I am also grateful for Dr. Kevin Pinney for taking me into his lab with no prior research experience. It was in his lab that I became aware of my passion for research. Dr. Charles Garner also took me in under his wing and taught me research basics. I am indebted to Dr. Jan Parker-Thornburg who hired me to work as a Research Technician in her lab at M.D. Anderson Cancer Center. She allowed me to attend graduate student seminars and courses within the Genes and Development program at GSBS where I became convinced that graduate school was the next step in my career.

Last but certainly not least, I would not have made it this far without the support of my family and friends. Thank you, mom and dad, for understanding my hectic schedule. I

thank my sisters Cameryn and Kyna for always asking me what the heck I was doing. You helped me prepare my lay abstracts early on! Thank you for the comic relief, reality checks, and all the support. I also thank my extended family for the encouraging words during my graduate career, especially Aunt Mary and Uncle Bob; thank you for your thoughts and prayers. Colleen and Renae: thank you for helping me relax during the holidays. I thank my extended Houston 'family' for their support and encouragement throughout the years. Nikki and Doug, thank you for your hospitality; Courtney thank you for your friendship and providing entertainment (Caleb); Bert thank you for your enthusiasm; and Ash thank you for your support and sarcasm and especially for keeping me sane and reminding me that there is life outside of lab.

REGULATION OF PROTEIN DEGRADATION IN THE HEART BY AMP-ACTIVATED PROTEIN KINASE

Publication No.: _____

Kedryn K. Baskin, BA

Supervisory Professor: Heinrich Taegtmeyer, M.D., DPhil

The degradation of proteins by the ubiquitin proteasome system is essential for cellular homeostasis in the heart. An important regulator of metabolic homeostasis is AMP-activated protein kinase (AMPK). During nutrient deprivation, AMPK is activated and intracellular proteolysis is enhanced through the ubiquitin proteasome system (UPS). Whether AMPK plays a role in protein degradation through the UPS in the heart is not known. Here I present data in support of the hypothesis that AMPK transcriptionally regulates key players in the UPS, which, under extreme conditions can be detrimental to the heart. The ubiquitin ligases MAFbx /Atrogin-1 and MuRF1, key regulators of protein degradation, and AMPK activity are increased during nutrient deprivation. Pharmacologic and genetic activation of AMPK is sufficient for the induction of MAFbx/Atrogin-1 and MuRF1 in cardiomyocytes and in the heart *in vivo*. Comprehensive experiments demonstrate that the molecular mechanism by which AMPK regulates MuRF1 expression is through the transcription factor myocyte enhancer factor 2 (MEF2), which is involved in stress response and cardiomyocyte remodeling. MuRF1 is required for AMPK-mediated protein degradation through the UPS in cardiomyocytes. Consequently, the absence of MuRF1 during chronic fasting preserves cardiac function, possibly by limiting degradation of critical metabolic enzymes. Furthermore, during cardiac hypertrophy, chronic activation of AMPK also leads to cardiac dysfunction, possibly through enhanced protein degradation and metabolic dysregulation. Collectively, my findings demonstrate that AMPK regulates expression of ubiquitin ligases which are required for UPS-mediated protein degradation in the heart. Based on these results, I propose that specific metabolic signals may serve as modulators of intracellular protein degradation in the heart.

LAY SUMMARY

METABOLIC CONTROL OF PROTEIN DEGRADATION IN THE HEART

Kedryn K. Baskin, BA

A cure for heart failure has thus far eluded researchers, although symptoms can be managed and side effects can be treated. More than 5 million Americans have been diagnosed with heart failure, and each year an estimated 550,000 of them die as a result of this condition, often less than 5 years after initial diagnosis. AMPK, a protein known as the “fuel gauge of the cell”, is the target for metformin, commonly used in the treatment of type 2 diabetes. This protein may potentially be a drug target to manage heart failure as well.

Heart failure is a complex disease caused by various factors including diabetes, obesity and high blood pressure. Heart failure patients often have hearts measuring up to three times the normal size, which is due to an the increased size of cells that make up the heart. The cells are bigger because they have more proteins than normal heart cells. Several studies have suggested that regulating cell size in the heart may be a way to combat the disease. Researchers also have known for some time that regulating the amount of healthy proteins within a cell regulates cell size. However, the details regarding how this process is regulated in the heart is not completely understood.

Enter AMPK, the “fuel gauge”. AMPK is the internal fuel gauge that tells the cell how to behave under different circumstances. When the cell has ample energy, AMPK does not allow the cell to take in more energy-producing material. When the cell is running low on energy, AMPK allows the cell to take in energy-producing material and possibly generate energy from other sources within the cell. Excess proteins in heart cells are disposed of in a highly organized manner through a process termed protein degradation. In this study I have shown that AMPK regulates protein degradation, which is another way to provide energy in the cell.

The current study links the cell’s energy needs to the regulation of protein degradation. When the cell’s fuel gauge, AMPK, is stimulated it causes certain genes involved in protein degradation to become active. These genes then regulate degradation of excess proteins. This process can be protective or detrimental to the heart depending on the condition of the heart prior to enhanced protein degradation.

TABLE OF CONTENTS

Approval Page	i
Title Page	ii
Dedication	iii
Acknowledgments	iv
Abstract	vii
Lay Abstract	viii
Table of Contents	ix
List of Illustrations	xii
List of Tables	xiv
Abbreviations	xv
Chapter 1. Introduction	1
1.1. Setting the Stage: Cardiac Hypertrophy and Heart Failure	2
1.2. Pathways of Protein Degradation in the Heart	5
1.3. Muscle Specific Ubiquitin Ligases (E3)	17
1.3.1. Regulation of Atrogin-1 and MuRF1	20
1.3.2. Targets of Atrogin-1 and MuRF1	26
1.4. Metabolic regulation of Cardiac Function: Focus on AMPK	30
1.4.1. Structural and Functional Aspects of AMPK	32
1.4.2. An Overview of the Central Role of AMPK in the Heart	35
1.5. AMPK: A Proposed Link Between Cardiac Metabolism and Protein Turnover	40
Chapter 2. Materials and Methods	42
2.1. Materials	43
2.1.1. Animals	43
2.1.2. Cell Lines	44
2.1.3. Equipment	44
2.1.4. Reagents	46
2.2. Methods	50
2.2.1. Maintenance of Mouse Lines	50
2.2.2. Transverse Aortic Constriction in Mice	50
2.2.3. Assessment of Cardiac Function	54
2.2.3.1. Echocardiography	54
	ix

2.2.3.2. Magnetic Resonance Imaging	56
2.2.4. Isolation of Neonatal Rat Ventricular Cardiomyocytes	58
2.2.5. Isolation of Adult Mouse Cardiomyocytes	60
2.2.6. Cell and Tissue Collection and Preservation	62
2.2.6.1. Total RNA Isolation and Quantification	62
2.2.6.2. Protein Isolation and Quantification	63
2.2.6.3. Nuclear Fractionation of Cells	63
2.2.6.4. Histology and Immunohistochemistry	64
2.2.7. Biochemical Assays	64
2.2.7.1. Luciferase Reporter Constructs and Activity Assays	64
2.2.7.2. β -galactosidase Activity Assays and Staining	65
2.2.7.3. MEF2 Activity Assay	66
2.2.7.4. Proteasome Activity Assay	67
2.2.7.5. Chromatin Immunoprecipitation Assay (ChIP)	67
2.2.8. Amplification and Quantification of Adenoviruses	69
2.2.9. Quantitative Real Time PCR (qRT-PCR) Transcript Analysis	73
2.2.9.1. Design and Verification of qRT-PCR Assays	73
2.2.9.2. Gene Expression Analysis using qRT-PCR Assays	73
2.2.10. SDS-PAGE, Western Blot Analysis and Quantification	77
2.2.11. Protein Turnover Assays	79
2.2.12. Statistical Analysis	80
Chapter 3. The Role of 5'-AMP-Activated Protein Kinase in Protein Degradation in the Heart	81
3.1. Nutrient Deprivation Upregulates Markers of Protein Degradation in Cardiomyocytes	82
3.2. AMPK Regulates the Expression of Ubiquitin Ligases <i>In Vitro</i> and <i>In Vivo</i>	85
3.3. AMPK Activation Regulates the Expression of MuRF1 <i>In Vitro</i> Through the Transcription Factor Myocyte Enhancer Factor 2	100
3.4. MEF2 Transcriptional Activity and MuRF1 Transcription Are Regulated by AMPK in the Heart	105
3.5. MuRF1 is Detrimental to the Heart During Fasting	108
Chapter 4. The Role of 5'-AMP-Activated Protein Kinase in Cardiac Hypertrophy	117
4.1. An Overview of AMPK in Cardiac Hypertrophy	118
4.2. Regulation of Cardiac Function by AICAR	119

4.3. Molecular Consequences of Chronic AMPK activation in the Heart	126
Chapter 5. Concluding Remarks and Outlook	137
References	142
Vita	178

LIST OF ILLUSTRATIONS

Figure 1.1. The concept of cardiac plasticity as proposed by Hill and Olson	3
Figure 1.2. Signaling pathways in cardiac hypertrophy according to Frey and Olson	4
Figure 1.3. Proteolytic systems according to Jackman and Kandarian	6
Figure 1.4. Sarcomeric cleavage by calpains	7
Figure 1.5. Pathway of macroautophagy according to Yang and Klionsky	9
Figure 1.6. Ubiquitin Proteasome System (UPS)	10
Figure 1.7. Ubiquitination of proteins according to Goldberg	12
Figure 1.8. Structure of the proteasome	16
Figure 1.9. The ubiquitin ligase Atrogin-1	18
Figure 1.10. The ubiquitin ligase MuRF1	19
Figure 1.11. Pathways regulating Atrogin-1 and MuRF1	22
Figure 1.12. The structure of mammalian AMPK	34
Figure 2.1. Cells used for mechanistic studies	45
Figure 2.2. Genotyping results	53
Figure 2.3. Transverse aortic constriction and Doppler measurements	55
Figure 2.4. Echocardiographic tracings in the mouse	57
Figure 2.5. Magnetic Resonance Images of the mouse heart	59
Figure 2.6. MuRF1 promoter sequence and ChIP primers	70
Figure 2.7. Quantitative Real Time RT-PCR analysis	76
Figure 3.1. Regulation of ubiquitin ligases and AMPK by nutrient deprivation in cardiomyocytes	83
Figure 3.2. Regulation of ubiquitin ligases and AMPK by glucose deprivation in cardiomyocytes	84
Figure 3.3. Regulation of protein degradation by nutrient deprivation in cardiomyocytes	86
Figure 3.4. Time-dependent regulation of AMPK, Atrogin-1, and MuRF1 by AICAR in cardiomyocytes	87
Figure 3.5. Dose-dependent regulation of AMPK, Atrogin-1, and MuRF1 by AICAR in cardiomyocytes	89
Figure 3.6. Regulation of Atrogin-1 and MuRF1 by AICAR and Compound C in cardiomyocytes	90

Figure 3.7. Regulation of AMPK, Atrogin-1, and MuRF1 by AICAR in the mouse heart	91
Figure 3.8. Regulation of Atrogin-1 and MuRF1 by AMPK in cardiomyocytes	93
Figure 3.9. Synergistic regulation of Atrogin-1 by pharmacologic and genetic activation of AMPK	95
Figure 3.10. Synergistic regulation of MuRF1 by pharmacologic and genetic activation of AMPK	96
Figure 3.11. Regulation of protein degradation by AMPK in cardiomyocytes	97
Figure 3.12. Life as a CRB student	99
Figure 3.13. Regulation of FOXO3a by AMPK in cardiomyocytes	101
Figure 3.14. Regulation of MEF2 transcription by AMPK in cardiomyocytes	103
Figure 3.15. Regulation of MuRF1 transcription by an AMPK-MEF2 axis in myocytes	104
Figure 3.16. Regulation of MEF2 and MuRF1 by AMPK in the heart	106
Figure 3.17. Regulation of HDAC5 by AMPK in the heart	107
Figure 3.18. Regulation of protein degradation in cardiomyocytes by AMPK requires MuRF1	109
Figure 3.19. Regulation of MuRF1 and cardiac mass during fasting	110
Figure 3.20. Regulation of AMPK, MyBPC, and TnI during fasting	113
Figure 3.21. Consequence of metabolic stress on protein degradation in the heart	116
Figure 4.1. Synergistic effects of TAC and AICAR on cardiac parameters	120
Figure 4.2. Synergistic effects of TAC and AICAR on cardiac function	122
Figure 4.3. Synergistic effects of TAC and AICAR on cardiac dimensions	123
Figure 4.4. MRI images depicting synergistic effects of TAC and AICAR on the heart	124
Figure 4.5. Synergistic effects of TAC and AICAR on heart and lung weight	125
Figure 4.6. Synergistic effects of TAC and AICAR on cardiac phenotype	127
Figure 4.7. Regulation of microvasculature in response to hypertrophy	128
Figure 4.8. Reactivation of the fetal gene program during hypertrophy	130
Figure 4.9. Regulation of the ubiquitin proteasome system in response to hypertrophy	131
Figure 4.10. Regulation of autophagy genes in response to hypertrophy	132
Figure 4.11. Regulation of signaling pathways with hypertrophy in response to AICAR	134

LIST OF TABLES

Table 1.1. Protein targets of Atrogin-1 and MuRF1	31
Table 1.2. AMPK transgenic and knockout mice	39
Table 2.1. Antibodies and dilutions	49
Table 2.2. Genotyping primer sequences	51
Table 2.3. Genotyping PCR protocols	52
Table 2.4. CHIP PCR primers and protocol	71
Table 2.5. Quantitative Real Time RT-PCR primer and probe sequences	75
Table 3.1. Left ventricular functional parameters in fed and fasted mice	112

ABBREVIATIONS

AA	Amino acids
aAMPK	active AMPK adenovirus
ACC	Acetyl-CoA carboxylase
AICAR	N-(β -D-Ribofuranosyl)-5-aminoimidazole-4-carboxamide
AID	Autoinhibitory domain
AKT	Protein Kinase B
AMCM	Adult mouse cardiomyocytes
AMP	Adenosine monophosphate
AMPK	5'AMP-actived protein kinase
ANF	Atrial natriuretic factor
APS	Ammonium persulfate
Atg	Autophagy regulated gene
ATP	Adenosine triphosphate
Bid	BH3 interacting-domain protein
BLAST	Basic Local Alignment Search Tool
BSA	Bovine serum albumin
C2C12	Muscle myoblast cell line
CBD	Carbohydrate binding domain
CBS	Cystathionine β -synthase domain
CC	Compound C; 6-[4-(2-Piperidin-1-yl-ethoxy)-phenyl]-3-pyridin-4-yl-
ChIP	Chromatin Immunoprecipitation
ChREBP	Carbohydrate response element binding protein
CK	Creatine kinase
CMA	Chaperone-mediated autophagy
cMyBP-C	cardiac myosin-binding protein C
CnA	Calcineurin A
CO	Cardiac output
CP	Core particle
CREB	cyclic AMP response element-binding
CRTC2	CREB regulated transcription coactivator -1
cTnl	Cardiac Troponin I
Cul1	Cullen1
DAB	3, 3'-diaminobenzidine

DAPI	4', 6-diamidino-2-phenylindole
DEPC	Diethylpyrocarbonate
DNA	Deoxyribonucleic acid
dnAMPK	dominant negative AMPK adenovirus
DOX	Doxorubicin
DRM	Desmin-related cardiomyopathy
DTT	Dithiothreitol
DUB	Deubiquitinating enzyme
E1	Ubiquitin activating enzyme (general)
E2	Ubiquitin conjugating enzyme
E3	Ubiquitin ligase
EDTA	Ethylenediaminetetraacetic acid
EDV	End diastolic volume
EF	Ejection Fraction
EGTA	Ethylene glycol tetraacetic acid
eIF3-f	Eukaryotic initiation factor 3 subunit 5
ERAD	Endoplasmic reticulum (ER) associated protein degradation
ESV	End systolic volume
FAM	fluorophore 6-carboxyfluorescein
FOXO	Forkhead box O transcription factor
FS	Fractional Shortening
GBD	Glycogen binding domain
GLUT1	Glucose transporter 1
GLUT4	Glucose transporter 4
GMEB1	Glucocorticoid modulatory element binding protein-1
GR	Glucocorticoid receptor
GRE	Glucocorticoid response elements
H&E	Hematoxylin and eosin
H9c2	Cardiac myoblasts
HDAC	Histone deacetylase
HECT	Homologous to the E6-AP carboxyl terminus
HEPES	4-(2-hydroxyethyl)-1-piperazineethanesulfonic acid
HIBADH	3-hydroxyisobutyrate dehydrogenase
HKII	Hexokinase II
HMG-CoA	3-hydroxy-3-methylglutaryl-coenzyme A

HR	Heart rate
hsc	Heat shock conjugate
I/R	Ischemia/reperfusion
IGF-1	Insulin-like growth factor 1
IL-1	Interleukin-1
IRS-1	Insulin receptor substrate 1
IVSd	interventricular septum in diastole
JNK	c-Jun N-terminal kinase
LAD	Left anterior descending coronary artery
LAMP-2A	Lysosome-associated membrane protein type 2a
LKB1	Liver kinase B1
LPS	Lipopolysaccharide
LV	Left ventricular/ Left ventricular
LVEDV	Left ventricular end-diastolic volume
LVESV	Left ventricular end-systolic volume
LVIDd	Left ventricular inner diameter in diastole
LVIDs	Left ventricular inner diameter in systole
LVPW	Left ventricular posterior wall
Lys	Lysine
MAFbx	Muscle Atrophy F-box
MAPK	Mitogen activated protein kinase
MEF2	Myocyte enhancer factor 2
MFC	MuRF family conserved region
MHC	Myosin Heavy Chain
MI	Myocardial infarction
MLC	Myosin Light Chain
MOI	Multiplication of infectivity
MRF	Myogenic regulatory factor
MRI	Magnetic Resonance Imaging
mTOR	Mammalian Target of Rapamycin
MuRF	Muscle RING Finger
MyoD	Myoblast determination protein 1
NADH	Nicotinamide adenine dinucleotide hydrate
NF- κ B	Nuclear factor kappa-light-chain-enhancer of activated B cells
NRVM	Neonatal rat ventricular cardiomyocytes

NTC	No template control
ONPG	O-nitrophenyl- β -D-galactopyranoside
PAK	p21-activated kinase
PBS	Phosphate buffered saline
PCR	Polymerase chain reaction
PDH	Pyruvate dehydrogenase
PDK2	Pyruvate dehydrogenase kinase 2
PGC-1 α	PPAR- γ coactivator-1 α
PI3K	Phosphatidylinositol 3-kinase
PKC	Protein kinase C
PP1	Phosphoprotein phosphatase 1
PPAR- γ	Peroxisome proliferator-activated receptor- γ
PQC	Protein quality control
PTEN	Phosphatase and tensin homolog
PVDF	Polyvinylidene fluoride pyrazolo[1,5-a] pyrimidine
qRT-PCR	Quantitative real time RT-PCR
RACK1	Receptor for activated protein kinase C-1
RAS	renin-angiotensin system
RING	Really Interesting new Gene
RNA	Ribonucleic acid
Roc1	Regulator of cullens
RP	Regulatory particle
RR	Respiration rate
SAPK	Stress-activated protein kinase
SCF	Skp1/Cul1/F-box
SDS	Sodium dodecyl sulfate
SIRT1	Silent information regulator two number 1
Skp1	S-phase-kinase-associated protein-1
SMAD3	Sma and Mad Related Family 3
SREBP-1c	Sterol response element binding protein-1c
SV	Stroke volume
TAC	Transverse aortic constriction
TAK1	TGF- β -activated kinase-1
TAMARA	tetramethylrhodamine

TBE	Tris base, boric acid, EDTA
T _{cap}	Telethonin
TEMED	Tetramethylethylenediamine
Tg	Transgenic
TGF-β	Transforming growth factor beta
TGF-β	Transforming growth factor--β
TNFα	Tumor necrosis factor
Tnl	Troponin I
TRIM	Tripartite motif protein
UBA6	Ubiquitin activating enzyme (specific)
UBE1	Ubiquitin activating enzyme (specific)
UCP	Uncoupling protein
UPS	Ubiquitin Proteasome System
ZMP	5-Amino-4-imidazolecarboxamide riboside (Z-riboside)

Chapter 1

INTRODUCTION

“...all we know is still infinitely less than all that remains unknown [1].”

~William Harvey, M.D. (1628)

1. Introduction

1.1. Setting the Stage: Cardiac Hypertrophy and Heart Failure

My thesis addresses certain molecular aspects of heart failure, a disease which claims the lives of more than 500,000 Americans every year. Heart failure is the leading cause of death in the United States [2]. To date there is no cure for heart failure because the cellular and molecular mechanisms are still not completely understood [3]. This is what is known: Heart failure is often preceded by pathological cardiac hypertrophy, which is driven by both endogenous (genetic) [4, 5] and exogenous (environmental) factors [6, 7]. In order for the heart to adapt to various types of stress, individual heart muscle cells (cardiomyocytes) change or “remodel” metabolically [8-11] and structurally [12]. Excessive remodeling results in enlarged cardiomyocytes, which translates into overall increased heart size (**Figure 1.1.**) [13, 14]. Over time, the enlarged cardiomyocytes fail to contract normally, and heart function declines leading to failure [15, 16]. Consequently it is critical to understand the mechanisms that can reverse cardiac hypertrophy in order to prevent or decrease the incidence of heart failure.

The regression of cardiac hypertrophy is associated with improved cardiovascular outcomes [17-19]. While these clinical results are promising, the regression of hypertrophy is correlated with the duration of treatment [20], and there is no guarantee that long term treatment of hypertrophy will also not result in contractile dysfunction [21]. Cardiac hypertrophy is regulated by a vast array of intracellular signaling pathways that are simultaneously activated and interlinked (**Figure 1.2.**) [21, 22]. The majority of pathways regulating cardiac hypertrophy lead to enhanced protein synthesis, structural remodeling, and enlarged cardiomyocyte size [23-25]. What is less well studied in the heart is the role of protein degradation and whether enhanced protein degradation can balance the enhanced protein synthesis that occurs in hypertrophy.

It has recently been suggested that protein degradation is critical for normal cardiovascular function [26]. The regulation of intracellular processes, such as protein degradation, is critical in the adult heart because it is mainly comprised of terminally differentiated cardiomyocytes [27]. Consequently, cell size, and the resulting heart size, is determined by the overall balance of protein synthesis and protein degradation within cardiomyocytes [28]. While it is known from pulse-chase experiments that protein degradation occurs in the heart, it is not completely known how protein degradation in the heart is controlled. Therefore I set out to elucidate one of the mechanisms by which protein

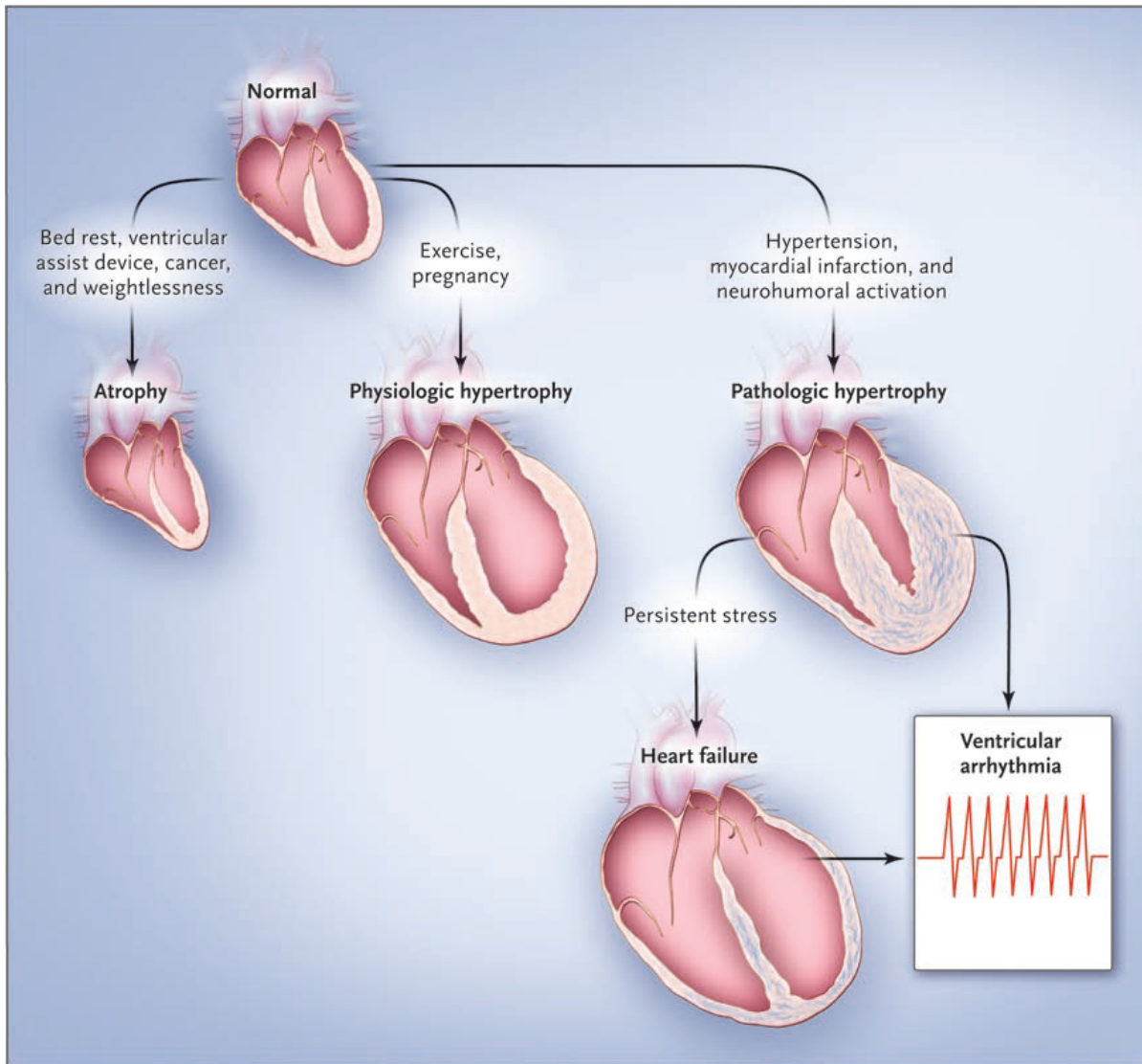


Figure 1.1. The Concept of Cardiac Plasticity as proposed by Hill and Olson [12].

The heart adapts to various types of stress by remodeling metabolically and structurally (shown here: atrophy on the left, hypertrophy on the right). The heart hypertrophies, either in a physiological or pathological manner. Exercise and pregnancy cause the heart to adapt through physiological hypertrophy. Stresses such as hypertension cause the heart to hypertrophy in a pathological manner which can eventually develop into heart failure. The heart can also atrophy under certain circumstances (Reviewed in [29]) Reprinted with permission from Massachusetts Medical Society (MMS) [12].

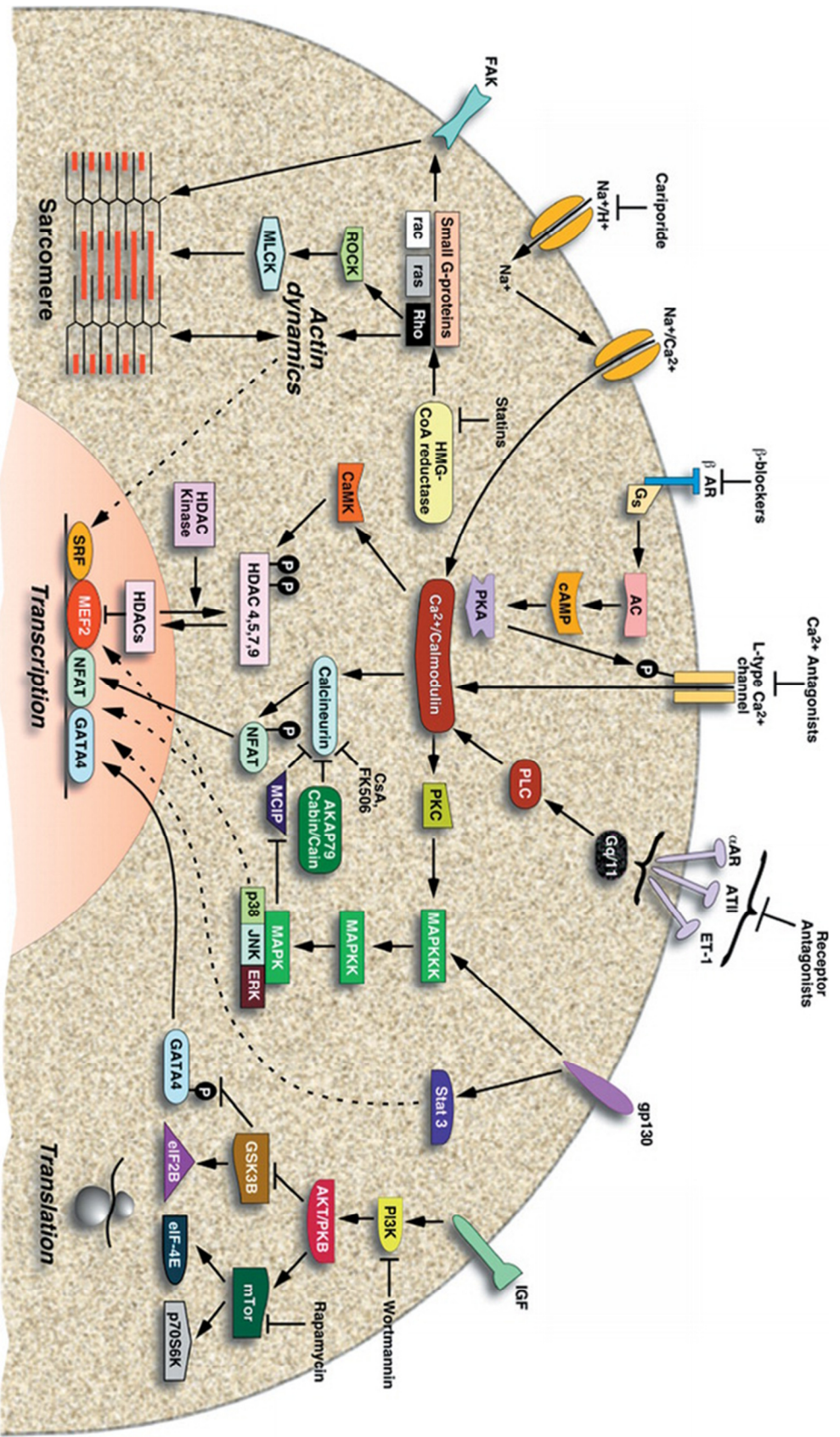


Figure 1.2. Simplified Signaling Pathways in Cardiac Hypertrophy according to Frey and Olson [21].

Cardiac hypertrophy is regulated by many different signaling pathways which are simultaneously activated and interlinked. A few pathways are shown here; however, many more pathways have been recently described which are not outline in this diagram. Reprinted with permission from Annual Reviews, INC [21].

degradation is controlled in the heart and to determine whether these mechanisms can decrease hypertrophy.

1.2. Pathways of Protein Degradation in the Heart

Much of what is known about protein degradation in the heart is based on studies in skeletal muscle [30]. Although the importance of protein degradation in the heart has been appreciated for some time [31], only recently have the specific proteolytic systems been investigated in detail. Protein degradation is regulated by three main proteolytic systems: the calpain system, the lysosomal-dependent autophagy system, and the Ubiquitin Proteasome System (UPS) (**Figure 1.3.**) [32]. The caspase system, specifically Caspase-3 is also thought to be involved in myofibrillar protein degradation [33-35], although it will not be discussed here.

The calpain system is composed of calcium-dependent cysteine proteases and calpastatin, a calpain-specific inhibitor [36]. At least 14 genes encoding calpains have been discovered, however, the most studied calpains are μ - and m-calpain (also referred to as Calpain 1 and 2) [37]. Calpains and calpastatin are expressed in all cell types investigated to date, however the levels of proteins in each cell differs [36]. In muscle, calpains cleave sarcomeric proteins [36] such as titin [38, 39], tropomyosin and troponins T and I [40], and myosin (**Figure 1.4.**) [41]. Calpain 3, which is mainly expressed in muscle, also cleaves titin, and loss-of-function mutations within this gene are associated with muscular dystrophy [42]. The calpain system has also been identified in the heart [43-45]. Recent studies have demonstrated that inhibition of calpain activity leads to the development of dilated cardiomyopathy with an accumulation of misfolded proteins, reviewed in [46]. Activation of calpains during reperfusion after ischemia contributes to apoptosis by cleavage of Bid and release of mitochondrial cytochrome C [47]. Calpains are also activated during hypertrophy and over-activation of calpains leads to atrial fibrillation and cardiac dysfunction, reviewed in [46] and [48]. The main calpain substrates are sarcomeric proteins, which are cleaved in a non-specific manner. Further degradation of specific sarcomeric proteins requires ubiquitin-mediated proteasomal degradation, which is discussed below.

Autophagy, a term first used by the Belgian Nobel laureate Christian de Duve [49] who also coined the terms “endocytosis” and exocytosis” [50], refers to a process that degrades intracellular material within a vacuole [51]. Autophagic processes can be further classified as follows. Macroautophagy, usually referred to as simply autophagy, involves the formation of cytosolic vesicles with a characteristic double membrane (autophagosomes) that are of non-lysosomal origin [52]. Autophagosomes fuse with lysosomes to form

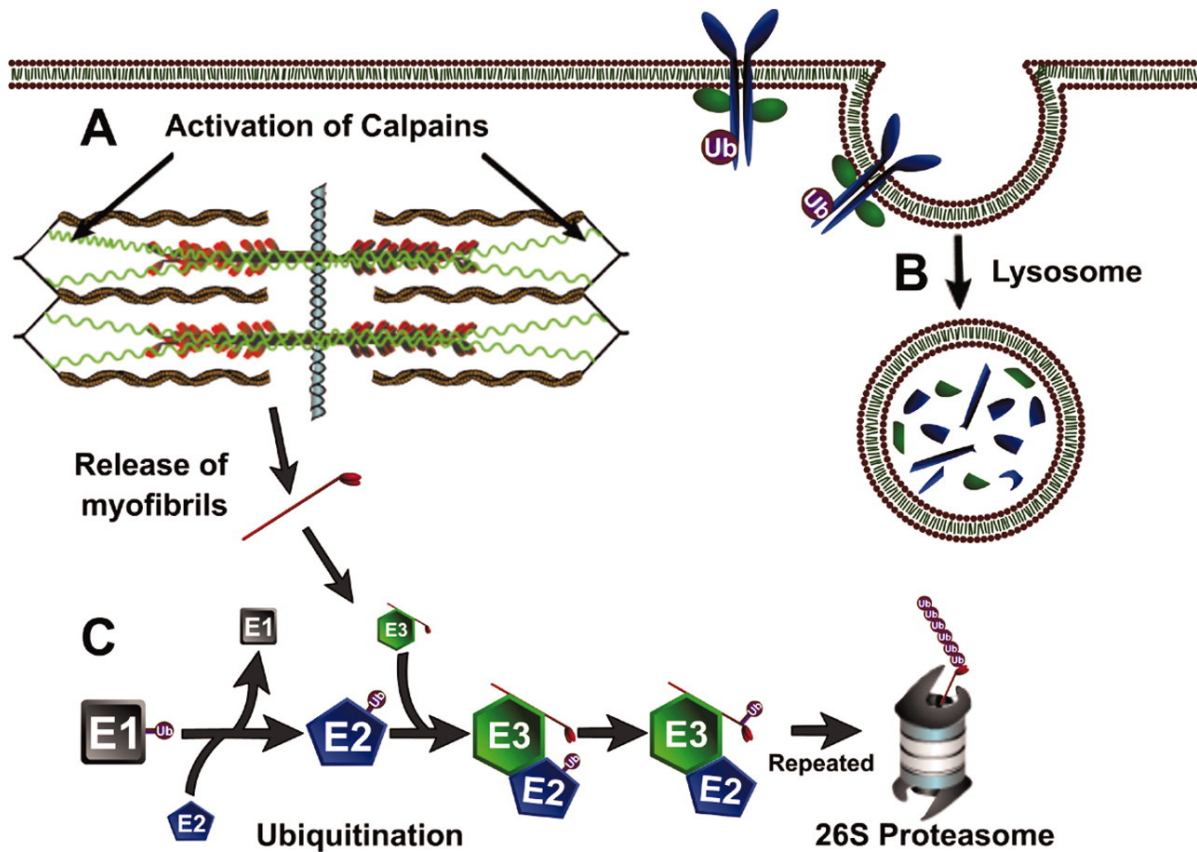


Figure 1.3. Proteolytic Systems according to Jackman and Kandarian [32].

Protein degradation is regulated by three main proteolytic systems. (A) The calpain system is thought to initiate sarcomere breakdown by cleaving large sarcomeric proteins in a non-specific, calcium-dependent manner (described in greater detail in Figure 1.4.). (B) The lysosomal-dependent autophagy system is described in more detail in Figure 1.5. (C) The ubiquitin proteasome system (UPS) is expanded upon in Figure 1.6. Reprinted with permission from The American Physiological Society [32].

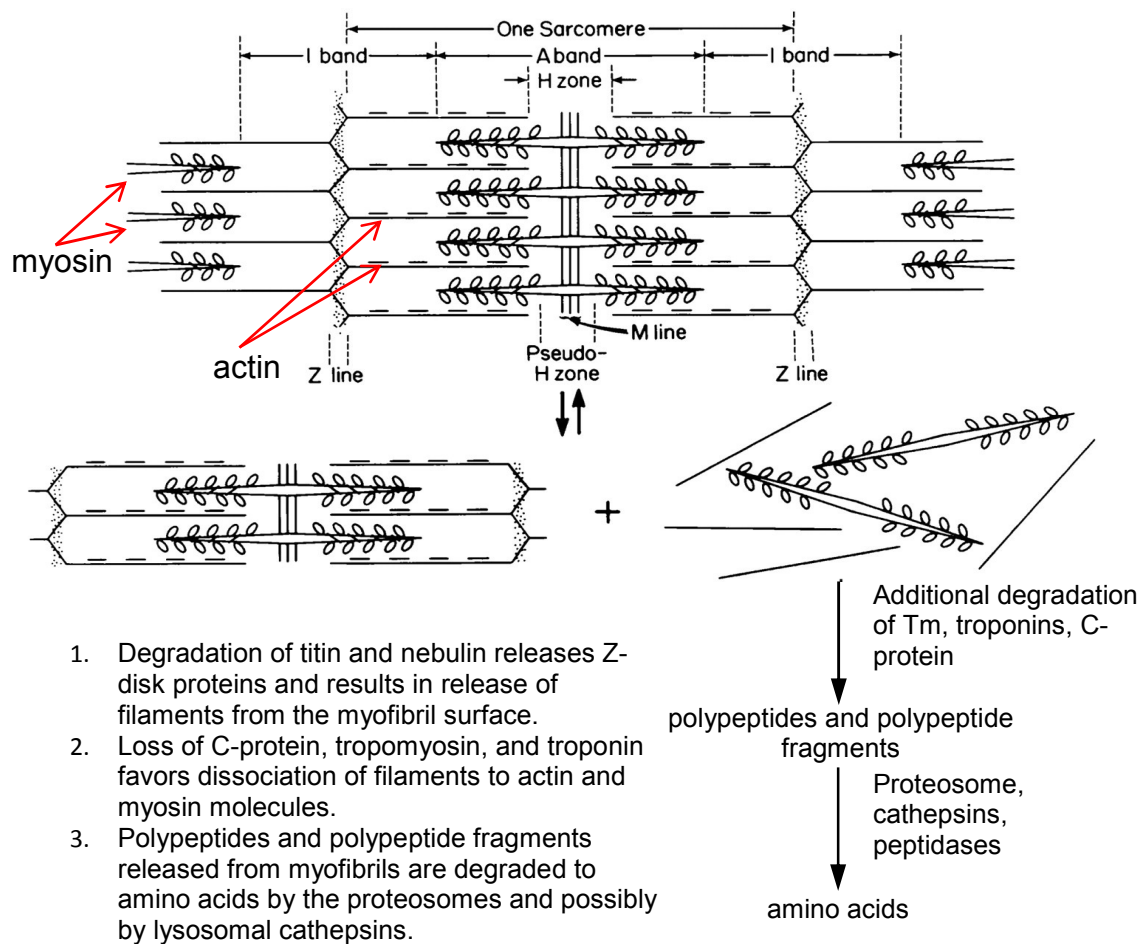


Figure 1.4. Sarcomeric Cleavage by Calpains.

(A) One sarcomere is represented with labeled regions. The Z lines outline each sarcomere and are where the actin filaments attach. The isotropic band (I band) of the sarcomere contains only actin filaments while the A band contains both actin and myosin. The middle region of the A band contains the H zone which is comprised of only myosin filaments. The H zone contains the M-line which is made up of many proteins. Titin (not shown here) links myosin filaments to the Z line. (B) The proposed process of calpain-induced sarcomere breakdown is described on the left and represented pictorially on the right. Tropomyosin (TM). Reprinted with permission from The American Physiological Society [36]

autolysosomes, and acid hydrolases degrade the content within the autolysosome (**Figure 1.5.**) [53]. Microautophagy refers to the selective or nonselective uptake of cytosol (including organelles) by the lysosome through protrusion, invagination, or septation of the lysosomal membrane [52]. Although considered a constitutively active form of autophagy involved in the turnover of long-lived proteins, the mechanism regulating microautophagy is not known presently [54]. The selective degradation of organelles, including lipophagy (degradation of lipid droplets), pexophagy (degradation of peroxisomes), reticulophagy (degradation of the endoplasmic reticulum), and ribophagy (degradation of ribosomes), is regulated by ubiquitination (discussed below) of adapter proteins or by receptors [52].

The most commonly investigated example of organelle-targeted degradation is mitophagy, the selective degradation of mitochondria [55]. The mechanisms regulating this process have recently been reviewed [56]. Another type of autophagy is chaperone-mediated autophagy (CMA) which degrades proteins containing the amino acid motif KFERQ by transporting them across the lysosomal membrane [52]. CMA requires the heat shock conjugate 70 (hsc70) and the integral membrane protein LAMP-2A [57]. Interestingly, mutations in LAMP-2 are associated with Danon's disease [58], a lysosomal glycogen storage disease characterized by cardiomyopathy [59].

Autophagy removes misfolded and dysfunctional proteins and organelles. The process can be triggered by nutrient deprivation and growth factor withdrawal [60]. The high energy demand of the heart, and the postmitotic nature of cardiomyocytes, deems basal autophagy an important housekeeping process for the removal of proteins that are either damaged or no longer needed [60]. Consequently, the disruption of autophagy can be detrimental to the heart. For example, the inhibition of autophagy can lead to hypertrophy and heart failure [61, 62]. Conversely, enhanced autophagy in the heart can lead to apoptosis during ischemia reperfusion [63] and pressure overload-induced heart failure [64]. The degree of autophagy and the context in which it occurs is linked to the differential effects of autophagy on the heart [65]. While it is still not clear whether it is beneficial or detrimental, the necessity of autophagy in the heart cannot be contested [66].

The ubiquitin proteasome system (UPS) is an ATP-dependent multi-enzymatic pathway that degrades the majority of intracellular proteins in a specific manner [67], and is the main focus of my dissertation (**Figure 1.6.**). The groundwork for the discovery of the UPS was laid by Alfred Goldberg in the 1970s when he established that ATP was required for protein breakdown [68, 69]. Shortly thereafter, the proteolytic component of the system (now known as the proteasome) was discovered simultaneously by Alfred Goldberg [70]

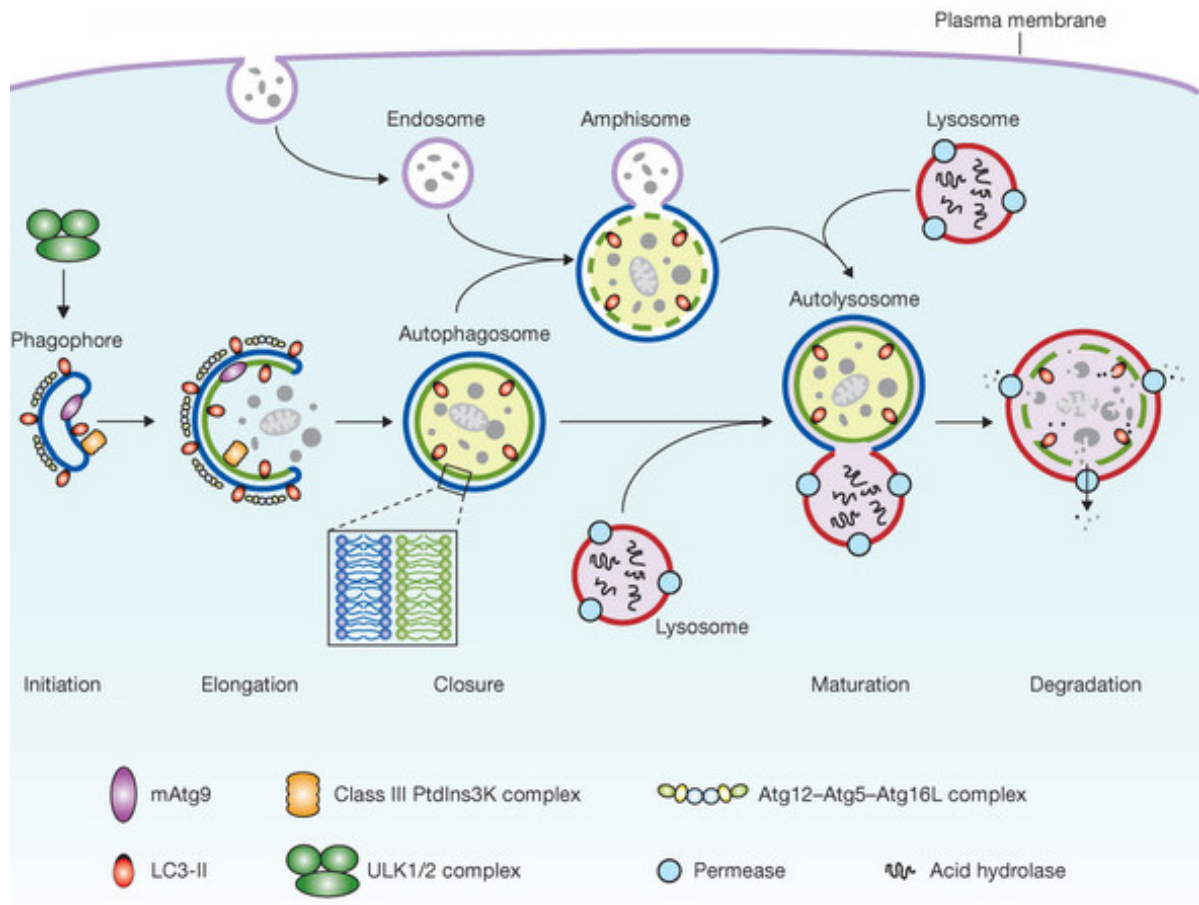


Figure 1.5. Pathway of Macroautophagy according to Yang and Klionsky [53].

Autophagy is initiated by phagophore formation followed by the elongation and expansion of the phagophore. The closure of the phagophore by completion of a double-membrane surrounding part of the cytoplasm creates an autophagosome. Autophagosomes mature by docking and fusing with an endosome or a lysosome, creating an amphisome or an autolysosome. After fusion, the contents of the autolysosome are degraded by acidhydrolases contained within the vesicle, and the products are recycled. The key regulators are show in the legended. Adapted from and reprinted with permission from Macmillan Publisher Ltd: [Nature Cell Biology] [53], copyright (2010).

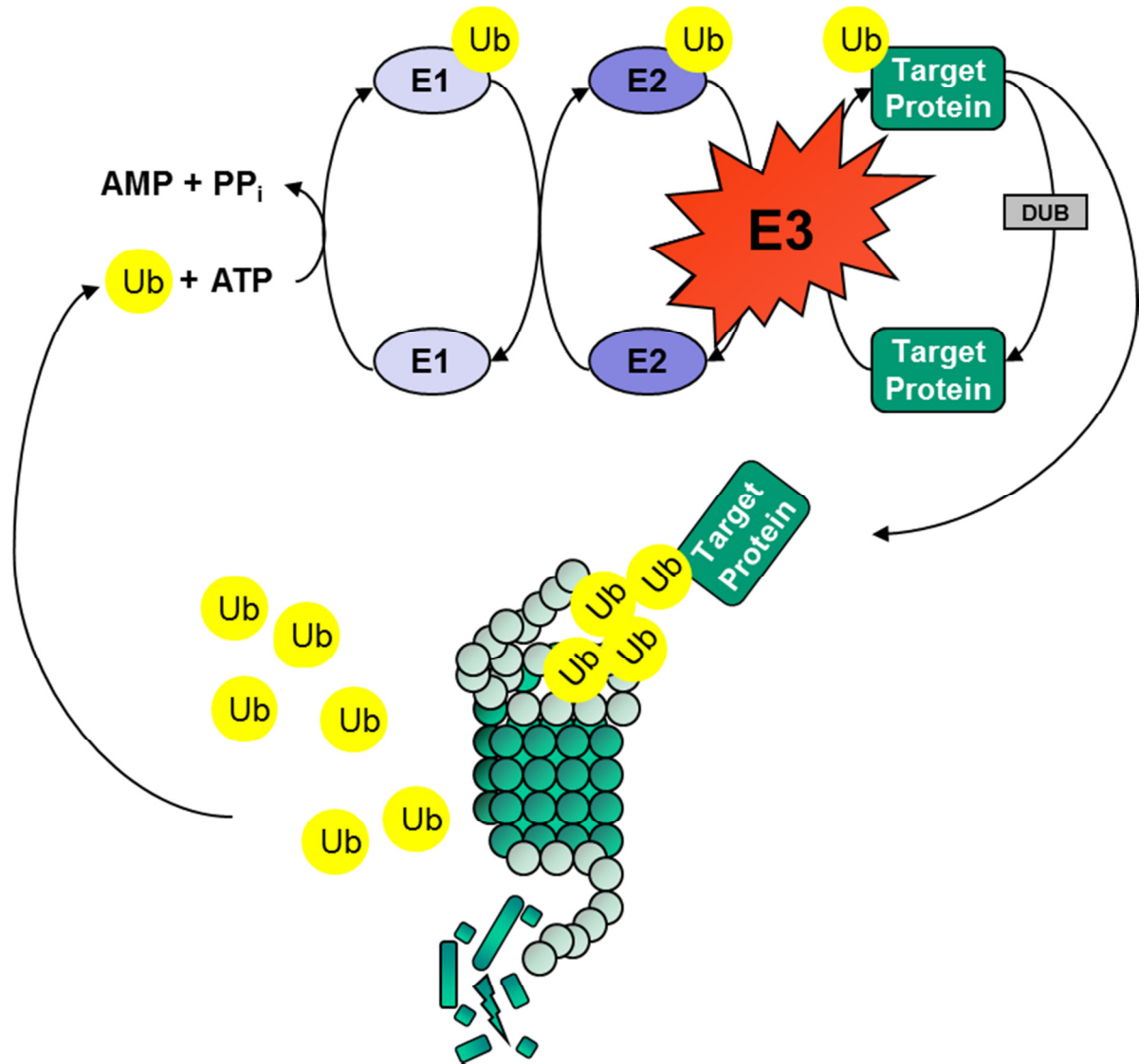


Figure 1.6. The Ubiquitin Proteasome System (UPS).

The Ubiquitin Proteasome System (UPS) consists of three enzymatic steps which degrade proteins in a targeted manner. Ubiquitin activating enzymes (E1) are first activated by ATP, followed by ubiquitin “charging”. Ubiquitin is then passed from the E1 to an ubiquitin conjugating enzyme (E2). E2s act with specific ubiquitin ligases (E3) to ubiquitinate proteins. E3s confer the specificity of the UPS by binding, ubiquitinating, and thus causing the degradation of targeted protein substrates. Proteins can also be deubiquitinated by deubiquitinating enzymes (DUB). Once protein substrates are ubiquitinated by a chain of at least 4 ubiquitin molecules, it is shuttled to the proteasome for degradation. The products of degradation (peptides, amino acids, and ubiquitin proteins) are recycled to make new proteins or are substrates for ATP production. Adapted from multiple sources.

and the Nobel laureates Avram Hershko, Aaron Ciechanover, and Irwin Rose [71]. The role of ubiquitin and the enzymatic steps required for the ubiquitination process were determined through several series of definitive experiments [72-76]. The culmination of these elegant studies defines what is widely recognized as the UPS.

What follows is a brief description of the UPS as we understand it today. Proteins degraded in the proteasome must first be ubiquitinated (**Figure 1.7.**) [77]. This process requires the activation of ubiquitin, a 76 amino acid protein, by an ubiquitin-activating enzyme (E1). The glycine residue on the C-terminus of ubiquitin forms a thiolester linkage with a cysteine residue on the E1, in an ATP-dependent reaction [78]. Once activated, ubiquitin is then transferred to a cysteine residue on an ubiquitin conjugating enzyme (E2), also called ubiquitin carrier proteins [79]. Enzymes belonging to the family of ubiquitin ligases (E3) confer the specificity of the system by binding to the protein substrate and transferring the ubiquitin from the E2 to the target protein [80]. Ubiquitin is linked to an ϵ -amino group of a lysine residue on the target protein. Multiple ubiquitin proteins are added to the protein substrate until the isopeptide chain contains at least 4 ubiquitin molecules (linked mainly through Lys48 on ubiquitin) [81]. The protein is then targeted to the 26S proteasome where it is degraded into peptides and amino acids. Ubiquitin molecules are removed by the 19S proteasome (the cap of the 26S) and reused [82].

The initial step in the UPS is the charging of ubiquitin. It was originally assumed that ubiquitin was only charged by the ubiquitin-activating enzyme UBE1, however several groups simultaneously discovered another enzyme also capable of activating ubiquitin, UBA6 [83-85]. The functions of UBE1 and UBA6 are not redundant because deletion of UBE1 in both yeast [86] and *C. elegans* [87] is lethal, and UBA6 knockout mice are embryonically lethal [85]. Both E1s activate ubiquitin but charge overlapping subsets of ubiquitin conjugating enzymes [84, 85].

To date there have been at least 38 human genes identified that encode ubiquitin conjugating enzymes (E2s) [79]. There are four classes of E2s but most E2s contain an active-site cysteine located within the conserved ubiquitin-conjugating (UBC) domain [88]. Conformational changes of E1s in response to ubiquitin charging allow for high affinity binding of the E1 to an E2 for ubiquitin transfer, and slight distinctions in these conformational changes allow for E2s to distinguish between the E1s [79]. Charging of E2s occurs quickly, and once charged with ubiquitin, E2s interact with E3s to catalyze ubiquitin transfer [84, 89] Although an E2 can interact with several E3s, there is evidence suggesting that certain amino acid residues on E2 are distinct for each E3 [90]. While E2-E3

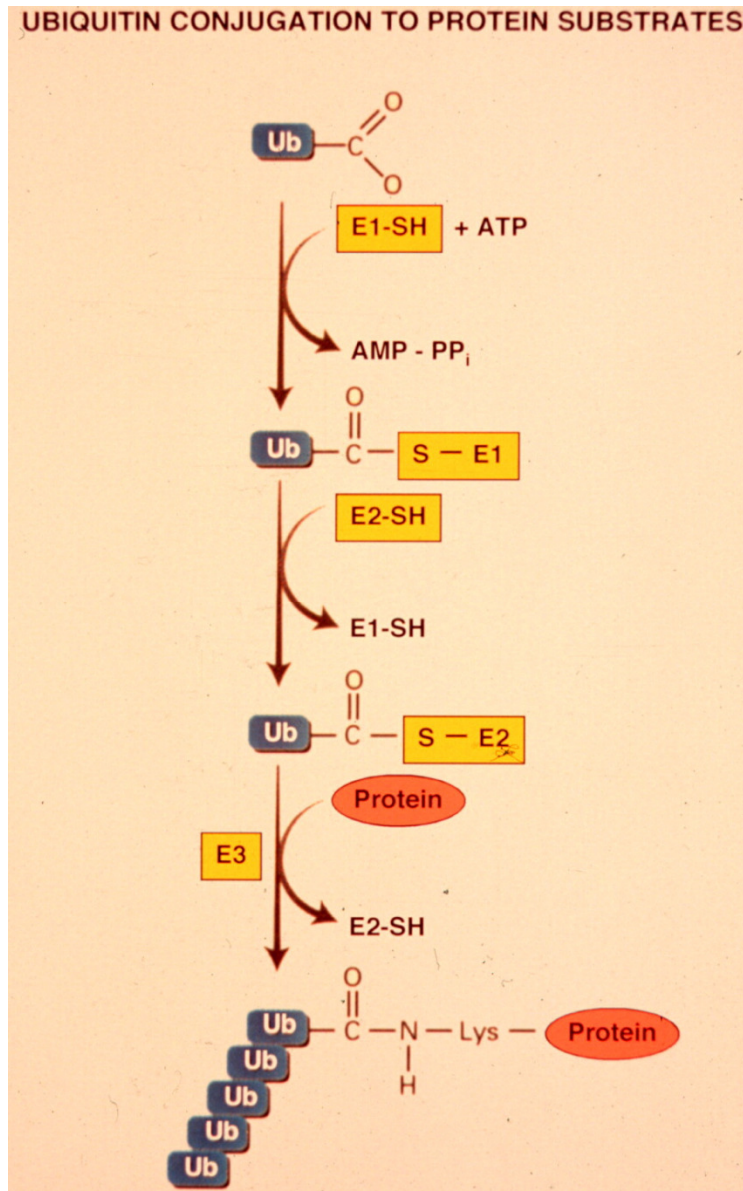


Figure 1.7. Ubiquitination of Proteins according to Goldberg [77].

The three steps required to ubiquitinate target proteins are shown here. The chemistry involved in ubiquitination is outlined, including the binding and transfer of ubiquitin. Details are found in the text. Reprinted from *Neuron*, 45/3, Goldberg, A.L., Nobel committee tags ubiquitin for distinction, 339-44, (2005), with permission from Elsevier.

interactions are weak, E3 binding induces conformational changes in the E2 allowing for ubiquitin transfer [91]. The E1 and E3s bind to overlapping regions on the E2 thus requiring several rounds of “ubiquitin charging” in order to polyubiquitinate a target protein [92].

E2s were originally dismissed as simple ubiquitin carrier proteins, but recent work has revealed that E2s regulate the length and topology of ubiquitin chains that are added to the target protein [79, 90]. Several E2s have been identified as strictly involved in ubiquitin chain initiation while others only function in ubiquitin chain elongation. Some E2s, however, are involved in both ubiquitin chain initiation and elongation. Additionally, a select few E2s are capable of pre-assembling ubiquitin chains to speed up the ubiquitination process thus increasing rates of degradation for certain proteins. Specific examples of each type of E2 are reviewed by Ye and Rape [79].

Yet another property of the E2 is the ability to regulate the type of ubiquitin linkage added to the target protein [79]. It is thought that the ubiquitin linkage can be regulated by several factors, including the ubiquitin binding domain. For example, the ubiquitin-binding domain NZF is specific for ubiquitin linkage through Lys63 [93]. At present there are at least 20 known ubiquitin binding domains and the structure of each domain is critical in determining the type of ubiquitin linkage E2s add to target proteins [94]. Although much more work is still needed to fully understand E2s, their functional output, the ubiquitination of target proteins, requires the presence of ubiquitin ligases (E3s) [91].

As already mentioned, ubiquitin ligases (E3s) confer the specificity of the UPS by determining which proteins are ubiquitinated and potentially degraded [95]. Thus far over 600 human genes have been identified that encode ubiquitin ligases. There are three types of E3s: HECT (homologous to the E6-AP carboxyl terminus)-type, RING (Really Interesting new Gene)-type, and U-box-type. While HECT-type ubiquitin ligases transfer ubiquitin to the active-site cysteine on the E3 before ligating the ubiquitin onto target proteins, RING-type and U-box-type ubiquitin ligases act more like scaffolds for the conjugation reaction [96]. Ubiquitin ligases regulate cellular processes including cell cycle and growth, transcription, cell signaling, and DNA repair [95]. Furthermore, discussed in detail in the next section, tissue or cell-specific ubiquitin ligases, such as TRIM9 expressed in the brain [97] and Atrogin-1 and MuRF1 expressed in striated muscle cells [98, 99], are critical regulators of organ function.

Much focus has been placed on ubiquitin ligases as they ubiquitinate target proteins; however recent work has highlighted the importance of the type of ubiquitin linkages conjugated to the target protein [93]. As previously mentioned, E2s also regulate

ubiquitin linkages. Ubiquitin is attached to ϵ -amino groups of lysine residues within ubiquitin binding domains of the target protein and of ubiquitin itself. Ubiquitin has 7 lysine residues giving rise to 7 possible types of homologous ubiquitin chains and many heterologous ubiquitin chains [94]. The most common ubiquitin chains are linked through Lys48 and Lys11, which target the protein for degradation, and Lys63 chains which play a role in DNA repair [94, 100]. An additional level of complexity in ubiquitination of proteins is that different lysines on the same protein can be ubiquitinated. The combination of the lysines that are ubiquitinated and which linkages are on each lysine can ultimately determine the fate of the protein.

Although ubiquitination is an important determinant of the cellular localization, function, and degradation of proteins, this process is also reversible. Deubiquitinating enzymes (DUB) are proteases with several functions, one of which is cleaving ubiquitin from ubiquitinated proteins [101]. DUBs appear to have high specificity and thus may be promising drug targets to regulate the UPS [102]. Proteasome-associated DUBs, which cleave polyubiquitin chains from proteins being degraded [103], are of particular interest due to the positive clinical outcomes of cancer patients treated with Bortezomib (proteasome inhibitor) [104]. It has been suggested that targeting proteasome-associated DUBs for cancer therapeutics may decrease the toxicity of anticancer drugs [105]. While many questions still need to be answered, it is apparent that DUBs add another layer of complexity to the regulation of the UPS [106].

The objective of the UPS is to degrade proteins in the proteasome [107]. The 26S proteasome is a multi-catalytic complex made up of the 20S core particle (CP) which carries out proteolysis, capped on either or both ends with homologous or heterologous regulatory particles (RP) [108]. There are three regulatory particles: the 19S particle (also known as PA700) which unfolds ubiquitin-tagged proteins [108], the 11S particle which degrades peptides in an ATP-independent manner [109], and the PA200 particle which regulates protein degradation during DNA repair [110]. The 20S has a barrel-like structure containing 4 heptameric rings organized in the following manner: $\alpha_{1-7}\beta_{1-7}\beta_{1-7}\alpha_{1-7}$ [111]. The β subunits are proteolytically active and have caspase-, trypsin-, and chymotrypsin-like activities [112]. The most common regulatory particle, 19S, is comprised of a base, containing 6 different ATPases (regulatory triple A proteins (Rpt) 1-6s) and 3 non-ATPase proteins (Rpn), and a lid containing 9 Rpn subunits (**Figure 1.8.**) [113]. While ATP binding to the 19S is required for proteasome function, ATP hydrolysis is not [114].

The proteasome itself is not the focus of my thesis, and thus not extensively reviewed here, however, it is an important aspect of the cardiac UPS to consider. The activity of the proteasome is a heavily investigated area with therapeutic implications in cancer [115], aging [116], neurodegenerative diseases [117], and cardiovascular diseases [118]. Akin to autophagy, the degree by which proteasome activity is activated or inhibited can be protective or detrimental to the heart. A lapse in protein quality control for example, by chaperone deficiency or uncontrolled protein synthesis, can lead to the accumulation and aggregation of misfolded proteins and thus decreased proteasome activity [119]. While uncontrolled protein synthesis, protein misfolding, and decreased proteasome activity are characteristics of desmin-related cardiomyopathy (DRM), DRM is also caused by mutations in sarcomeric proteins which consequently lead to protein aggregation and proteasome insufficiency [119].

Various stresses on the heart can lead to proteasome dysfunction. Proteasome activity is decreased in the heart during ischemia/reperfusion (I/R) [120], and the degree of proteasome dysfunction during reperfusion depends on the length of time the heart is subjected to ischemia [121]. Inhibition of the proteasome reduces infarct size and preserves cardiac function after I/R [122]. Ischemic preconditioning also improves proteasome dysfunction by decreasing the oxidative damage to the proteasome. These studies suggest that proteasome dysfunction during I/R is due to modification of the proteasome [123]. Furthermore, enhanced proteasome function during I/R (by overexpressing proteasome subunits) protects the heart from I/R-induced dysfunction [124]. Taken together these studies demonstrate that proteasome function is decreased after I/R and this may contribute to cardiac dysfunction.

Proteasome activity is also altered during cardiac hypertrophy. Chronic hypertrophy induced by aortic banding increases trypsin- and chymotrypsin-like 26S proteasome activities and expression of proteasome subunits [125]. Additionally, isoproterenol-induced hypertrophy increases 26S proteasome activity and modifies the subpopulations of proteasomes in the heart [126]. The proteasome inhibitor epoxomicin prevents the development of hypertrophy after aortic banding suggesting that enhanced proteasome activity is required for the development of cardiac hypertrophy [125]. Furthermore, inhibition of the proteasome after the onset of cardiac hypertrophy reduces cardiomyocyte size and apoptosis, stabilizes ejection fraction, and decreases the incidence of heart failure [127]. Collectively these findings show that enhanced proteasome activity leads to cardiac hypertrophy. Although proteasome function is critical for proper protein degradation, ubiquitination of proteins by ubiquitin ligases is required.

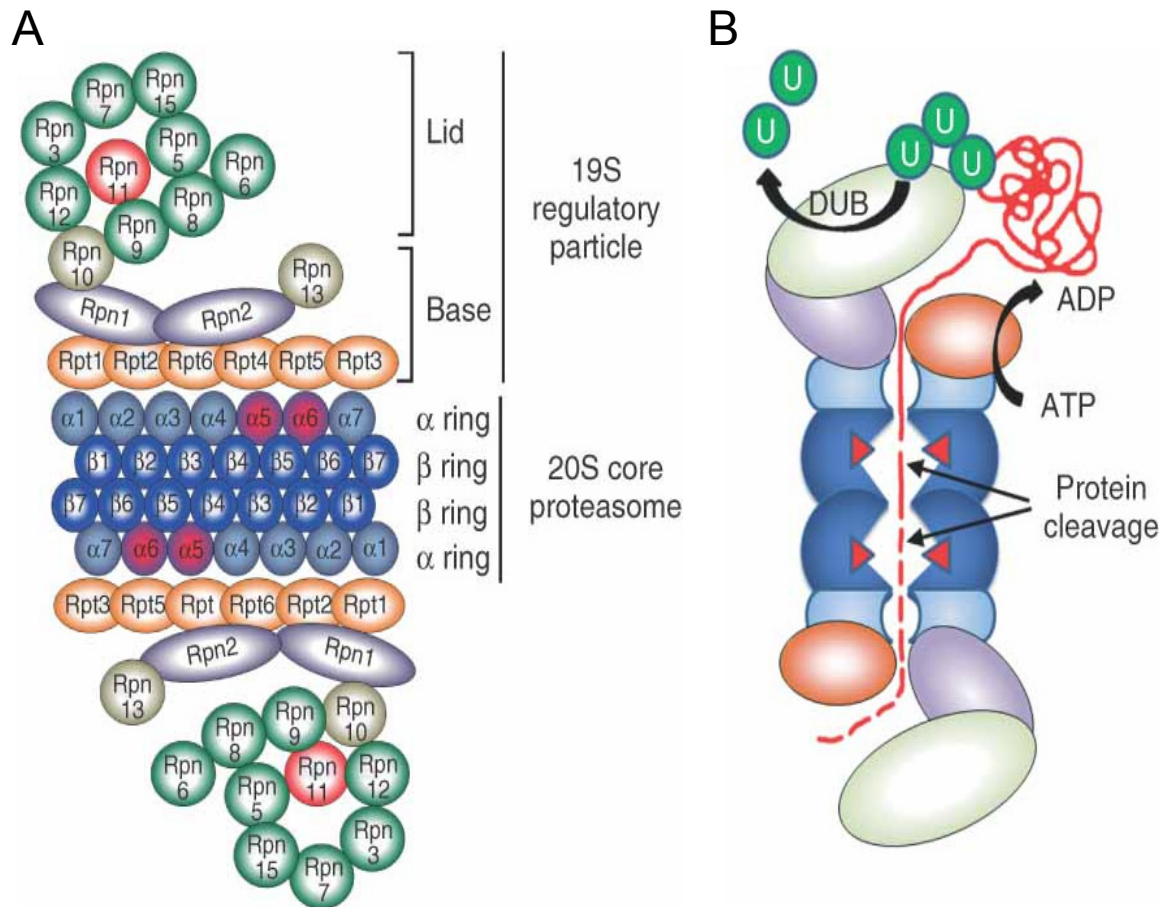


Figure 1.8. Structure of the Proteasome.

(A) A detailed illustration of the 26S proteasome containing 2 lids, 2 bases, and the 20S core. Descriptions of the subunits are found in the text. (B) A cross section of the 26S demonstrating unfolding and deubiquitination of the target protein by the 19S, the cleavage of the unfolded protein within the core, and peptide release from the lid. Reprinted with permission from John Wiley & Sons Ltd. [128].

1.3 Muscle Specific Ubiquitin Ligases (E3s)

The ubiquitin ligases discussed in detail below, Atrogin-1 and MuRF1, are both RING-type ubiquitin ligases, although of different classes. It interacts with Skp1 (S-phase-kinase-associated protein-1), Cul1 (Cullen1), and Roc1 to form an SCF complex (**Figure 1.9.**) [98, 99, 129]. Cullen1 provides the RING domain, which by binding E2s, mediates ubiquitination of the target protein. Atrogin-1 contains an F-box domain through which it binds Skp1, the scaffolding protein required for complex formation [130]. Atrogin-1 also contains a substrate recognition domain [131] and recognizes the motif “LQALL” on target proteins [132].

MuRF1 is also a RING-type ubiquitin ligase, but it ubiquitinates proteins solely with an E2 and does not require scaffolding proteins. MuRF1 has two coiled-coil domains which are important for protein-protein interactions; it has been found as hetero- and homodimers (**Figure 1.10.**) [133]. The B-box domain is required for E2 binding [134] and the RING domain contains the ligase “activity” which is important for ubiquitin transfer to the target protein [130]. MuRF1 also contains a MFC domain (MuRF family conserved region) which binds target proteins, but the specific function of this domain is unclear.

Muscle Atrophy F-box (MAFbx) [99] also known as Atrogin-1 [98] was simultaneously discovered in two independent studies investigating the molecular mechanisms of skeletal muscle atrophy and muscle wasting. In all models of skeletal muscle atrophy investigated, including hindlimb suspension, immobilization, denervation, cancer, diabetes, fasting, and renal failure, Atrogin-1 was universally upregulated at the transcript level [98, 99]. Additionally, glucocorticoid treatment, a model used to investigate sepsis and cancer-induced cachexia, also increases Atrogin-1 expression [98].

Muscle RING Finger 1 (MuRF1), a muscle-specific member of the RING family ubiquitin ligases, was originally identified in a yeast two-hybrid screen for binding partners that interact with titin, a sarcomeric kinase [135]. MuRF1 binds the N-terminus of titin, a region of the kinase localized on the M-line of sarcomeres [136, 137]. Three MuRF family proteins were identified and have high sequence homology but diverge at their C-terminus (**Figure 1.10.**) [135]. MuRF1 heterodimerizes with MuRF2 and MuRF3 but only MuRF1

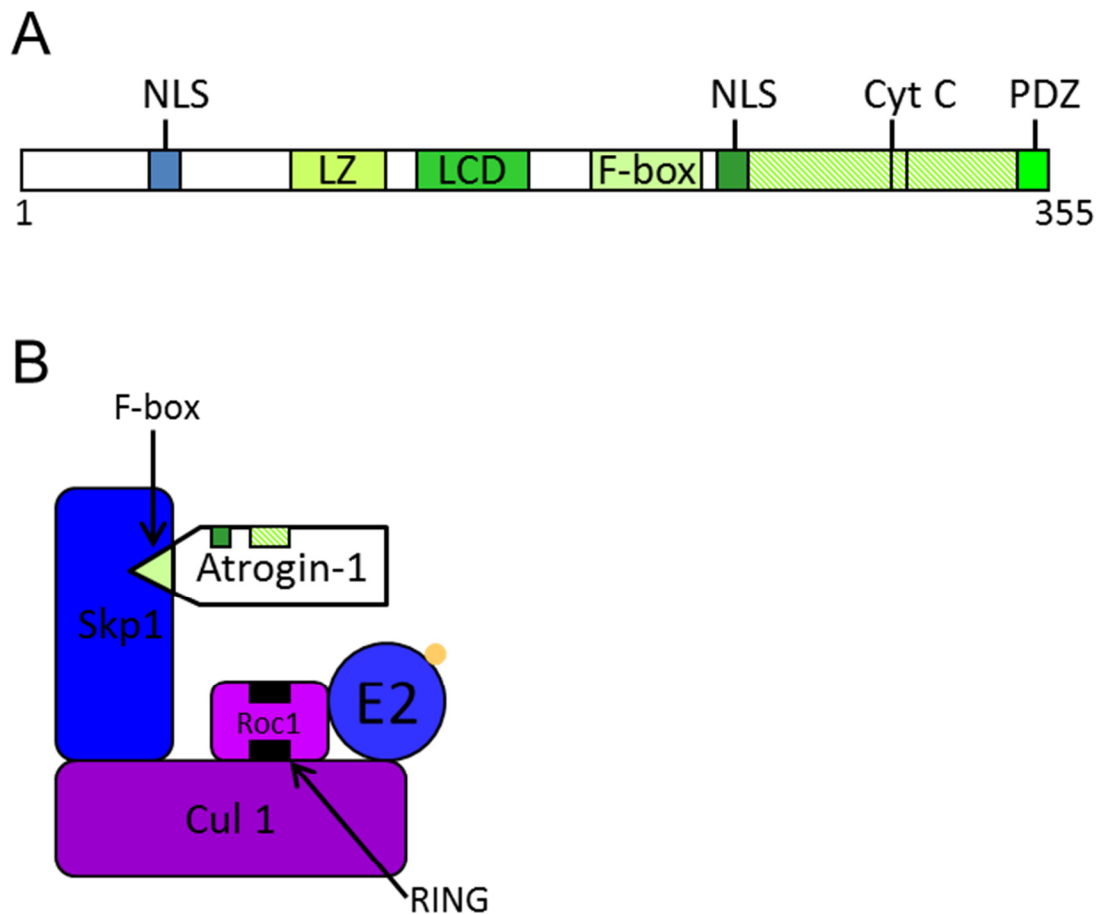


Figure 1.9. The Ubiquitin Ligase Atrogin-1.

(A) Linear structure of Atrogin-1 containing protein domains. NLS, nuclear localization sequence; LZ, leucine zipper; LCD, leucine charged domain; Cyt C, cytochrome c heme family binding site; PDZ, postsynaptic density-95 (PSD-95)/Discs large/zona occludens-1 domain. This research was originally published in the *Journal of Biological Chemistry*. Lionel A. Tintignac, Julie Lagirand, Sabrina Batonnet, Valentina Sirrill, Marie Peirre Leibovitch, and Serge A. Leibovitch. Degradation of MyoD Mediated by the SCF (MAFbx) Ubiquitin Ligase. *J Biol Chem*. 2005; 280:2847-56. [138]. (B) The SCF complex containing Atrogin-1. See text for details. Adapted with permission from Wolters Kluwer Health [131].

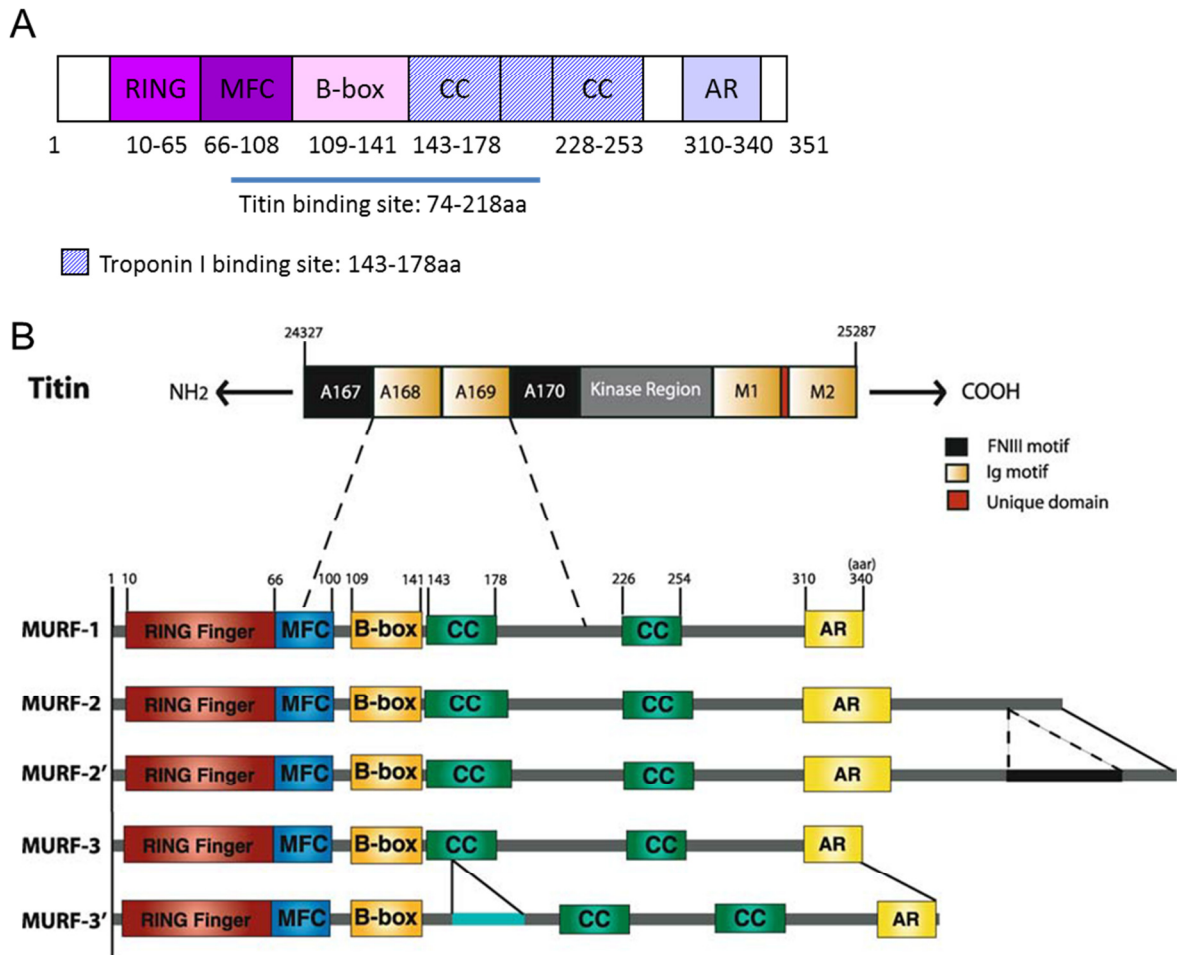


Figure 1.10. The Ubiquitin Ligase MuRF1.

(A) The linear structure of MuRF1 containing protein domains. The titin and troponin binding sites are noted. Adapted with permission [133]. (B) Linear alignment of the MURF family. Splice variants are shown as MURF-2' and MURF-3'. A region of titin is shown above the alignment and the regions where MuRF1 binds titin is outlined. Reprinted with permission from Springer [139]. RING, Really Interesting new Gene domain; MFC, MuRF family conserved region; CC, coiled-coil domain; AR, acidic region.

associates with titin. MuRF3, the first in the family to be identified, is involved in microtubular stabilization, which is important in myofibrillar assembly and contractile function [140]. While MuRF1 and 3 localize to the Z-lines of sarcomeres, MuRF3 is not found at the M-line [135]. MuRF1 and 3 are muscle specific; however, MuRF1 is expressed in all developmental stages, while MuRF3 seems to be important during development. MuRF2, on the other hand, is found in the liver in addition to striated muscle and is highly expressed in the fetal heart [135]. MuRF1, like Atrogin-1, was also found to be upregulated in several models of skeletal muscle atrophy [99].

The first *in vivo* investigations on the functional implications of Atrogin-1 and MuRF1 were performed using mice deficient for Atrogin-1 or MuRF1 [99]. Both strains of mice are resistant to skeletal muscle atrophy (induced by denervation), and the overexpression of Atrogin-1 in C2C12 muscle cells *in vitro* causes atrophy [99]. Since their original discovery, numerous reports have validated the importance of both ubiquitin ligases and have clarified their mechanistic regulation. Although most of what we know comes from studies performed in skeletal muscle and myotubes, the importance of these specific ubiquitin ligases in the heart has been validated and is a current field of investigation.

1.3.1. Regulation of Atrogin-1 and MuRF1

The earliest signaling pathways investigated in the regulation of Atrogin-1 and MuRF1 were growth signaling pathways. In addition to multiple skeletal muscle atrophy models, Atrogin-1 and MuRF1 expression are induced by food deprivation [141], suggesting that the inhibition of growth stimulating pathways positively regulates their expression. In skeletal muscle cells, insulin-like growth factor 1 (IGF-1) suppresses mRNA expression of Atrogin-1 and MuRF1 and inhibition of IGF-1 (through the PI3K-Akt pathway) increases Atrogin-1 expression and proteolysis [142]. Starvation-induced atrophy in C2C12 muscle cells decreases the Phosphatidylinositol 3-kinase - Protein Kinase B (PKB, also known as AKT) pathway, or PI3K-AKT pathway for short. Consequently, Forkhead box O (FOXO) transcription factors are activated thus increasing Atrogin-1 expression. Overexpression of IGF-1 or AKT inhibits FOXO3A and Atrogin-1 expression, and constitutively active FOXO3A regulates Atrogin-1 expression directly in skeletal muscle [143]. In the heart, FOXO3A overexpression also increases Atrogin-1 expression and prevents IGF-1-induced cardiac hypertrophy [144]. Furthermore, inhibition of FOXO1 by AKT also prevents the expression of Atrogin-1 and MuRF1 in muscle cells [145]. Glycogen synthase kinase 3 beta (GSK3 β), also negatively regulated by AKT, mediates FOXO1-induced expression of Atrogin-1 to decrease cardiac hypertrophy [146], and in skeletal muscle, basal and atrophy-induced

Atrogin-1 mRNA expression requires GSK3 β [147]. These and other pathways are outlined in **Figure 1.11**.

The regulation of Atrogin-1 and MuRF1 expression through the PI3K-Akt pathway has been demonstrated by many groups in various experimental settings. Diabetes has been shown to induce skeletal muscle wasting, and indeed, streptozotocin (STZ)-induced diabetes increases both ubiquitin ligases [148]. Insulin deficiency in muscle suppresses PI3K, increases the inhibitory phosphorylation of IRS-1 (Insulin receptor substrate 1), and increases muscle proteolysis [149]. Furthermore, mice heterozygous for Phosphatase and tensin homolog (PTEN), a negative regulator of the PI3K-AKT signaling pathway, exhibit decreased protein degradation and reduced expression of Atrogin-1 and MuRF1 in muscle [150].

Additional studies on muscle atrophy and the PI3K-AKT pathway suggest that transcription of Atrogin-1 and MuRF1 also occurs downstream of mammalian target of rapamycin (mTOR), but independent of FOXO [151]. Furthermore, the regulation of FOXO3A, independent of the PI3K-AKT pathway also regulates Atrogin-1 expression. The histone acetyltransferase (HAT) p300/cyclic AMP-response element-binding protein (CREB), known as p300/CREB, represses FOXO3A activity and thus decreases Atrogin-1 expression, suggesting that acetylation by p300/CREB may differentially regulate the FOXO isoforms and more specifically direct atrophic signaling [152].

In the heart, chronic left ventricular dysfunction caused by myocardial infarction (MI) leads to cardiac and skeletal muscle atrophy. In response to MI there is enhanced protein ubiquitination, increased proteasome activity, activation of FOXO-mediated transcription, and increased Atrogin-1 expression. Local IGF-1 injection, however, prevents MI-induced muscle atrophy [153]. Congestive heart failure associated with hypertension (the activation of renin-angiotensin system (RAS)) also leads to skeletal muscle wasting. Angiotensin-II infusion in rats increases muscle proteolysis and Atrogin-1 and MuRF1 expression, which is reversed by inducing IGF-1 expression [154]. While Atrogin-1 expression in the heart is regulated by FOXO1/3A, Atrogin-1 also inhibits AKT-induced physiological cardiac hypertrophy by binding to, ubiquitinating (through Lys63 linkages), and thus transcriptionally co-activating FOXO1/3A. Consequently, IGF-1-induced physiological cardiac hypertrophy is decreased in Atrogin-1 transgenic mice due to increased activity of FOXO1/3A. Moreover, Atrogin-1^{-/-} hearts hypertrophy to a greater extent after exercise [155]. This study unveils a feed forward mechanism for FOXO1/3A-Atrogin-1 in the heart, although the ramifications of this pathway under normal conditions have yet to be reported [156].

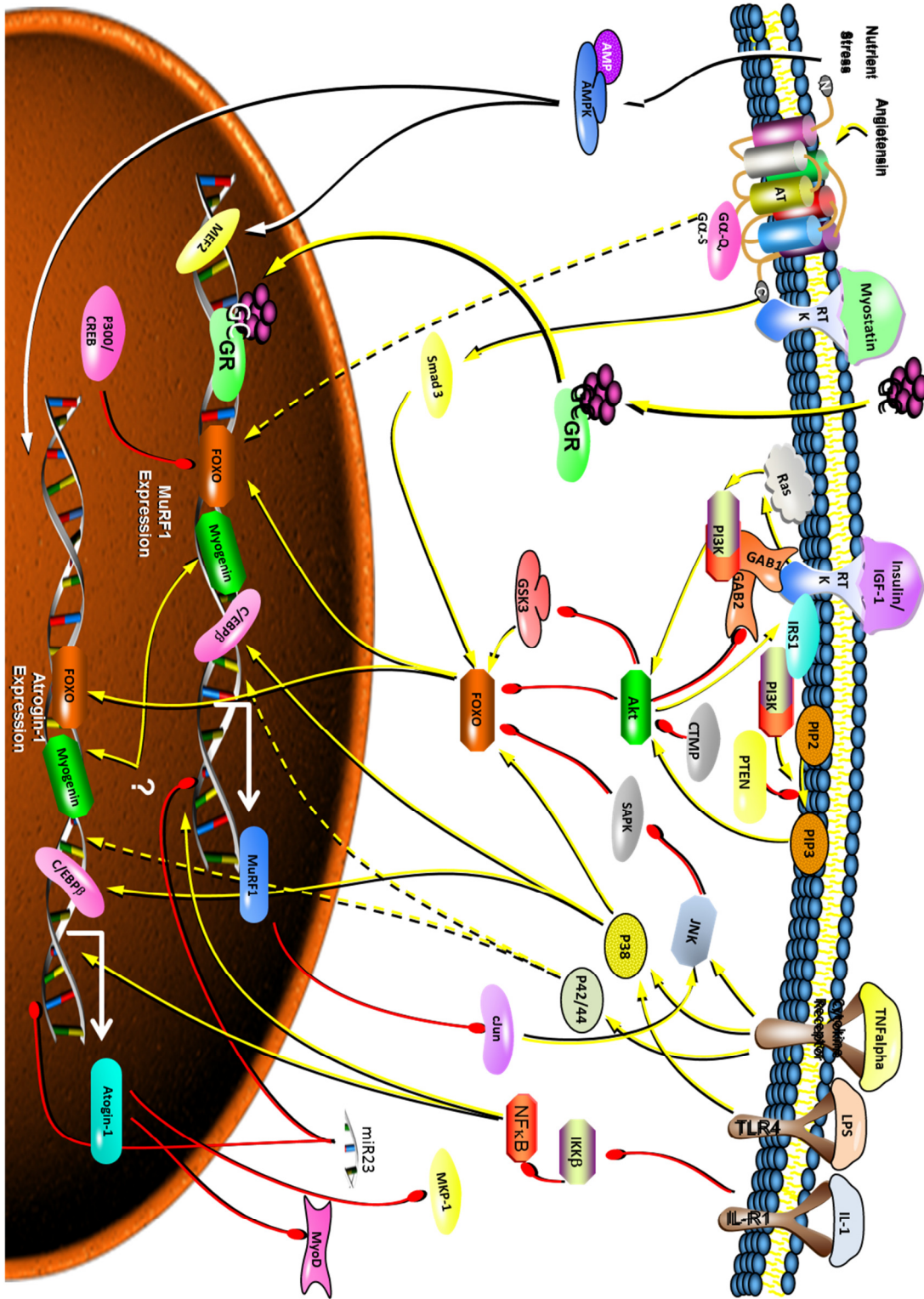


Figure 1.11. Pathways regulating Atrogin-1 and MuRF1.

Detailed pathways regulating Atrogin-1 and MuRF1 expression. Yellow arrows symbolize activation; red lines symbolize inhibition; white lines are the topic of Chapter 3. See text for details. Designed using resources from SA Biosciences.

Another signaling pathway that regulates Atrogin-1 and MuRF1 is the transforming growth factor beta (TGF- β) signaling pathway (**Figure 1.11.**). Myostatin, a member of the TGF- β super family, induces skeletal muscle wasting (cachexia) in part by increasing the expression of Atrogin-1 and MuRF1. Myostatin reverses the PI3K-AKT signaling pathway by inhibiting AKT phosphorylation [157, 158]. Myostatin^{-/-} mice have increased muscle size and overexpression of myostatin in C2C12 myotubes attenuates IGF-1-induced hypertrophy [159]. Myostatin is also required for Dexamethasone (glucocorticoid)-induced skeletal muscle atrophy [160]. TGF β family members, including myostatin, signal through the transcription factor Smad3 (mothers against decapentaplegic homolog 3) in muscle. Smad3 is sufficient and necessary for myostatin-induced Atrogin-1 expression through FOXO1, but is not required for MuRF1 expression [161].

Tumor necrosis factor (TNF α), a cytokine involved in inflammation, also induces muscle wasting under conditions such as cachexia and sepsis. TNF α causes atrophy in C2C12 cells in part by increasing Atrogin-1 expression [162], and this is partially reversible with IGF-1 treatment [163] (**Figure 1.11.**). Injection of TNF α into skeletal muscles of mice also induces Atrogin-1 mRNA expression, and inhibition of p38 mitogen activated protein kinase (MAPK) blunts the increase of Atrogin-1. These studies demonstrate that the TNF α /p38 pathway regulates Atrogin-1 expression in skeletal muscle [162]. TNF α also regulates Atrogin-1 through FOXO4, independent of AKT, in muscle cells [164]. Muscle wasting in cancer-induced cachexia increases Atrogin-1 by activating p38 [165]. Activated p38 regulates Atrogin-1 transcription by phosphorylating and thus activating the transcription factor CCAAT/enhancer-binding protein beta (C/EBP β), which then induces Atrogin-1 expression independent of FOXO1/3 [165].

In chronic heart failure, TNF α levels are increased, which induces expression of Atrogin-1 and MuRF1. Like in muscle cells, TNF α enhances Atrogin-1 expression in a p38-dependent manner, while MuRF1 requires p42/44 in cardiomyocytes. TNF α also increases troponin I (TnI) degradation and decreases contractility of cardiomyocytes [166]. Furthermore, occlusion of the left anterior descending coronary artery (in the heart) (LAD) also increases TNF α levels and Atrogin-1 and MuRF1 expression [167]. Doxorubicin (DOX) treatment, an anti-neoplastic agent that intercalates DNA, causes cardiomyopathy. DOX increases Atrogin-1 expression, however, inhibiting p38 abrogates DOX-mediated increases in Atrogin-1 [168]. While Atrogin-1 ubiquitinates target proteins for degradation, Atrogin-1 itself is ubiquitinated, which is enhanced in the presence of Skp1-Cul1-Roc1 and the E2 UbCH3. Atrogin-1 ubiquitination and degradation is increased when p38 is inhibited

[169]. These data suggest that p38 is a switch regulating the expression of Atrogin-1 (summarized in **Figure 1.11.**).

Inflammatory signaling pathways, such as $\text{TNF}\alpha$ discussed above, can also activate c-Jun N-terminal kinase (JNK), potentially through p21-activated kinase 1 and 2 (PAK1 and PAK2) [170]. FOXO3A is not only inhibited by AKT, but also by stress-activated protein kinase (SAPK). This process involves JNK signaling, but is independent of AKT. Activation of SAPK decreases Atrogin-1 expression in C2C12 cells [171] (**Figure 1.11.**). In the heart, ischemia/reperfusion (I/R) induces apoptosis and JNK signaling to enhance Atrogin-1 expression. Furthermore, Atrogin-1 sustains JNK in its activated form by ubiquitinating and degrading the MAPK phosphatase-1 (MKP-1) [172]. Unlike Atrogin-1, MuRF1 is protective in ischemia/reperfusion by decreasing cell death through inhibition of JNK signaling by ubiquitinated degradation of phospho c-Jun [173].

Another signaling pathway activated during stress and in the presence of cytokines is the nuclear factor kappa-light-chain-enhancer of activated B cells (NF- κ B). Muscle atrophy caused by hindlimb immobilization increases NF- κ B activation in part by downregulating its inhibitor I κ B. However, overexpressing I κ B by *in vivo* electroporation inhibits unloading-induced atrophy and expression of Atrogin-1 [174]. Additionally, the overexpression of active I κ B kinase beta, which activates NF- κ B, causes muscle wasting that correlates with increased MuRF1 expression in muscle [175]. Interleukin-1 (IL-1) treatment decreases I κ B, increases NF- κ B, and thus increases the expression of Atrogin-1 and MuRF1 in C2C12 muscle cells [176] (**Figure 1.11.**). Collectively, these studies provide evidence that Atrogin-1 and MuRF1 regulate muscle proteolysis in response to cytokines.

Lipopolysaccharide (LPS) is used *in vitro* and *in vivo* to elicit an immune response and therefore activate several signaling pathways mentioned above. LPS treatment increases Atrogin-1 and MuRF1 expression [177] and increases the alpha subunits of the proteasome in muscle [178]. LPS-induced muscle atrophy is reduced by curcumin, a non-toxic anti-inflammatory reagent [179]. LPS activates the inflammatory receptor toll-like receptor 4 (TLR-4), which consequently increases expression of Atrogin-1 and MuRF1 in a p38-dependent manner [180]. Sepsis occurs in response to LPS, consequently inducing muscle atrophy [181]. Sepsis-induced muscle wasting increases the transcriptional activity of FOXO1/3A but not FOXO4 [182]. Furthermore, muscle wasting is partially inhibited with the calpain inhibitors calpeptin or BN82270, but the expression of Atrogin-1 and MuRF1 is

unaffected by calpain inhibition. This study demonstrates that in muscle the UPS is regulated independently of calpains during sepsis [183].

Denervation causes skeletal muscle atrophy and upregulates myogenin, a member of the myogenic regulatory factor (MRF) family of transcription factors involved in muscle development, repair, and differentiation [184]. Denervation, which regulates Atrogin-1 and MuRF1 expression, does so through myogenin, while denervated myogenin^{-/-} mice do not have increased Atrogin-1 and MuRF1 expression [185]. Atrogin-1 is a *bona fide* target for myogenin as its promoter contains binding sites for myogenin and MyoD, another member of the MRF transcription factor family [186]. MyoD is an important trophic mediator during skeletal muscle hypertrophy and atrophy. Interestingly, Atrogin-1 targets MyoD for degradation by ubiquitinating MyoD on Lys133 [138] in several models of muscle atrophy [187]. Moreover, the MAP kinase MEK1 phosphorylates MyoD and inhibits its ubiquitination and degradation by Atrogin-1, allowing for muscle differentiation [188]. These studies provide further evidence for importance of Atrogin-1-mediated protein degradation in skeletal muscle atrophy (**Figure 1.11.**).

Glucocorticoids regulate MuRF1 transcription, presumably through the glucocorticoid response elements (GRE) found within the MuRF1 promoter, but MuRF1 is synergistically regulated by FOXO1 and the glucocorticoid receptor in skeletal muscle [189]. The glucocorticoid dexamethasone induces cachexia by increasing MuRF1 expression. Consequently, protein levels of myosin heavy chain (MHC) are decreased but MHC levels are spared in dexamethasone treated MuRF1^{-/-} mice [190]. Glucocorticoids are sufficient to induce skeletal muscle wasting; however daily injections of the glucocorticoid receptor (GR) antagonist RU-486 neither prevent atrophy after hindlimb casting, nor prevented Atrogin-1 and MuRF1 expression [191]. These results do not rule out the possibility of the direct effect of glucocorticoids on Atrogin-1 and MuRF1 mRNA transcription or stability independent of the GR. Tillis et.al. have recently reported that dexamethasone stabilizes surfactant protein-B mRNA in a posttranscriptional manner, which may be the case with Atrogin-1 and MuRF1 [192]. Collectively these studies suggest that glucocorticoids regulate Atrogin-1 and MuRF1 but may not be the predominant pathway controlling muscle atrophy (**Figure 1.11.**).

Another mediator of muscle atrophy is the class of statin drugs used to treat hypercholesterolemia. Statins inhibit HMG-CoA reductase which is involved in cholesterol synthesis. Lovastatin increases Atrogin-1 and removal of Atrogin-1 prevents muscle damage mediated by lovastatin [193]. Lovastatin causes damage, presumably by altering

post translational modifications, specifically inhibiting geranylgeranylation; however the mechanism by which this occurs is unknown [194].

Because Atrogin-1 and MuRF1 are induced under a variety of stimuli leading to muscle proteolysis and atrophy, there will most likely be more pathways uncovered in the future that regulate Atrogin-1 and MuRF1. As I began work on my thesis project, several papers were published demonstrating, in line with our hypothesis, that AMPK was involved in the regulation of the ubiquitin ligases Atrogin-1 and MuRF1; however, the studies were correlative and not mechanistic in nature. These reports are discussed in more detail in chapter 3.

Atrogin-1 and MuRF1 are expressed at differing levels at baseline in skeletal muscle and in the heart. While many transcriptional regulators of these ligases have been described, only one inhibitor of their expression has recently been identified. MicroRNA (miRNA) are short RNA (roughly 22 nucleotides) that act as post-transcriptional modifiers of gene expression. They bind to complementary sequences on target mRNA to repress or degrade the mRNA [195]. miR23 promotes cardiac hypertrophy and its expression is regulated through NFATc3, a pro-hypertrophy transcription factor [196]. miR23 suppresses translation of Atrogin-1 and MuRF1 and the ectopic expression of miR23a protects against skeletal muscle atrophy [197] (**Figure 1.11.**). These initial descriptions of the repression of Atrogin-1 and MuRF1 are presumed to be the first, with many more to come.

1.3.2. Targets of Atrogin-1 and MuRF1

As discussed above, studies identifying pathways that regulate Atrogin-1 and MuRF1 were initially performed in skeletal muscle. On the other hand, the identification of the targets of the ligases has been mainly performed in cardiomyocytes and in the heart. In yeast two-hybrid screens using Atrogin-1 as bait, Li and colleagues found that Atrogin-1 interacts with Calcineurin A (CnA) and α -actinin-2. Both of these proteins are localized to the Z-disc in cardiomyocytes and CnA is an important mediator in pathological hypertrophy. Atrogin-1 overexpression enhances the ubiquitination of CnA and in Atrogin-1 transgenic mice (Tg), the hypertrophic response is blunted, presumably due to decreased CnA levels. This group also discovered that Atrogin-1 displays ubiquitin ligase activity in complex with Skp1-Cul1-Roc1, and the E2 with which Atrogin-1 ubiquitinates some proteins is UbcH3/CDC34 [129] (**Figure 1.9.**).

Recently, the endogenous role of Atrogin-1 in cardiac hypertrophy was reported [198]. Transverse aortic constriction (TAC), an *in vivo* model that induces cardiac

hypertrophy (see chapter 2 for a detailed description), leads to increased Atrogin-1 expression in the heart, verifying previously published results from our lab [199]. Atrogin-1^{-/-} mice did not hypertrophy to the same extent as wild type animals after TAC and have less cardiac fibrosis. Surprisingly, CnA levels were inhibited in the Atrogin-1^{-/-} hearts. Microarray analysis revealed that NF- κ B-regulated genes were down-regulated in Atrogin-1^{-/-} hearts after TAC, indicating a potential pathway protecting the heart from the development of pathological hypertrophy. Furthermore, Atrogin-1 regulates ubiquitination and degradation of I κ B-alpha in cardiomyocytes, which leads to the activation of NF- κ B [198]. Although these *in vivo* TAC studies provide mechanistic insight into the role of Atrogin-1, their conflicting results make it difficult to conclusively determine whether Atrogin-1 is protective or detrimental to the heart during cardiac hypertrophy.

Another target of Atrogin-1 has been the focus of several reports. In muscle, Atrogin-1 targets eukaryotic initiation factor 3 subunit 5 (eIF3-f) for degradation, and siRNA against Atrogin-1 prevents the degradation of eIF3-f during atrophy. The overexpression of eIF3-f causes hypertrophy and increases expression of muscle structural proteins, while knockdown of eIF3-f induces atrophy [200]. Atrogin-1 ubiquitinates the C-terminus of eIF3-f but mutating 6 Lysine residues within this region causes hypertrophy and protects against starvation-induced muscle atrophy [201]. The overexpression of Atrogin-1 induces skeletal muscle atrophy and leads to degradation of eIF3-f; however, an eIF3-f mutant insensitive to Atrogin-1 abrogates these changes [202]. While this has not yet been investigated, it will be interesting to determine whether eIF3-f is targeted by Atrogin-1 in the heart.

In the heart, MuRF1 binds to and co-localizes with RACK1 (receptor for activated protein kinase C), which associates with protein kinase C (PKC ϵ) during hypertrophy. The overexpression of MuRF1 prevents PKC ϵ localization to focal adhesions and thus focal adhesion formation, a critical step in the development of cardiomyocyte hypertrophy. Furthermore, overexpression of MuRF1 abolishes the hypertrophic response to phenylephrine in cardiomyocytes [203]. Thus enhanced MuRF1 expression might be one way to decrease cardiac hypertrophy.

Another anti-hypertrophic protein has been identified as a target for MuRF1-mediated degradation in cardiomyocytes. Cardiac troponin I (cTnI) is part of the troponin complex and plays an inhibitory role in contraction by binding actin and preventing it from binding myosin in the relaxed phase. cTnI localizes to the M-line, coimmunoprecipitates with MuRF1, and is directly ubiquitinated by MuRF1 [133]. Interestingly, MuRF1 differentially ubiquitinates troponin I depending on which E2 is utilized. MuRF1, when

working with the E2 UbcH1, ubiquitinates Tnl using Lys48 linkages, which leads to the degradation of Tnl. However, when MuRF1 works with the E2 UbcH13/Uev1a, Tnl is ubiquitinated with Lys63 linkages and is not degraded. Furthermore, MuRF1 interacts with the E2 Ubc9 [204] and ubiquitinates proteins with Lys48, Lys63, Lys11, and forked ubiquitin linkages using the E2 UbcH5, although the consequence of differential ubiquitination is at present unknown [205].

Additional binding partners of MuRF1 were found using yeast two-hybrid screenings. MuRF1 interacts with the myofibrillar proteins telethonin (Tcap), myotilin, nebulin, nebulin-related protein, troponin T1 and T3, and myosin light chain 2 (MLC-2). MuRF1 also interacts with proteins involved in energy metabolism including muscle creatine kinase, NADH dehydrogenase, adenylate kinase, aldolase A, pyruvate kinase, and pyruvate dehydrogenase kinase, to name a few. Although this study has identified additional targets for MuRF1, functional studies are still needed to conclusively verify ubiquitination of these proteins [206]. The potential metabolic consequences of MuRF1-mediated degradation of these proteins is discussed in Chapter 5.

Several follow-up studies have focused on MuRF1 regulation of target proteins mentioned above, one being muscle creatine kinase (CK). CK is involved in energy reservation during the resting state of muscle contraction. When CK is damaged, or otherwise unnecessary, it becomes oxidized and thus inactive. MuRF1 degrades the oxidized form of CK [207]. Mice starved of amino acids (AA) (a proteinogenic diet) *in vivo*, used here as a model of skeletal muscle atrophy, have decreased levels of muscle CK, while MuRF1^{-/-} on the same diet have increased levels of CK. Additionally, AA-starved MuRF1^{-/-} mice also have decreased plasma AA and branched chain AA (BCAA), and enhanced levels of muscle protein synthesis. Moreover, glucocorticoid modulatory element binding protein-1 (GMEB1), a transcription factor that regulates gene expression in response to glucocorticoid levels, and 3-hydroxyisobutyrate dehydrogenase (HIBADH), an essential enzyme in valine catabolism, were increased in muscles of AA-starved MuRF1^{-/-} mice [208].

Transgenic mice overexpressing MuRF1 16-fold in skeletal muscle have decreased protein levels of pyruvate dehydrogenase (PDH) and its regulator pyruvate dehydrogenase kinase 2 (PDK2), two enzymes initially discovered in yeast-two hybrid screens, discussed above. MuRF1 Tg mice have higher blood insulin levels, lower glycogen levels in the liver, and during glucose tolerance tests, insulin levels are further increased in Tg mice. MuRF1 seems to preserve energy by inhibiting rate-limiting catabolic pathways [209]. These *in vivo*

studies support findings of yeast-two hybrid screens by providing indirect evidence that MuRF1 is involved in degrading metabolic enzymes in muscle.

MuRF1 interacts with sarcomeric proteins, also initially described in yeast-two hybrid studies. In myofibrils, MuRF1 ubiquitinates myosin light chains 1 and 2 (MyLC1, MyLC2) and the degradation of these proteins leads to thick filament disassembly and myosin heavy chain (MyHC) ubiquitination by MuRF1[210]. While calpains are assumed to be required for initial breakdown of sarcomeres, MuRF1 regulated myofibril degradation may be independent of the calpain system as MuRF1 also ubiquitinates skeletal muscle actin [211], although, this has not yet been tested directly. However, in support of this hypothesis, MuRF1 and MuRF2 were found to be required for type-II muscle fiber maintenance through the regulation of myozenin-1/calsarcin-2, an inhibitor of calcineurin, and a determinant of muscle fiber-type [212]. MuRF1 also functions redundantly with MuRF3 (through the E2s UbcH5a, -b, -c) to degrade β Myosin Heavy Chain (MHC) and MHCII α in muscle and in the heart. Deletion of both MuRF1 and MuRF3 in mice causes abnormal accumulation of proteins (MHCs) within the sarcomere leading to muscle dysfunction and myopathy [213].

MuRF1^{-/-} mice have an exacerbated hypertrophic response to pressure overload compared to wild type mice or MuRF2^{-/-} mice, suggesting that MuRF1 negatively regulates cardiac hypertrophy [214]. Furthermore, pathological hypertrophy induced by TAC is not reversible with the removal of TAC in the absence of MuRF1, even though gene expression patterns in WT and MuRF1^{-/-} mice returned to baseline [215]. Interestingly, older mice (greater than 6 months of age) lacking MuRF1 have enlarged hearts, however cardiac function is normal. However, AKT signaling is increased and proteasome activity is decreased in the absence of MuRF1 in the hearts of older mice [216]. MuRF1 Tg mice overexpressing 45-fold in the heart have a mild cardiac phenotype at baseline (thinner left ventricular (LV) wall thickness, increased LV dimension, and decreased fractional shortening (FS)) but this does not progress with age, and cardiac dysfunction does not develop. With TAC, MuRF1 Tg mice develop rapid heart failure with significant decline in LV wall thickness, increase in LV dilation, and decrease in FS, all characteristics of eccentric cardiac hypertrophy. MuRF1 Tg mice also have decreased CK activity and display a cardiac metabolic phenotype. PGC1 is increased in MuRF1 Tg mice after TAC indicating a possible cardiometabolic defect [217].

The majority of studies reported to date have focused on the degradation of proteins by either Atrogin-1 or MuRF1; however, one study has reported redundancy of the ubiquitin ligases in regulating cardiac myosin-binding protein C (cMyBP-C). Familial hypertrophic

cardiomyopathy can result from mutations in cMyBP-C resulting in C-terminal truncated mutant protein which is not detected in the tissue of patients. Using the premise that the absence of detection may denote rapid degradation of cMyBP-C in cardiomyocytes, experiments provide evidence that Atrogin-1 targets a mutated form of cMyBP-C (M7t-cMyBP-C) for degradation. Additionally, MuRF1 indirectly reduces cMyBP-C by regulating transcription of myosin heavy chain [218].

Atrogin-1 and MuRF1 are the main ubiquitin ligase studied in muscle and heart, and their target proteins are summarized in **Table 1.1**. The abundance of predicted ubiquitin ligases (over 600) suggests that others may be required or necessary for atrophy. Indeed, a recent study described Cbl-b, an E3 ligase that is upregulated during skeletal muscle unloading. Cbl-b interacts with, ubiquitinates, and degrades IRS-1. Consequently decreased PI3K-AKT signaling activates FOXO3-dependent induction of Atrogin-1. Mice deficient for Cbl-b are resistant to unloading [219]. Although not completely independent of Atrogin-1 and MuRF1, this study suggests that we are just beginning to understand ubiquitin ligases and their role and regulation in protein degradation.

1.4. Metabolic Regulation of Cardiac Function

Like all living cells, heart muscle cells liberate the energy contained in organic molecules to support their function. This process is both highly regulated and oxygen dependent. It produces ATP from fatty acids, glucose, lactate, ketone bodies, and (under extreme circumstances) amino acids [220]. For a given environment the source of ATP production can be changed from one fuel to another, and the heart has therefore been termed a “metabolic omnivore” [221]. In the fasted state and under resting conditions the heart prefers fatty acids [222] while carbohydrates become a major fuel for the stressed heart [8].

A key enzyme involved in the metabolic response to stress in the heart is AMP-activated protein kinase (AMPK). AMPK, also known as the “fuel gauge” of the cell [223], is activated under a variety of conditions that decrease the ratio of [ATP]/[AMP]. AMPK regulates processes involved in ATP production, such as glucose uptake, glycolysis, fatty acid oxidation, and mitochondrial biogenesis. At the same time, AMPK inhibits processes involved in high ATP consumption, such as protein synthesis, glycogen synthesis, gluconeogenesis, and fatty acid synthesis [224]. Details on the regulation of AMPK and the consequences of AMPK activation on cardiac metabolism are discussed in more detail in the following section.

Protein targets of Atrogin-1 and MuRF1			
Target Protein	Targeted by	Consequence of interaction	Reference
Titin	MuRF1	Binds, ubiquitinates	[136, 137]
RACK1/PKC ϵ	MuRF1	Binds, localization	[203]
cTnl	MuRF1	Ubiquitinates, degrades	[133]
CK	MuRF1	Ubiquitinates, degrades	[207]
GMEB1	MuRF1	Unknown, increased in MuRF1 ^{-/-}	[208]
HIBADH	MuRF1	Unknown, increased in MuRF1 ^{-/-}	[208]
PDH	MuRF1	Unknown, decreased in MuRF1 Tg	[209]
PDK2	MuRF1	Unknown, decreased in MuRF1 Tg	[209]
MyLC1	MuRF1	Ubiquitinates, degrades	[210]
MyLC2	MuRF1	Ubiquitinates, degrades	[210]
MyHC	MuRF1	Ubiquitinates	[210]
β MHC	MuRF1	Ubiquitinates, degrades	[213]
MHC α	MuRF1	Ubiquitinates, degrades	[213]
PGC1	MuRF1	Unknown, increased in MuRF1 Tg	[217]
cMBP-C	MuRF1, Atrogin-1	Ubiquitinates, degrades	[218]
CnA	Atrogin-1	Ubiquitinates, degrades	[129]
α -actinin	Atrogin-1	Binds, colocalizes	[129]
I κ B α	Atrogin-1	Ubiquitinates, degrades	[198]
eIF3-f	Atrogin-1	Ubiquitinates, degrades	[200-202]

Table 1.1. Protein targets of Atrogin-1 and MuRF1.

A summary of the protein targeted by Atrogin-1 and MuRF1, including which ligase targets the protein, and what the consequence of the interaction is. There are other potential targets of Atrogin-1 and MuRF1 that have been describe using yeast-two hybrid sreens, however, they have not been validated *in vitro*.

1.4.1. Structural and Functional Aspects of AMPK

AMP-activated protein kinase (AMPK) is a serine threonine kinase comprised of a catalytic subunit, α , and two regulatory subunits: β and γ , each subunit existing as several isoforms ($\alpha 1$, $\alpha 2$, $\beta 1$, $\beta 2$, $\gamma 1$, $\gamma 2$, $\gamma 3$) [225]. The catalytic $\alpha 1$ subunit is expressed in all tissues, while $\alpha 2$ is mainly expressed in the heart and skeletal muscle [226, 227]. Akin to the catalytic subunit, $\beta 1$ is ubiquitously expressed and $\beta 2$ is expressed at very high levels in heart and skeletal muscle [228, 229]. The $\gamma 1$ regulatory subunit is also ubiquitously expressed and most of the complexes found within the heart contain this isoform (at least during ischemic conditions) [230]. The $\gamma 2$ subunit has 2 splice variants: one is expressed in most tissues excluding the heart, and the other *vice versa* [231]. The $\gamma 3$ subunit is only expressed in skeletal muscle [231]. The details of the isoform specificity are not completely known, but proposed functions include subcellular localization and differential signaling of AMPK isoform combinations [232].

The protein domains of the AMPK subunits are well documented and several crystal structures have been reported [233-235]. The catalytically active subunit of AMPK (α) contains an N-terminal kinase domain with an activation loop. Thr172 within the activation loop is phosphorylated by upstream kinases, thereby activating AMPK [236]. The C-terminus of α AMPK contains an autoinhibitory domain and a β -subunit interacting domain. The β regulatory subunit acts as a scaffold between the α and γ subunits, and may potentially be involved in intracellular localization [237]. This subunit contains a glycogen binding domain (GBD), or carbohydrate binding domain (CBD), and a C-terminal subunit binding sequence that binds both α and γ [238]. The other regulatory subunit, γ , contains four bateman domains or CBS motifs, which are adenylyl binding sites. CBS1 and CBS3 can be occupied by AMP or ATP, CBS4 is only occupied by AMP, while CBS2 is occupied by ADP (**Figure 1.12.**) [234].

The “adenylate energy charge” hypothesis describes the allosteric regulation of enzyme activity by the ratio of $[ATP]/[ADP][AMP]$ [239]. This concept was originally thought to be the regulatory mechanism of acetyl-CoA carboxylase (ACC), which we now know is regulated by AMPK [240]. More correctly, AMPK is an example of the “adenylate energy charge” hypothesis, and consequently, ACC is directly affected. As a result, the phosphorylation status of ACC is measured as the indicator of the activation status of AMPK.

Although only first described in 1988 [241], much is known about the regulation and function of AMPK. In addition to its allosteric regulation by the ratio [ATP]/[AMP], AMPK can also be regulated by other metabolic signals. As mentioned above, the β -subunit contains a GBD and indeed, AMPK binds glycogen, which then inhibits AMPK activity [242]. Therefore, AMPK is also known as a glycogen sensor. β AMPK can also be myristoylated, which results in decreased AMPK activity and localization to cellular membranes. Although not well defined, myristoylation of AMPK may be another regulatory mechanism of intracellular localization and localized activity [243].

The catalytic subunit of AMPK has been investigated in detail and it is well established that AMPK requires phosphorylation in order to be active [244]. What is less understood is the autoinhibitory/autoregulatory domain (AID) of the catalytic subunit. The AID, a sequence of 23 amino acids (313-335) (**Figure 1.12.**) [245], is thought to modulate the kinase domain and block activity; however, proof of this mechanism is lacking [238]. C-terminal to the AID is a less characterized region, now termed the α -hook (**Figure 1.12.**). In an elegant study published earlier this year, structural analysis of AMPK provided new evidence that there is a direct interaction between the α and γ subunits, which potentially regulates kinase activity. The α -hook interacts with CBS3 on the γ subunit when it is bound to AMP, protecting the exchange of AMP with ATP at this site. Moreover, this interaction protects AMPK Thr172 from dephosphorylation through an overarching structural stabilizing conformation [235]. Thus, not only does adenylate binding regulate AMPK activity, the conformational changes that occur as a result of adenylate binding are also critical for AMPK activation.

AMPK is allosterically activated by AMP under conditions of nutrient stress, which changes the ratio of [ATP]/[AMP]. Allosteric activation of AMPK initially increases its kinase activity fivefold [231]. AMP binding not only deems AMPK a better substrate for phosphorylation by its upstream kinases [244], but also prevents dephosphorylation by phosphatases [246]. AMPK is phosphorylated on Thr172 by LKB1 (liver kinase B1), a serine threonine kinase which acts in a complex with the scaffolding protein MO25 and pseudokinase STRAD (also known as protein kinase LYK5) [247]. The recent generation of LKB1^{-/-} mice [248, 249], specifically in the heart [250], has further demonstrated the importance of LKB1 regulation of AMPK. AMPK can also be phosphorylated by Ca²⁺/Calmodulin-dependent protein kinase kinases (CaMKK α and β) [251, 252], although its implications in the heart have not been investigated. Another kinase that phosphorylates AMPK on Thr172 is TGF- β -activated kinase-1 (TAK1), although this kinase is not well

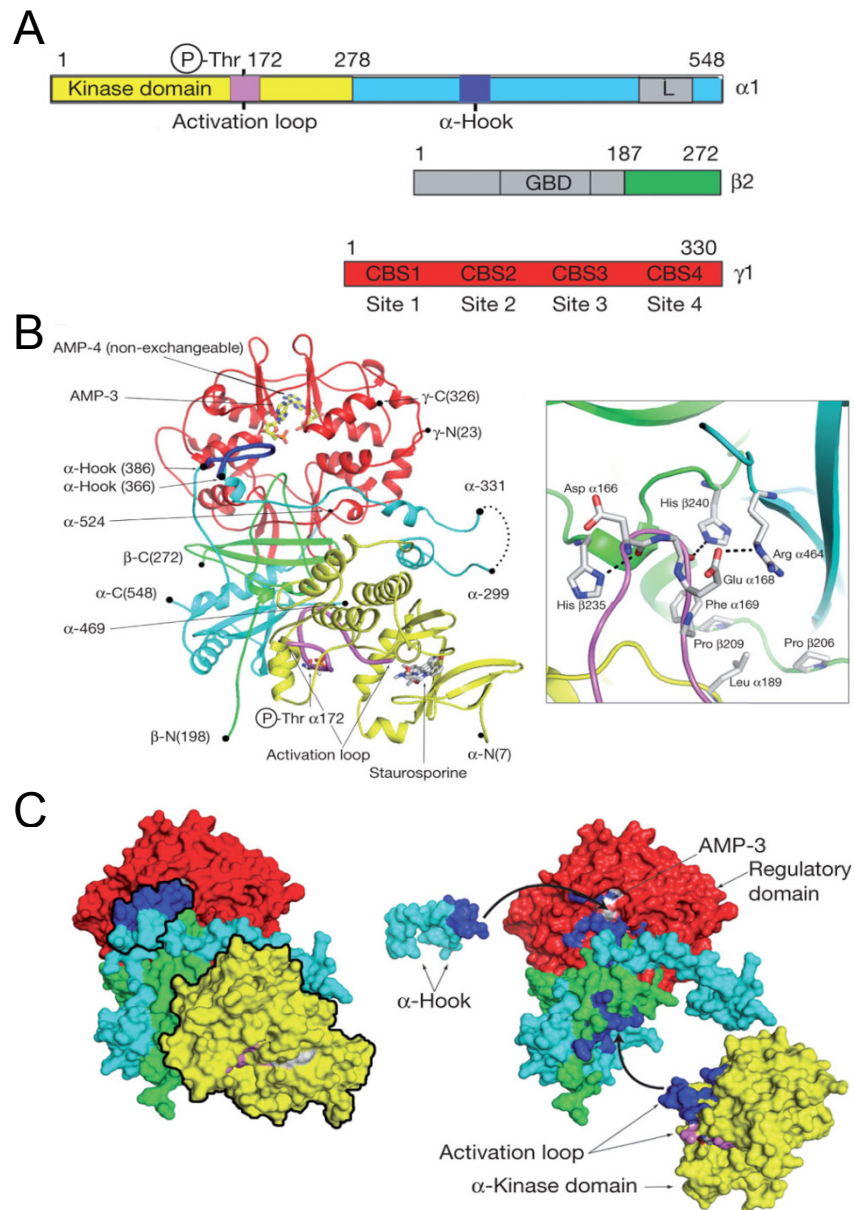


Figure 1.12. The structure of mammalian AMPK.

(A) The linear structure of AMPK containing protein domains of the α 1, β 2, and γ 1 subunits. The kinase domain of α 1 (and α 2, not shown) contains Thr172 within the activation loop. The β -subunit binding domain (L) is also labeled. Domains within the β 2 subunit include the glycogen binding domain (GBD), and shown in green, the α - and γ - subunit binding sequence. Shown in red on the γ 1-subunit are the bateman domains (CBS1-4) which are responsible for adenylate binding. (B) Ribbon diagram of the structure of AMPK showing the interaction between all three subunits. The inset is a zoomed-in view of the activation loop. Key amino acid residues are labeled. (C) A space filling model of the 3 dimensional structure of AMPK. Colors identifying domains within the subunits are consistent throughout the figure. Reprinted with permission from Macmillan Publishers Ltd. [Nature] [235].

characterized [253, 254]. Other phosphorylation sites on α AMPK have been identified such as Thr258 and Ser485/491: however, the kinases involved have not been determined [255].

AMPK activity is not only prevented by its autoinhibitory domain within its catalytic subunit as previously discussed, it is also attenuated by several protein phosphatases (PP). AMPK can be dephosphorylated by PP1 [256], PP2A [257] and PP2C [246, 258]. The tissue specificity and other details regarding AMPK dephosphorylation is an area that requires more investigation.

While the regulatory mechanisms of AMPK activity have been investigated mostly *in vitro*, the *in vivo* consequences of AMPK activation on metabolism, organ function, and disease continue to be a hot topic of investigation. Because of the vast amount of knowledge on AMPK, only a minor fraction will be discussed here, with an emphasis on AMPK in the heart, the focus of the next section.

1.4.2. An Overview of the Central Role of AMPK in the Heart

AMPK is activated under conditions of metabolic stress, as discussed above. In the heart specifically, such conditions include ischemia and exercise. While it is clear that AMPK is an important factor in heart disease, conflicting reports complicate our understanding of the role of AMPK in conditions of pressure overload, volume overload, and various models of heart failure. Whether AMPK activation is a cause or consequence in these settings is yet to be determined [259, 260].

During ischemia, decreased delivery of substrates to cardiomyocytes results in decreased ATP production, increased levels of AMP, and consequently activation of AMPK in the heart [261]. Once activated, AMPK increases glycolysis, glucose uptake, and fatty acid oxidation [261-263]. Initially during ischemia, when oxygen levels are low and the energy demand of the heart is high, glycogen stores are mobilized to glucose, which is metabolized further to produce ATP [264]. AMPK also promotes glucose uptake through the translocation of the glucose transporter GLUT4, although the exact mechanisms through which this occurs are still uncertain [265]. Activation of AMPK enhances fatty acid oxidation by inhibiting acetyl-CoA carboxylase (ACC), which carboxylates acetyl-CoA to malonyl-CoA. Because malonyl-CoA inhibits fatty acid entry into the mitochondria for β oxidation, decreased malonyl-CoA levels lead to enhanced fatty acid oxidation, which occurs in the heart during ischemia [261]. Thus, activation of AMPK during ischemia seems to protect the heart by providing the necessary fuel for cardiac function through increased glucose uptake and enhanced fatty acid oxidation.

Prolonged ischemia and reperfusion after ischemia can be detrimental to the heart, partially due to activated AMPK. As mentioned above, activation of AMPK during the initial phase of ischemia leads to glycogen breakdown, specifically by glycogen phosphorylase through AMPK-mediated activation of phosphorylase kinase. However, with continual low oxygen availability during instances of severe prolonged ischemia, the heart relies almost exclusively on ATP derived from glycolysis [266]. Accumulation of the byproducts from glycolysis is detrimental to the heart and can lead to apoptosis and cardiac dysfunction [267]. AMPK is also activated during reperfusion after ischemia, which can be injurious to the heart [261]. AMPK increases fatty acid oxidation during acute ischemia. Upon reperfusion, the high levels of fatty acid oxidation contribute to decreased cardiac function [266].

While the role of AMPK during cardiac hypertrophy is still unclear and is somewhat controversial, a brief discussion is necessary. The first report of AMPK in the hypertrophic heart showed increased AMPK phosphorylation after 17 weeks of ascending aortic banding [268]. It is not clear from this study whether AMPK activation was cause or consequence of hypertrophy, but after 17 weeks hearts from banded rats displayed a severe cardiac metabolic phenotype. The ratio of [ATP]/[AMP] was significantly decreased, AMPK activity was increased, and glucose uptake was enhanced [268]. An independent study found that in late stage hypertrophy, glycolysis was also increased [269]. *In vitro* evidence suggests that AMPK activation is a consequence of hypertrophy as phenylephrine-treated cardiomyocytes hypertrophy but show no signs of AMPK phosphorylation [270]. Furthermore, rats treated with the AMPK activator AICAR showed signs of decreased hypertrophy after 7 weeks of banding [271]. Although many more studies are still required, it is tempting to speculate that the activation of AMPK occurs after the onset of hypertrophy as the heart metabolically adapts to the stress. Continual hemodynamic stress, however, leads to chronic AMPK activation, causing metabolic derangements which lead to maladaptation [272], and ultimately heart failure.

AMPK is a critical metabolic enzyme; however, it is also involved in other cellular processes not generally thought to be “metabolic” in nature. When investigating the role of AMPK in hypertrophy, Chan et.al. discovered that in cardiomyocytes activation of AMPK reverses phenylephrine-induced hypertrophy [270]. AMPK attenuates hypertrophy by inhibiting protein synthesis through inactivation of the mTOR signaling pathway [273, 274]. Protein synthesis is an energetically demanding process. Therefore when the cell experiences energetic stress it is reasonable that protein synthesis would be decreased to preserve energy and that this process would be regulated by AMPK. In keeping with this

reasoning, it is logical that AMPK would concomitantly enhance protein degradation, a reservoir of substrates for ATP production via amino acid catabolism.

The ATP requirement for protein degradation has been recognized for some time [31, 68], but the direct role that AMPK plays in regulating this process has only recently been investigated. The first evidence that AMPK is directly involved in protein degradation, specifically through autophagy, was reported 10 years ago in a mutant yeast strain that had deficient glycogen stores. The gene responsible for this defect, *snf1*, is the yeast homologue of mammalian AMPK. Furthermore, two regulators of autophagy, Apg1 and Apg13, that are required for maintenance of glycogen storage, were found to be regulated by AMPK [275, 276]. Recent studies have demonstrated that AMPK is also required for autophagy in mammalian cells [277, 278]. Moreover, the importance of AMPK-regulated autophagy in the heart, particularly during glucose deprivation and ischemia/reperfusion has been reported [279]. Recent developments in AMPK-regulation of autophagy are reviewed in [280].

At the onset of my thesis project nothing had been reported on AMPK-mediated protein degradation through the ubiquitin proteasome system. However, after the generation of my early results suggesting the positive effect of AMPK on proteasome-mediated protein degradation, several reports with conflicting results were published (see chapter 5 for further discussion). One report suggested that AMPK activation by AICAR reduced proteasome activity and that this could be rescued by ectopic expression of dominant negative AMPK [281]. The same group reported that AMPK interacts with a subunit of the proteasome, PSMD11, using a yeast two-hybrid screen [282]. Although initially identified by its interaction with β 2MPK, coimmunoprecipitation experiments found that PSMD11 also interacts with and is phosphorylated by α 2AMPK [282]. The AMPK phosphorylation site on PSMD11 has not been determined and it is unclear whether AMPK-mediated phosphorylation of PSMD11 decreases proteasome activity [282]. The yeast two-hybrid screening in this study was performed using human skeletal muscle cDNA library. Interestingly, some of the same proteins found to interact with Atrogin-1 and MuRF1 were also identified as potential binding partners with AMPK. This study identified tropomodulin 1 and myozenin 1 as α 2AMPK binding partners, and the receptor for activated protein kinase C (RACK1) as a binding partner for β 2AMPK [282]. Although follow-up studies have not been reported, these results provide insight into AMPK localization within muscle cells, and AMPK-regulated processes yet to be defined. These intriguing discoveries and their ramifications are discussed in more detail chapter 5.

Another cellular process regulated by AMPK which has been the focus of recent studies is transcriptional regulation [283]. Early reports focused on the transcriptional regulation of metabolically-regulated genes by AMPK in the liver [284]. AMPK inhibits gluconeogenesis and does so in part by phosphorylating and inactivating carbohydrate response element binding protein (ChREBP), thereby decreasing transcription of pyruvate kinase [285]. Additionally, AMPK phosphorylates the CREB regulated transcription coactivator -1 (CRTC2), which consequently inhibits transcription of phosphoenolpyruvate carboxylase and glucose-6-phosphate [286]. AMPK-mediated inhibition of fatty acid synthesis and storage also occurs in a transcriptional manner. AMPK phosphorylates and inactivates sterol response element binding protein-1c (SREBP-1c) in liver, subsequently decreasing expression of the lipogenic genes fatty acid synthase and acetyl-CoA carboxylase in liver [287]. AMPK inhibits fatty acid storage partly by phosphorylating the transcriptional coactivator p300 and thus decreasing its interaction with peroxisome proliferator-activated receptor- γ (PPAR- γ) [288].

AMPK also positively regulates transcription. Activation of AMPK enhances glycolysis by increasing hexokinase II (HKII) through phosphorylation of the transcription factor CREB [289]. This same mechanism also increases expression of uncoupling protein 3 (UCP3) thereby enhancing ATP production [290]. Additionally, AMPK enhances mitochondrial biogenesis at the transcriptional level by two known mechanisms. First, AMPK increases the expression of PPAR- γ coactivator-1 α (PGC1- α) [291] and second, AMPK activates silent information regulator two number 1 (SIRT1) [292]. The most commonly investigated metabolic consequence of AMPK activation is enhanced glucose uptake, which is also regulated at the transcriptional level. AMPK activates MEF2-regulated expression of GLUT4 [293] in an HDAC 5-dependent manner in skeletal muscle [294]. Perhaps the most intriguing finding to date is that AMPK appears to regulate transcription of entire “gene programs”. In mammalian cells, AMPK phosphorylates histone 2B, thus allowing for a more global transcriptional response during metabolic stress [295, 296].

In an effort to delineate the role of AMPK in the heart, numerous mouse models have been generated and are summarized in **Table 1.2** and reviewed in [297]. A major obstacle in this effort is the multidimensional nature of AMPK (three isoforms with some containing splice variants) as discussed previously. The first mouse models generated were transgenic mice overexpressing a mutant form of AMPK α 2 resulting in the expression of a dominant negative kinase. AMPK α 2 D157A expressed in the heart (Tg) resulted in normal

Genetically Engineered AMPK Mice					
Name	Gene	Mutation	Promoter	Disease/ Phenotype	Reference
$\alpha 1^{-/-}$	PRKAA1 ($\alpha 1$)	KO	Endogenous	None	[299]
$\alpha 2^{-/-}$	PRKAA2 ($\alpha 2$)	KO	Endogenous	Glucose intolerance, increased catechoalamines	[300]
Tg $\alpha 2^{\text{DN}}$	PRKAA2 ($\alpha 2$)	D157A	α MHC	Decreased glucose uptake	[298]
Tg $\alpha 2^{\text{DN}}$	PRKAA2 ($\alpha 2$)	K45R	Creatine kinase	Decreased glucose uptake and ischemic tolerance	[301]
Tg ^{R302Q}	PRKAG2 ($\gamma 2$)	R302Q	α MHC	PRKAG2 cardiomyopathy, glycogen storage	[302]
Tg ^{N488I}	PRKAG2 ($\gamma 2$)	N488I	α MHC	PRKAG2 cardiomyopathy, glycogen storage	[303]
Tg ^{R531G}	PRKAG2 ($\gamma 2$)	R531G	α MHC	PRKAG2 cardiomyopathy	[304]

Table 1.2. AMPK transgenic and knockout mice.

A list of transgenic and knockout mouse pertinent to the heart. See text for detailed description of the disease and phenotype of each mouse. Reprinted with permission from M Arad, CE Seidman, and JG Seidman, AMP-activated protein kinase in the heart: role during health and disease, *Circulation Research*, 100, 4, 474-488 [305].

cardiac phenotype at baseline [298]. During ischemia, hearts from Tg mice fail to increase glucose uptake and develop left ventricular dysfunction. Hearts from whole body AMPK α 2^{-/-} mice are phenotypically normal, based on echocardiographic measurements. In response to ischemia, ACC was not phosphorylated in the heart. The hearts from these mice, like the AMPK α 2 D157A Tg mice, failed to adapt metabolically to ischemia but were still able to functionally recover during reperfusion [306]. Moreover, AMPK α 2^{-/-} mice subjected to 7 days of isoproterenol injections developed greater hypertrophy than WT mice [307]. These studies support initial claims that AMPK α 2 is the prominent catalytic subunit in the heart and is required for adaptation to stress.

Another AMPK α 2 transgenic mouse was generated using a creatine kinase promoter, resulting in transgenic expression in both skeletal muscle and heart. AMPK α 2 K45R, like D157A, results in a dominant negative kinase. These mice were exclusively used to study the consequences of inactive AMPK in muscle [301]. Akin to the D157A mutation, K45R results in decreased glucose uptake in muscle, although the ramifications of this mutation on the heart are not known at present. Mice deficient for AMPK α 1, like the AMPK α 2^{-/-} mice, are phenotypically normal, although the cardiovascular phenotype in these mice has not been investigated [299].

The γ -subunit has been well studied in the mouse heart. Patients with hypertrophic cardiomyopathy characterized by enhanced glycogen storage and electrical abnormalities seen in Wolff-Parkinson-White syndrome, have genetic mutations within *prkag2*, the gene encoding for AMPK α 2 [305]. As a result, three different strains of mice have been generated to investigate the different human genetic mutations on *prkag2*. All three mutations in the heart result in cardiomyopathy, whereas only the R302Q and N488I mutation lead to glycogen storage [302, 303, 308]. All mouse models discussed above have been instrumental to our understanding of AMPK; however, much more work is required to completely understand the complex regulation of AMPK and the consequences of its activation in the heart.

1.5. AMPK: A Proposed Link Between Cardiac Metabolism and Protein Turnover

It is well established that AMPK inhibits protein synthesis and increases autophagy, but whether AMPK regulates the ubiquitin proteasome system in the heart is not known. Stress, particularly nutrient stress has been shown to increase protein degradation in the heart [309]. Nutrient stress also alters the ratio of [ATP]/[AMP] and thus activates AMPK is activated in the heart. Furthermore, the ubiquitin ligases Atrogin-1 and MurF1 are

significantly increased in response to nutrient deprivation in muscle [141]. Based on these studies I set out to test the hypothesis that AMPK regulates the ubiquitin proteasome system in the heart, potentially through regulation of ubiquitin ligases.

Chapter 2

MATERIALS AND METHODS

“The techniques have galloped ahead of the concepts. We have moved away from studying the complexity of the organism; from processes and organisation to composition [310].”

~Sir James W. Black, (1988) Nobel Prize for the invention of propranolol [311]

2. Materials and Methods

2.1. Materials

2.1.1. Animals

All animals were cared for according to the National Institutes of Health guidelines. The protocols were approved by the Animal Welfare Committee of The University of Texas Health Science Center at Houston.

For some of the experiments I used rats. Neonatal Sprague-Dawley rats (1-2 days old, Texas Animal Specialties, Humble, TX) were used for the isolation of neonatal rat cardiomyocytes (NRVM), see section “2.2.4. Isolation of neonatal rat ventricular cardiomyocytes”.

For some of the experiments I used genetic mouse models. Mice heterozygous for MAFbx/Atrogin-1 or MuRF1 were kindly provided by Regeneron Pharmaceuticals (Tarrytown, NY) [99]. The research group was headed by Dr. David Glass (now with Novartis, Cambridge, MA), and they discovered the muscle specific ubiquitin ligases MAFbx and MuRF1 in screens for so-called “atrogenes”, genes involved in the regulation of skeletal muscle atrophy [99]. Simultaneously, Dr. Alfred Goldberg’s group, Harvard Medical School, Boston, MA, identified Atrogin-1 (MAFbx) as a key ubiquitin ligase in muscle induced by fasting, diabetes, cancer, and renal failure [98]. Both MAFbx/Atrogin-1^{+/-} or MuRF1^{+/-} strains were previously backcrossed into C57BL/6 mice. Heterozygous mice were bred to generate MAFbx/Atrogin-1^{-/-}, MuRF1^{-/-}, MAFbx/Atrogin-1^{-/-} MuRF1^{-/-} (double knockout), and MAFbx/Atrogin-1^{+/+} MuRF1^{+/+} (wild type, WT) mice.

Transgenic mice expressing desMEF2-LacZ were kindly provided by Drs. Eric Olson and Rhonda Bassell-Duby, The University of Texas Southwestern Medical Center, Dallas, TX [312]. These mice harbor a *lacZ* reporter gene downstream of three tandem repeats of the MEF2 binding site flanked by *desmin* enhancer sequences. *LacZ* is expressed in the heart and muscle during development, particularly during embryonic days 7.5-14.5. The expression of *lacZ* declines after birth, and is not basally expressed in the adult heart and muscle. Although MEF transcription factors are not solely expressed in the heart and muscle, *lacZ* expression in this mouse line is driven by the desmin promoter, which is. Therefore, this transgenic line is a valuable tool to study MEF2-regulated processes in the heart and muscle [312].

2.1.2. Cell Lines

H9c2(2-1) cardiac myoblasts (**Figure 2.1.**) were purchased and cultured according to American Type Culture Collection (ATCC, Manassas, VA) guidelines. These cells are a subclone of the original H9c2 cells derived from BDIX rat heart tissue (embryonic day 13) using a modified selective serial passage technique [313]. The ventricular portion of the embryonic rat heart was cultured and passaged for two months. The resulting cells were spindle-shaped and grew in a parallel fashion. The cells from the H9c2(2-1) subclone resemble skeletal muscle because they can fuse to form multinucleated tube-like structures when confluent. The cell line displays many properties characteristic of both skeletal muscle and cardiomyocytes such as the existence of T-tubules and the ability to generate action potentials [313]. H9c2 cells have been further characterized as having cardiac L-type calcium currents (slow depolarization, compared to skeletal muscle) [314, 315].

Because primary cardiomyocytes are difficult to genetically manipulate without the use of viral transduction, H9c2 myoblasts were used for *lacZ* reporter assays and some preliminary experiments. Upon arrival on dry ice, H9c2 cells (approximately 1mL) were thawed at 37°C, resuspended in preincubated media (10mL), and cultured in a sterile incubator at 37°C in 95% air, 5% CO₂. Cells were passaged every 3-4 days to prevent over-confluency, which changes the phenotype of the cells. Cells to be passaged were rinsed once with warm sterile PBS and incubated for several minutes with Trypsin (0.25% w/v) - EDTA (0.53 mM) until they lifted off the plate. Cells were split at a 1:4 ratio and subcultures were preserved in freezing medium (FBS [20%], Complete medium [60%], DMSO [20%]) at -20°C for 24 hours and then stored at -80°C. Experiments were performed in low passage H9c2 cells to prevent loss of cardiac phenotype.

HEK293 cells were kindly provided by Dr. Carmen Dessauer; The University of Texas Health Science Center at Houston, Department of Integrative Biology and Pharmacology. These cells were used for the propagation and titration of adenoviruses as they are currently the only cell line available to generate high titer adenoviruses [316]. The cells were passaged every 3-4 days and grown to 90% confluency according to ATCC guidelines.

2.1.3. Equipment

The following equipment was used for my experiments. ABI Prism® 7000 Sequence Detection System (Applied Biosystems, Carlsbad, CA); Axioskop 40 fluorescent microscope (Carl Zeiss MicroImaging, LLC, Thornwood, NY); Baker Company SterilGARD

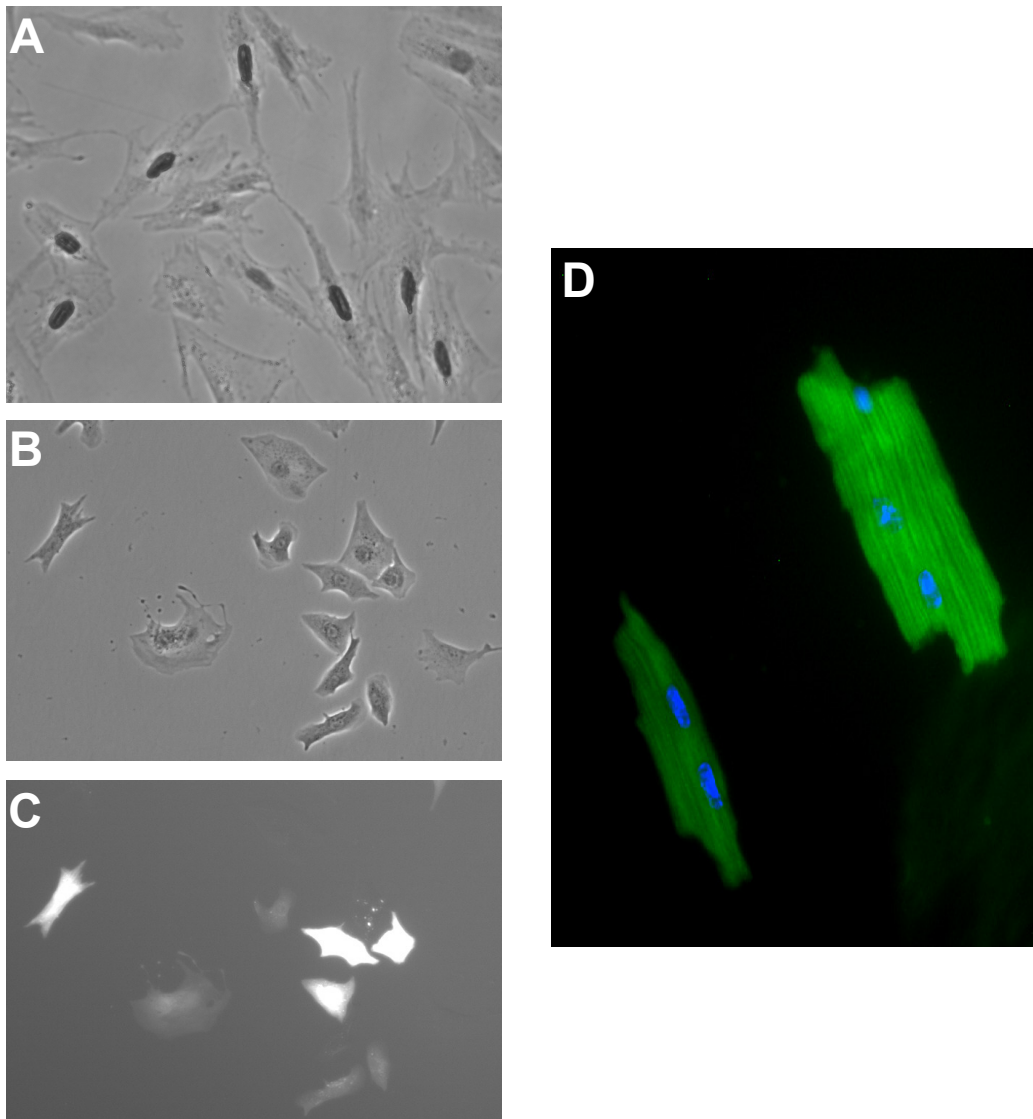


Figure 2.1. Cells used for mechanistic studies.

(A) H9c2 cardiac myoblasts expressing nuclear β -galactosidase in bright field. (B) Neonatal rat ventricular cardiomyocytes (NRVM) in bright field. (C) NRVM expressing green fluorescent protein (GFP) in bright field. (D) Immunocytochemistry of WT adult mouse cardiomyocytes (AMCM); alpha-actinin in green and nucleus in blue (DAPI stain).

VBM-400 Biological Safety Hood (Artisan Scientific Corporation, Champaign, IL); Beckman Coulter Allegra 25R centrifuge (Beckman Coulter, Brea, CA); Biospec USR70/30 magnetic resonance imager (MRI) (Bruker Biospin MRI, Billerica, MA); Doppler Signal Processing Workstation (Indus Instruments, Webster, TX); ELx800 Absorbance Microplate Reader (BioTek, Winooski, VT); Eppendorf 5804R refrigerated centrifuge (Eppendorf, Hauppauge, NY); Gemini Cautery System (SouthPointe Surgical Supply, Inc., Coral Springs, Florida); Hermle Z300 Centrifuge (HERMLE Labortechnik GmbH, Wehingen, Germany); IN835 Inverted Compound Microscope (Nova, Portland, OR); Isotemp* Economy Analog-Control Water Bath (ThermoFisher Scientific, Waltham, MA); Isotemp* PPO Heating Circulator (Fisher Scientific, Waltham, MA); Mouse Cardiovascular Research System (MVRS) Doppler and electrode board (Indus Instruments, Webster, TX); MyCycler Thermal Cycler (Bio-Rad, Hercules, CA); NanoDrop® ND-1000 spectrophotometer (Nanodrop Technologies, Wilmington, DE); Ohaus AS120 scale (Ohaus, Florham Park, NJ); Packard 2200 liquid scintillation counter (Packard Instruments, Warrenville, IL); POLARstar OPTIMA fluorometer (BMG LABTECH, Cary, NC); Power Gen 35 Micro Homogenizer (Omni International, Kennesaw, GA); Professional Cell Culture CO₂ Incubator (Sanyo Electric Biomedical Co., Ltd., Moriguchi City Osaka, Japan); PTC-100 Thermoblock (MJ Research, Waltham MA); Revco® -80°C freezer (Thermo Scientific, Asheville, NC); Small animal monitoring system Model 1025 (Small Animals Instruments, Inc., Stony Brook, NY); SRX-101A Medical Film Processor (Konica Minolta Medical Imaging USA, Inc., Wayne, NJ); TD-1000R Bi-O-Vision Dual-Light Transilluminator (Spectroline, Westbury, NY); Precision 2870 Reciprocal Shaking Bath (Thermo Fisher Scientific, Waltham, MA); Variable-Flow Peristaltic Pump (ThermoFisher Scientific, Waltham, MA); Vevo 770 ultrasound system (Visual Sonics Inc., Toronto, Ontario, Canada); Sanyo® -20°C freezer (Sanyo Scientific, Bensenville, IL).

2.1.4. Reagents

The following chemicals of analytical or appropriate grade were used. From Sigma (St. Louis, MO): 0.25% (w/v) Trypsin-0.53 mM, Ethylenediaminetetraacetic acid (EDTA), 2,3-butanedione monoxime (BDM), 3-Methyladenine (3-MA), Agarose, Ammonium persulfate (APS), β-glycerophosphate, β-mercaptoethanol, Boric acid, Bovine Serum Albumin, Bromophenol blue, Calcium Chloride (CaCl₂), Dimethyl sulfoxide (DMSO), Disodium hydrogen orthophosphate (Na₂HPO₄), Dithiothreitol (DTT), Ethylenediaminetetraacetic acid (EDTA), Ethylene glycol tetraacetic acid (EGTA), Ethanol (100%), Ethidium bromide, Formaldehyde, Glucose, Gluteraldehyde, Glycine, Hydrochloric acid (HCl), HEPES (4-(2-hydroxyethyl)-1-piperazineethanesulfonic acid), Isopropanol

(100%), Isoproterenol, Lithium chloride (LiCl), Magnesium sulfate (MgSO_4), Magnesium sulfate heptahydrate ($\text{MgSO}_4 \cdot 7\text{H}_2\text{O}$), Methanol, Monopotassium phosphate (KH_2PO_4), Monosodium phosphate (NaH_2PO_4), Octyl phenoxypolyethoxyethanol (Nonidet P-40), Pancreatin, Pencillin G Potassium Salt, Paraformaldehyde, Phenol red, Phenylephrine (PE), Potassium chloride (KCl), Potassium ferricyanide ($\text{K}_3\text{Fe}(\text{CN})_6$), Potassium ferrocyanide ($\text{K}_4\text{Fe}(\text{CN})_6$), Proteinase K (10mg/mL), Sodium ATP (Na-ATP), Sodium azide, Sodium bicarbonate (NaHCO_3), Sodium chloride (NaCl), Sodium-deoxycholate, Sodium Fluoride (NaF), Sodium-HEPES, Sodium molybdate (Na_2MoO_4); Sodium pentobarbital, Sodium pyrophosphate ($\text{Na}_4\text{P}_2\text{O}_7$), Taurine, Tergitol-type nonyl phenoxypolyethoxyethanol (NP-40), Tetramethylethylenediamine (TEMED), Trichloroacetic acid (TCA), Tris base, Tris-buffered phenol, Tris-HCl, Trisodium phosphate (Na_3PO_4), Triton X-100, and Tween 20.

The following chemicals and reagents were obtained from EMD Biosciences (San Diego, CA): Compound C, Cyclosporin A, DAB substrate buffer, and Rapamycin. Additional chemicals used were from different vendors and are listed as follows: Bortezomib (Selleck Chemicals, Houston, TX), Bovine Serum Albumin protein standard (1mg/mL) and Chloroform (Invitrogen, Carlsbad, CA), 30 % Acrylamide/Bis and Precision Plus Protein All Blue Standards and Sodium dodecyl sulfate (SDS) (BioRAD, Hercules, CA), Collagenase II (Worthington Biochemical Corporation, Lakewood, NJ), Heparin (MP Biomedicals, Irvine, CA), N-(β -D-Ribofuranosyl)-5-aminoimidazole-4-carboxamide (AICAR) (Toronto Research Company, Ontario, Canada), Percoll (Pfizer, New York, NY), Protease inhibitor complete tablet (Roche, San Francisco, CA), and Radiolabeled phenylalanine (Perkin Elmer, Boston, MA).

The following reagents were from Sigma (St. Louis, MO): Bradford Reagent, Insulin/Transferrin, Selenium (ITS, medium supplement), Ponceau Stain, and Synthesized oligonucleotide primers/ probes/ cDNA.

The following reagents were from Thermo Fisher Scientific (Waltham, MA): Bovine Calf Serum, Calf serum (Hyclone, Logan, UT), Newborn Calf Serum, and Ultima Gold® liquid Scintillation Cocktail.

The following reagents were from VWR (Radnor, PA): CellGro DMEM 4.5g/L Glucose & L-Glut, w/o Sodium Pyruvate, Diethylpyrocarbonate (DEPC)-treated water, FK506, and Laminin coating solution.

The following reagents were from Invitrogen (Carlsbad, CA): β -Galactosidase Assay Kit, MEM (Eagle's with HBSS), Penicillin/Streptomycin (100U/mL), Phosphatase inhibitor cocktails I-III, Phosphate Buffered Saline (PBS; without calcium and magnesium),

Prolong Gold mounting media with DAPI, Proteinase K, Reverse transcriptase and PCR reaction buffers, and Superscript II.

Additional reagents used were from Eton Biosciences (San Diego, CA): aAMPK adenovirus, dnAMPK adenovirus, and a null adenovirus; and from Promega Corporation (Madison, WI): β -galactosidase (1 unit/ μ L), β -galactosidase Enzyme Assay System, Luciferase Assay System, and QuantiLum® Recombinant Luciferase. The β -galactosidase expression vector [317] was kindly provided by Dr. Joseph Alcorn (University of Texas Medical School, Houston). Additional reagents used were from different vendors and are listed as follows: PolyJet™ (SigmaGen® Laboratories, Rockville, MD); Taq polymerase (recombinant origin, isolated in the lab from *Escherichia coli*), TRI® Reagent (Molecular Research Center, Cincinnati, OH), Western Blotting Luminol Reagent (Santa Cruz, Santa Cruz, CA), and X-Gal (5-bromo-4-chloro-3-indolyl-beta-D-galacto-pyranoside (Fermentas, Ontario, Canada).

The following kits were used according to the manufacturer's instructions: AdEasy viral titer kit (Stratagene, La Jolla, CA), DNeasy Blood & Tissue Kit (Qiagen, Germantown, MD), Nuclear Extract Kit and TransAM™ MEF2 Transcription Factor Assay Kit (Active Motif, Carlsbad, CA).

The following antibodies were used (**Table 2.1**). All antibody dilutions were made in non-fat powdered milk (5%, in Tris-Buffered Saline containing Tween 20 [0.4%], [TBST]). Primary antibodies were preserved with sodium azide [0.2% in ddH₂O]. AMPK α (1:1000), phospho-AMPK α (Thr172, 1:1000), Acetyl CoA Carboxylase (ACC) (1:1000), phospho-ACC (Ser79, 1:1000), β -Tubulin (9F3, 1:1000), Forkhead transcription factor 3 (FOXO3A) (1:500), phospho-FOXO3A (Ser253, 1:500), AKT (1:1000), phospho-AKT (Thr308, 1:500), mammalian target of Rapamycin (mTOR) (1:1000), phospho-mTOR (Ser2488, 1:500), and CD31 (Platelet Endothelial Cell Adhesion Molecule-1: PECAM-1) (1:200) antibodies were from Cell Signaling Technology (Danvers, MA). Histone deacetylase 5 (1:500), phospho-histone deacetylase 5 (Ser498, 1:500), MuRF1 (1:500), and anti-adenovirus hexon protein (1:1000) antibodies were from Abcam (Cambridge, MA), the Atrogin-1 antibody (1:1000) was from ECM biosciences LLC (Versailles, KY), the Glyceraldehyde-3-phosphate dehydrogenase (GAPDH, 1:60,000) antibody was from Fitzgerald Industries International (Acton, MA), and the MEF2 (C-21) antibody was from Santa Cruz Biotechnology, Inc. (Santa Cruz, CA).

The following items from Thermo Fisher Scientific (Waltham, MA) were also used: Cell strainer, Hemacytometer, Primaria cell culture plates.

Antibodies and Dilutions			
Name	Dilution	Molecular Weight (kDa)	Vender/Product
AMPK α	1:1000	62	Cell Signaling/ 2532
pAMPK α (Thr172)	1:1000	62	Cell Signaling/ 2531
ACC	1:1000	280	Cell Signaling/ 3662
pACC (Ser79)	1:1000	280	Cell Signaling/ 3661
β -Tubulin	1:1000	55	Cell Signaling/ 2128
FOXO3A	1:500	82-97	Cell Signaling/ 9467
pFOXO3A (Ser253)	1:500	82-97	Cell Signaling/ 9466
AKT	1:1000	60	Cell Signaling/ 4685
pAKT (Thr308)	1:500	60	Cell Signaling/ 4056
mTOR	1:1000	289	Cell Signaling/ 2972
pmTOR (Ser2488)	1:500	289	Cell Signaling/ 2971
CD31	1:200	Used for staining	Cell Signaling/ 2538
HDAC5	1:500, 2 μ g for ChIP	122	Abcam/ ab1439
pHDAC5 (Ser498)	1:500	122	Abcam/ ab47283
MuRF1	1:500	40	Abcam/ ab77577
anti-adenovirus hexon protein	1:1000	Used for staining	Abcam/ ab21116
Atrogin-1	1:1000	41	ECM biosciences LLC/ AP2041
GAPDH	1:60,000	37	Fitzgerald Industries International/ 10R- G109A
MEF2	2 μ g for ChIP	Used for IP	Santa Cruz/ C-21

Table 2.1. Antibodies and dilutions.

Detailed list of antibodies used. See text for details.

2.2. Methods

2.2.1. Maintenance of Mouse Lines

The following mouse lines were maintained: MAFbx/Atrogin-1^{-/-}, MuRF1^{-/-}, MAFbx/Atrogin-1^{+/+} MuRF1^{+/+} (wild type, WT) all from Regeneron (Tarrytown, NY) through Dr. David Glass (now at Novartis, Cambridge, MA). Single knockout mice were crossed to generate MAFbx/Atrogin-1^{-/-} MuRF1^{-/-} (double knockout) mice, and desMEF2-*LacZ* transgenic mice from Dr. Eric Olson (The University of Texas Southwestern, Dallas, TX) were also maintained. Breeding pairs successfully produced 6-8 litters and were retired thereafter. Mice were routinely genotyped by PCR using genomic DNA extracted from the tail. Tails were clipped (<0.5mm) at age 3 weeks and cauterized to prevent bleeding. Tails were digested and DNA was isolated using the DNeasy Blood & Tissue Kit (Qiagen) according to the manufacturer's instructions. The primer sequences and PCR protocols for MAFbx/Atrogin-1, MuRF1, and desMEF2-*LacZ* genotyping are shown in **Table 2.2.** and **2.3.** For double knockout and WT mice, MAFbx/Atrogin-1 and MuRF1 genotyping PCR reactions were performed independently. PCR products (20μL) were mixed with DNA loading buffer (5μl of glycerol [3mL of 100%], bromophenol blue [25mg], ddH₂O [7mL]) and run on a 1% agarose gel in TBE buffer (Tris base [1.08g], Boric acid [5.5g], EDTA [20mL of 0.5M] in 1L DEPC-treated water) at 150mV (**Figure 2.2**). Genotyping results, mouse identification and location, breeding pairs, and experimental setup were all recorded in a database using Microsoft® Access.

2.2.2. Transverse Aortic Constriction in Mice

Transverse aortic constriction (TAC), originally described by Rockman et.al., is a surgical procedure used to induce cardiac hypertrophy *in vivo* [318]. Although hypertrophy develops more rapidly than what occurs physiologically, this method allows for the reproducible development of extreme hypertrophy and is used to investigate mechanisms of development, inhibition, and reversal of cardiac hypertrophy. These experiments were performed in collaboration with Drs. Aarif Khakoo and Vishnu Chintalgattu at The University of Texas MD Anderson Cancer Center (presently at Amgen, San Francisco, CA). Animal protocols were approved by the Animal Welfare Committee of The University of Texas MD Anderson Cancer Center.

Male mice (C57/BL6, 8 weeks old) were kept under continuous anesthesia with isoflurane (2%) and taped to a heated procedure board (37°C) containing ECG electrodes in the supine position. Mice were intubated, ventilated, and a cervical incision was made

Primer Name	Primer Sequence
MAFbx/Atrogin-1 forward primer (MA61 KO, F1)	5' – AACAAAGAGACGGGGCAGCG – 3'
MAFbx/Atrogin-1 KO forward primer (MA61 KO, LacZ)	5' – TGAGGGGACGACGACAGTATCG – 3'
MAFbx/Atrogin-1 reverse primer (MA61 KO, R1)	5' –TCGGCGAATGTCCTCACCTG– 3'
MuRF1 forward primer (MA16 KO5'F2)	5' – CTCCTGGGGCTCATGTGACAGAGG – 3'
MuRF1 KO forward primer (LacZ-R)	5' – TAGATGGGCGCATCGTAACCGTGC – 3'
MuRF1 reverse primer (MA16 5'R2)	5' – GATGTCGTTGGCACACTTCCGGCA – 3'
LacZ 3'	5' – CAGTACAGCGCGGCTGAAATC – 3'
LacZ 5'	5' – CAAACTGGCAGATGCACGGTTAC – 3'

Table 2.2. Mouse genotyping primers.

PCR was performed on mouse tail DNA using the primers above. Atrogin-1^{-/-} mice were genotyped using two reactions: one to detect the WT gene (using MA61KO, F1 and MA61KO, R1) and one to detect the knockout gene (using MA61KO, F1 and MA61KO, LacZ). MuRF1^{-/-} mice were genotyped using one reaction with MA16KO5'F2, LacZ-R, and MA16KO5'R2. MEF2-LacZ transgenic mice were genotyped using one reaction with LacZ 3' and LacZ 5'.

PCR Reaction Mix		PCR Protocol	Amplicon Length
MAFbx/Atrogin-1 WT		95°C x 5 minutes 94°C x 30 seconds 65°C x 45 seconds cycles 72°C x 50 seconds 72°C x 2 minutes 4 °C x ∞	422 base pairs
10X PCR Buffer MgCl ₂ (50mM) dNTP's (2.5mM) MA61 KO, F1 Primer MA61 KO, R1 Primer Taq (Invitrogen) DEPC-treated H ₂ O DNA	2.0μL 1.0μL 2.0μL 0.2μL 0.2μL 0.2μL 12.2μL 2.0μL		
MAFbx/Atrogin-1 KO		95°C x 5 minutes 94°C x 30 seconds 65°C x 45 seconds cycles 72°C x 50 seconds 72°C x 2 minutes 4 °C x ∞	553 base pairs
10X PCR Buffer MgCl ₂ (50mM) dNTP's (2.5mM) MA61 KO, F1 Primer MA61 KO, LacZ Primer Taq (Invitrogen) DEPC-treated H ₂ O DNA	2.0μL 1.0μL 2.0μL 0.2μL 0.2μL 0.2μL 12.2μL 2.0μL		
MuRF1		94°C x 5 minutes 94°C x 30 seconds 63°C x 30 seconds cycles 72°C x 50 seconds 72°C x 2 minutes 4 °C x ∞	WT: 324 base pairs KO: 470 base pairs
10X PCR Buffer MgCl ₂ (50mM) dNTP's (2.5mM) MA16 KO5'F2 Primer LacZ-R Primer MA16 5'R2 Primer Taq (In-house) DEPC-treated H ₂ O DNA	2.00μL 1.00μL 2.00μL 0.05μL 0.05μL 0.20μL 12.65μL 2.00μL		
desMEF2-LacZ Tg		95°C x 5 minutes 95°C x 30 seconds 60°C x 30 seconds cycles 72°C x 30 seconds 72°C x 10 minutes 4 °C x ∞	Tg: 400 base pairs
10X PCR Buffer MgCl ₂ (25mM) dNTP's (10mM) LacZ 3' Primer LacZ 5' Primer Taq (Invitrogen) DEPC-treated H ₂ O DNA	2.5μL 1.5μL 0.5μL 0.5μL 0.5μL 0.5μL 1.0μL 1.0μL		

Table 2.3. Genotyping PCR protocols and amplicon lengths.

PCR was performed on DNA from mouse tails as described in the text and according to the protocols above.

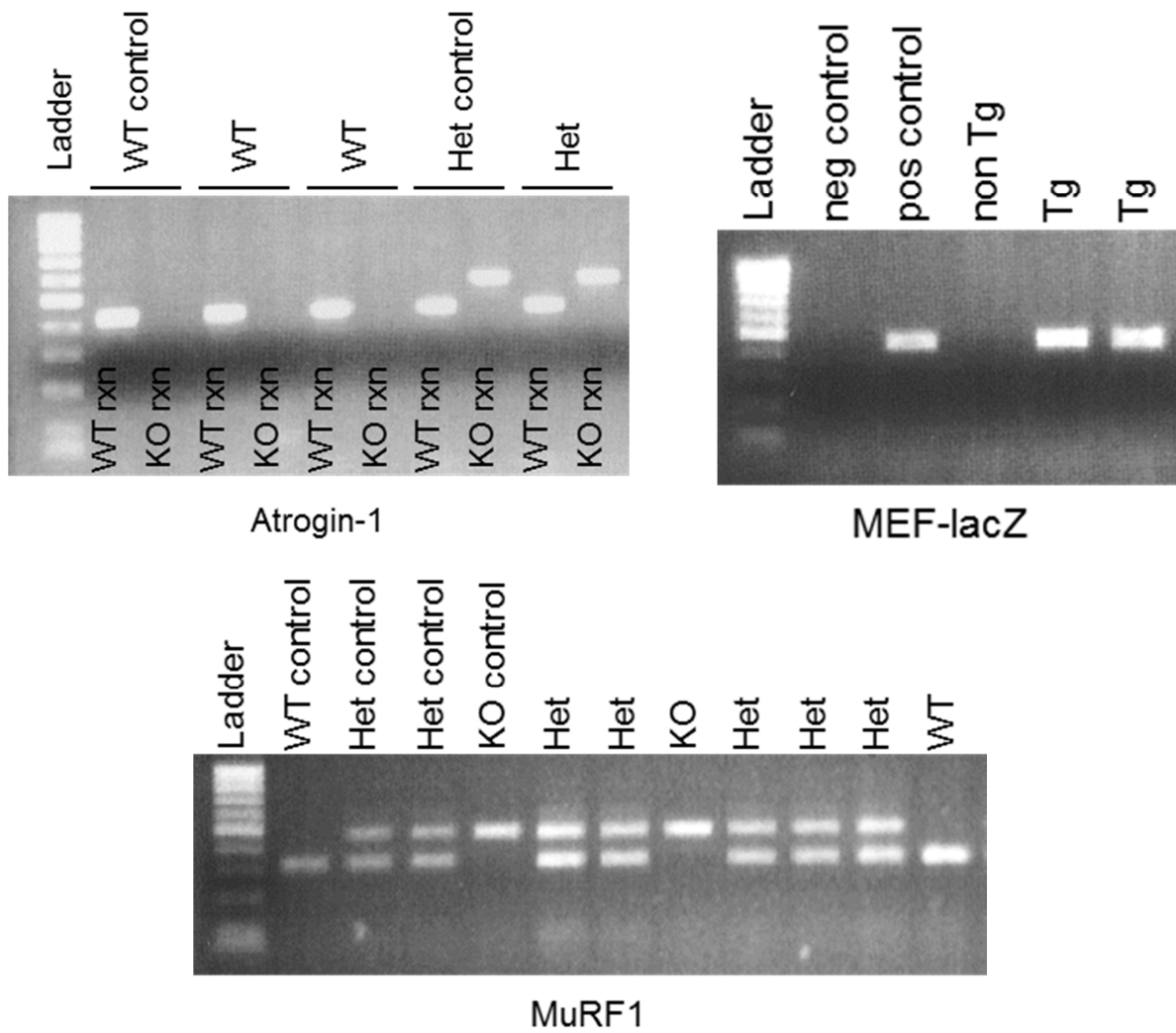


Figure 2.2. Genotyping Results.

Genotyping PCR reaction products. (A) Atrogin-1 PCR performed using two reactions: one with primers detecting the WT allele, one with primers detecting the KO allele (labeled below the gel). The genotyping results are labeled above the gel; DNA from control animals are also labeled. (B) MEF2-lacZ PCR performed in one reaction. The genotyping results (including controls) are labeled above the gel. (C) MuRF1 PCR performed in one reaction. The genotyping results (including controls) are labeled above the gel. See text for more details.

exposing the trachea and carotid arteries. The aortic arch was isolated and a 27-gauge needle was tied to the transverse aorta using 7.0 silk suture (**Figure 2.3.A.**). The needle was removed creating an aortic stenosis of 0.4mm diameter (originally 1.0mm diameter). The chest was surgically closed, the animal was allowed to recover, and the animal was monitored daily. Sham operations were also performed using the same procedure except for the tying of the suture. Non-invasive Doppler imaging was performed the day after TAC surgery to verify successful placement of the suture and pressure differences across the carotid arteries [319]. Mice were anesthetized and placed on a procedure board as described above. Cardiac parameters and blood velocity signals from the right and left carotid arteries were obtained using a 2-mm-diameter 20-MHz Doppler probe connected to a Doppler Signal Processing Workstation (Indus Instruments, Webster, TX). After TAC surgery 90% of mice displayed an increase in peak blood velocity in the right carotid artery and a decrease in peak blood velocity in the left carotid artery (**Figure 2.3.B.**) [320, 321]. Heart function was analyzed (see section 2.2.5.2. Magnetic Resonance Imaging) 7, 14, 21, and 28 days after surgery, and tissues were collected 29 days after surgery and processed as described below (2.2.6. Cell and Tissue Collection and Preservation).

2.2.3. Assessment of Cardiac Function

2.2.3.1. Echocardiography

Echocardiography uses high frequency sound waves (ultrasound) to transmit live 2-dimensional images of the heart. We used the Vevo 770 ultrasound system (above) to calculate cardiac dimensions (interventricular septal thickness in diastole [IVSd] and systole [IVSs], left ventricular posterior wall thickness [LVPW], left ventricular inner diameter in diastole [LVIDd] and systole [LVIDs], and left ventricular mass), cardiac volumes (left ventricular volume in diastole and systole), and functional parameters (heart rate [HR], stroke volume [SV], cardiac output [CO], fractional shortening [FS], and ejection fraction [EF]) [322, 323].

Cardiac parameters and function was assessed in mice using echocardiography [324]. Mice were anesthetized (2% isoflurane) and the body fur was shaved from the anterior thorax and upper abdominal area. Acoustic coupling gel was applied to the abdomen. Mice were placed in the supine position with all four limbs taped to electric plates on a temperature-controlled board with leads used for electrocardiographic monitoring. Mice were maintained under 1% isoflurane during analysis of cardiac function (Vevo 770

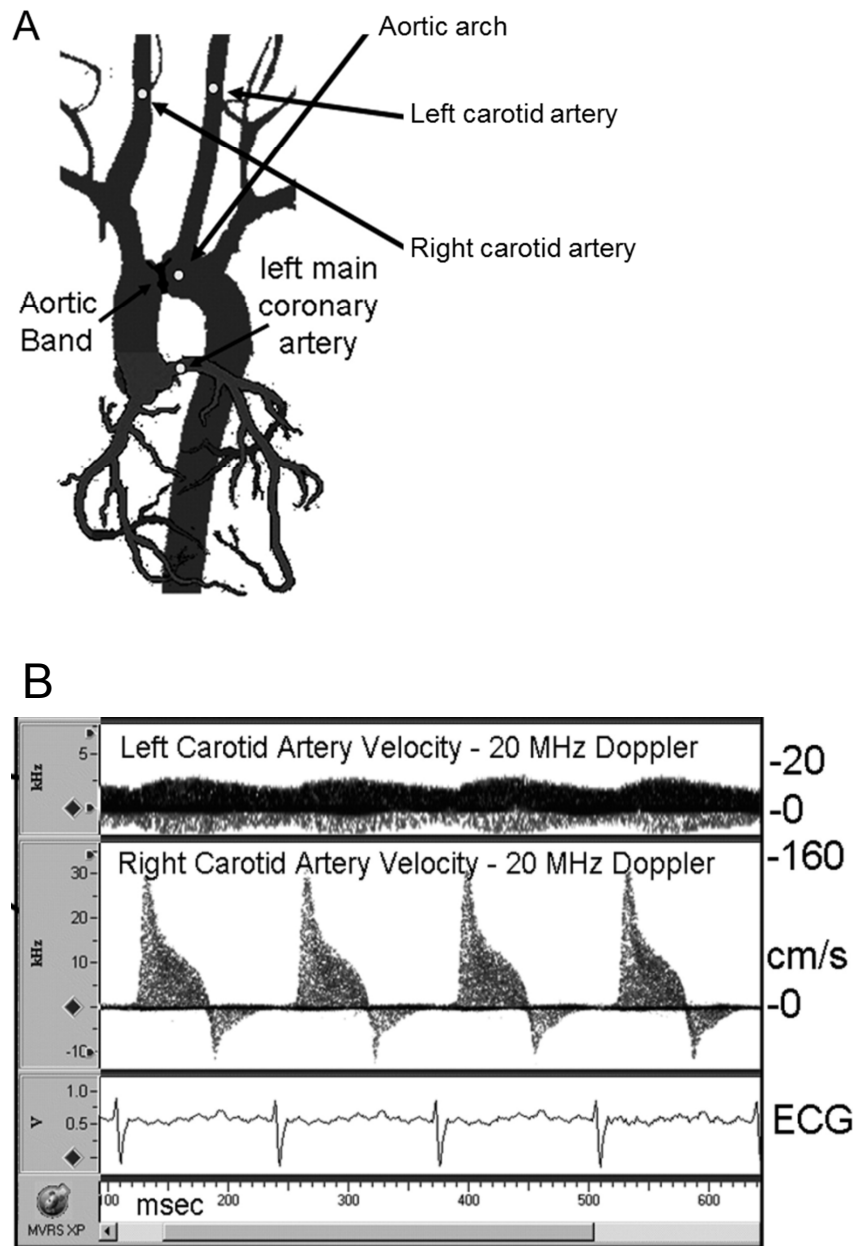


Figure 2.3. Transverse aortic constriction and Doppler measurements.

(A) Suture placement for transverse aortic constriction (TAC) surgery. (B) Doppler measurements 24 hours after surgery. Velocity of blood flow through the left carotid artery is blunted due to placement of the aortic band (top frame) whereas velocity of blood flow through the right carotid artery is normal (middle frame). Electrocardiogram (ECG) tracings of the banded heart (bottom frame). Reprinted from *Ultrasound Med Biol*, 34/6, Hartley CJ, Reddy AK, Madala S, Michael LH, Entman ML, Taffet, GE, Doppler estimation of reduced coronary flow reserve with pressure overload cardiac hypertrophy, Pages 892901, (2008), with permission from Elsevier[321]

ultrasound system, Visual Sonics). After echocardiography was performed, mice were monitored as they recovered from anesthesia.

M-mode parasternal short-axis scans were used to quantify ventricular diameters in diastole and systole. Left ventricular diameters in diastole and systole were determined by making 5 measurements for each parameter (IVSd, LVPW, LVIDd, LVIDs) on four different images of each mouse heart (**Figure 2.4.**). Based on these measurements, the Vevo 770 software estimates the end-diastolic volume (EDV) and end-systolic volume (ESV). The parameters were then used to assess cardiac function using the following equations.

$$\text{Stroke volume (SV)} = \text{EDV} - \text{ESV}$$

$$\text{Cardiac output (CO)} = \text{HR} \times \text{SV}$$

$$\text{Ejection Fraction (EF, \%)} = \frac{\text{SV}}{\text{EDV}} \times 100$$

$$\text{Fractional Shortening (FS, \%)} = \frac{(\text{LVEDd} - \text{LVESd})}{\text{LVEDd}} \times 100$$

2.2.3.2. Magnetic Resonance Imaging

Magnetic Resonance Imaging (MRI) was used to obtain high resolution images of the heart. A magnetic field within the MRI machine aligns protons within the specimen and radio frequency pulses alter the alignment of the protons. Consequently, protons produce a rotating magnetic field that is detected and recorded. Fourier transformation converts the collected signals into images. Gradient magnets are rapidly turned on and off to alter the magnetic field in a local region of the specimen, producing slices (200-300 μm) of images [325]. MRI is optimized for cardiac imaging by using electrocardiography (ECG) gating and rapid imaging sequences. ECG gating allows for cardiac images to be acquired by synchronizing frequency pulses with the beating heart, enabling the visualization of cardiac motion and the accurate evaluation of cardiac output [326-328].

Mice were anesthetized with isofluorane (2%), and parameters were monitored using a small animal monitoring system (Model 1025, Small Animals Instruments, Stony Brook, NY). Body temperature was maintained at 37°C using a circulating water-filled imaging platform, heart rate (HR) was kept between 350-500 beats per minute (bpm) and respiration rate (RR) was kept between 25-40 (breaths per minute). Mice were placed on the imaging platform and positioned using sagittal and coronal images; short axis images

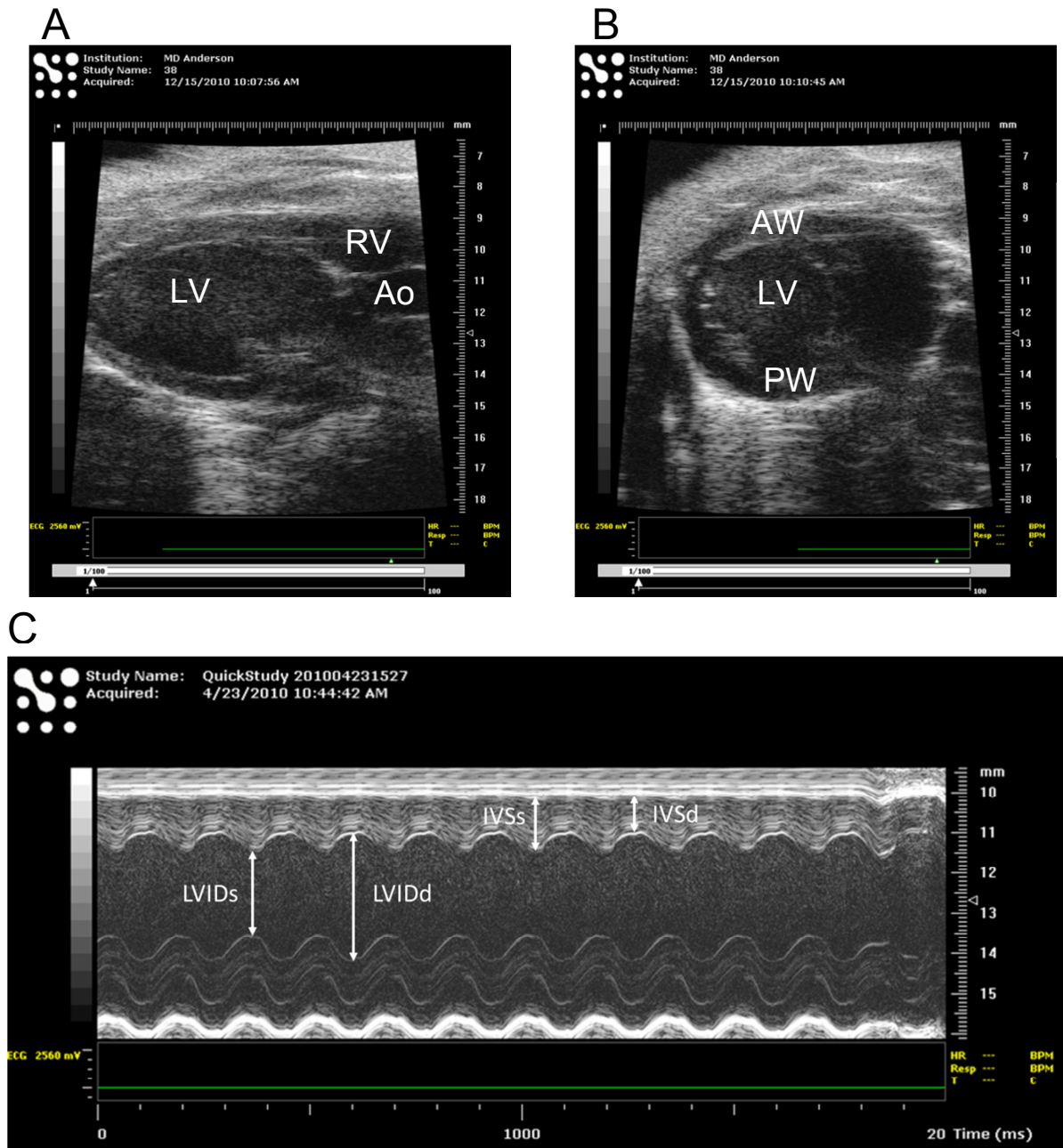


Figure 2.4. Echocardiographic tracings in the mouse.

(A) Parasternal-long-axis B-mode image and (B) Short-axis B-mode image of an adult mouse heart. (C) M-mode image depicting left ventricular structure and function in an adult mouse. Functional calculations are based on measurements taken for LVIDs, LVIDd, IVSs, and IVSd. LV, left ventricle; RV, right ventricle; Ao, aorta; AW, anterior wall; LVIDd, left ventricular inner diameter in diastole; IVSs, interventricular septum in systole; IVSd, interventricular septum in diastole. Images courtesy of Meredith Rees, Taegtmeier laboratory.

were used for analysis of cardiac structure and function. Slices of the heart (1mm) were imaged every 6 milliseconds with 3 milliseconds between pulses. Using the Paravision® MRI Software, six slices (images) of the heart taken during different phases of contraction and relaxation were used for analysis, including end-diastolic and end-systolic images (**Figure 2.5**). For each slice, the interventricular septal and posterior wall thickness (mm) was measured, the contours of the left ventricle were traced, and the ventricular area was calculated. The area and slice thickness were used to calculate left ventricular end-systolic (LVESV) and diastolic (LVEDV) volumes using Simpson's rule algorithm for volume determination:

$$LVESV = \sum_{Apex}^{Base} (end - systolic\ area) \times (Slice\ thickness)$$

$$LVEDV = \sum_{Apex}^{Base} (end - diastolic\ area) \times (Slice\ thickness)$$

Other cardiac parameters (EF, SV, and CO) were calculated as described in section 2.2.5.1. Echocardiography. Serial MRIs were taken at days 7, 14, 21, and 28 after TAC. After imaging, mice were monitored as they recovered from anesthesia. These experiments were performed in collaboration with Drs. Aarif Khakoo and Vishnu Chintalgattu at The University of Texas MD Anderson Cancer Center (presently at Amgen, San Francisco, CA). Animal protocols were approved by the Animal Welfare Committee of The University of Texas MD Anderson Cancer Center.

2.2.4. Isolation of Neonatal Rat Ventricular Cardiomyocytes (NRVM)

The isolation of neonatal rat ventricular cardiomyocytes (NRVM) was performed under sterile conditions in a biological safety hood and all solutions were made in the hood and/or sterile filtered. This protocol is adapted from a method used in Dr. Diane Bick's lab at The University of Texas Health Science Center at Houston, Department of Pathology [329]. Neonatal Sprague-Dawley rats (1-2 day old) were quickly washed in 70% ethanol, and decapitated. Their heads were placed in liquid nitrogen. The chest cavity was opened and the heart was removed and placed in 1X ADS buffer (NaCl [6.8g], KCl [0.4g], glucose [1.0g], NaH₂PO₄ [1.5g], MgSO₄ [0.1g], HEPES [4.76g], and pH adjusted to 7.38 with HCl/NaOH in 1L total volume of double distilled water [ddH₂O]) at room temperature until all hearts were collected. Hearts were then rinsed once with 1X ADS buffer using a transfer pipet, cut in half, and transferred to a 25mm² culture flask containing enzyme buffer (9-15mL of 1X ADS containing Pancreatin [0.6mg/mL] and Collagenase Type II [73U/mL]) with

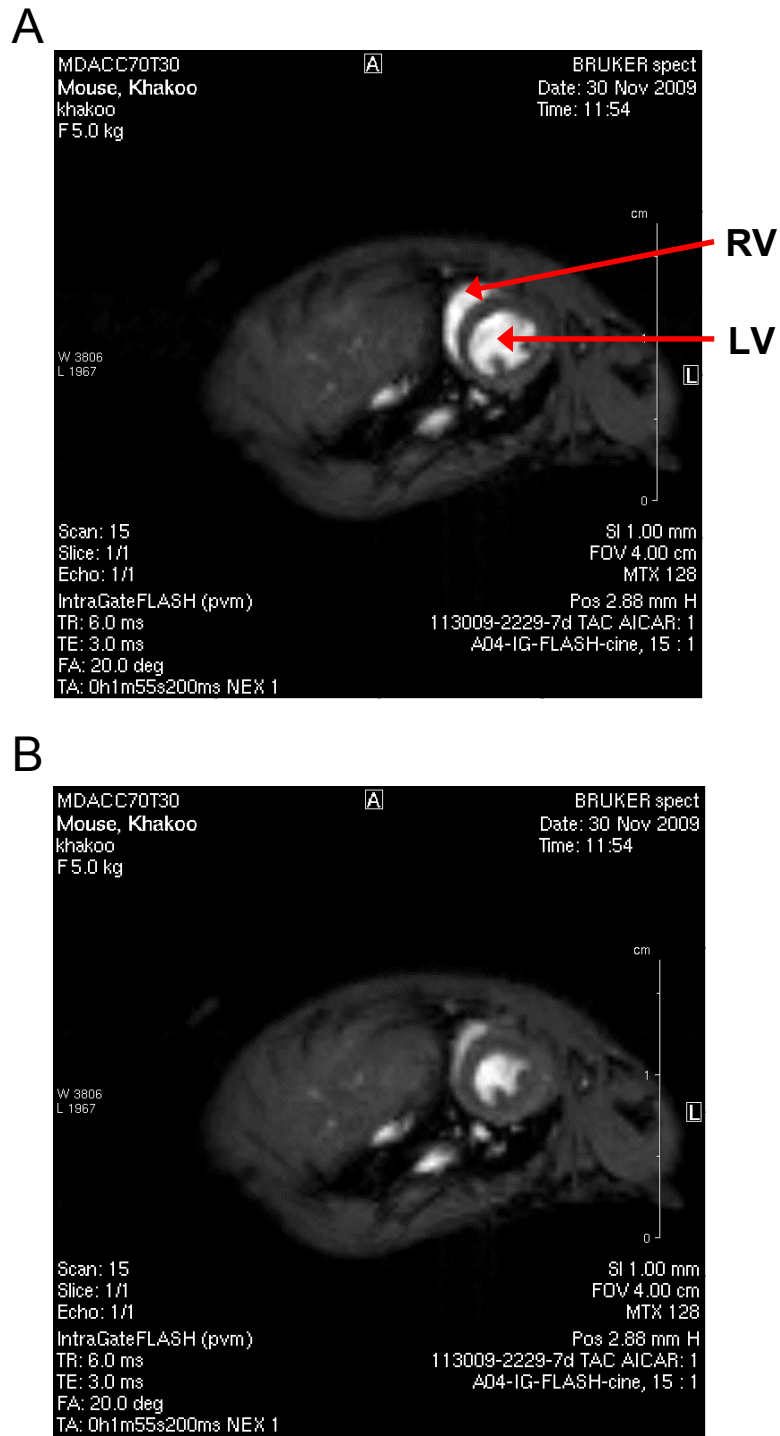


Figure 2.5. Magnetic Resonance Images of the mouse heart.

(A) Short axis MRI image of an adult mouse in diastole and (B) systole. Cardiac parameters were calculated based on measurements made using the Paravision® MRI Software. See text for details. RV; right ventricle, LV; left ventricle.

15 cut hearts per flask. Flasks were incubated for 20 minutes at 37°C with shaking (110-120rpm) and the supernatant fraction was discarded and replaced with fresh enzyme buffer. The same digestion step was performed four additional times, 25 minutes of incubation for each step. The supernatant fraction from each digestion was collected, centrifuged for 5 minutes at 300g and the pellet was resuspended in 2-3mL newborn calf serum and kept in the incubator.

Cell pellets from all four digestion steps were pooled together, centrifuged for 5 minutes at 300g and the pellet was resuspended in 4mL of Percoll gradient (1.082 g/mL). Percoll gradient tubes were prepared by adding 4mL of each gradient: 1.05g/mL, 1.062g/mL, and 1.082g/mL containing cells. Gradients were added in increasing density by slowly pipetting the gradient into the bottom of the tube through a 15 gauge filling needle so as not to disturb the layers. Percoll gradients were then centrifuged for 25 minutes at 1000g in a swing bucket rotor at room temperature. The cardiomyocytes remain in the percoll gradient layer (1.082 g/mL), and were collected in 1X ADS (for a final volume of 30mL containing phenol red), and centrifuged for 5 minutes at 300g. The supernatant fraction was discarded; the pellet was again resuspended in 1X ADS (30mL), and centrifuged for 5 minutes at 300g. The supernatant fraction was discarded and the myocytes were resuspended in complete media (1 mL per heart, comprised of DMEM [500 mL], BCS [50 mL], and Penicillin/Streptomycin [10 mL of 100U/mL]). Cardiomyocytes were then counted and plated at a density of 2 million cells per 60mm dish or 0.75 million cells per well in a 6-well plate, and media was replaced the next morning. NRVM spontaneously contract after brief culture and continue to do so for up to 7 days, at which time they lose viability. Although structurally distinct from adult cardiomyocytes (**Figure 2.1.**), NRVM express cardiomyocyte structural properties such as T-tubules and sarcomeres [330]. Always difficult to manipulate genetically, the ease and abundance of NRVMs per single isolation (compared to adult cardiomyocytes) makes them the model of choice for investigating mechanisms *in vitro* in the cardiomyocyte [331].

2.2.5. Isolation of Adult Mouse Cardiomyocytes (AMCM)

The isolation of adult mouse cardiomyocytes (AMCM) was performed under semi-sterile conditions. All solutions were made in the hood and/or sterile filtered and surgical equipment was sterilized by autoclaving, but the cell isolation was not performed under the hood until the culture of the AMCM. This protocol is adapted from O'Connell et.al. [332]. Preparation for this procedure is crucial to a successful isolation. Key steps include: priming the perfusion apparatus, preparing the buffers (perfusion, digestion, and stopping buffer),

preparing and pre-incubating plating and culturing medium, laminating the plates for culturing cardiomyocytes, and sterilizing the surgical tools.

Mice (6-10 weeks old) were anesthetized using pentobarbital (0.5mL of 5mg/mL). Once anesthetized, Heparin (0.2mL of 1000U/mL) was injected intraperitoneally. When fully anesthetized and unresponsive to the toe-pinch reflex test, a thoracotomy was performed. The beating heart was removed with the lungs and immediately placed in ice-cold PBS. The lungs were dissected away, the thymus peeled back and removed to reveal the aorta. The thoracic aorta was traced up to the aortic arch, the aortic branches were identified, and the aorta was trimmed at the ascending aorta. The aorta was cannulated using a 22 gauge catheter cover on a 1mL sterile syringe containing perfusion buffer (NaCl [120.4mM], KCl [14.7mM], KH_2PO_4 [0.6mM], Na_2HPO_4 [0.6mM], $\text{MgSO}_4 \cdot 7\text{H}_2\text{O}$ [1.2mM], Na-HEPES [10mM], NaHCO_3 [4.6mM], Taurine [30mM], BDM [10mM], and glucose [5.5mM] in cell culture grade water and adjusted to pH 7.0 with HCl). The heart was fastened to the cannula using a micro clip and the syringe was depressed to verify the absence of leaks in the aorta. The cannula and heart were then connected to the primed water-jacket of the Langendorff-style apparatus containing perfusion buffer at 37°C. The heart was perfused in a retrograde manner at 4mL/minute with perfusion buffer for 3 minutes, followed by perfusion with 15mL digestion buffer (perfusion buffer with Collagenase Type II) and finally re-circulated digestion buffer with calcium (40 μM).

After the extracellular matrix of the heart was digested by perfusing for a total of 16-20 minutes, the heart was removed from the perfusion apparatus and placed in a 60mm² dish (non-tissue-culture treated) containing 5mL stopping buffer (18mL perfusion buffer, 2mL Calf serum, and CaCl_2 at a final concentration of 100mM). The heart was minced in stopping buffer and further mechanically digested using a transfer pipet. The digested suspension was filtered through a cell strainer (100 μM), transferred to a 15mL conical tube, and centrifuged at room temperature at 20g for 3 minutes. The supernatant fraction was removed and the cell pellet was resuspended in stopping buffer (5-10mL containing CaCl_2 [100 μM]), incubated at room temperature for 2 minutes, and centrifuged at 20g for 3 minutes. This step was repeated with stopping buffer containing CaCl_2 [400 μM] and then CaCl_2 [900 μM] to slowly restore calcium to near physiological concentration in the cardiomyocyte. After centrifugation in stopping buffer containing CaCl_2 [900 μM], supernatant fraction was removed and cardiomyocytes were resuspended in plating medium (MEM [Eagle's with HBSS] containing Calf serum [10%], BDM [10mM], Penicillin [100U/mL], and ATP [2mM]) and plated with appropriate cell densities. Cells were

incubated for one hour at 37°C in 2% CO₂ and the medium was changed to culture medium (MEM [Eagle's with HBSS] containing BSA [1mg/mL] and Penicillin [100U/mL]). For long term culture, medium was supplemented with ITS (insulin [5µg/mL], transferrin [5µg/mL], and selenium [5ng/mL]) and BDM [10mM] to inhibit contraction.

Cardiomyocyte density is determined by counting the number of rod-shaped cardiomyocytes (**Figure 2.1.**). The quality of the isolation is determined by the total number of cardiomyocytes obtained and the ratio of rod-to-round-shaped cells. The higher the percentage of rod-shaped cells that is obtained (>60%), the higher the quality of the isolation. Adenoviral transductions and pulse-chase experiments in AMCM were started two hours after initial plating of the cells.

2.2.6. Cell and Tissue Collection and Preservation

2.2.6.1. Total RNA Isolation and Quantification

Total RNA was isolated using TRI Reagent® per the manufacturer's protocol with slight modifications [333]. Cells were scraped off plates using of TRI Reagent® (0.5-1.0 mL). Lysate was either snap frozen in liquid nitrogen or passed several times through a pipette tip. Frozen tissue was pulverized under liquid nitrogen using a mortar and pestle and 50mg was added to TRI Reagent® (1.0 mL) in a 2.0 mL eppendorf tube. The suspension was kept on ice and homogenized using a micro homogenizer. To separate the RNA (aqueous phase) from DNA and protein (organic phase), chloroform (0.2 mL) was added to the TRI Reagent® (per 1.0 mL), the samples were shaken vigorously, incubated at room temperature for 5-10 minutes, and centrifuged at 11,500g for 15 minutes at 4°C. The RNA in the aqueous phase was then precipitated with roughly the same volume of isopropanol (100%) for 5-10 minutes at room temperature. The precipitated RNA was pelleted by centrifugation at 11,500g for 10 minutes at 4°C. The supernatant fraction was removed and the RNA pellet was washed with ethanol (70% in DEPC-treated water [0.75 mL]), followed by centrifugation at 11,500g for 5 minutes at 4°C. The supernatant fraction was removed and the pellet was briefly air-dried and resuspended in DEPC-treated water (25-50µL). Following complete solubilization, total RNA was quantified using the NanoDrop 100 spectrophotometer.

The purity of isolated RNA is determined by the 260nm:280nm and 260nm:230nm ratios. The Beer Lambert Law ($A=ELC$; where A =absorbance, E =molar extinction coefficient, C =concentration, L =length light travels through the sample) is used to calculate the concentration of RNA, given that the average extinction coefficient for single-stranded

RNA at 260nm is 0.027 ug/mL/cm. The accepted 260:280 ratio for “pure” RNA is 1.8-2.0. Organic contaminants absorb light at 230nm, thus samples with a 260:230 ratio below 1.8 have significant contamination [334].

2.2.6.2. Protein Isolation and Quantification

Protein was isolated using cell lysis buffer (Stock cell lysis buffer [7.4mL] containing HEPES [5mM, pH 7.4], EDTA [0.1mM, pH 8.0], MgCl₂ [0.1mM], DTT [0.1mM], Triton [1%], NaCl [150mM], and protease and phosphatase inhibitor cocktails) for cells or tissue lysis buffer (HEPES [30mM], EGTA [2.5mM], EDTA [2.5mM], KCl [20mM], β-glycerophosphate [40mM], NaF [40mM], Na₄P₂O₇ [4mM], protease and phosphatase inhibitor cocktails) for tissue. Cells were washed twice with ice-cold PBS and collected in cell lysis buffer (0.2-0.5mL) on ice. Lysate was passed through a 1mL 27.5 gauge syringe five times (on ice), the lysate was centrifuged at 13,500g for 5 minutes at 4°C, and the supernatant fraction was collected in a new tube on ice. Frozen tissue was pulverized under liquid nitrogen using a mortar and pestle and 50mg was added to tissue lysis buffer (0.2 mL) in a 2.0 mL eppendorf tube. The suspension was kept on ice and homogenized using a microhomogenizer, the lysate was centrifuged at 13,500 g for 5 minutes at 4°C, and the supernatant fraction was collected in a new tube on ice.

Protein concentration was quantified using the Bradford method [335]. Proteins in solution form a complex with Brilliant Blue G dye causing a shift in the absorption of the dye from 465nm to 595nm. The absorption is proportional to the amount of protein present in the sample. A series of known protein concentrations were diluted to generate a standard curve (50-1000 μg/μL). Protein samples were diluted (1:5-1:20), diluted sample (5μL) was added to Bradford Reagent (200μL) in a 96-well plate, and the absorbance was read at 595nm using an absorbance microplate reader. Protein concentration was calculated based on the standard curve values.

2.2.6.3. Nuclear Fractionation of Cells

Nuclear extracts were isolated from NRVM or H9c2 myoblasts plated on 100mm² dishes using a modified protocol and reagents from the Nuclear Extract Kit (Active Motif). Cells were washed on ice with ice cold PBS (containing phosphatase inhibitors), gently scraped in 3mL of the same into pre-chilled 15mL conical tubes, and centrifuged at 500rpm for five minutes at 4°C. The supernatant fraction was removed, cells were resuspended in Hypotonic Buffer (500μL containing Hepes [20mM at pH 7.5], NaF [5mM], Na₂MoO₄ [10μM], and EDTA [0.1mM]), and cells were incubated on ice for 15 minutes. Detergent

(25 μ L, Active Motif) was added and lysate was vortexed for 10 seconds and centrifuged at 14,000g for 30 seconds at 4°C. The supernatant (cytoplasmic) fraction was snap frozen in liquid nitrogen and stored at -80°C for other experiments. The pellet (nuclear fraction) was resuspended in Complete Lysis Buffer (DTT [2.5 μ L of 10mM], Protease Inhibitor Cocktail [0.25 μ L], and Lysis Buffer AM1 [22.25 μ L]), vortexed for 10 seconds, and incubated for 30 minutes with gentle rocking on ice and at 4°C. The nuclear lysate was then vortexed for 30 seconds, centrifuged at 14,000g for 10 minutes at 4°C, and the supernatant (nuclear) fraction was transferred to a new tube. A Bradford assay was performed to determine the protein concentration of the nuclear protein.

2.2.6.4. Histology and Immunohistochemistry

A thoracotomy was performed on terminally anesthetized mice, hearts were removed, rinsed in ice cold PBS and a transverse slice of the apex was fixed in paraformaldehyde (4% in PBS) at 4 °C overnight. The remainder of the heart was snap-frozen in liquid nitrogen and used for biochemical analysis. Tissue was processed and stained by Tommy Reese (Department of Pathology, St. Luke's Episcopal Hospital, Houston, TX). Briefly, after fixation, heart tissue was dehydrated by incubating the tissue with increasing concentrations of ethanol (50%, 70%, 95%, and 100%). Tissue was cleared in xylene, imbedded in paraffin, sectioned using a microtome, and mounted on microscope slides. Slides were prepared for staining by removing the paraffin, rehydrating the sample with alcohol (100%), and rinsing (distilled water). Several slides from each animal were stained with hematoxylin and eosin (H&E). Hematoxylin stains nuclei blue and the counterstain eosin stains proteins pink. H&E staining was used to determine the outline of cardiomyocytes in order to quantify cell size and number. Several slides from each animal were also stained with CD31 (Platelet Endothelial Cell Adhesion Molecule-1: PECAM-1) and the number of capillaries were counted.

2.2.7. Biochemical Assays (Luciferase, β -galactosidase, CHiP)

2.2.7.1. Luciferase Reporter Constructs and Activity Assays

The following luciferase reporter constructs were designed and submitted to GenScript Corporation (Piscataway, NJ) for synthesis. The promoter region and upstream sequence (1kB) of the rat MuRF1 gene containing a putative MEF2 binding site was subcloned into a luciferase reporter plasmid pGL4.10 (Promega, Madison, WI). The same construct containing three adenine-to-cytosine mutations in the putative MEF2 binding site was also subcloned into the luciferase reporter plasmid pGL4.10 (Promega). Previous studies

have used A→C mutations within MEF2 binding domains to study MEF2-dependent transcription [336]. Luciferase reporter constructs pGL4.10 (1μg) were cotransfected with a vector encoding β-galactosidase (1μg) into H9c2 cells using the polymer-based DNA transfection reagent, PolyJet™ (SignaGen® Laboratories, Rockville, MD).

H9c2 myoblasts were grown to 85% confluency in 6-well plates and the medium (1mL) was changed one hour before transfection. Transfection mixtures (100μL) containing PolyJet™ (3μL), DNA (1μg of the MuRF1 promoter or the mutated MuRF1 promoter and β-galactosidase), and serum-free culture medium were added to each well; 12 hours later medium was replaced with fresh medium and treatments were started (AICAR and Compound C). For luciferase expression in response to aAMPK or dnAMPK, H9c2 myoblasts were transformed with either aAMPK, dnAMPK, or a null adenovirus (MOI 10) and 24 hours later were transfected with luciferase and β-galactosidase constructs using the same protocol. Twenty-four hours after transfection, cells were washed with ice-cold PBS and collected in 1X Reporter Lysis Buffer (100μL, Promega). Lysate was vortexed for 15 seconds, frozen in liquid nitrogen and thawed at 37°C, vortexed again for 15 seconds to completely lyse the cells, and centrifuged for 1 minute at 12,000g at 4°C. Samples were kept on ice for immediate analysis or snap frozen for future analysis.

Luciferase is an enzyme that catalyzes the oxidation of luciferin to oxyluciferin in the presence of ATP and magnesium. The reaction generates a luminescent signal with a half-life of 10 minutes that is detected by a fluorescent plate reader. A luciferase standard curve (consisting of tenfold dilutions from 5×10^{-12} to 5×10^{-21} moles/μL) was generated using Quantilum® Recombinant Luciferase (Promega) diluted in 1X Reporter Lysis Buffer (Promega) containing BSA (2mg). Luciferase activity was quantified in duplicate in wells containing luciferase standards, blank wells, and cell lysate (20μL). The POLARstar OPTIMA fluorescent plate reader (BMG Labtech) was set to take 10-one-second luminescent end point readings after automated injections of Luciferase Assay Reagent (100μL, Promega), with a Gain Adjustment (background) automatically detected at 4095. Values were averaged and normalized to β-galactosidase activity (see below).

2.2.7.2. β-galactosidase Activity Assays and Staining

A β-galactosidase expression plasmid was kindly provided by Dr. Joseph Alcorn, The University of Texas Health Science Center at Houston, Department Pediatrics. This plasmid comprises gene fusions between the simian virus 40 early promoter and *E.coli lacZ* [317]. β-galactosidase is an enzyme that cleaves β-galactosidic linkages, hydrolyzing

ONPG (o-nitrophenyl- β -D-galactopyranoside, colorless) to o-nitrophenol (yellow). The reaction is terminated with sodium carbonate and the reaction is analyzed spectrophotometrically by taking an absorbance reading at 420nm [334].

H9c2 myoblasts were transfected using PolyJet™ (SignaGen® Laboratories), collected in 1X Reporter Lysis Buffer (100 μ L, Promega), and lysed as described above. A standard curve was generated (0 - 6.0 milliunits) using β -galactosidase (1 unit/ μ L, Promega). Assay 2X Buffer (sodium phosphate buffer [200mM at pH 7.3], MgCl₂ [2mM], β -mercaptoethanol [100mM], and ONPG [1.33mg/mL], Promega) was added to cell lysate (50 μ L) in a 96-well plate. Samples were mixed well, covered, and incubated at 37°C for 3 hours. During this time a faint yellow color developed. The reaction was terminated with sodium carbonate (150 μ l of 1M) and the absorbance was read at 420nm using an ELx800 Absorbance Microplate Reader (BioTek). β -galactosidase activity was used to normalize luciferase activity in gene reporter assays.

β -galactosidase staining was performed on whole hearts from WT or desMEF2-*LacZ* transgenic mice using a modified protocol [337, 338]. Mice were anesthetized with pentobarbital and hearts extracted as described above. Hearts were rinsed with ice-cold PBS and incubated on ice in β -galactosidase fixative (paraformaldehyde [2%], gluteraldehyde [0.2%], EGTA [5mM at pH 8.0], MgCl₂ [2mM], and Na₃PO₄ [100mM at pH 8.0] in ddH₂O) for 90 minutes. Hearts were washed three times with washing buffer (MgCl₂ [2mM] sodium deoxycholate [0.01%], Nonidet P-40 [0.02%], and phosphate buffer [100mM at pH 8.0] in ddH₂O) for 20 minutes each wash. Hearts were incubated in β -galactosidase staining solution (K₄Fe(CN)₆ [5mM], K₃Fe(CN)₆ [5mM], X-gal [1mg/mL] in washing buffer) at room temperature overnight and photographed the next morning.

2.2.7.3. MEF2 Activity Assay

The activity of transcription factors, or the ability of transcription factors to bind to their respective DNA binding motifs, can be measured using an Enzyme-linked immunosorbent assay (ELISA)-based TransAM™ method (Active Motif). The consensus binding sequence for MEF2 is immobilized on a 96-well plate and the ability of “active” MEF2 in cell lysate to bind to the sequence is detected as follows. The immobilized MEF2 from cell lysate is detected with a primary antibody against MEF2, the MEF2 antibody is detected with a secondary antibody conjugated to HRP, and HRP intensity is quantified spectrophotometrically.

Nuclear fractions from NRVM and H9c2 myoblasts were isolated as described above and nuclear lysate (22 μ g in Complete Binding Buffer, 40 μ L total volume) was added to each well. Positive controls were provided by Active Motif and added to the plate as well. The plate was sealed and incubated for one hour at room temperature with gentle shaking. Wells were washed 3 times with 1X Wash Buffer (200 μ L, Active Motif), and incubated with a MEF2 antibody (100 μ L of 1:1000 in 1X Antibody Binding Buffer, Active Motif) for one hour at room temperature, covered. Washes were repeated and wells were incubated with an HRP-conjugated secondary antibody (100 μ L of 1:1000 in 1X Antibody Binding Buffer, Active Motif) for one hour at room temperature, covered. Washes were repeated and Developing Solution (100 μ L, Active Motif) was added to the wells. The plate was incubated for 2-10 minutes in the dark until a blue color was visible in the wells. The reaction was terminated using Stop Solution (100 μ L, Active Motif), and a yellow color was produced. The absorbance was read at 450nm and raw values were used to compare MEF2 “activity” between samples.

2.2.7.4. Proteasome Activity Assay

The proteasome “core” is made up of multiple subunits collectively referred to as the 20S proteasome [70, 71, 339]. The proteasome degrades proteins via trypsin and chymotrypsin proteases within its core. To measure proteasome activity, a fluorogenic substrate (Suc-Leu-Leu-Val-Tyr-AMC) is incubated with cell lysate [340]. Chymotrypsin proteases within the 20S proteasome (in the lysate) cleave the substrate which emits a signal at 460nm after excitation at 380nm.

20S proteasome activity was measured using a modified protocol and reagents from EMD Biosciences. Cells were collected or tissue was homogenized on ice as described above except in 1X Reaction Buffer (HEPES [25mM] and EDTA [0.5mM at pH 7.6]). Protein concentration was determined using the Bradford Assay. To each well in a black 96-well plate the following was added in order for a reaction volume of 190 μ L: protein lysate (20 μ g), 1X Reaction Buffer, and SDS (2 μ l of 3% [w/v]). The reaction was initiated by the addition of Substrate solution (10 μ L of 200 μ M fluorogenic substrate) and the fluorescence was recorded. Results are expressed as fold change of 20S proteasome activity.

2.2.7.5. Chromatin Immunoprecipitation Assay (ChIP)

Chromatin Immunoprecipitation (ChIP) is a method used to investigate interactions between proteins (such as transcription factors) and DNA [341, 342]. H9c2 myoblasts were grown in 100cm² dishes (a large amount of cells is required for this assay). Formaldehyde (final concentration of 1%) was added to the media to crosslink proteins and DNA. Cells

were incubated for 20 minutes with gentle shaking at room temperature. The cross-linking reaction was terminated by adding glycine (0.125M final concentration) to the media and gently rocking for 5 minutes. Media was poured off and cells were washed twice with ice-cold PBS. Cells (2 plates per condition were pooled together) were scraped in 5mL PBS per plate and were centrifuged for 5 minutes at 4000rpm at 4°C. The supernatant fraction was discarded and the pellet was resuspended in nuclei lysis buffer (250µL containing HEPES [50mM at pH 7.5], EDTA [1mM], NaCl [140mM], Triton X-100 [1%], Na-deoxycholate [0.1%], SDS [0.1%], and protease inhibitors) and incubated on ice for 10 minutes. Cells were sonicated on ice in the cold room (20 times for 5 seconds with at least 30 second intervals between each sonication). Samples were centrifuged for 10 minutes at 14,000rpm at 4°C. The supernatant fraction was transferred to a new tube and the lysate was precleared with Protein A agarose beads (50uL, Santa Cruz) for one hour at 4°C with rotation. The lysate was centrifuged for 5 minutes at 4,000rpm at 4°C and the supernatant fraction was transferred to a new tube. Ten percent of this “input” fraction was snap frozen in liquid nitrogen and stored at -80°C. MEF2 antibody (10µL, Santa Cruz) was added and the samples were incubated overnight at 4°C with rotation.

After incubation with the antibody, Protein A agarose beads (50uL, Santa Cruz) were added and the samples were incubated for 2 hours at 4°C with rotation. Samples were centrifuged for 2 minutes at 4,000rpm at 4°C. The supernatant fraction was discarded and the pellets were washed a total of 8 times with the following buffers: twice with ice-cold nuclei lysis buffer (1mL containing HEPES [50mM at pH 7.5], EDTA [1mM], NaCl [140mM], Triton X-100 [1%], Na-deoxycholate [0.1%], SDS [0.1%], and protease inhibitors), twice with ice-cold nuclei lysis buffer (1 mL containing HEPES [50mM at pH 7.5], EDTA [1mM], NaCl [500mM], Triton X-100 [1%], Na-deoxycholate [0.1%], SDS [0.1%], and protease inhibitors), twice with ice-cold buffer (1mL containing Tris base [20mM of pH 8.0], EDTA [1mM], LiCl [250mM], NP-40 [0.5%], Na-deoxycholate [0.5%]), and twice with ice-cold TE (1mL containing Tris-HCl [1M] and EDTA [0.5M]). For each wash the samples were incubated for 10 minutes at 4°C with rotation and then centrifuged for 1 minute at 4,000rpm at 4°C. After each wash, the resuspended pellet was transferred to a new tube to reduce the background.

After the last wash the antibody-protein-DNA complexes were eluted with IP elution buffer 1 (1mL containing SDS [1%], EDTA [1mM], and Tris-HCl [10mM at pH 8.1]), incubated at 65°C for 15 minutes, and centrifuged for 3 minutes at 14,000rpm at 4°C. The supernatant fraction was transferred to a new tube, and elution buffer 2 (1mL containing

SDS [0.67%], EDTA [1mM], and Tris-HCl [10mM at pH 8.1]) was added to the pellet, mixed well, and centrifuged for 3 minutes at 14,000rpm at 4°C. The supernatant was combined with the eluent from IP elution buffer 1 and SDS (20µL of 10%), and the volume was brought up to 250µL with TE. Samples were incubated overnight at 65°C to reverse the formaldehyde crosslinks.

Samples were centrifuged for 1 minute at 14,000rpm at 4°C, TE (250µL) and proteinase K (10µL of 10mg/mL) were added to each sample, and the samples were incubated for 1-2 hours at 37°C. LiCl (55µL of 4M) was added to each sample and the DNA was extracted once with Tris-buffered phenol (500µL) and once with chloroform (500µL), vortexing both times. Glycogen (2µL of 20mg/mL) was added to each sample, mixed well, ethanol was added (900µL of 100%), and DNA was precipitated on ice for 10 minutes. Samples were centrifuged for 30 minutes at 14,000 rpm at 4°C, the supernatant fraction was discarded, and pellets were air dried and resuspended in TE (20µL).

Immunoprecipitant products were amplified by PCR; the location within the MuRF1 promoter and the sequences of the primers are shown in **Figure 2.6.** and the PCR protocol is described in **Table 2.4.** PCR products were visualized by adding DNA loading buffer (5µL) and running the samples on 3% agarose gel with ethidium bromide at 50mV for several hours.

2.2.8. Amplification and Quantification of Adenoviruses

Adenoviruses expressing active AMPK α 2 (aAMPK), dominant-negative AMPK α 2 (dnAMPK), or a null control were purchased from Eton Biosciences Inc. (San Diego, CA). The adenovirus encoding aAMPK expresses a truncated form (amino acids 1-312) of the alpha (active) subunit of AMPK. Amino acids 1-312 lack the $\beta\gamma$ binding domains and auto-inhibitory domain but retain the activating phosphorylation site (Thr192), thus encoding an active kinase [343]. The adenovirus encoding dnAMPK contains a K45R mutation within the kinase domain and thus lacks kinase activity, acting as a dominant negative form of the kinase [344].

Adenoviruses expressing active AMPK α 2 (aAMPK), dominant-negative AMPK α 2 (dnAMPK), or a null control were amplified in HEK293 cells using a modified protocol [345]. HEK293 cells were grown to 80% confluency, medium (Eagle's MEM with 10% FBS) was replaced, and four-100mm² plates of confluent cells were infected with 15µL of stock aAMPK, dnAMPK, or null adenovirus (2x10⁹ PFU/mL). Cells were incubated for 5

CCTCCCAGATGACAAGCATGTCCAGGACACAGACAGCAGCAAGGCCCTCCCCTTTA
 CACACCGCTGATCCAAACCCACTCTCCACTGCCTGGGCTGCTCTTGTTGCCTTCCGCT
 CGAGCTGTTCTTCAGGACA **GGATTTCCTTCGTAGTCCTTGGTTT**TCATCTCTCCCTTC
 CCCTCCCCCTCAGGTGATCTGAATGTATCAACCTGTTCCCAAACACACCTCCACAGAG
 ACACAAGCTCGTTAGGGGCTGTGTCTCAGAGCCACCGCTGCTGGCTGTGTGACTTTTC
GGGGTTGCTATGCCTCTCTGGCCTAACCTGTCTGTCCACGAATGGGGGTGCAAGG
 GTTCTCCCACTGTAGACTGTTCAAGGTGGAGACTTGAACCTAAGCCCTAATCCCATATG
 CTAGGCAAGTGCTCTATCATTAAAGCCATATTGCTAGCTTTCTTTTTTTAAAAACCCTTTT
 TAAATAAAATTTATTTTTCTTCTTCATGTGCGTGTTTTGCATGAATGCATTTCTGTACACC
 ATGTTCAAGCCAGAAAAGGTATCGGATCCCTTGGAACTAGAGTTTCAGACAATTGTGAA
 CTAAAACGTGGGTGCTGGGATTTGAACCCAGGTCTCTGAAAGAGCAGCTGGGATTCT
 TAGCCGATGAGCTATCTCTAGCCCCTACTATTTTAAAATTTTAATTTTTTTTTATTTTA
 TGTATATTATGTGCCTCACAAGCATGCAGTTCTCATGCCGCCAGAAGAGGGAGCCAG
 ACCTCCTGGAAGTGAATAACTTGCGAGCTGCCACCTGGATGCCAGGAACCAAACCCT
 GGTCTTCTGCTCTGTCTTTTTACTTTTTAAAACGCATTTTTAAACAAGGAGATGGTGACA
 CACACCTTCAATCCTAGTACTTGGGGGTGGGGGGGCAGATGTTTACAAAGCACGTTCC
 ATGATAGCCAGGACCACAGCAACTCTGTCTCTTAAAACCTAAAACCAAACCAAAA
 CAAAAACCCCATATTTAATACCTGTTCTTTTGGGGTTTGTGGTGAGGGGTCTGGGTG
 GTGACTGGGGGTGTGTAGTGACATTATTTTGTATTTTGTGATAGGGTCTCATATAGTC
 CAGGCTTGCTTTGAACTCCTGCCTCTGCCTTCTAAGTACTGGGGTTATTGGCATTACC
 CATCATGCCCTGCTTTACCTTTTATTCCAAGACATGATATCACTATGTAGCTCATGGCC
 TTAACCTTTGGATCCTCCTGCCTCAGCCTCCTGAGGAGCTGGGAATATAGGCTGCAGA
 TCACCCGCTCTTAGAACTCTGTTCACTCCTGTCTCCAGAGAACCCCATATTCCAATGCC
 CCGGAAGTTCTTCTGGGACCCAAGAATGAACACATATGTAAAGAGTCCAGTGGAGCC
 TCCTGTATCCACAGGTGTCAGGGCAGGTTCTGAGGCAGCACAGGAAGTTCCTGTTTGT
 CTCTGGGCTGTGAGCATGGCAGTTCAGGGAAAACACAGGAACCTGGGAAGGCAAGTT
 GTCAGCCTTGGCGGCAAGCACCTTTACCCACTGAGCCATCGAGCTGGCCCTCATGAA
 ACCCTTGTGAGCATGTAGTGTGATGATTGGCTGAGGGCTGTCAGGGTGGGCTGCCCA
 ACATGGGAGTCTCAAAGACTCTAGTGAATGCTTGACTGGAGTCTGGGGCAGGAGA
 AAGCCCTTTCACAGAAGGGCTATCCCAAGGCCTTAGAGCTGTTTCAAGTCCAGAAGGG
 GAACAGACTTAGGTTGGTACAGGGGCGCTGGCTGTTAATCTTGTGTATGCCAACCCCA
 CCCCCACCCAAGTTCCTACTCCCTTACTCCCAATCACTGGAGGGGCAGGAGGGTGG
 AGACCAACTTCTTCATGAACTAGGGTACCTGGCCCTCCCCTGAACCTGGCTCTGAAC
 AATCTGTTCTTGTTTACGACCCCCATTGCAGGGCAACAGCGATTGCTCACCCCTGCAT
 GTGATCTGAGAGGGCCAAATCTTTGAGGCCTGGAGGAACTCAAGCCCTGCCAGCCG
CTTGGCTTCGGAATGCTCAGCTGGTCCCCTCCTGGGGCTCATGTGACTGAAGGGCAG
CTATCCCTATCAGAAGGGCCTCAGACCAAGACAGAAGCCGGGTGTT **CGGGGAGGAAG**
ACAAAGAGGATCCGAGTGGGATCCCTTCCACTCGGTGTGACGCAGGTGGAAGAGACA
 GTCGCAGTTTCGAAGCAAT **ATG**GATTATAAATCTGGCTTGATTCCGGACGGAAATGCT
 ATGGAGAACCTGGAGAAGCAG

Figure 2.6. MuRF1 promoter sequence and ChIP primers.

Rat MuRF1 promoter sequence was used to generate primers for amplification of MEF2 ChIP products. **Yellow** highlighted sequence: potential MEF2 binding sequence; **Red** highlighted sequence: Start codon; **Blue** highlighted sequences: ChIP primers, MEF2 binding region; **Green** highlighted sequences: ChIP primers, distal region.

PCR Reaction Mix		PCR Protocol
10X PCR Buffer	5.0 μ L	95°C x 3 minutes
MgCl ₂ (50mM)	1.5 μ L	94°C x 45 seconds 60°C x 45 seconds 72°C x 45 seconds } x 32 cycles
dNTP's (2.5mM)	4.0 μ L	
Forward Primer	2.5 μ L	
Reverse Primer	2.5 μ L	
Taq (Invitrogen)	0.3 μ L	72°C x 10 minutes
DEPC-treated H ₂ O	7.2 μ L	
DNA	2.0 μ L	4 °C x ∞

Table 2.4. ChIP PCR primers and protocol.

PCR was performed on DNA from chromatin immunoprecipitation. The primers are listed in Figure 2.6. See text for details.

days until cytopathic effects were evident in 80% of the cells. Cells were collected, pooled, and centrifuged at room temperature for 5 minutes at 1000rpm. The supernatant fraction was stored at -20°C while the pellet was resuspended in 10mL of the supernatant fraction. The cell pellet was lysed by three consecutive freeze-thaw cycles in liquid nitrogen and in a 37°C water bath and vortexed after each thaw cycle. After the third cycle, debris was centrifuged at room temperature for 5 minutes at 1000rpm, and the pellet was discarded.

The viral titer in the crude lysate (combined with the supernatant fraction stored at -20°C) was determined using a modified version of the protocol available in the AdEasy™ Viral Titer Kit (Stratagene) [346]. HEK293 cells were plated in a 24-well plate at a density of 2.2×10^5 per well in 0.5mL media. Several hours after plating 10-fold serial dilutions of the viral stock from 10^{-1} to 10^{-5} were made and added (85µL of each dilution) to the cells in duplicate. After 18 hours of incubation at 37 °C in 95% air, 5% CO₂, media was removed and plates were dried for 5 minutes at room temperature. Cells were fixed by incubating with ice-cold methanol (0.5mL of 100%) at -20°C for 10 minutes, washed twice with PBS (0.5mL containing BSA [1%]), and incubated with an anti-hexon primary antibody (1:500 PBS with 1% BSA) at 37 °C for an hour. This antibody recognizes the hexon protein, a major coat protein on adenoviruses. Cells were washed twice with PBS (0.5mL containing BSA [1%]), and incubated with an HRP-conjugated secondary antibody (1:1000 PBS with 1% BSA) at 37 °C for an hour. The secondary antibody was removed and the cells were washed twice with PBS (0.5mL containing BSA [1%]) and incubated with DAB (3,3' Diaminobenzidine) substrate for 15-20 minutes at room temperature. In the presence of horseradish peroxidase (HRP-conjugated secondary antibody), DAB produces a brown precipitate visible using a light microscope.

To determine the titer of the amplified viruses, the number of DAB-positive cells was quantified. The infectious units per milliliter of virus (IFU) were calculated using the following formula:

$$IFU = \frac{\text{Average number of positive cells per field} \times \text{Number of fields per well}}{\text{volume of diluted virus per well (mL)} \times \text{dilution factor}}$$

The IFU values were then used to calculate the volume of adenovirus needed for experiments using the following equations, where MOI is multiplication of infectivity.

$$\text{Cells per well or plate} \times \text{desired MOI} = \text{Total IFU needed}$$

$$\frac{\text{Total IFU needed}}{IFU} = \text{virus needed per well or plate (mL)}$$

Due to high amplification, experiments performed using these viruses required a low MOI.

2.2.9. Quantitative Real Time RT-PCR (qRT-PCR) Transcript Analysis

Quantitative real time RT-PCR (qRT-PCR) is a method used to analyze expression of specific RNA sequences. RNA is reverse transcribed to DNA using a gene-specific reverse primer. The DNA is then amplified using gene-specific forward and reverse primers and a gene-specific probe. The probe is conjugated on either end to a fluorophore and a quencher, and when in close proximity, the fluorophore is quenched. As Taq polymerase amplifies the DNA, its exonuclease activity breaks down the probe, disrupting the reporter-quencher proximity and allowing for the detection of the fluorescent signal. The amount of fluorescence detected is proportional to the amplified sequence.

2.2.9.1. Design and Verification of qRT-PCR Assays

Assays for quantitative real time RT-PCR (qRT-PCR) were designed using Primer Express® Software. The coding DNA sequence of the gene of interest, including the splice sites, was obtained and exported into Primer Express. Forward and reverse primers were designed with the following parameters: 18-26 nucleotides in length, melting temperature (T_m) between 59-61°C, GC content between 40-60% with no GC clamp residues, no more than 3G/C nucleotides in a row, low primer dimer formation, and contain a secondary structure that is easily linearized. Probes were designed with the following parameters: 27-30 nucleotides in length and no more than 3G/C nucleotides in a row with the fluorophore 6-carboxyfluorescein (FAM) conjugated to the 5'-end of the probe and the quencher tetramethylrhodamine (TAMRA) conjugated to the 3'-end. Assays were designed to be 80-120 nucleotides in length and the sequences of the amplicons were tested for specificity *in silico* using BLAST (Basic Local Alignment Search Tool) [347]. The assays were tested using the buffers and protocol below, and the product was run on a 2% agarose gel in TBE buffer (Tris base [1.08g], Boric acid [5.5g], EDTA [20mL of 0.5M] in 1L DEPC-treated water) to verify the specificity of the amplicon.

2.2.9.2. Gene Expression Analysis using qRT-PCR Assays

Gene expression analysis was performed on total RNA (60-120ng) as previously described [199, 348]. cDNA standards spanning the entire length of each amplicon, reverse and forward primers, and Taqman® probes were purchased (**Table 2.5.**) (Sigma). For each gene expression assay cDNA was serially diluted to generate a standard curve ranging from 20pg-0.2fg. Additionally, non-template controls (NTC, without mRNA) and non-amplification controls (NAC, without reverse transcriptase) were used. qRT-PCR was performed in two

steps in the same 96 well plate. RNA was reverse transcribed with Superscript™ II (Invitrogen) using a modified version of the manufacturer's protocol. Reverse transcription buffer (5X First-Strand Buffer [1μL] (containing Tris-HCl [250mM, pH 8.3 at room temperature], KCl [375mM], and MgCl₂ [15mM]), dNTP mixture [1.2μL of 2.5mM], DTT [0.6μL of 0.1M], reverse primer [0.1μL of 20μM], DEPC-treated water [0.6μL], and Superscript™ II [0.03μL]) was added to the RNA sample (1.5μL), incubated at 50°C for 30 minutes, and the reaction was inactivated at 75°C for 5 minutes. Samples were then placed on ice and mixed with PCR buffer (10X PCR buffer [2.5μL, comprised of Tris-HCl [200mM, pH 8.4] and KCl [500mM]), dNTP mixture [2.5μL 2.5mM], MgCl₂ [1.3μL of 50mM], reverse primer [0.6μL of 20μM], forward primer [0.6μL of 20μM], Taqman™ probe [0.25μL of 10μM], DEPC-treated water [11.75μL], and Taq polymerase [0.5μL]). The DNA was denatured at 95°C for 1 minute and amplified with 40 cycles of PCR (95°C for 12 seconds, 60°C for 1 minute).

Gene expression was analyzed using ABI Prism® 7000 Sequence Detection System Software. The results are visualized on an amplification plot comparing the cycle number (independent value) and the ΔR_n (magnitude of the fluorescent signal, dependent value) (**Figure 2.7.A.**). When the ΔR_n is plotted on a linear scale the baseline can be determined (**Figure 2.7.B.**). The baseline is the initial PCR cycles that yield no or little fluorescence signal. Once the baseline is set, the threshold can be defined by plotting ΔR_n on a logarithmic scale. The threshold is set above baseline and intersects with the amplification plot to define the C_T , the cycle number in which the fluorescence passes through the threshold. Once the baseline and threshold have been defined, the standard curve can be evaluated. The standard curve is plotted on a linear scale: C_T versus the concentration of cDNA [Log(CO)]. The efficiency (E) of the PCR can be determined from the slope of the standard curve (**Figure 2.7.C.**) using the following formula:

$$E = 10 \times \frac{-1}{\text{slope}} - 1$$

A good PCR reaction should have an efficiency between 90-110% or a slope between -3.58 and -3.10 and the coefficient of correlation (R^2) for the standard curve should be >0.99 [349-352]. Once all settings were adjusted, the absolute copy number of each transcript, measured in triplicate, was used for comparison between samples.

Quantitative Real Time RT-PCR (qRT-PCR) primer and probe sequences		
Transcript	Primer/Probe	Sequence
mAtrogin-1	590F (forward primer)	TGTATCGGATGGAGACCATTTC
	677R (reverse primer)	GTGATCGTGAGGCCTTTGAAG
	620T (probe)	AGCAGCAGCTGAATAGCATCCAGATCA
mMuRF1	29F (forward primer)	ATGGAAACGCTATGGAGAACCCT
	170R (reverse primer)	GGATTCGCAGCCTGGAAGAT
	115T (probe)	TGCCAACACAACCTCTGCCGGAA
rAtrogin-1	371F (forward primer)	GGCTGTTGGAGCTGATAGCA
	505R (reverse primer)	CATGACTTTTCAGGAACCTTCTGGTCCG
	rAtrogin-1 (probe)	CACATCCCTGAGTGGCATCGCC
rMuRF1	487F (forward primer)	TTCCAAGGACAGAAGACTGAACTG
	582R (reverse primer)	TTCTTGGTCACTCGGCAG
	519T (probe)	CATCTCCATGCTGGTGGCAGGGAAC
r/mUCP3	r/mUCP3 (forward primer)	GTGACCTATGACATCATCAAGGA
	r/mUCP3 (reverse primer)	GCTCCAAAGGCAGAGACAAAG
	r/mUCP3 (probe)	CTGGACTCTCACCTGTTCACTGACAACCTTCC
r/mGLUT4	783F (forward primer)	CCCCGATACCTCTACAT
	872R (reverse primer)	CTGCCCGAAAGAGTCTAAAGCGCCT
	r/mGLUT4 (probe)	GCATCAGACACCATCAGCCCAG
mMHCα	1907F (forward primer)	GCAAAGGAGGCAAGAAGAAAGG
	1990R (reverse primer)	TGAGGGTGGGTGGTCTTCAG
	1942T (probe)	ACAGTGTCTGCTCTCCACCGGGAA
mMHCβ	1650F (forward primer)	AGGGCGACCTCAACGAGAT
	1744R (reverse primer)	CAGCAGACTCTGGAGGCTCTT
	mMHC β (probe)	AGCTCAGCCATGCCAACCGTA
rANF	rANF (forward primer)	AGTGCGGTGTCCAACACAG
	rANF (reverse primer)	CTTCATCGGTCTGCTCGCT
	rANF (probe)	TCTGATGGATTTCAAGAACCCTGCTAGACCAC
rGLUT1	697F (forward primer)	CATCGTCTGGTGGGATCCTTA
	749R (reverse primer)	GAGACAGTAGAGGCCACAAGTCT
	rGLUT1 (probe)	AGGTGTTCCGGCTTAGACTCCATCATGG
m/rAtg12	195F (forward primer)	AGGCTGTAGGAGACACTCCATAA
	276R (reverse primer)	GAAGTCGATGAGTGCTTGGACAGT
	m/rAtg12 (probe)	AAAACGAAGAAATGGGCTGTGGAGCGG
h/m/rBeclin	466F (forward primer)	CCTCAGCCGAAGACTGAAGGT
	547R (reverse primer)	CTCACAGAGTGGGTGATCCACAT
	h/m/rBeclin (probe)	TTTGACATCATGTCCGGCC
m/rAtg5	m/rAtg5 (forward primer)	GGTGATCAACGAAATGCAGAGAA
	m/rAtg5 (reverse primer)	GTCCAAAACCTGGTCAAATCTGTCA
	m/rAtg5 (probe)	ACCACAAGCAGCTCTGGATGGGACTG
LC3	LC3 (forward primer)	GTGGAAGATGTCCGGCTCAT
	LC3 (reverse primer)	CTCCCCCTTGTATCGCTCTATAATCA
	LC3 (probe)	AGCAGCACCCACCAAGATCCCA

Table 2.5. Quantitative Real Time RT-PCR (qRT-PCR) primer and probe sequences.

Forward primers, reverse primers, and probes used to analyze specific mRNA levels. See text for details.

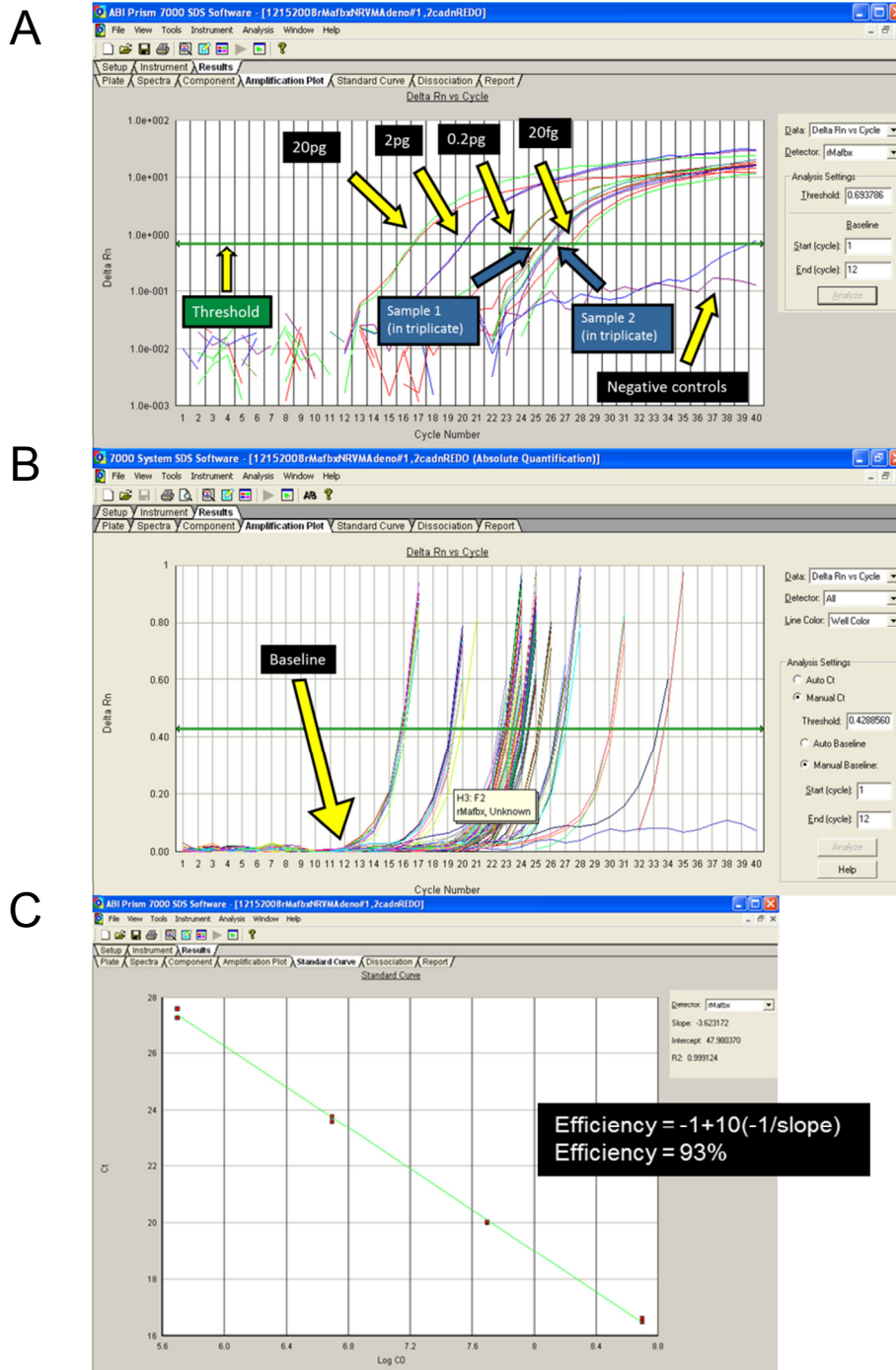


Figure 2.7. Quantitative Real Time RT-PCR analysis.

(A) An amplification plot comparing the cycle number (independent value) and the ΔR_n (magnitude of the fluorescent signal, dependent value). 10 fold dilutions of the cDNA are used as a standard curve. The concentration of cDNA used (20pg – 20fg) is labeled in black. Two representative samples are shown in triplicate and labeled in blue. The threshold is shown in green. (B) 82-97 R_n is plotted on a linear scale to determine the baseline (shown here: cycle 12) and the start cycle (baseline cycle minus 3; in this case 9). (C) The standard curve is plotted on a linear scale to determine the efficiency of the reaction. See text for details.

2.2.10. SDS-PAGE, Western Blot Analysis and Quantification

Proteins are separated by charge and mass using polyacrylamide gel electrophoresis (PAGE). While nondenaturing PAGE separates proteins according to their mass-to-charge ratio, denaturing /reducing SDS-PAGE separates proteins solely by mass. SDS denatures proteins and makes them evenly negatively charged, thus they migrate from a negatively to a positively charged electrode. SDS-polyacrylamide gels ranging from 8-12% were used to analyze protein content and posttranslational modifications of proteins. A lower percentage gel is used to separate larger proteins and higher percentage gel for smaller proteins.

Gels were cast in a two-step fashion. The lower “resolving” gel contained the percentage desired for separation, and the upper “stacking” gel (comprised of lower percent acrylamide and lower pH) concentrated proteins before being resolved. To cast two gels, components were combined in the following order. For 10% resolving gels: 8mL resolving/lower buffer stock (Tris base [36.3g], SDS[0.8g], adjusted to pH 8.8 in ddH₂O [200mL]), Acrylamide/Bis (10.5mL of 30%), water (13.4mL), APS (540μL), and TEMED (54μL). For stacking/upper gels: 2.5mL stacking/upper buffer stock (Tris HCl [6g], SDS [0.4g], adjusted to pH 6.8 in ddH₂O [100mL]), Acrylamide/Bis (1.5mL of 30%), water (6.0mL), APS (90μL), and TEMED (9μL). Once the resolving gel was poured (80% of total casting height), a layer of isopropanol was slowly pipetted over the gel to ensure a smooth transition from stacking to resolving gels. Once the resolving gel had solidified, the isopropanol was poured out, the stacking gel was poured, and the combs were put in place. When the stacking gel was solidified, the gel running apparatus was assembled, the combs were removed, running buffer (Tris base [6g], Glycine [28.8g], SDS [1g] in water [1L]) was added, and the wells were rinsed with running buffer.

Protein (10-20μg/μL in 5X loading buffer) (Tris base [312.5mM], glycerol [10%], and SDS [11.5%]) was boiled for 5 minutes at 100°C and cooled to room temperature before running gels. One lane was loaded with a protein standard (10μL) and the other lanes with the appropriate amount of protein. Gels were run at 50mV until the protein traveled through the stacking gel and 100mV thereafter.

Separated proteins were immobilized for analysis by transferring them to a PVDF (PolyVinylidene Fluoride) membrane by western blotting using a wet transfer method. The principle behind the electrophoretic transfer of proteins to a membrane is based on Ohm's law.

$$V (\text{voltage}) = I (\text{current}) \times R (\text{resistance})$$

Proteins migrate to the membrane following a current generated by applying a voltage across electrodes.

PVDF membranes were briefly soaked in methanol, rinsed several times with ddH₂O, and stored in transfer buffer (Tris base [144g], Glycine [30g], SDS [0.5g] in water [1L]) until used. Sponges and filter paper were also soaked in transfer buffer until used. A “sandwich” was created between the plastic supports of a transfer cassette such that the order from the bottom of the cassette (the side facing the cathode) to top (the side facing the anode) was sponge, filter paper, gel, PVDF membrane, filter paper, sponge. Air bubbles between the gel and membrane were gently rolled out of the sandwich using a conical tube and the cassette was closed and placed in the proper orientation within the cassette case. An ice pack was added to the cassette case which was then filled with transfer buffer. Gels were transferred at 4°C for 75 minutes at 110mV with stirring.

Once transferred, membranes were briefly rinsed with water and placed in Ponceau stain with gentle shaking for several minutes. Ponceau stain has a negative charge and binds to positively charged amino acids of proteins for visible detection on the membrane. This stain is used to verify the even transfer of proteins and to aid in cutting membranes at different molecular weights for simultaneous detection of several proteins. Ponceau stain is easily removed by rinsing with water, but complete removal of the stain is not necessary because there is no noticeable change in antibody detection of proteins. Once rinsed, membranes were incubated with primary antibodies overnight at 4°C with gentle rocking. Membranes were washed 3 times for 5-10 minutes in TBST with gentle shaking and incubated with HRP (horseradish peroxidase)-conjugated secondary antibody (in 5% milk in TBST) for 1 hour at room temperature. Membranes were then washed 3 times for 5-10 minutes in TBST with gentle shaking and developed using Western Blotting Luminol Reagent. HRP (conjugated to secondary antibodies) converts the substrate in the luminol reagent to a chemiluminescent precipitate which is then captured on film. After developing, antibodies were removed from the membrane by incubating them in stripping buffer (Tris HCl [6mL of 1M at pH 6.8], SDS [19.2mL of 10%], β-mercaptoethanol [0.675mL], ddH₂O [70mL]) for 75 minutes at 60°C with gentle shaking. Membranes were briefly rinsed with ddH₂O and washed 3 times for 10 minutes in TBST with gentle shaking. Membranes were then reprobed for other proteins using the same protocol.

To quantify protein levels, films were scanned and Adobe Photoshop was used to convert the films to a standard black and white setting for consistent analysis. Images were

saved as tiff files and densitometric analysis was performed with ImageJ software. The densities of proteins on the same film were compared using a normalizing protein such as β -tubulin or GAPDH.

2.2.11. Protein Turnover Assays

Protein turnover was assessed using pulse-chase analysis. Radiolabeled amino acids in the cell culture medium are incorporated into newly synthesized proteins during the “pulse” period. Cells are collected over time and radioactivity measurements are used to calculate rates of protein synthesis. To determine protein degradation, the cells are pulsed with radiolabeled amino acids. After the “pulse” period, medium containing radiolabeled amino acids is washed away and replaced with non-radioactive medium. Aliquots of medium over time are taken during the “chase” period, and the radioactivity measurements are used to calculate protein degradation rates. The amino acid used for pulse-chase analysis is critical in order to accurately determine protein turnover rates. The intracellular concentration of the amino acid used must be stable. Additionally, the amino acid must be readily taken up by the cell and have a detectable rate of incorporation into proteins, but should not be synthesized, degraded, or converted to other amino acids within the cell. In the heart, phenylalanine (Phe) fits all criteria and thus has been used to measure protein turnover in the heart and in isolated cardiomyocytes [353, 354].

Radioactivity is assessed using liquid scintillation counting [355]. Radioactive samples are mixed with scintillation fluid containing an aromatic solvent and one or several luminophors (scintillants). Samples containing carbon-14, for example, emit β particles that transfer energy to the solvent and subsequently to the luminophors. The excited luminophors emit light that is detected by the scintillation counter. Radioactivity is measured as counts per minute (CPM), the detectable decay of atoms per minute. CPM is then converted to disintegrations per minute (DPM), the “corrected” number of atoms that have decayed per minute. DPM values were used for comparisons between samples.

To measure protein synthesis rates, NRVM or AMCM were incubated with pulse medium containing radiolabeled Phe (1 μ Ci/mL [14 C]) and cells were collected at various time points. Cells were washed with ice-cold PBS and cells were incubated at 4°C overnight in TCA (700 μ L of 10% in ddH₂O per well in a 6-well plate). Cells were scraped and collected in eppendorf tubes and centrifuged at 21,000g for 5 minutes at 4°C. The supernatant fraction was discarded and the cell pellet was resuspended in buffer (100uL of Triton X-100 [1%] and NaOH [1M]). The lysate (85uL) was added to glass scintillation vials (containing scintillation

fluid [10mL]) and counted using the following counting protocol: 2 counting cycles with 1 minute count time and no sigma coincidence [356].

To measure protein degradation rates, NRVM or AMCM were incubated with “pulse” medium containing radiolabeled Phe (1 $\mu\text{Ci}/\text{mL}$ [^{14}C]) for 24 hours prior to adenovirus infection or 48 hours prior to treatments. After 48 hours of incubation, media were switched to chase medium. Aliquots of chase medium (500 μL) were collected over 24 hours, combined with TCA (500 μL of 20% in ddH₂O) and incubated at 4°C overnight to precipitate proteins. Precipitated proteins were centrifuged 9600g for 5 minutes at 4°C. The supernatant fraction (950 μL) was added to glass scintillation vials (containing scintillation fluid [10mL]) and counted using the protocol described above. Cells were also collected and the radiolabeled Phe remaining in the cells was measured as described above. The acid-soluble radioactivity from the chase medium was used to denote the amount of protein degraded over time while total protein was used for normalization. Results are expressed as percent protein degradation or fold change over control [356].

2.2.12. Statistical Analysis

Results are expressed as means \pm SEM. Analysis was performed using two-tailed, unpaired Student's t test or one-way ANOVA with Tukey post hoc test. A value of $P < 0.05$ was considered significant.

Chapter 3

THE ROLE OF 5'-AMP-ACTIVATED PROTEIN KINASE IN PROTEIN DEGRADATION IN THE HEART

“Scientific principles and laws do not lie on the surface of nature. They are hidden, and must be wrested from nature by an active and elaborate technique of inquiry [357].”

~John Dewey, PhD. (1920)

3.1. Nutrient Deprivation Upregulates Markers of Protein Degradation in Cardiomyocytes

As outlined already in Chapter 1, protein degradation, specifically protein degradation through the ubiquitin proteasome system (UPS), has been extensively studied in skeletal muscle. Comparatively less is known about the cardiac UPS. In skeletal muscle and in the heart, nutrient deprivation *in vivo* leads to enhanced protein degradation. Nutrient deprivation increases expression of the ubiquitin ligases Atrogin-1 and MuRF1 in myotubes [141], but whether the absence of nutrients regulates expression of Atrogin-1 and MuRF1 in cardiomyocytes is not known.

To test the hypothesis that Atrogin-1 and MuRF1 are regulated by nutrient deprivation in cardiomyocytes, I first isolated and cultured neonatal rat ventricular cardiomyocytes (NRVM) under a variety of nutrient deprivation conditions. Complete nutrient deprivation significantly increased Atrogin-1 and MuRF1 expression over time. Atrogin-1 mRNA levels increased quickly (3.5 fold increase with 2 hours of nutrient deprivation) and continued to increase to greater than 5 fold after 24 hours. MuRF1 mRNA also increased over time, nearly 4 fold after 24 hours (**Figure 3.1.A.**).

To determine the consequence of enhanced expression of the ubiquitin ligases, I analyzed their protein levels. After 24 hours of nutrient deprivation, both Atrogin-1 and MuRF1 protein levels increased. Furthermore, AMPK activity, denoted by its phosphorylation status, was significantly enhanced (**Figure 3.1.B.**). It is an established fact that nutrient deprivation decreases the ratio of [ATP]/[AMP] and, consequently, activates AMPK [224]. My results now demonstrate that nutrient deprivation also activates AMPK in cardiomyocytes, and thus activation is associated with increased mRNA and protein levels of Atrogin-1 and MuRF1.

The IGF-1/AKT pathway is downregulated with nutrient deprivation in skeletal muscle which permits FOXO to initiate transcription of target genes [145]. Indeed, FOXO3A regulates Atrogin-1 in the heart [144]. Because Atrogin-1 and MuRF1 are upregulated under a variety of conditions, and complete nutrient deprivation can affect multiple pathways simultaneously, I focused on an as yet unexplored pathway that could regulate their expression, namely AMPK.

To determine whether AMPK is involved in regulating Atrogin-1 and MuRF1, NRVM were incubated without glucose. Glucose deprivation activates AMPK. Even though glucose deprivation activates other pathways as well, potentially fewer pathways are activated than what occurs with complete nutrient deprivation. Glucose deprivation increased Atrogin-1

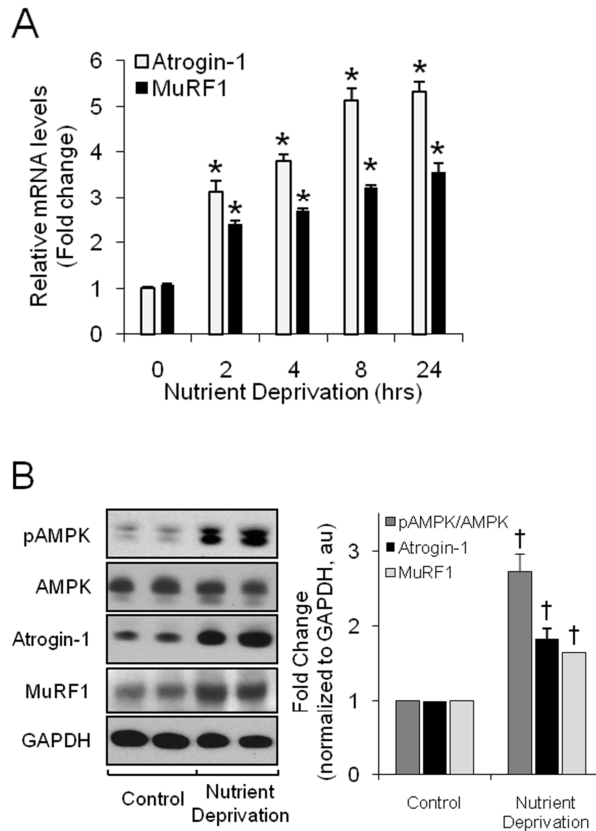


Figure 3.1. Regulation of ubiquitin ligases and AMPK by nutrient deprivation in cardiomyocytes.

(A) Atrogin-1 and MuRF1 expression in response to nutrient deprivation. NRVM were isolated as described in “2.2.4. Isolation of Neonatal Rat Ventricular Cardiomyocytes” and incubated overnight in culture medium. NRVM were washed twice with phosphate buffered saline (PBS) and incubated in PBS for the remainder of the experiment. NRVM were collected in TRI Reagent® 0, 2,4,8, and 24 hours after PBS incubation. RNA was isolated and quantified as described in “2.2.6.1. Total RNA Isolation and Quantification”. Quantitative real time PCR was performed as described in “2.2.9. Quantitative Real Time PCR (qRT-PCR) Transcript Analysis”. Data are expressed as mean fold change \pm SEM of 3 independent experiments performed in triplicate. (B) Atrogin-1, MuRF1, pAMPK, and AMPK protein levels in response to nutrient deprivation. NRVM were incubate in PBS for 24 hours, collected in cell lysis buffer, and protein concentration was determined as described in “2.2.6.2. Protein Isolation and Quantification”. Protein and phosphorylation levels were determined as described in “2.2.10. SDS-PAGE, Western Blot Analysis and Quantification”. A representative western blot is shown on the left. Data are expressed as mean fold change \pm SEM of 3 independent experiments performed in duplicate. * $P < 0.01$ versus control, † $P < 0.01$ versus respective controls. pAMPK, phosphorylated AMP-activated protein kinase; AMPK, AMP-activated protein kinase; GAPDH, Glyceraldehyde 3-phosphate dehydrogenase. Reprinted with permission from KK Baskin and H Taegtmeier, AMP-activated protein kinase regulates E3 ligases in rodent heart, *Circulation Research*, 109, 10, 1153-1161 [358].

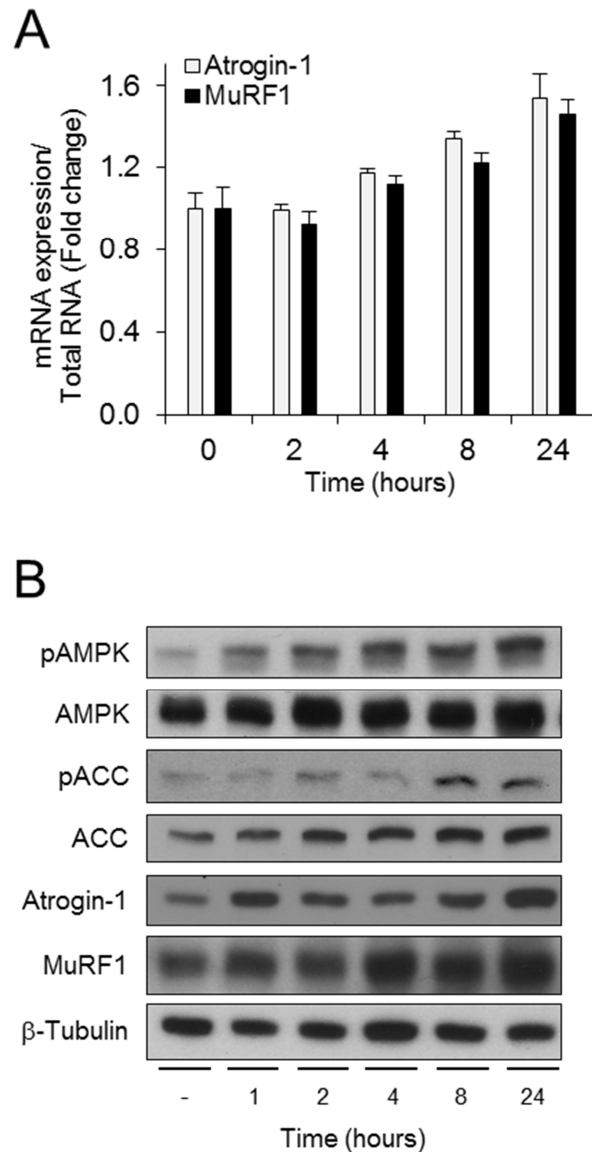


Figure 3.2. Regulation of ubiquitin ligases and AMPK by glucose deprivation in cardiomyocytes.

(A) Atrogin-1 and MuRF1 expression in response to glucose deprivation. NRVM were isolated and incubated overnight in culture medium. NRVM were washed twice with phosphate buffered saline (PBS) and cultured in glucose-free culture medium for the remainder of the experiment. RNA was isolated from NRVM collected at the times indicated and qRT-PCR was performed. Data are expressed as mean fold change \pm SEM of 3 independent experiments performed in triplicate. (B) Atrogin-1, MuRF1, pAMPK, AMPK, pACC, and ACC protein levels in response to nutrient deprivation. A representative western blot from NRVM incubated in glucose-free medium for the times indicated is shown here. pACC, phosphorylated acetyl-CoA carboxylase; ACC, acetyl-CoA carboxylase.

and MuRF1 mRNA expression (**Figure 3.2.A.**); albeit to a lesser extent than with complete nutrient deprivation. Protein levels of both ligases were also significantly increased with glucose deprivation, most prominently, after 24 hours (**Figure 3.2.B.**). These data demonstrate a correlation between nutrient deprivation, AMPK activation, and Atrogin-1 and MuRF1 expression. However, the consequence of nutrient deprivation had not been investigated in cardiomyocytes before.

Fasting also increases protein degradation in the heart *in vivo*, but the mechanisms by which this occurs have not yet been explored [309, 359]. As a first step I investigated the consequence of nutrient deprivation on protein degradation in NRVM using pulse-chase analysis (as described in Chapter 2 in section 2.2.11. “Protein Turnover Assays”). The results shown in **Figure 3.3.** are expressed as percent total protein degraded after 24 hours of nutrient deprivation. To determine the relative contribution of proteasome- and autophagy-mediated protein degradation, I used inhibitors for both pathways (Bortezomib and 3-methyladenine (3-MA), respectively). Protein degradation was significantly decreased with Bortezomib or with 3-MA treatment under complete nutrient conditions (**Figure 3.3.**). However, protein degradation was enhanced with nutrient deprivation but could be reduced by treatment with either Bortezomib or 3-MA. Inhibition of both the proteasome and autophagy under complete nutrients or nutrient deprivation was not possible due to considerable cell death. Collectively, these data suggest that nutrient deprivation activates AMPK, which leads to enhanced expression of ubiquitin ligases and increased protein degradation.

3.2. AMPK Regulates the Expression of Ubiquitin Ligases *In Vitro* and *In Vivo*

To test the hypothesis that AMPK is responsible for the increased expression of Atrogin-1 and MuRF1 under nutrient deprivation conditions, NRVM were treated with AICAR, an activator of AMPK. AICAR is an adenosine analog which is rapidly phosphorylated upon entry into the cell (to ZMP) [360]. Accumulation of ZMP leads to activation of AMPK in the absence of metabolic stress (such as nutrient deprivation) [361]. Previous studies in NRVM used between 0.5mM and 2.0mM AICAR to activate AMPK. Initial time course studies were performed using AICAR (1.0mM) to define conditions for additional experiments. AICAR treatment increased phosphorylation of AMPK and acetyl-CoA carboxylase (ACC), a direct target of AMPK. Phosphorylation occurred quickly with AICAR (1.0mM) (in less than 30 minutes, not shown) and both AMPK and ACC remained phosphorylated for at least 24 hours in the presence of AICAR. After 36 hours

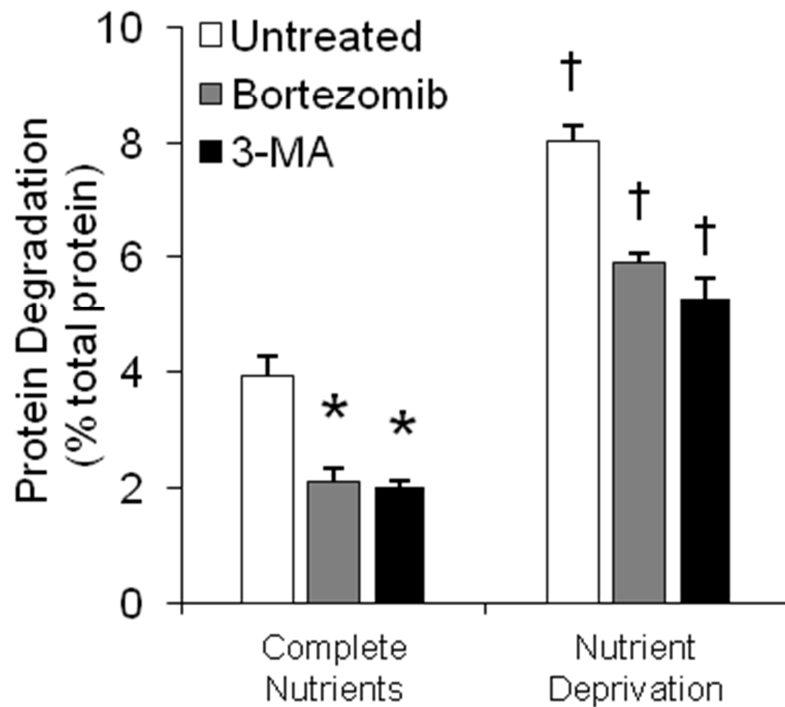


Figure 3.3. Regulation of protein degradation by nutrient deprivation in cardiomyocytes.

Protein degradation in response to nutrient deprivation. NRVM were isolated and several hours later incubated in pulse medium containing radiolabeled Phe ($1\mu\text{Ci}/\text{mL}$ [^{14}C]), as described in “2.2.11. Protein Turnover Assays”. After 48 hours NRVM were washed twice with complete medium and incubated in chase medium with or without nutrients containing vehicle, Bortezomib ($1\mu\text{mol}/\text{L}$), or 3-methyladenine (3-MA, $10\mu\text{mol}/\text{L}$). Chase medium was collected over 24 hours and rates of protein degradation were calculated as described in “2.2.11. Protein Turnover Assays”. Results are expressed as mean percent protein degradation \pm SEM of 3 independent experiments performed in triplicate. * $P < 0.01$ versus untreated, † $P < 0.01$ versus complete nutrients. Reprinted with permission from KK Baskin and H Taegtmeier, AMP-activated protein kinase regulates E3 ligases in rodent heart, *Circulation Research*, 109, 10, 1153-1161 [358].

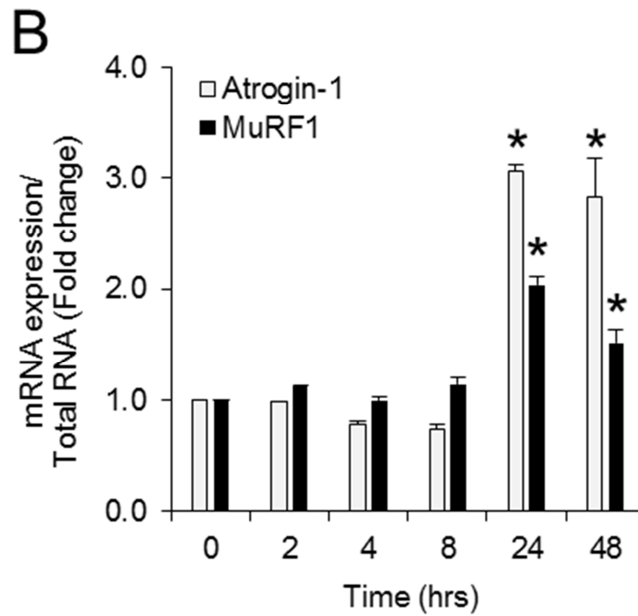
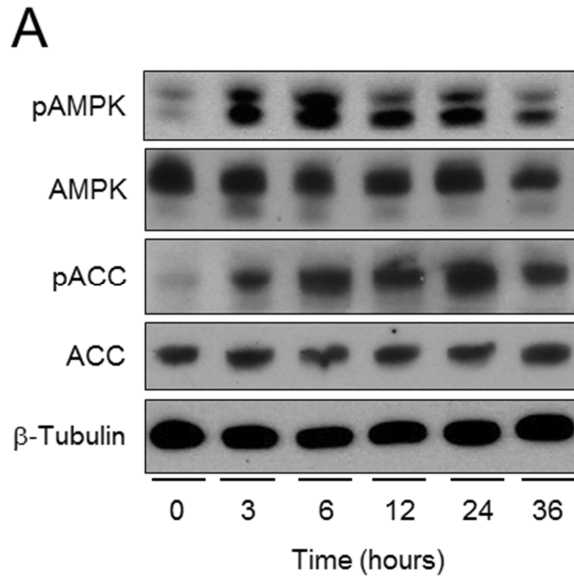


Figure 3.4. Time-dependent regulation of AMPK, Atrogin-1, and MuRF1 by AICAR in cardiomyocytes.

(A) Activation of AMPK in response to AICAR. NRVM were isolated and incubated overnight in culture medium, washed twice with phosphate buffered saline (PBS), and incubated with AICAR (1.0mM) in culture medium for the designated times. A representative western blot from AICAR-treated NRVM is shown. (B) Atrogin-1 and MuRF1 expression in response to AICAR treatment. Data are expressed as mean fold change \pm SEM of 3 independent experiments performed in triplicate. $*P < 0.01$ versus 0 hours.

phosphorylation of AMPK and ACC declined (**Figure 3.4.A.**). Consequently, Atrogin-1 and MuRF1 expression increased in response to AICAR (1.0mM) treatment, but at a slow rate (**Figure 3.4.B.**). Atrogin-1 and MuRF1 expression significantly increased 3 and 2 fold, respectively, 24 hours after AICAR treatment. Therefore all subsequent experiments were performed at 24 hours.

To further characterize the regulation of Atrogin-1 and MuRF1 by AMPK through AICAR, I performed dose-response experiments. Atrogin-1 and MuRF1 expression was increased by up to three fold in a dose-dependent manner after 24 hours of AICAR treatment (**Figure 3.5.A.**). Additionally, AMPK and ACC phosphorylation were increased at a relatively low concentration of AICAR (0.25mM) and continued to increase in a dose-dependent manner as well (**Figure 3.5.B.**). Atrogin-1 and MuRF1 protein levels also increased in response to AICAR treatment, but required a higher dose. The protein levels of Atrogin-1 and MuRF1 were significantly increased with AICAR (1.0mM) and subsequent experiments were therefore performed using this concentration.

To determine whether the increase of Atrogin-1 and MuRF1 was due to AMPK activation through AICAR, and not through another AICAR-mediated pathway, AMPK was inhibited using Compound C [287]. Compound C decreased AMPK phosphorylation to the same extent with or without AICAR. ACC was equally responsive to AICAR and Compound C, but phosphorylation of ACC was much lower with Compound C alone compared to the combined AICAR and Compound C treatment (**Figure 3.6.A.**). Atrogin-1 and MuRF1 expression was also significantly decreased with Compound C treatment, in a dose-dependent manner. AICAR treatment increased Atrogin-1 and MuRF1 expression nearly three fold, and addition of Compound C abrogated these changes (**Figure 3.6.B.**).

The consequence of AMPK activation by AICAR was also determined *in vivo*. AICAR was delivered by intraperitoneal (IP) injection, and the effects of AICAR on AMPK, ACC, Atrogin-1, and MuRF1 in the heart were examined (**Figure 3.7.A.**). Acute treatment, one injection of AICAR, significantly increased Atrogin-1 and MuRF1 mRNA in a time-dependent manner. Six hours after AICAR delivery, Atrogin-1 expression significantly increased (two fold) and further increased (to three fold) at 24 hours after AICAR injection. MuRF1 expression was increased, although not significantly, six hours post injection and was significantly increased to the same extent as Atrogin-1 24 hours post injection. Chronic AICAR treatment, by daily injections for 7 days, significantly increased both Atrogin-1 and MuRF1 expression (each by more than 5 fold) (**Figure 3.7.A.**). AMPK regulates the transcription of GLUT4 [293] and UCP3 [290], which were quantified in the heart as positive

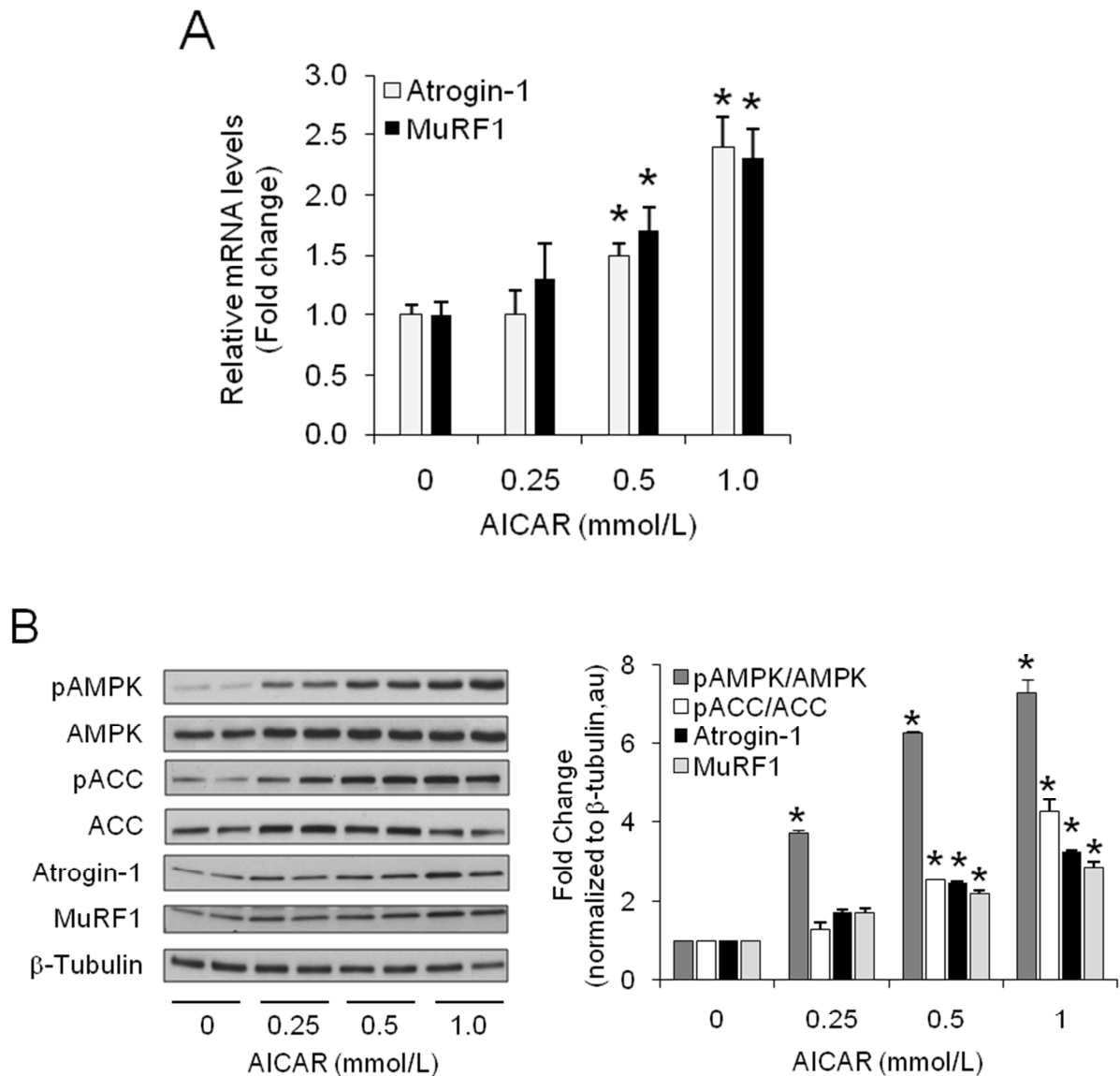
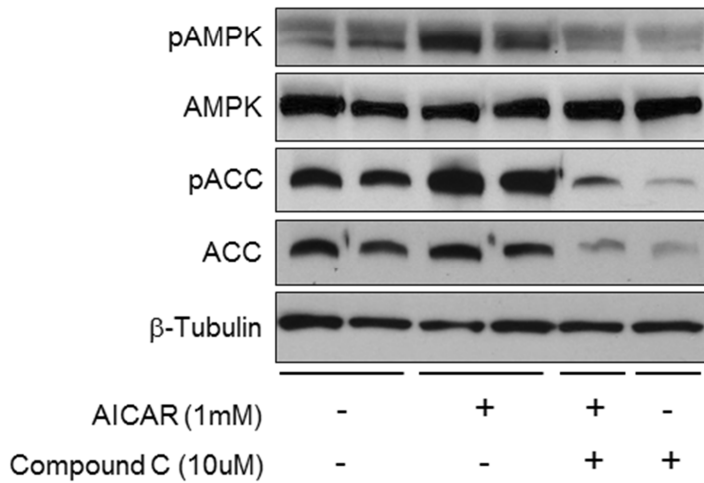


Figure 3.5. Dose-dependent regulation of AMPK, Atrogin-1, and MuRF1 by AICAR in cardiomyocytes.

(A) Atrogin-1 and MuRF1 expression in response to AICAR treatment. NRVM were isolated and incubated overnight in normal culture medium, washed twice with phosphate buffered saline (PBS), and incubated with AICAR (0.25mM, 0.5mM, or 1.0mM) in culture medium for 24 hours. Data are expressed as mean fold change \pm SEM of 3 independent experiments performed in triplicate. (B) AMPK activation and Atrogin-1 and MuRF1 protein levels in response to AICAR treatment. A representative western blot is shown on the left. Data are expressed as mean fold change \pm SEM of 3 independent experiments performed in duplicate. * $P < 0.01$ versus untreated. Reprinted with permission from KK Baskin and H Taegtmeier, AMP-activated protein kinase regulates E3 ligases in rodent heart, *Circulation Research*, 109, 10, 1153-1161 [358].

A



B

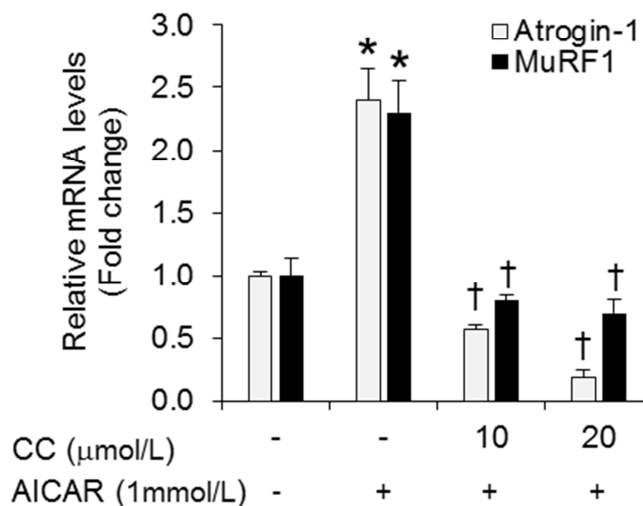


Figure 3.6. Regulation of Atrogin-1 and MuRF1 by AICAR and Compound C in cardiomyocytes.

(A) AMPK activation and inhibition and Atrogin-1 and MuRF1 protein levels in response to AICAR and/or Compound C treatment. NRVM were isolated and incubated overnight in culture medium, washed twice with phosphate buffered saline (PBS), and incubated with AICAR (1.0mM) and/or Compound C (10 μ M) in culture medium for 24 hours. A representative western blot is shown. (B) Atrogin-1 and MuRF1 expression in response to AICAR and Compound C treatment. Data are expressed as mean fold change \pm SEM of 3 independent experiments performed in triplicate. * P <0.01 versus untreated, † P <0.01 versus AICAR. Reprinted with permission from KK Baskin and H Taegtmeier, AMP-activated protein kinase regulates E3 ligases in rodent heart, *Circulation Research*, 109, 10, 1153-1161 [358].

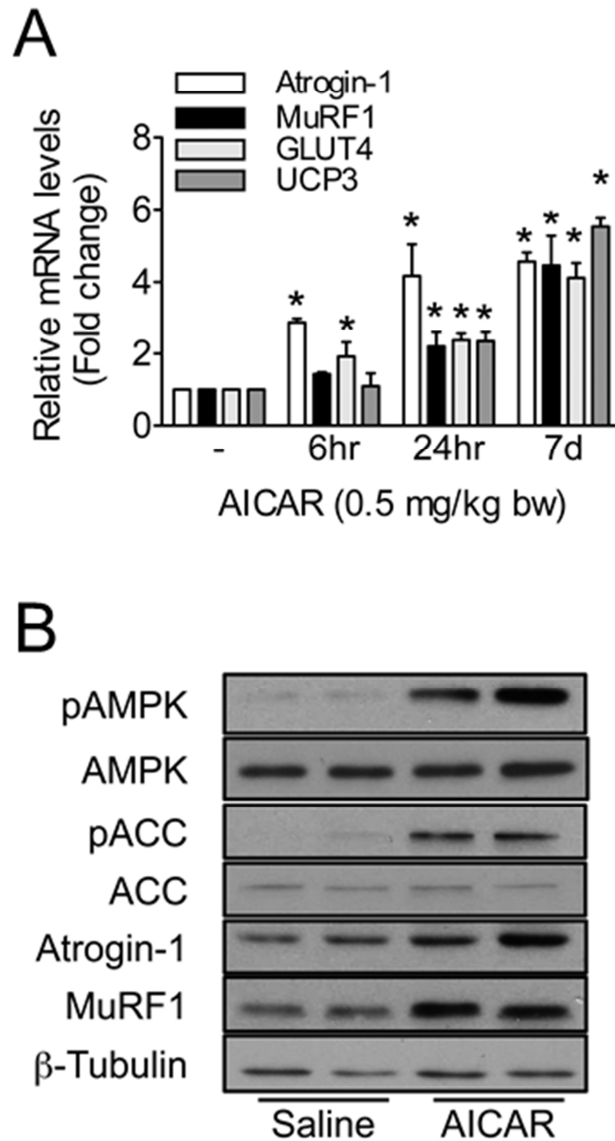


Figure 3.7. Regulation of AMPK, Atrogin-1, and MuRF1 by AICAR in the mouse heart.

(A) Atrogin-1, MuRF1, GLUT4, and UCP3 expression in the heart in response to AICAR injection(s). Mice were injected with AICAR (0.5mg/kg bw) (see text for details). Hearts were extracted, rinsed in ice-cold PBS, and snap frozen in liquid nitrogen. RNA was isolated from heart tissue and quantified as described in “2.2.6.1. Total RNA Isolation and Quantification”. Data are expressed as mean fold change \pm SEM, $n=6-8$ per group, qRT-PCR was performed in triplicate for each heart. $*P<0.01$ versus saline controls. (B) AMPK activation, Atrogin-1 and MuRF1 protein levels in the heart in response to AICAR injection(s). A representative western blot is shown on samples from the 7d saline control and AICAR group. GLUT4, glucose transporter 4; UCP3, uncoupling protein 3. Reprinted with permission from KK Baskin and H Taegtmeyer, AMP-activated protein kinase regulates E3 ligases in rodent heart, *Circulation Research*, 109, 10, 1153-1161 [358].

controls. GLUT4 and UCP3 expression in the heart also increased in a time-dependent manner in response to AICAR treatment (**Figure 3.7.A.**). As expected, chronic AICAR treatment also increased AMPK and ACC phosphorylation. Moreover, Atrogin-1 and MuRF1 protein levels were significantly increased in the heart with chronic AICAR treatment (**Figure 3.7.B.**). Taken together (**Figures 3.1. – 3.7.**), these results demonstrate that Atrogin-1 and MuRF1 are regulated in cardiomyocytes and in the heart by AMPK.

To exclude the possibility that the results described above were caused by off-target effects of pharmacological treatment, I used genetically modified AMPK adenoviruses in cardiomyocytes. NRVM are difficult to manipulate genetically, as most primary cells are. Therefore adenoviruses expressing active or dominant negative forms of AMPK were used in the following experiments. For a detailed description of the adenoviruses see Chapter 2 (2.2.8., “Amplification and Quantification of Adenoviruses”). NRVM were infected with increasing amounts of virus (multiplicity of infection, MOI) and the expression of Atrogin-1 and MuRF1 was determined. Atrogin-1 mRNA was significantly increased with the overexpression of active AMPK (aAMPK) in NRVM. Low expression of AMPK (MOI 1) led to a nearly two fold increase, while overexpression of dominant negative AMPK (dnAMPK) had no effect on baseline levels of Atrogin-1 (**Figure 3.8.A.**). MuRF1 mRNA was also significantly increased in response to aAMPK nearly two fold, and like Atrogin-1, MuRF1 expression was also not affected by dnAMPK (**Figure 3.8.B.**).

Active AMPK is expressed as a truncated form of AMPK α 2 that lacks the autoinhibitory domain and β -subunit binding domain (see Chapter 2 for details). Thus, the AMPK antibody used to determine protein levels in NRVM recognizes a lower molecular weight species of AMPK (**Figure 3.8.C.**). Unfortunately, the phospho-AMPK antibody did not detect phosphorylation of this species. Therefore, ACC phosphorylation was used as an indicator of active AMPK. ACC phosphorylation was enhanced with increasing expression of aAMPK (**Figure 3.8.C.**). Furthermore, the protein levels of Atrogin-1 and MuRF1 were increased by expression of aAMPK. It is not clear whether the AMPK antibody detects dnAMPK because with increasing amounts of dnAMPK adenovirus, neither total nor phosphorylated AMPK levels were altered (**Figure 3.8.D.**). However, ACC was responsive to dnAMPK as its phosphorylation status decreased in response to increasing amounts of dnAMPK expression (**Figure 3.8.D.**). Dominant negative AMPK also decreased the protein levels of Atrogin-1 and MuRF1 (**Figure 3.8.D.**). It is interesting that Atrogin-1 and MuRF1 mRNA levels were unaffected by dnAMPK expression while their protein levels were decreased. Although further investigation is still necessary, it is possible that the steady

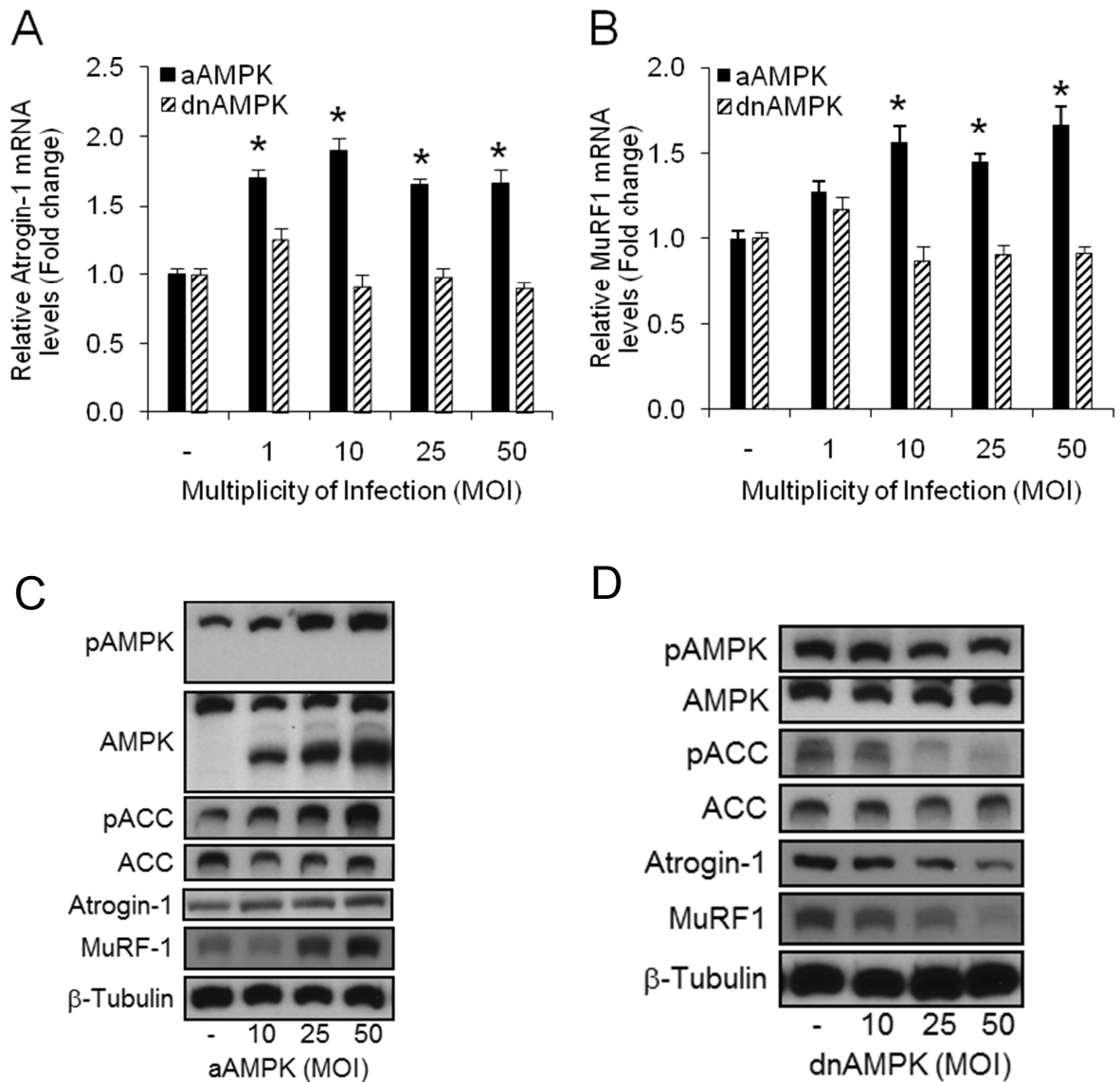


Figure 3.8. Regulation of Atrogin-1 and MuRF1 by AMPK in cardiomyocytes.

(A) Atrogin-1 expression and (B) MuRF1 expression in response to active AMPK (aAMPK) or dominant negative AMPK (dnAMPK) adenovirus expression. NRVM were isolated and cultured overnight in culture medium and infected with adenovirus (1, 10, 25, 50 MOI). Six hours post infection NRVM were washed twice with PBS and cultured an additional 18 hours in culture medium. Data are expressed as mean fold change \pm SEM of 3 independent experiments performed in triplicate. * $P < 0.01$ versus empty virus control. (C and D) AMPK, ACC, Atrogin-1, and MuRF1 protein levels in response to dnAMPK and aAMPK. Representative western blots are shown. See text for details. Reprinted with permission from KK Baskin and H Taegtmeier, AMP-activated protein kinase regulates E3 ligases in rodent heart, *Circulation Research*, 109, 10, 1153-1161 [358].

state levels of Atrogin-1 and MuRF1 are altered by dnAMPK at the protein level but not at the mRNA level.

Although, as shown above, aAMPK appears to be expressed in an active state, its phosphorylation status could not be verified directly using commercially available antibodies. Therefore I wondered whether aAMPK could be further stimulated by AICAR, thus enhancing the expression of Atrogin-1 and MuRF1. I infected NRVM with aAMPK or dnAMPK, and treated them with AICAR and/or Compound C. As previously shown, AICAR and aAMPK (to a lesser extent) increased expression of Atrogin-1, while Compound C alone decreased Atrogin-1 expression. dnAMPK, as shown in **Figure 3.8.A.**, had no significant effect on Atrogin-1 expression (**Figure 3.9.**). AICAR and aAMPK had an additive effect on Atrogin-1 expression, while Compound C treatment decreased Atrogin-1 expression in the presence of aAMPK. These data suggest that aAMPK is also pharmacologically regulated by AICAR and Compound C. Although the active site within dnAMPK is mutated, NRVM expressing dnAMPK treated with AICAR and/or Compound C were still responsive to the treatment (as evidenced by changes in Atrogin-1 expression). It is possible that these effects are due to endogenous AMPK; however, this has yet to be demonstrated.

The additive effects of pharmacological treatment and genetic expression on MuRF1 mRNA levels were also determined. The expression of MuRF1 in response to AICAR, Compound C, aAMPK, and dnAMPK, in this set of experiments was the same as previously discussed and shown in **Figure 3.8.B.** Like Atrogin-1, MuRF1 expression was increased with AICAR treatment and further increased with AICAR and expression of aAMPK. Unlike Atrogin-1, MuRF1 expression was not altered by AICAR when dnAMPK was expressed; however, was decreased with Compound C when dnAMPK was expressed (**Figure 3.10.**). Taken together, these studies validate the usage of aAMPK and dnAMPK in NRVM, and demonstrate that genetic modification of AMPK does not completely activate or abolish total AMPK pools within the cardiomyocyte. These data provide evidence that AMPK, pharmacologically and/or genetically, regulates the expression of Atrogin-1 and MuRF1.

To determine the consequence of genetic activation and inhibition of AMPK on protein degradation, I performed more pulse chase experiments in NRVM (using aAMPK and dnAMPK, MOI 10). Active AMPK, like nutrient deprivation, increased protein degradation in cardiomyocytes, while dnAMPK decreased protein degradation. Bortezomib, a proteasome inhibitor that decreases protein degradation, was used as a control (**Figure**

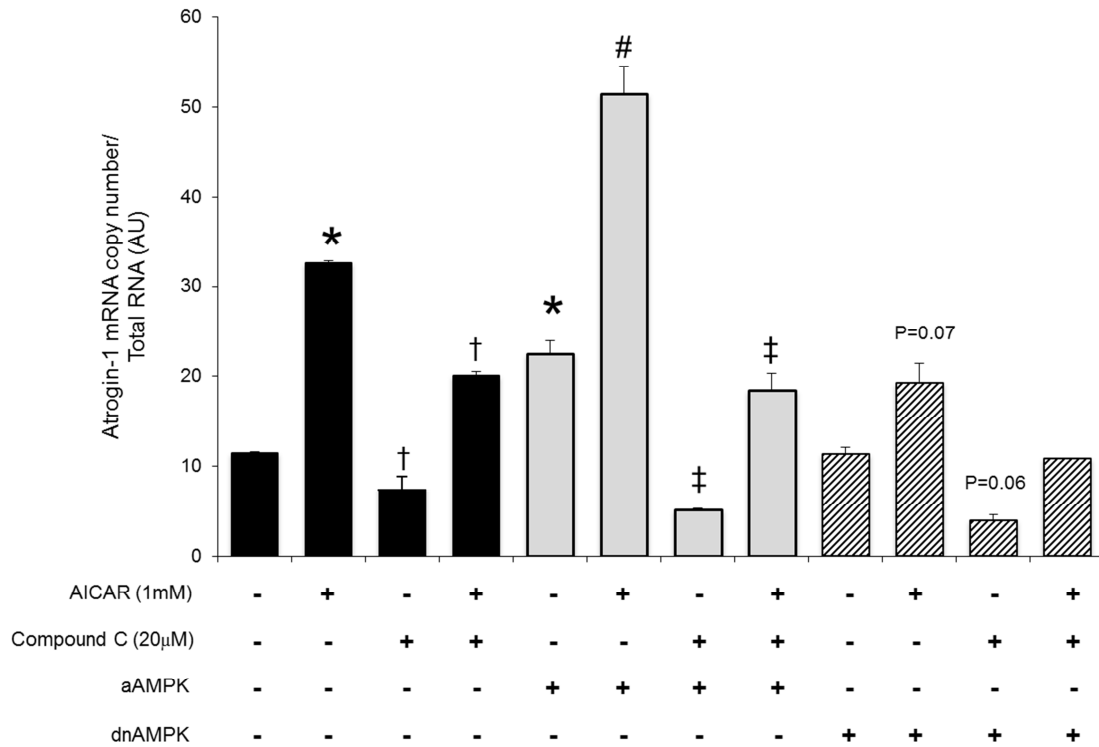


Figure 3.9. Synergistic regulation of Atrogin-1 by pharmacologic and genetic activation of AMPK

Atrogin-1 expression in response to AMPK activation and inhibition. NRVM were isolated and cultured as described in **Figure 3.8.** except that 24 hours after virus infection with aAMPK or dnAMPK (MOI 10), AICAR and/or Compound C were added to the culture medium and NRVM were incubated 24 hours longer. Control NRVM were infected with empty virus (MOI 10) and is shown in the green bars on the left, NRVM infected with aAMPK are shown in the middle in grey, NVRM infected with dnAMPK are shown on the right in the pattern-filled bars. Data are expressed as mean expression \pm SEM of 3 independent experiments performed in triplicate. * P <0.01 versus untreated empty virus control, † P <0.01 versus AICAR, # P <0.01 versus virus, ‡ P <0.01 versus virus + AICAR.

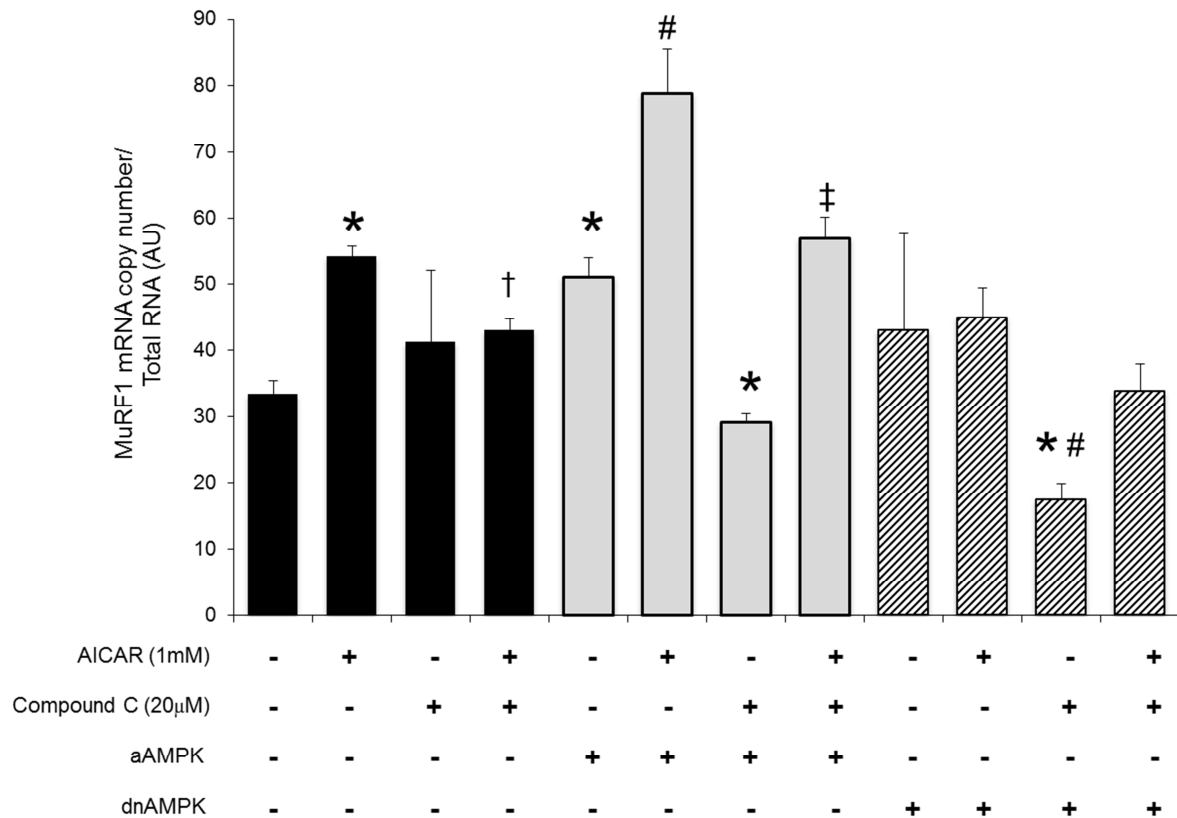


Figure 3.10. Synergistic regulation of MuRF1 by pharmacologic and genetic activation of AMPK

MuRF1 expression in response to AMPK activation and inhibition. NRVM were isolated and cultured as described in **Figure 3.8.** except that 24 hours after virus infection with aAMPK or dnAMPK (MOI 10), AICAR and/or Compound C were added to the culture medium and NRVM were incubated 24 hours longer. Control NRVM were infected with empty virus (MOI 10) and is shown in the black bars on the left, NRVM infected with aAMPK are shown in the middle in grey, NVRM infected with dnAMPK are shown on the right in the pattern-filled bars. Data are expressed as mean expression \pm SEM of 3 independent experiments performed in triplicate. * $P < 0.01$ versus untreated empty virus control, † $P < 0.01$ versus AICAR, # $P < 0.01$ versus virus, ‡ $P < 0.01$ versus virus + AICAR.

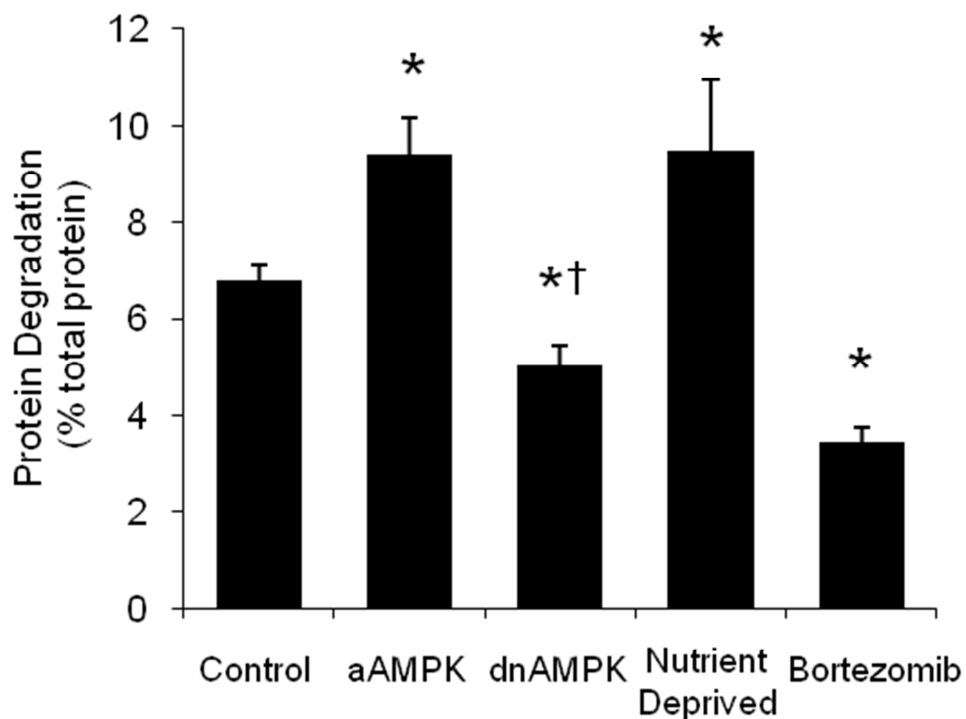


Figure 3.11. Regulation of protein degradation by AMPK in cardiomyocytes.

Protein degradation in response to aAMPK and dnAMPK. NRVM were isolated and cultured as described in Figure 3.3. NRVM were infected with aAMPK (MOI 10) and dnAMPK (MOI 10) 24 hours prior to changing the medium from pulse to chase medium. At the onset of the “chase”, NRVM were incubated in culture medium (control, aAMPK, dnAMPK), PBS (nutrient deprived), or culture medium with Bortezomib (1 μ mol/L). Data are expressed as mean percent protein degradation \pm SEM of 3 independent experiments performed in triplicate. * P <0.01 versus control. † P <0.01 versus aAMPK. Reprinted with permission from KK Baskin and H Taegtmeier, AMP-activated protein kinase regulates E3 ligases in rodent heart, *Circulation Research*, 109, 10, 1153-1161 [358].

3.11.). Collectively, these results demonstrate that AMPK regulates the ubiquitin ligases Atrogin-1 and MuRF1 in cardiomyocytes (and in the heart) by enhancing their expression at the mRNA and protein level. In other words, AMPK increases protein degradation in cardiomyocytes.

The hypothesis that AMPK could be involved in UPS-mediated protein degradation had not been considered until I began working on my thesis project, or so we thought. Much to my despair, and rather unfortunate for the lab, some of the work described thus far in my dissertation was published by several groups (although all experiments were performed in skeletal muscle). These studies are discussed in detail below. This situation offered itself as a learning experience, and I followed the advice of my mentor, “Dr. T.”, and “stuck with it.” This experience, and a cartoon illustrating the advancements and setbacks in AMPK research [362], inspired my T-shirt design for the 2011 annual Cell and Regulatory Biology (CRB) spring retreat (**Figure 3.12.**).

Similar to our results presented thus far, experiments reported by Krawiec et.al. demonstrated that Atrogin-1 and MuRF1 mRNA was increased with AICAR treatment in a dose-dependent manner in C₂C₁₂ cells, a skeletal muscle cell line [363]. Their data support our findings that the expression of MuRF1 in response to AICAR increases in a time-dependent manner, but at a slower rate compared to the increase in Atrogin-1 expression. They also found that Metformin, another activator of AMPK, increased Atrogin-1 and MuRF1 expression. Despite this finding in C₂C₁₂ cells, Metformin failed to increase the expression of either ligase in NRVM in our hands (data not shown). This could be due to differential metabolic demand and regulation in the heart compared to skeletal muscle, as Metformin does not activate AMPK directly [287]. Furthermore, the investigators used other methods to activate AMPK rather than nutrient deprivation, namely 2-deoxyglucose (2DG). 2DG is a glucose analogue that enters the cell and is phosphorylated by hexokinase, but cannot be metabolized. Cells are essentially “glucose deprived”, however phosphorylated 2DG may have other negative effects on intracellular signaling (S. Sen, H. Taegtmeyer, unpublished results). Although the data of Krawiec et. al. support our initial findings, they did not investigate the consequence of AMPK activation on protein degradation.

Another study published shortly thereafter also found, in C₂C₁₂ cells, that AICAR increases the expression of Atrogin-1 and to a lesser extent, MuRF1 [364]. Additionally, AICAR treatment increases protein degradation in muscle cells. Nakashima et. al. attributed these findings to increased FOXO activity, although only reported FOXO1 and FOXO3A mRNA expression and not protein or phosphorylation levels. I also wondered whether

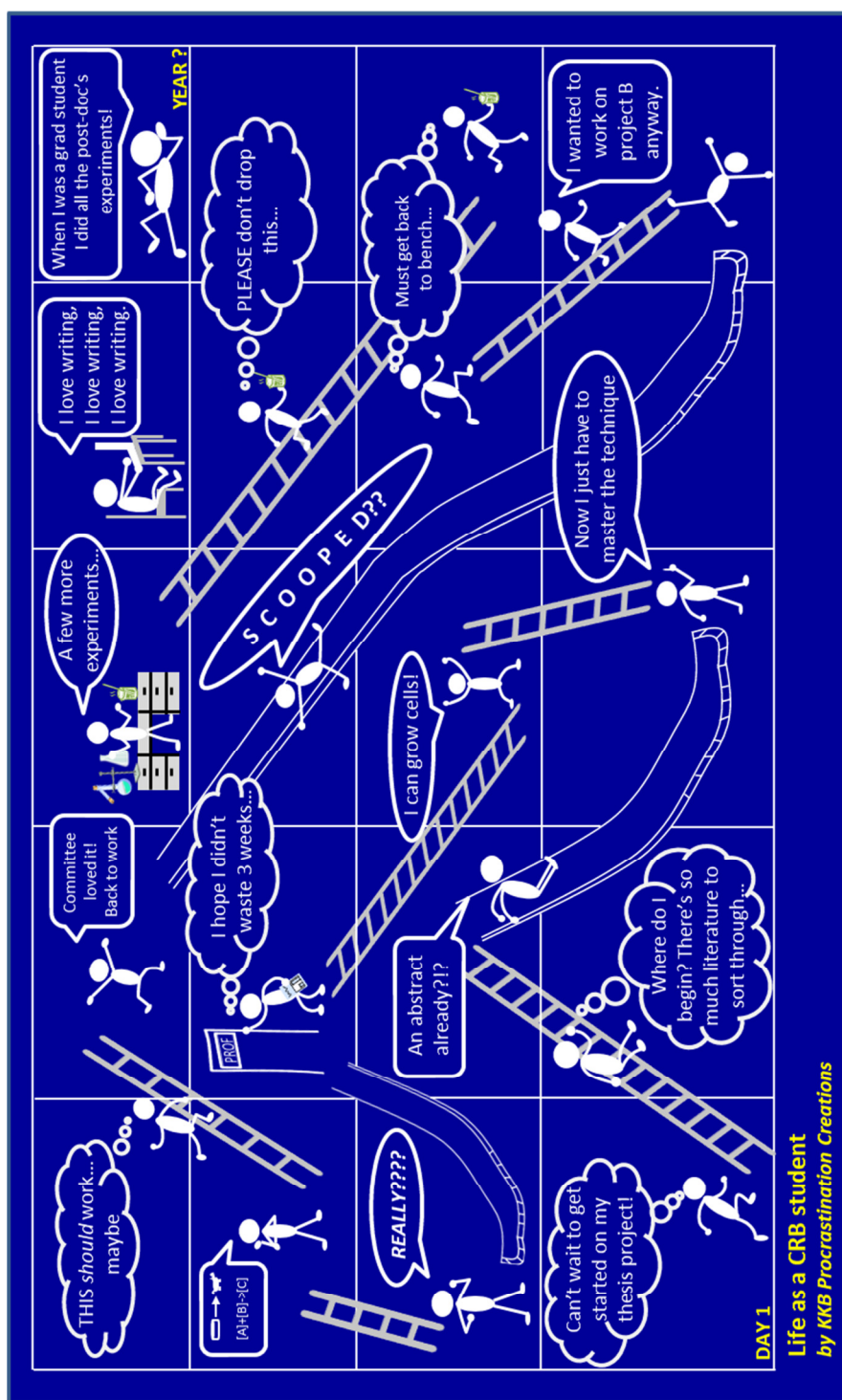


Figure 3.12. Life as a CRB student.

This cartoon depicts a simplified overview of life as graduate student. Many life lessons can be learned in this stage of a scientific career. The two most important: take the good with the bad, and embrace sarcasm. Special thanks to 'Piled Higher & Deeper a grad student comic strip' for finding humor in daily lab scenarios.

(<http://www.phdcomics.com/comics.php>)

AMPK could be affecting FOXO3A activity in cardiomyocytes thus leading to increased expression of Atrogin-1 and MuRF1. At the time I performed the following set of experiments, it was already known that FOXO3A regulates Atrogin-1 expression in the heart [144]; however it was not known whether AMPK could regulate FOXO. Therefore, I determined the phosphorylation status of FOXO3a in NRVM expressing aAMPK or dnAMPK. Neither aAMPK nor dnAMPK expression affected the phosphorylation status of FOXO3a, at least on Ser253 (**Figure 3.13.**). Therefore, I proceeded to search for an alternative novel mechanism whereby AMPK regulates Atrogin-1 and MuRF1 expression.

Shortly after I performed the experiments described in (**Figure 3.13.**), Greer et.al. identified phosphorylation sites on FOXO3 (including Ser588) which were regulated by AMPK. The consequence of FOXO phosphorylation on this site, however, was not described [365]. Although presumably important, no additional studies reported the regulation of FOXO3A by AMPK until recently. AMPK was shown to interact with and phosphorylate FOXO3A on Ser588. Although the expression of Atrogin-1 and MuRF1 was not investigated, autophagy gene expression was increased through FOXO3A-mediated transcription, as was the number of autophagosomes in muscle cells [366]. This study identifies another pathway by which AMPK regulates autophagy, however little is still known about AMPK-mediated protein degradation through the UPS in the heart.

Data in support of our hypothesis that AMPK regulates the UPS by mediating Atrogin-1 and MuRF1 expression was also published by Tong et.al. [367]. This group demonstrated that AMPK activation was sufficient to increase Atrogin-1 and MuRF1 expression, even in the presence of IGF-1, activation of AKT, and inhibition of FOXO3A [367]. The authors suggest that AMPK antagonizes the inhibition of FOXO3A-mediated transcription by AKT through phosphorylation of FOXO3A on other/multiple regulatory sites. This study does not exclude the possibility that AMPK regulates Atrogin-1 and MuRF1 expression independent of FOXO3A, which we have found to be the case, and is the topic of discussion below.

3.3. AMPK Activation Regulates the Expression of MuRF1 *In Vitro* Through the Transcription Factor Myocyte Enhancer Factor 2

As already mentioned, previous studies in liver [285] and in skeletal muscle [289] have demonstrated that AMPK regulates transcription of several genes. AMPK regulates the transcription of GLUT4 in skeletal muscle through the transcription factor myocyte enhancer factor 2 (MEF2) [293]. Because MEF2 is a transcription factor involved in metabolic and structural remodeling in cardiomyocytes [368], and Atrogin-1 and MuRF1 are

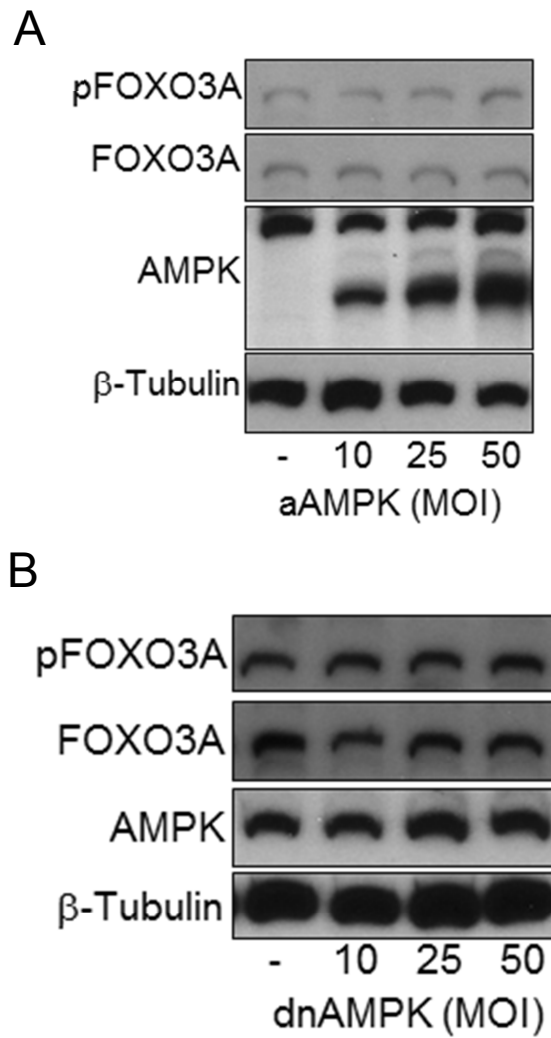


Figure 3.13. Regulation of FOXO3a by AMPK in cardiomyocytes.

FOXO3A protein and phosphorylation levels in response to dnAMPK and aAMPK expression. Representative western blots are shown. See text for details.

as well, it seemed very likely to me that a connection between AMPK, MEF2, and Atrogin-1 and MuRF1 exists.

To explore potential transcriptional mechanisms by which AMPK regulates ubiquitin ligases, *in silico* experiments were performed to identify transcription factor binding sites within the Atrogin-1 and MuRF1 promoters. A well-established MEF2 binding site (CTAaAAATAG) was identified within the MuRF1 promoter (**Figure 3.14.A.**). Because AMPK-regulation of MEF2 has never been described in cardiomyocytes, I determined MEF2 transcriptional activity in response to AMPK activation. An ELISA-like assay containing a stationary MEF2 recognition sequence binds to MEF2 in its active state. MEF2 binding is then detected using antibodies conjugated to HRP (horseradish peroxidase). Activation of AMPK with AICAR and aAMPK increased MEF2-DNA binding while Compound C (CC) and dnAMPK decreased MEF2-DNA binding (**Figure 3.14.B.**). These results strongly suggest that MEF2-regulated transcription may be mediated by AMPK.

To determine whether MEF2 binds the MuRF1 promoter and regulates its transcription in cardiomyocytes, gene reporter and chromatin immunoprecipitation assays (ChIP) were performed. Gene reporter assays were generated using 1kb of the endogenous MuRF1 promoter upstream of luciferase. The “MuRF1 promoter” construct contains the MuRF1 promoter with the potential MEF2 binding site intact. The “mutated MuRF1 promoter” construct contains the MuRF1 promoter with the potential MEF2 binding site mutated (**Figure 3.15.A.**). The MuRF1 promoter or the mutated MuRF1 promoter construct were cotransfected with a construct encoding β -galactosidase (β -gal) into H9c2 cardiomyoblasts. After transfection and treatment cells were collected and assayed for luciferase and β -galactosidase activity. AMPK activation with AICAR or aAMPK increased luciferase activity of the endogenous promoter, while AMPK inhibition with CC or dnAMPK decreased luciferase activity (**Figure 3.15.B.**). These results indicate that AMPK directly regulates MuRF1 transcription. The mutated MuRF1 promoter, however, was not responsive to AMPK activation or inhibition, but was still transcribed in the absence of nutrients (**Figure 3.15.B.**). These data demonstrate that MEF2 is required for AMPK-mediated MuRF1 transcription, but that MEF2 is not required for MuRF1 transcription during nutrient deprivation (**Figure 3.15.B.**).

To determine whether MEF2 binds directly to the MuRF1 promoter, ChIP assays were performed. Myocytes were infected with adenovirus (MOI 10) and MEF2 was immunoprecipitated from nuclear extracts. DNA isolated from the extracts was amplified

A

5' - CTAaAAATAG - 3' MEF2 consensus binding site
5' - CTATAAATAT - 3' Potential MEF2 binding site
in MuRF-1 promoter

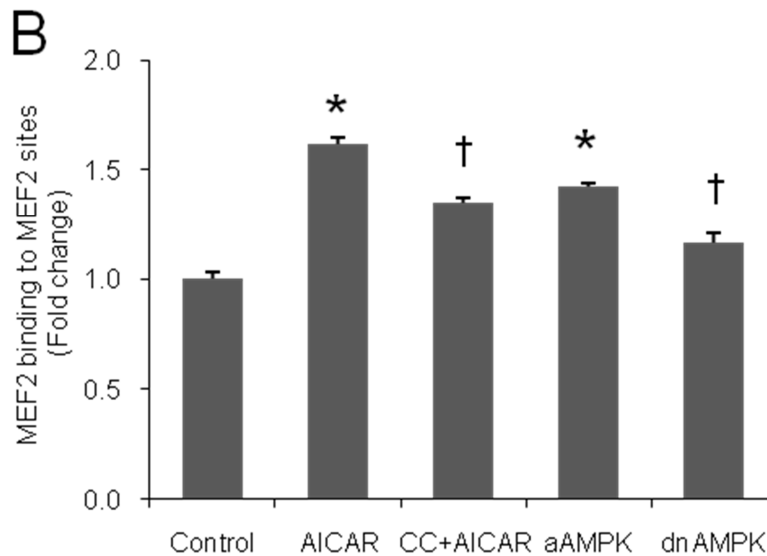


Figure 3.14. Regulation of MEF2 transcription by AMPK in cardiomyocytes.

(A) MEF2 consensus binding site and the potential MEF2 binding site identified *in silico*. (B) MEF2 binding activity in response to AMPK activation and inhibition. NRVM were treated for 24 hours with AICAR (1.0mM), CC (10 μ M) + AICAR (1.0mM), aAMPK (MOI 10), or dnAMPK (MOI 10). Nuclear fractions were isolated as described in “2.2.6.3. Nuclear Fractionation of Cells” and used to determine MEF2 –DNA binding as described in “2.2.7.3. MEF2 Activity Assay”. See text for details. Data are expressed as mean fold change \pm SEM of 3 independent experiments performed in triplicate. * P <0.01 versus control. † P <0.01 versus AICAR or aAMPK. Reprinted with permission from KK Baskin and H Taegtmeier, AMP-activated protein kinase regulates E3 ligases in rodent heart, *Circulation Research*, 109, 10, 1153-1161 [358].

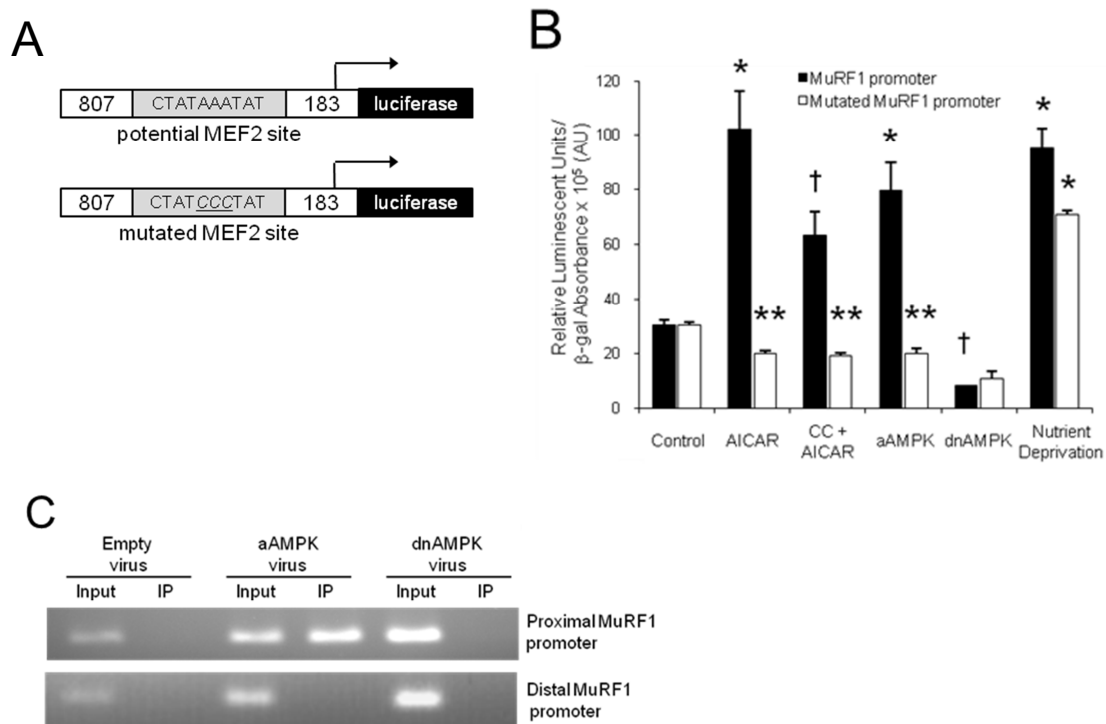


Figure 3.15. Regulation of MuRF1 transcription by an AMPK-MEF2 axis in myocytes.

(A) Gene reporter assay constructs containing the endogenous MuRF1 promoter sequence with the potential MEF2 binding site intact or mutated (alanine to cytosine, AAA →CCC) upstream of luciferase. (B) MuRF1 transcription in response to AMPK activation or inhibition in myocytes. H9c2 myoblasts were cotransfected with luciferase reporter constructs (1 μg) and a vector encoding β-galactosidase (1 μg) using PolyJet™ transfection reagent as described in “2.2.7.1. Luciferase Reporter Constructs and Activity Assays”. Myocytes were incubated in culture medium containing AICAR (1.0mM) or CC (10 μM) + AICAR (1.0mM), or in PBS (nutrient deprivation) for 24 hours. For adenovirus conditions, myocytes were infected 24 hours prior to transfection of luciferase reporter constructs. Myocytes were collected in reporter lysis buffer and enzyme activities were assayed as described in “2.2.7.1. Luciferase Reporter Constructs and Activity Assays” and “2.2.7.2. β-galactosidase Activity Assays and Staining”. Data are expressed as mean relative luminescent units (RLU) normalized to β-galactosidase absorbance ± SEM of 3 independent experiments performed in triplicate. **P*<0.01 versus control. † *P*<0.01 versus AICAR or aAMPK. (C) MEF2 binding to the MuRF1 promoter. Myocytes were infected with empty, aAMPK, or dnAMPK adenovirus (MOI 10). 24 hours post infection DNA was cross-linked to proteins and myocytes were collected. Chromatin immunoprecipitation (ChIP) was performed as described in “2.2.7.5. Chromatin Immunoprecipitation Assay (ChIP)”. See text for more details. Reprinted with permission from KK Baskin and H Taegtmeyer, AMP-activated protein kinase regulates E3 ligases in rodent heart, *Circulation Research*, 109, 10, 1153-1161 [358].

using primers specific for the potential MEF2 binding region on the MuRF1 promoter. A distal sequence on the MuRF1 promoter was used as a negative control. Myocytes expressing aAMPK resulted in MEF2 binding to the endogenous MuRF1 promoter, while myocytes expressing dnAMPK or an empty virus did not (**Figure 3.15.C.**). Furthermore, MEF2 binding was specific for the identified site because MEF2 immunoprecipitation did not result in amplification of the distal region of the MuRF1 promoter (**Figure 3.15.C.**). Collectively, these experiments provide evidence that MEF2 binds the MuRF1 promoter and regulates the transcription of MuRF1 in an AMPK-dependent manner.

3.4. MEF2 Transcriptional Activity and MuRF1 Transcription Are Regulated by AMPK in the Heart

To confirm the role of AMPK-mediated MEF2 transcription in the heart, we obtained MEF2-lacZ reporter mice from Dr. Eric Olson's lab (UTSWMC, Dallas). These mice express β -galactosidase upon stimulation of MEF2 transcription (see section "2.1.1. Animals" for a detailed description of this mouse strain). MEF2-lacZ mice were treated with AICAR daily for seven days to chronically activate AMPK in the heart. As a positive control, mice were treated with isoproterenol, which has previously been shown to regulate MEF2 transcriptional activity [337]. Isoproterenol (ISO) and AICAR induced β -galactosidase expression, as evidenced by patches of blue staining within the treated hearts (**Figure 3.16.A.**). Additionally, β -galactosidase activity, quantified using an enzyme activity assay, was also enhanced by AICAR, to the same extent as with ISO treatment (**Figure 3.16.B.**). Furthermore, AICAR treatment also increased MuRF1 expression in hearts from MEF2-lacZ mice (**Figure 3.16.C.**). These experiments provide evidence in support of the hypothesis that MEF2-mediated MuRF1 transcription is regulated by AMPK in the heart.

Studies in skeletal muscle have shown that AMPK phosphorylates histone deacetylase 5 (HDAC5), a repressor of MEF2-mediated transcription [294]. To determine whether AMPK mediates MEF2 transcriptional activity by inhibition of HDAC5 in cardiomyocytes, I first analyzed the phosphorylation status of HDAC5 in response to AMPK activation. As suggested in skeletal muscle, AICAR treatment increased, and Compound C decreased, HDAC5 phosphorylation in NRVM (**Figure 3.17.A.**). Phosphorylation of HDAC5 facilitates its export from the nucleus by 14-3-3 scaffolding proteins [369]. Despite enhanced HDAC5 phosphorylation, HDAC5 localization, determined by subcellular fractionation of NRVM, was not significantly affected by AMPK activation (**Figure 3.17.B.**). However, HDAC5 does not appear to inhibit MuRF1 transcription when AMPK is activated, as it was not detected on the MuRF1 promoter by chromatin immunoprecipitation (ChIP)

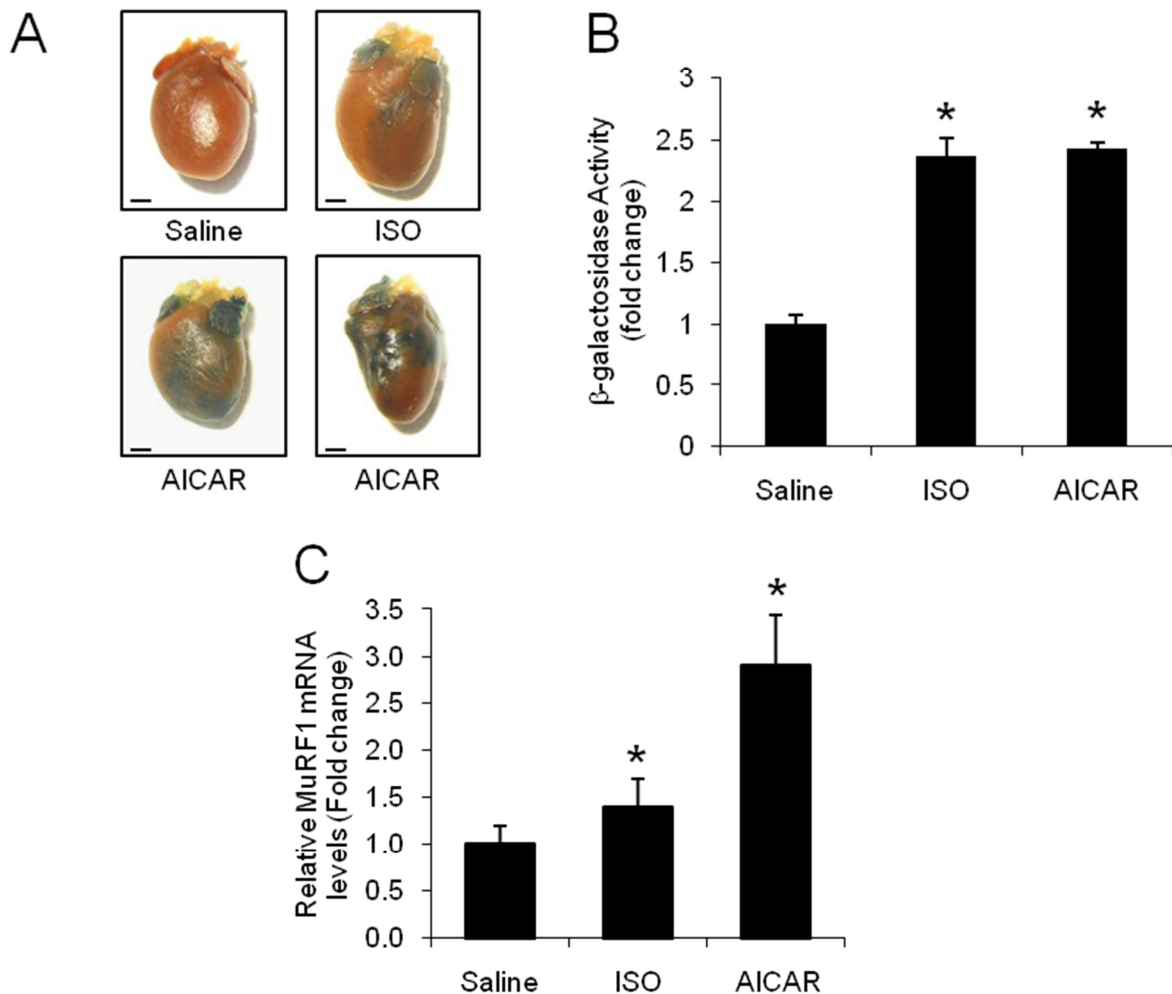


Figure 3.16. Regulation of MEF2 and MuRF1 by AMPK in the heart.

(A) MEF2 activity (β -galactosidase expression) in response to AMPK activation. MEF2-lacZ transgenic mice were treated with AICAR (1 mg/g bw) or isoproterenol (15 mg/kg bw) once a day for seven days. Hearts were extracted and stained for β -galactosidase as described in “2.2.7.2. β -galactosidase Activity Assays and Staining”. (B) β -galactosidase activity in response to AMPK activation. Heart lysate from treated mice was assayed for β -galactosidase activity. (C) MuRF1 expression in response to AMPK activation in MEF2-lacZ mice. Data are expressed as mean fold change \pm SEM, $n=6-8$ per group, qRT-PCR was quantified in triplicate for each heart. * $P<0.01$ versus saline controls. Reprinted with permission from KK Baskin and H Taegtmeier, AMP-activated protein kinase regulates E3 ligases in rodent heart, *Circulation Research*, 109, 10, 1153-1161 [358].

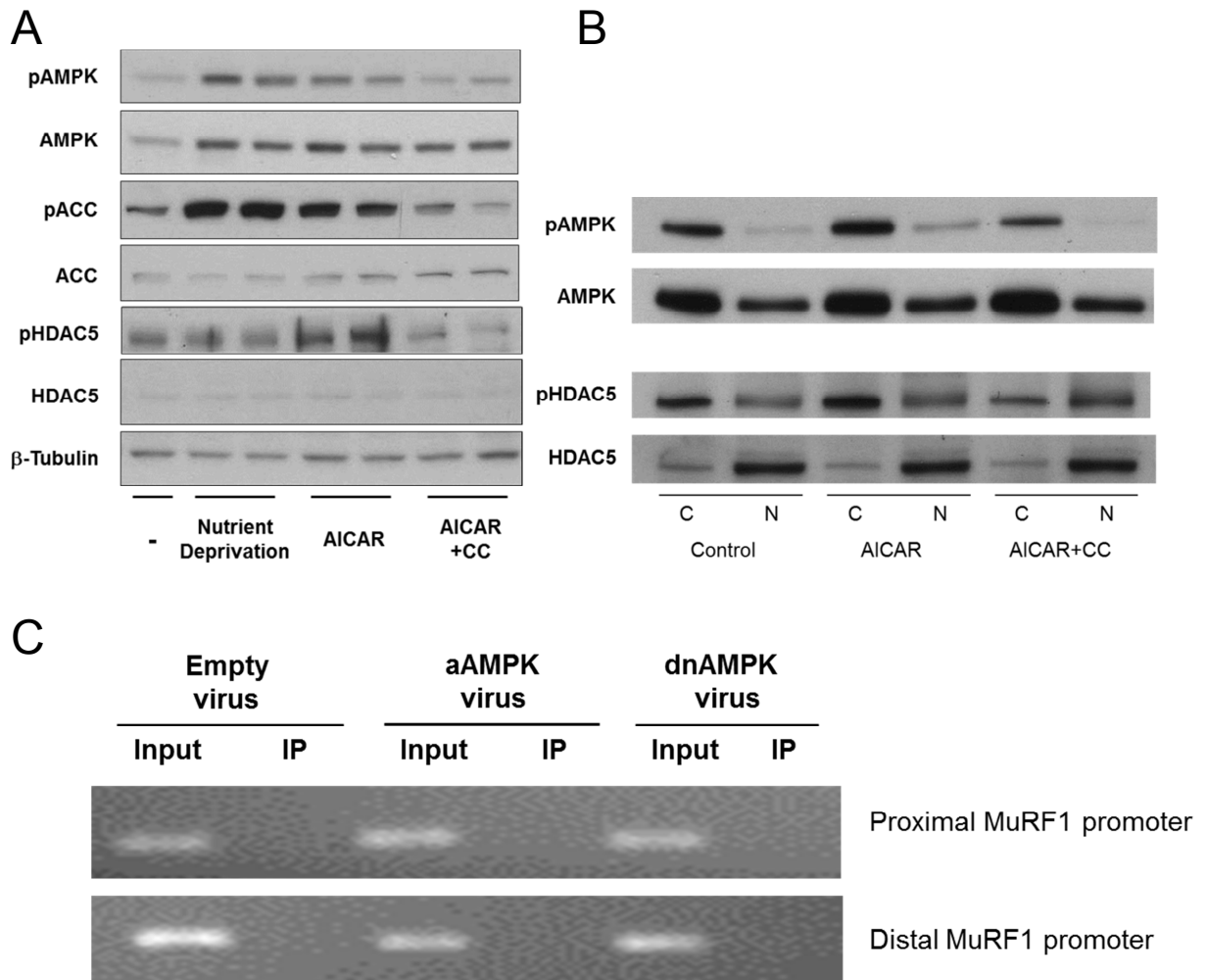


Figure 3.17. Regulation of HDAC5 by AMPK in the heart.

(A) HDAC5 protein and phosphorylation levels in response to AMPK activation. NRVM were isolated and cultured as previously described. A representative western blot is shown. (B) Nuclear localization of HDAC5 in response to AMPK activation. NRVM were cultured as previously described. Myocytes were collected as described in 2.2.6.3. “Nuclear Fractionation of Cells”. A representative western blot is shown: C, cytosolic fraction; N, nuclear fraction. (C) HDAC5 binding to the MuRF1 promoter. ChIP was performed as described in **Figure 3.15**, except cross-linked DNA was immunoprecipitated using an HDAC5 antibody.

(**Figure 3.17.C.**). These data suggest that AMPK regulates MEF2 transcription of MuRF1, independent of HDAC5.

To investigate the necessity of MuRF1 in AMPK-mediated protein degradation, adult cardiomyocytes isolated from WT or MuRF1^{-/-} mouse hearts were used. Protein degradation in adult cardiomyocytes was determined in pulse-chase experiments as described above. WT and MuRF1^{-/-} myocytes were responsive to bortezomib indicating that proteasome-mediated degradation was not altered in the absence of MuRF1 (**Figure 3.18.**). Nutrient deprivation increased protein degradation in WT cardiomyocytes by nearly 3 fold. Although nutrient deprivation also increased protein degradation in MuRF1^{-/-} myocytes compared to control MuRF1^{-/-} myocytes, the response was much less than what was observed in WT myocytes. These results indicate that MuRF1 is required for protein degradation in response to nutrient deprivation, at least in part. Furthermore, activation of AMPK (aAMPK) increased (by 2 fold), and inhibition of AMPK (dnAMPK) decreased (by half), protein degradation in WT cardiomyocytes. Interestingly, protein degradation in MuRF1^{-/-} myocytes was not significantly altered with either activation or inhibition of AMPK (**Figure 3.18.**). Thus, this set of experiments defines the requirement for MuRF1 in AMPK-mediated protein degradation in cardiomyocytes.

3.5. MuRF1 is detrimental to the Heart during Fasting

The results summarized above and illustrated in **Figure 3.18.** were initially very surprising because they suggest that during nutrient deprivation, MuRF1 is the major regulator of protein degradation in cardiomyocytes. Experiments performed up until this point provided evidence for the involvement of AMPK and MuRF1 in protein degradation in the heart, but the extent of this regulation was not clear. It was unexpected that MuRF1 would be required for orchestrating protein degradation in response to AMPK activation. However, in support of these findings, *in vivo* experiments have demonstrated that MuRF1 is necessary for the plasticity of the heart in the recovery from hypertrophic stress. MuRF1 is required for improved cardiovascular function and normalization of cardiac size upon removal of aortic constriction [215]. We therefore wondered whether MuRF1 was required for cardiac remodeling under conditions other than changes in hemodynamic load, such as during fasting.

Fasting causes skeletal muscle atrophy in part through enhanced protein degradation through the UPS [370]. During fasting expression of Atrogin-1 and MuRF1 are significantly increased in skeletal muscle [141, 371]. To determine whether MuRF1 in the

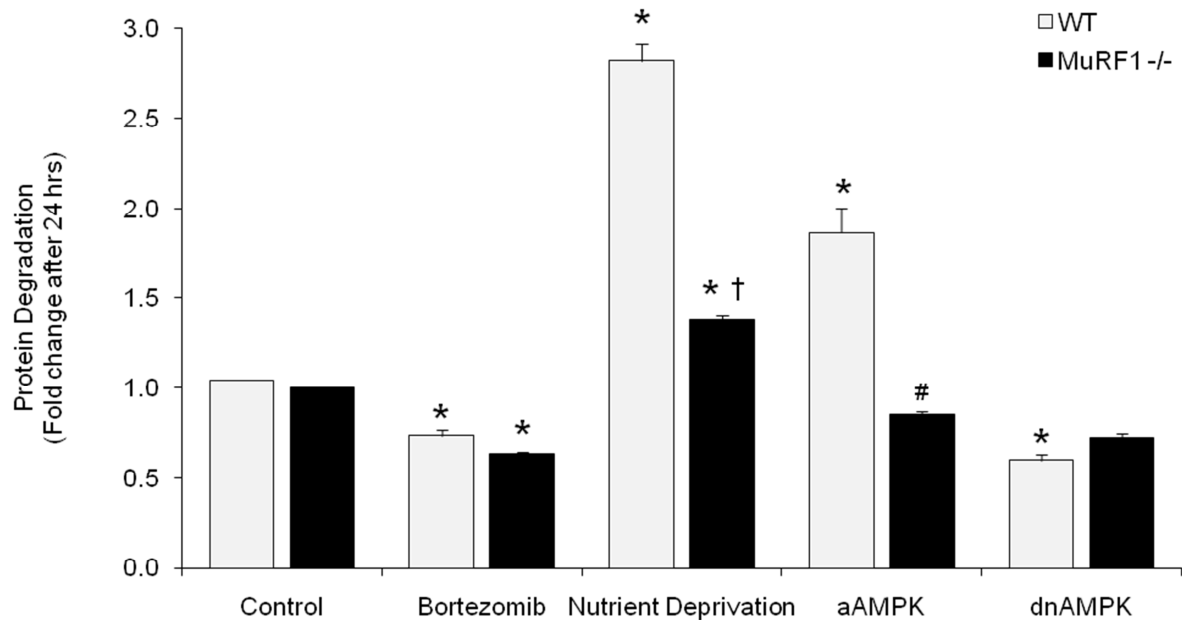


Figure 3.18. Regulation of protein degradation in cardiomyocytes by AMPK requires MuRF1.

Protein degradation in response to aAMPK and dnAMPK. Adult cardiomyocytes (AMCM) from WT and MuRF1^{-/-} mice were isolated and cultured as described in “2.2.5. Isolation of Adult Mouse Cardiomyocytes”. Immediately after plating, AMCM were incubated in pulse medium containing radiolabeled Phe (1μCi/mL [¹⁴C]), as described in “2.2.11. Protein Turnover Assays”. AMCM were infected with aAMPK (MOI 10) and dnAMPK (MOI 10) 24 hours prior to changing the medium from pulse to chase medium. At the onset of the “chase” AMCM were incubated in culture medium (control, aAMPK, dnAMPK), PBS (nutrient deprived), or culture medium with Bortezomib (1 μmol/L). Data are expressed as mean fold change in protein degradation ± SEM of 3 independent experiments performed in triplicate. **P*<0.01 versus respective controls. † *P*<0.01 versus WT nutrient deprivation, # *P*<0.01 versus WT aAMPK. Reprinted with permission from KK Baskin and H Taegtmeyer, AMP-activated protein kinase regulates E3 ligases in rodent heart, *Circulation Research*, 109, 10, 1153-1161 [358].

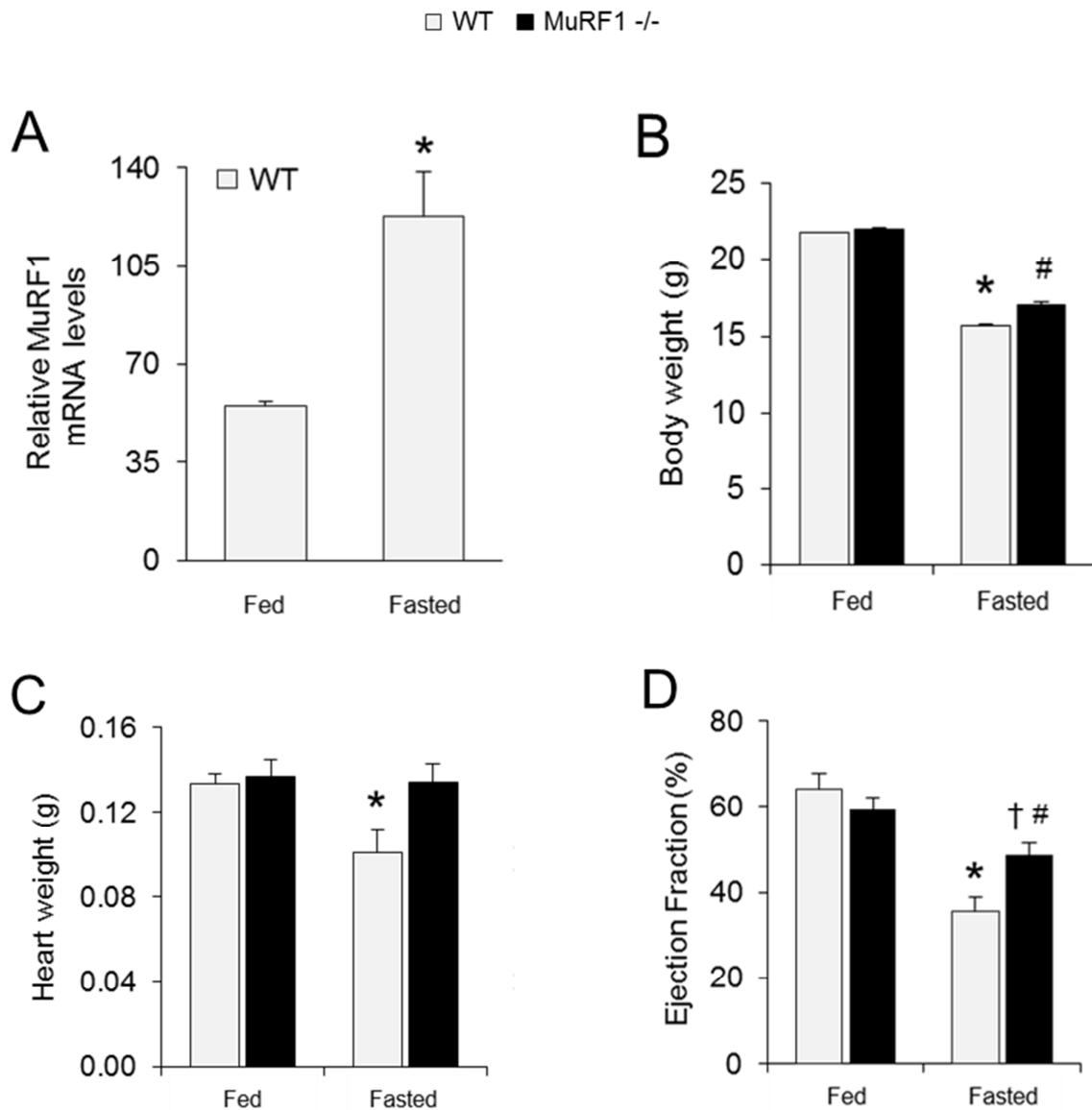


Figure 3.19. Regulation of MuRF1 and cardiac mass during fasting.

(A) MuRF1 expression in the heart in response to fasting. (B) Body weight (g) in response to fasting. (C) Heart weight (wet weight, g) in response to fasting. (D) Cardiac function in response to fasting. Echocardiography was performed on fed and fasted mice as described in “2.2.3.1. Echocardiography”. M-mode parasternal short-axis images were used to calculate cardiac functional parameters, such as ejection fraction. See text for details. Data are expressed as mean or mean percent \pm SEM, $n=6-8$ per group. qRT-PCR was quantified in triplicate for each heart. * $P<0.01$ versus saline controls, # $P<0.01$ versus MuRF1^{-/-} fed, † $P<0.01$ versus WT fasted. Adapted with permission from KK Baskin and H Taegtmeier, AMP-activated protein kinase regulates E3 ligases in rodent heart, *Circulation Research*, 109, 10, 1153-1161 [358].

heart, like in skeletal muscle, is regulated by fasting, MuRF1 expression was quantified after chronic food deprivation. MuRF1 expression was significantly increased in the heart in response to fasting (**Figure 3.19.A.**). Fasting caused significant loss of body weight in WT and MuRF1^{-/-} mice alike (**Figure 3.19.B.**). These results are in accordance with a report on the role of MuRF1 in skeletal muscle during amino acid (AA) deprivation [208]. This study found that WT and MuRF1^{-/-} mice lost weight with AA deprivation, and also had decreased muscle size. These data suggest that MuRF1 is not required for fasting-induced muscle or cardiac atrophy.

To date, numerous studies have demonstrated that the mechanisms regulating protein degradation in muscle and in heart are very similar. Therefore we expected that the heart would respond analogous to the muscle during fasting. Despite a similar decrease in body weight between WT and MuRF1^{-/-} mice, further investigation of the heart in MuRF1^{-/-} mice revealed an unanticipated result. Unexpectedly, the absence of MuRF1 preserved heart weight during fasting (**Figure 3.19.C.**). Moreover, ejection fraction, although depressed with fasting, was preserved in MuRF1^{-/-} mice (**Figure 3.19.D.**). Although other functional parameters were not significantly altered, fractional shortening was also preserved with fasting in MuRF1^{-/-} mice (**Table 3.1.**).

MuRF1 ubiquitinates and leads to the degradation of sarcomeric proteins. It is possible that under fasting conditions, enhanced MuRF1-mediated protein degradation leads to loss of sarcomeric proteins in the heart, which contributes to the decline in cardiac function. To determine the effect of fasting on the molecular level, several protein targets of MuRF1 were investigated. As previously reported, and as shown above in cardiomyocytes, fasting (nutrient deprivation) leads to the activation of AMPK. Consequently, ACC is phosphorylated. AMPK was activated (pAMPK and pACC) to the same extent in hearts from WT and MuRF1^{-/-} mice in response to fasting. Cardiac myosin-binding protein C (MyBP-C) protein levels were decreased in hearts of WT mice suggesting that an increase in MuRF1 leads to enhanced degradation of MyBP-C. However, MyBP-C levels were also decreased in the heart after fasting in the absence of MuRF1 (**Figure 3.20.**). This could be due to the fact that Atrogin-1 also targets MyBP-C for degradation, albeit through a different molecular mechanism [218].

Another sarcomeric protein that is degraded by MuRF1 is cardiac troponin I (TnI). The degradation of TnI by MuRF1 has been shown to decrease contractility in isolated cardiomyocytes [166] and hence may lead to the cardiac dysfunction seen with fasting.

LV functional parameters in Fed and Fasted Wild Type and MuRF1 ^{-/-} mice				
	Wild Type Fed	Wild Type Nutrient Deprived	MuRF1 ^{-/-} Fed	MuRF1 ^{-/-} Nutrient Deprived
IVSd, mm	0.681 ± 0.078	0.608 ± 0.050	0.596 ± 0.087	0.760 ± 0.105
LVPW, mm	0.837 ± 0.092	0.752 ± 0.069	0.874 ± 0.122	0.956 ± 0.150
LVIDd, mm	3.518 ± 0.203	3.677 ± 0.322	3.314 ± 0.276	3.650 ± 0.278
LVIDs, mm	2.544 ± 0.293	2.862 ± .0404	2.498 ± 0.214	2.778 ± 0.374
FS, %	34.28 ± 2.68	20.93 ± 2.47*	28.59 ± 2.51	25.72 ± 3.21

Table 3.1. Left ventricular functional parameters in fed and fasted mice.

Echocardiography was performed on mice as described in “2.2.3.1. Echocardiography”. M-mode parasternal short-axis images were used to calculate cardiac functional parameters. Data are expressed as mean or mean percent ± SEM, n=6-8 per group. **P*<0.01 versus WT fed. IVSd, interventricular septum in diastole; LVPW, left ventricular posterior wall; LVIDd, left ventricular inner diameter in diastole; LVIDs, left ventricular inner diameter in systole; FS, fractional shortening. Reprinted with permission from KK Baskin and H Taegtmeyer, AMP-activated protein kinase regulates E3 ligases in rodent heart, *Circulation Research*, 109, 10, 1153-1161 [358].

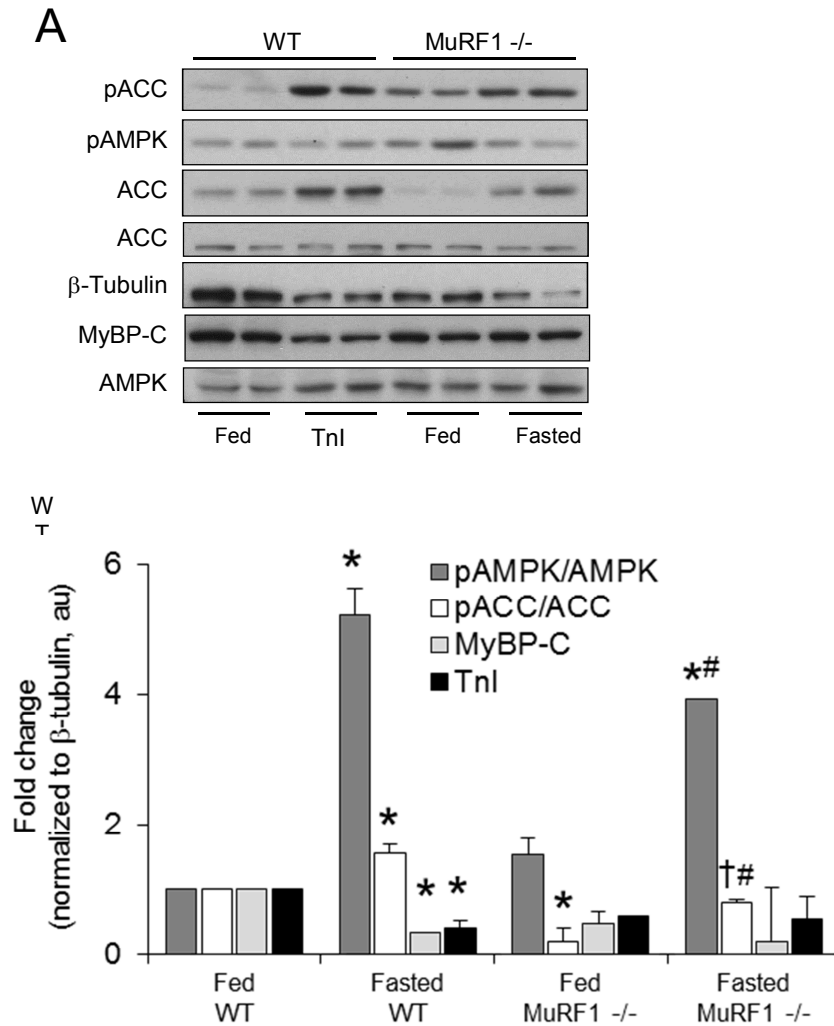


Figure 3.20. Regulation of AMPK, MyBPC, and Tnl during fasting.

(A) AMPK activation and MuRF1-target protein levels in response to fasting. Mice were subjected to fasting for 3 days. Hearts were extracted as previously described. A representative western blot is shown. (B). Densitometric quantification of western blots. Data are expressed as mean \pm SEM, n=6-8 per group. * P <0.01 versus fed WT controls, # P <0.01 versus fed MuRF1^{-/-}. Reprinted with permission from KK Baskin and H Taegtmeier, AMP-activated protein kinase regulates E3 ligases in rodent heart, *Circulation Research*, 109, 10, 1153-1161 [358].

Indeed, TnI levels were decreased with fasting in hearts from WT mice. Interestingly, TnI levels were not altered by fasting in MuRF1^{-/-} mice (**Figure 3.20.**). These data suggest that the absence of MuRF1 is protective during fasting in part by preservation of sarcomeric proteins.

Many other sarcomeric proteins may be targeted for degradation by MuRF1, including telethonin (Tcap), myotilin, nebulin, nebulin-related protein, troponin T1 and T3, and myosin light chain 2 (MLC-2) [206]. The levels of these proteins were not investigated as many of these targets originally identified in yeast-two hybrid screens have not been validated *in vitro* or *in vivo*.

MuRF1 may also play a role in metabolic adaptation and metabolic remodeling of the heart during fasting, in addition to its involvement in sarcomeric protein degradation. A recent study demonstrated that fasting decreases cardiac function [372] and in support of our findings, mice deficient for MuRF1 were spared from muscle and cardiac atrophy during fasting [208]. However, mechanistic experiments were not performed in either study. MuRF1 has been shown to target enzymes involved in ATP production for degradation, such as pyruvate dehydrogenase (PDH), which is downregulated in MuRF1 Tg mice [209]. PDH converts pyruvate to acetyl-CoA for entry into the Krebs cycle to produce reducing equivalents and, ultimately ATP. Consequently, decreased PDH potentially decreases ATP production in the cell, which could contribute to cardiac dysfunction, as we observe with long term fasting. Furthermore, activation of AMPK in response to decreased ATP levels, could feed forward to induce higher expression of MuRF1, leading to persistently lower intracellular ATP concentrations. Although we have not directly investigated the role of PDH in our model, the protective effects of fasting-induced metabolic derangements in the absence of MuRF1 in the heart, due to preservation of PDH-regulated ATP production, is an attractive hypothesis.

Other metabolic changes occur in the heart during fasting such as enhanced glycogen storage and elevated citrate levels [373]. Citrate inhibits phosphofructokinase, a regulatory enzyme in the glycolytic pathway which phosphorylates fructose-6-phosphate to fructose-1,6-bisphosphate. During atrophy, MuRF1 is upregulated and phosphofructokinase is downregulated [99]. Since MuRF1 and phosphofructokinase localize to the M-line of sarcomeres [135, 374], it is tempting to speculate that MuRF1 ubiquitinates phosphofructokinase thereby leading to its degradation. As suggested above, upregulation of MuRF1 during starvation could lead to the downregulation of metabolic enzymes, decreased ATP production from glycolysis and/or inhibition of the conversion of pyruvate to

acetyl-CoA, and ultimately decreased cardiac function. In support of this hypothesis, we have preliminary data (not shown) suggesting that glucose oxidation rates in hearts from MuRF1^{-/-} mice are at least three-fold higher than in the hearts from WT mice.

In summary, I have shown that nutrient deprivation and pharmacologic and genetic activation of AMPK increases Atrogin-1 and MuRF1 expression in cardiomyocytes and in the heart. Activation of AMPK leads to increase proteasome-mediated protein degradation. AMPK transcriptionally regulates MuRF1 through the transcription factor MEF2, although the exact mechanism by which this occurs in the heart is still not known. AMPK-mediated protein degradation requires MuRF1 in the heart, suggesting a more general role for MuRF1 in protein degradation, potentially in autophagy-mediated degradation. AMPK-mediated MuRF1 expression in the heart in response to fasting is detrimental to cardiac function. Not only does MuRF1 degrade sarcomeric proteins required for contractility, but MuRF1 also potentially negatively regulates cardiac metabolism, which has yet to be investigated. These findings are summarized in our working model described in **Figure 13.21**.

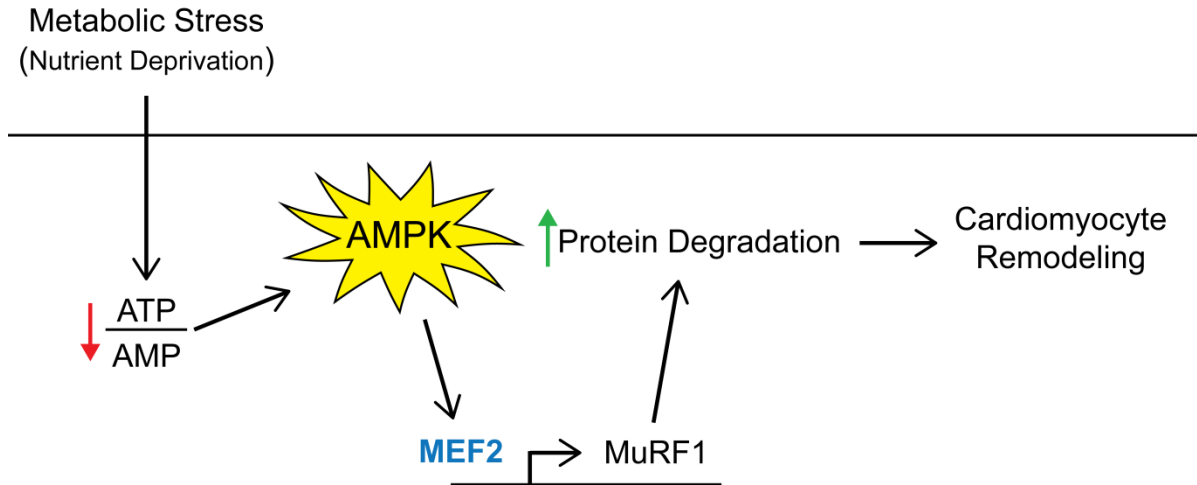


Figure 3.21. Consequence of metabolic stress on protein degradation in the heart.

Metabolic stresses such as nutrient deprivation or fasting lead to a decrease in the ratio of [ATP]/[AMP], thus activating AMPK. AMPK regulates the expression of a key ubiquitin ligase, MuRF1, through the transcription factor MEF2. Consequently, protein degradation in the heart is increased. This leads to cardiomyocyte remodeling, both structurally and metabolically. Continual metabolic derangements, such as what occurs during chronic fasting, leads to maladaptive cardiac remodeling, ultimately contributing to cardiac dysfunction. See text for details. Reprinted with permission from KK Baskin and H Taegtmeyer, AMP-activated protein kinase regulates E3 ligases in rodent heart, *Circulation Research*, 109, 10, 1153-1161 [358].

Chapter 4

A ROLE FOR 5'-AMP-ACTIVATED PROTEIN KINASE IN CARDIAC HYPERTROPHY

“Science, in the very act of solving problems, creates more of them [375].”

~Abraham Flexner, Educational reformer and author

4.1. An Overview of AMPK in Cardiac Hypertrophy

AMP-activated protein kinase (AMPK), as discussed in Chapter 1, is a key metabolic enzyme involved in many aspects of cellular signaling. In the preceding chapter I have shown that AMPK regulates ubiquitin ligases and proteasome-mediated protein degradation in the nutrient deprived heart [358]. The role of AMPK in cardiac hypertrophy, however, is presently not completely understood. Initial studies demonstrated that AMPK α 1 expression and activity is increased in the rat heart after 17-19 weeks of ascending aortic constriction in rats [268]. AMPK is also increased in the rat heart 8 weeks after abdominal aortic constriction to induce pressure overload [269]. These results suggest that AMPK may be activated during hypertrophy but the details are not known.

The heart adapts to hemodynamic stress by remodeling structurally and metabolically (**Figure 1.1.**). Consequently, intracellular reorganization occurs in cardiomyocytes during the development of hypertrophy. Hypertrophy is initially an adaptation to stress. However, chronic hemodynamic stress leads to maladaptation of the heart, and eventually heart failure. In the studies mentioned above, cardiac function was not assessed during, or at the termination, of the experiments. Therefore, whether activation of AMPK was a cause or consequence of hypertrophy and/or heart failure is not known.

AMPK has been shown to inhibit protein synthesis in muscle, in part by decreasing mTOR signaling [376]. AMPK also inhibits phenylephrine- and AKT-mediated hypertrophy by inhibiting protein synthesis in cardiomyocytes [270]. Therefore, according to Chan and Dyck, AMPK could be a target to reduce hypertrophy through inhibition of protein synthesis [377]. In support of this hypothesis my findings also suggest that AMPK can increase proteasome-mediated protein degradation [358], in addition to autophagy [277].

While long term pressure overload leads to AMPK activation, short term pressure overload does not. In fact, AMPK activation is decreased within 30 minutes of aortic constriction in mice [378]. Cardiomyocytes treated with the hypertrophic stimulus Angiotensin II also exhibit decreased AMPK phosphorylation levels, and protein synthesis is decreased under these conditions. Treatment with AICAR, however, abrogates these effects [378]. Taken together, these studies suggest that activation of AMPK does not cause hypertrophy, but rather AMPK is activated during the maladaptation of the heart to chronic pressure overload. My results demonstrating that activation of AMPK also increases protein degradation in NRVM through regulation of ubiquitin ligases (see Chapter 3) suggest that AMPK could be a target to slow the progression of hypertrophy, by inhibiting protein synthesis and activating protein degradation.

4.2. Regulation of Cardiac Function by AICAR

To test the hypothesis that activation of AMPK reduces cardiac hypertrophy, we investigated the role of AICAR-mediated AMPK activation in a model of pressure overload. Mice (male, age 8 weeks), were subjected to 4 weeks of transverse aortic constriction (TAC) as described in Chapter 2 (section 2.2.2. “Transverse Aortic Constriction in Mice”); sham surgeries were performed on the control group. A subset of animals were treated with AICAR (0.5mg/ g bw) daily for several days prior to, and daily for four weeks after, surgery. Cardiac function was monitored throughout the experiment by magnetic resonance (MR) scanning at 7, 14, 21, and 28 days after TAC, as described in Chapter 2 (see section 2.2.3.2. “Magnetic Resonance Imaging”). Cardiac parameters were calculated as described in 2.2.3. “Assessment of Cardiac Function”. This study was performed at MD Anderson Cancer Center in collaboration with the laboratory of Dr. Aarif Khakoo. Dr. Khakoo provided the surgery and MRI facilities, and Dr. Vishnu Chintalgattu performed TAC surgeries, Doppler measurements for the verification of TAC, trained me to use the MRI machine, and assisted in data analysis. Both are currently at Amgen in San Francisco, CA.

MRI images taken throughout the study were used to determine left ventricular end-diastolic (LVED) volume, left ventricular end-systolic (LVES) volume, and stroke volume. Interventricular septal and posterior wall thickness and ventricular area were also determined. Cardiac output and ejection fraction were then calculated as described in Chapter 2. As expected, left ventricular end diastolic (LVED) volume did not change in the saline-treated sham controls throughout the 4 weeks. Chronic AMPK activation with AICAR treatment also had no significant effect on LVED volume (**Figure 4.1A.**). However, as previously reported, LVED volume increased over time in response to pressure overload (by TAC). Surprisingly, LVED volume in TAC animals increased with AICAR treatment (**Figure 4.1A.**). Neither saline nor AICAR affected left ventricular end systolic (LVES) volume (**Figure 4.1A.**). But, like LVED, LVES volume was increased in response to TAC and further increased with AICAR treatment (**Figure 4.1B.**). Consequently, stroke volume was unchanged in saline and AICAR treated sham animals while stroke volume decreased over time with TAC and even more so with AICAR (**Figure 4.1C.**).

Cardiac output, a measure of cardiac function, was determined throughout the experiment at the same time points. There was no change in cardiac output in either the sham saline treated or sham AICAR treated mice. However, with TAC cardiac output declined significantly 7 days after surgery and slowly continued to decline (**Figure 4.2.A.**). AICAR treatment further decreased cardiac output with TAC at seven days after surgery,

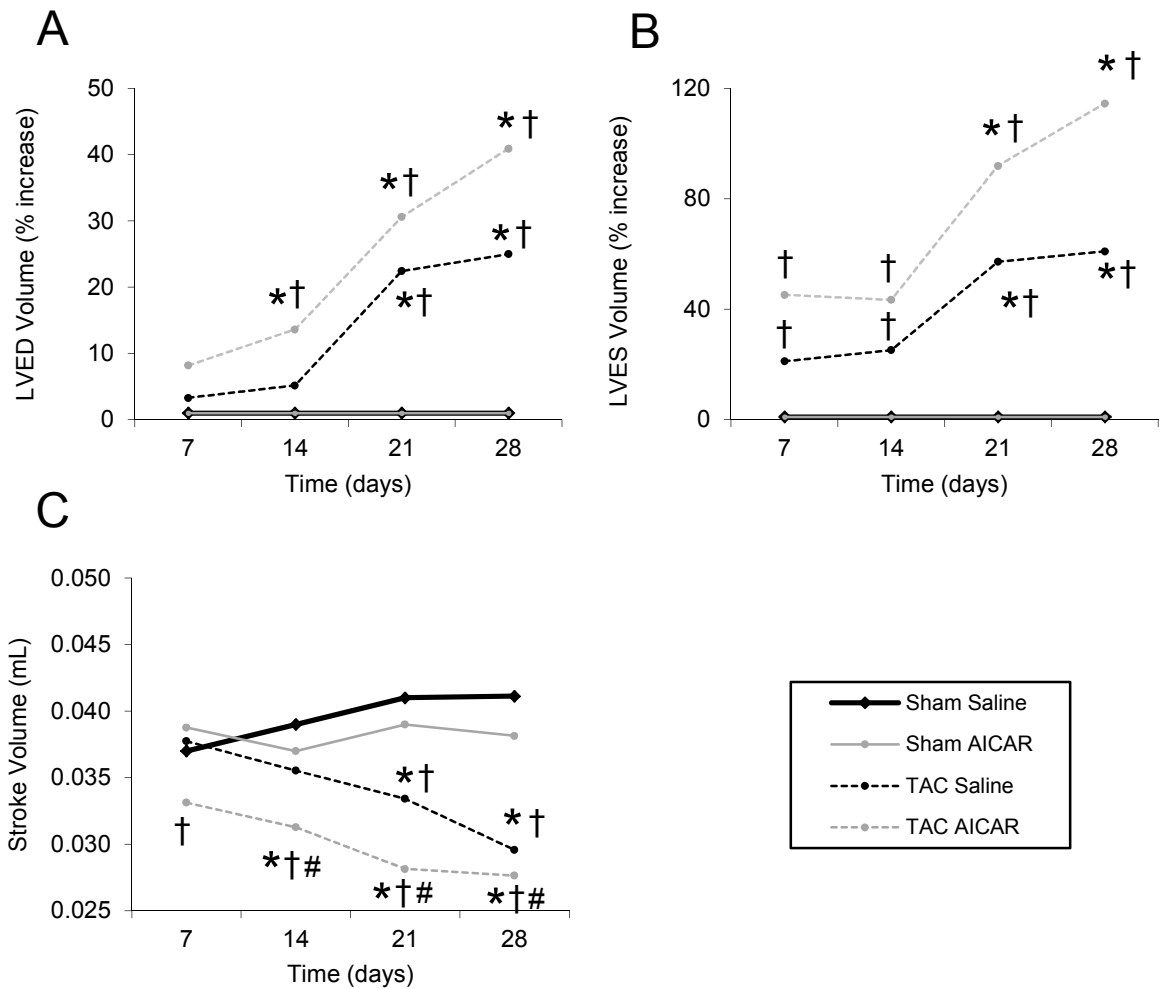


Figure 4.1. Synergistic effects of TAC and AICAR on cardiac parameters.

(A) Left ventricular end diastolic volume (LVED), (B) Left ventricular end systolic volume (LVES), and (C) Stroke volume in response to AICAR treatment and/or transverse aortic constriction (TAC) at 7, 14, 21, and 28 days after surgery. Male mice (C57/BL6, 8 weeks old, $n=6-8$ per group) were subjected to TAC as described in 2.2.2. “Transverse Aortic Constriction in Mice”. AICAR treatment (0.5mg/g bw/ day) was given intraperitoneally daily for 4 weeks, beginning several days before surgery. The day after surgery, Doppler measurements were taken as described in 2.2.2. “Transverse Aortic Constriction in Mice” to verify successful placement of the sutures. MRI scans were performed, measurements were taken, and calculations made as described in 2.2.3.2. “Magnetic Resonance Imaging”. * $P<0.01$ versus same group at 7 days, † $P<0.01$ versus sham with same treatment at matched time point, # $P<1.01$ versus TAC Saline at matched time point.

and throughout the duration of the experiment (**Figure 4.2.A.**). Like cardiac output, ejection fraction was not affected by AICAR treatment (**Figure 4.2.B.**). TAC decreased ejection fraction seven days after surgery and continued to decrease ejection fraction for 28 days. AICAR further decreased ejection fraction with TAC (**Figure 4.2.B.**). These data demonstrate that chronic AMPK activation does not affect basal cardiac function. However, contrary to what we expected, AMPK activation worsened cardiac function with pressure overload.

The dimensions of the heart, interventricular septal and posterior wall thickness, can be used to determine the degree of cardiac hypertrophy that develops with pressure overload. It is well established that posterior wall thickness increases with TAC, and then declines with continuous pressure, an indication of cardiac dilation and heart failure. In our study, AICAR treatment did not affect septal (**Figure 4.3.A.**) or posterior wall thickness in the sham-operated animals (**Figure 4.3.B.**). TAC increased both septal and posterior wall thickness throughout the 4 week experiment. Initially, AICAR further increased septal and posterior wall thickness after TAC. However, after 3 and 4 weeks, posterior wall thicknesses declined. These data suggests that AICAR accelerates dilation and possibly heart failure symptoms during pressure overload-induced hypertrophy (**Figure 4.3.A and B.**).

The functional data described above are easily visualized in MRI images shown in **Figure 4.4.** Enlargement of the left ventricle is seen with TAC. Although AICAR appears to increase cardiac dimensions, the averaged parameters were not significant throughout the study. However, hearts from AICAR treated TAC animals are larger than saline treated TAC animals, and is due to enlargement of both ventricles. Consistent with these findings, heart weight (normalized with either body weight or tibia length) was increased with TAC, but not with AICAR treatment. AICAR treated TAC animals had an even greater increase in heart weight compared to saline treated TAC animals (**Figure 4.5.A and B.**). Because AICAR treated TAC animals showed signs of left ventricular dilation and decreased wall thickness, lung weight was determined at the end of the experiment. Indeed, lung weight was significantly increased in AICAR treated TAC animals compared to saline treated TAC animals (**Figure 4.5.C.**). These characteristics are indicative of pulmonary edema and heart failure.

Because AICAR treated TAC animals had depressed cardiac function, as compared to saline treated TAC animals, we wondered whether they had increased fibrosis. However, no sign of enhanced fibrosis was seen in cross sections of these hearts (**Figure 4.6.A.**).

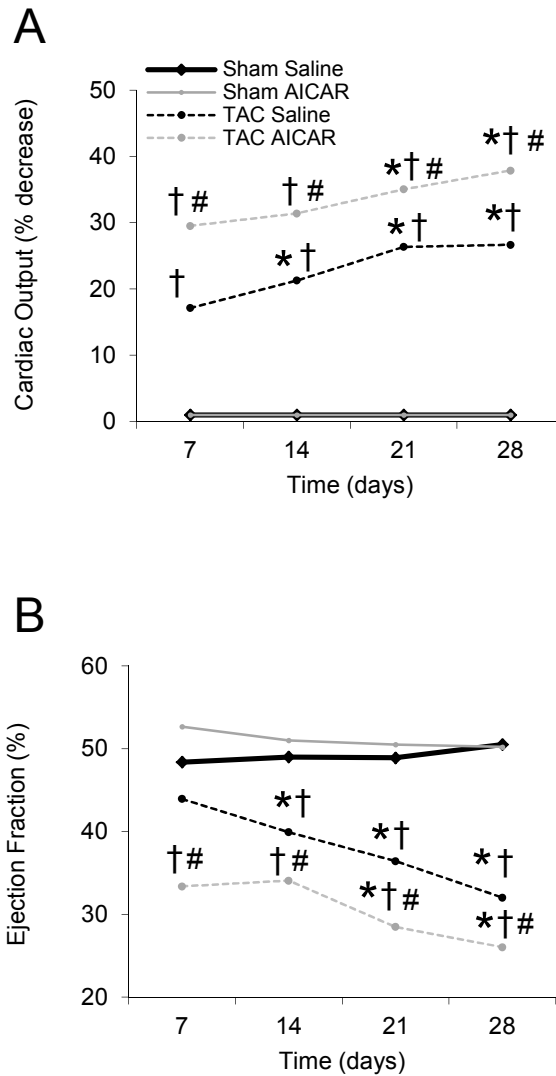


Figure 4.2. Synergistic effects of TAC and AICAR on cardiac function.

(A) Cardiac output and (B) Ejection fraction in response to AICAR and/ or TAC. Calculations were made based on measurements take from MRI images at the designated time. * $P < 0.01$ versus same group at 7 days, † $P < 0.01$ versus sham with same treatment at matched time point, # $P < 1.01$ versus TAC Saline at matched time point.

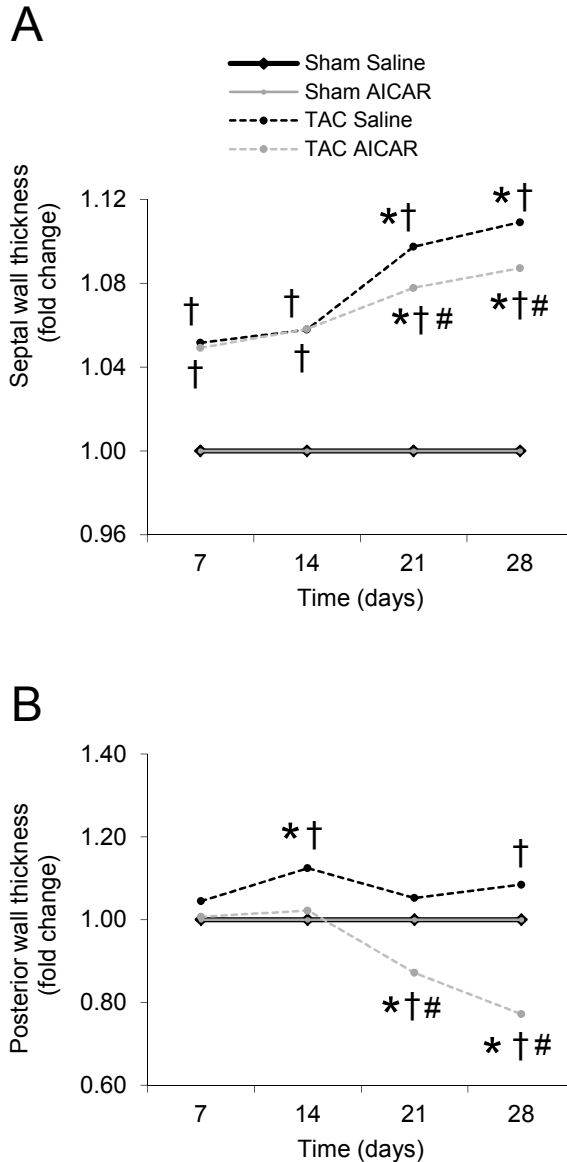


Figure 4.3. Synergistic effects of TAC and AICAR on cardiac dimensions.

(A) Septal and (B) Posterior wall thickness in response to AICAR and/ or TAC. Calculations were made based on measurements take from MRI images at the designated time. * $P < 0.01$ versus same group at 7 days, † $P < 0.01$ versus sham with same treatment at matched time point, # $P < 1.01$ versus TAC Saline at matched time point.

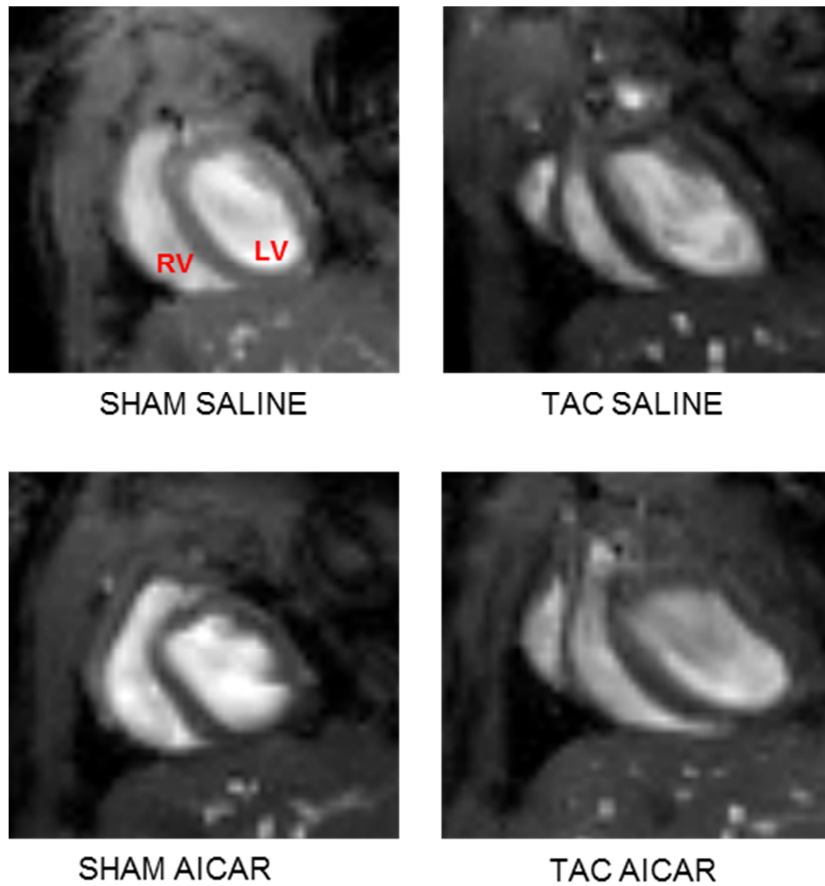


Figure 4.4. MRI images depicting synergistic effects of TAC and AICAR on the heart.

Representative MRI image of the heart in diastole in response to AICAR and/ or TAC. LV, left ventricle; RV, right ventricle.

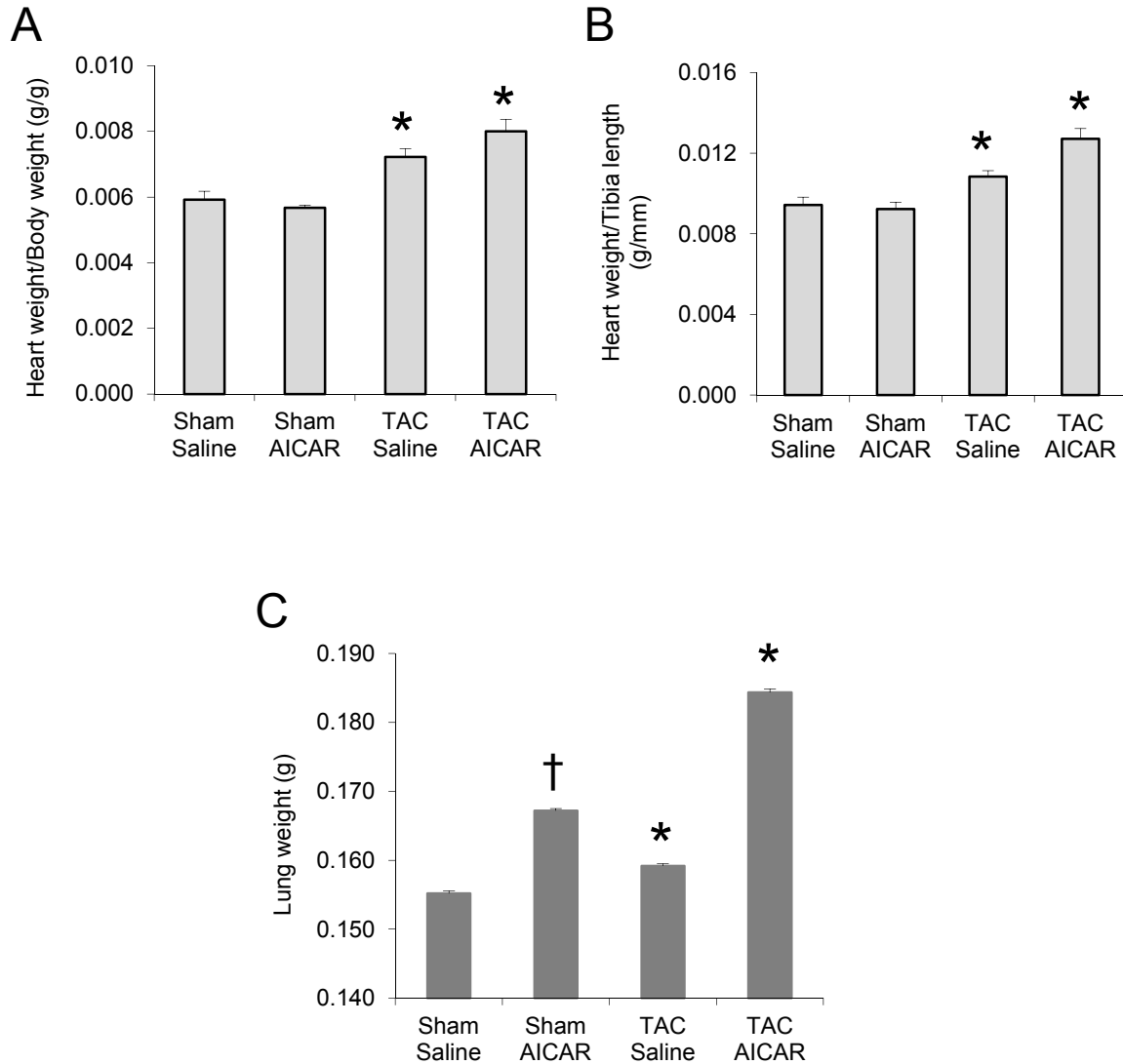


Figure 4.5. Synergistic effects of TAC and AICAR on heart and lung weight.

(A) Heart weight to body weight ratios, (B) heart weight to tibia length, and (C) lung weight in response to AICAR and/ or TAC. Twenty-four hours after the last MRI scans, hearts, tibia, and lungs were collected as described in 2.2.6. "Cell and Tissue Collection and Preservation". * $P < 0.01$ versus respective Sham group, † $P < 0.01$ versus Sham saline.

Differences in cardiomyocyte diameter were observed and quantified in **Figure 4.6.B**. Myocyte diameter was significantly increased with TAC, and further increased with AICAR. Although, not significant, AICAR treatment alone showed a tendency to decrease myocyte diameter, consistent with studies performed in isolated cardiomyocytes.

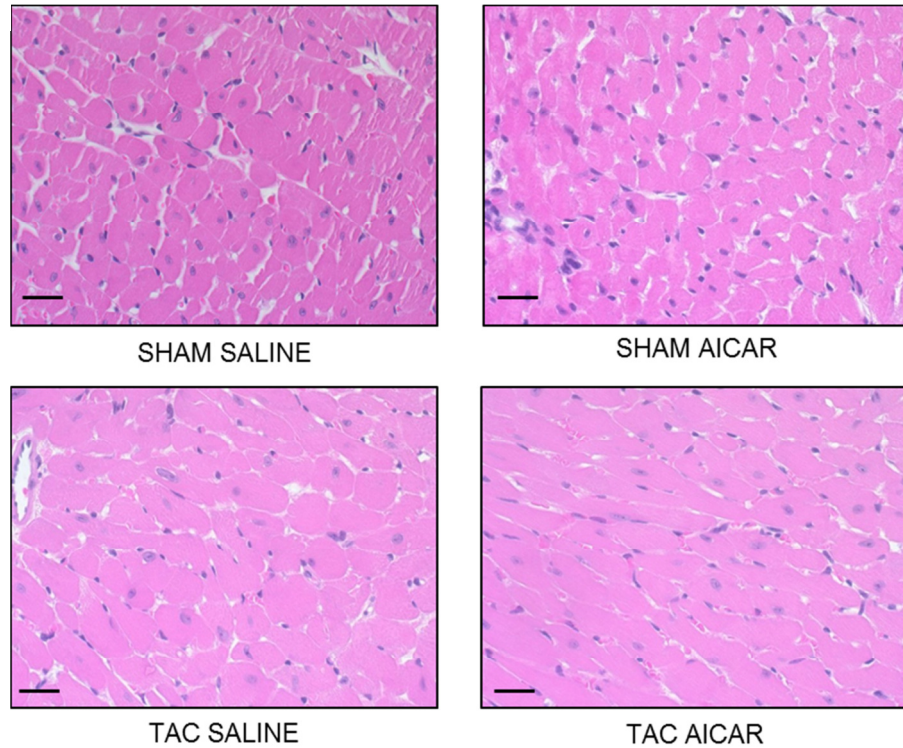
Angiogenesis occurs in the heart during hypertrophy and can be determined by the ratio of coronary microvessels per myocyte [319]. In muscle, AMPK regulates vascular endothelial growth factor (VEGF) thereby enhancing angiogenic repair during ischemia [379]. It is unclear whether AMPK plays a role in angiogenesis in the heart during hypertrophy. Therefore we evaluated the microvasculature by staining for CD31, a marker for endothelial cells within blood vessels. The number of capillaries per myocyte was increased with AICAR treatment and with TAC, and there was a slight, but insignificant, additive effect of AICAR treatment on TAC animals (**Figure 4.7.**). The collective results were somewhat puzzling to us at first. What could be causing the “protective” effect of AICAR to be detrimental to the heart in the setting of cardiac hypertrophy (*in vivo*)?

4.3. Molecular Consequences of Chronic AMPK activation in the Heart

We were initially surprised by the additive effects AICAR had with aortic constriction on cardiac phenotype and function. We had reasoned that activation of AMPK in hypertrophy would be cardioprotective during hemodynamic stress due to AMPK's role in regulating protein synthesis and degradation, in addition to its role in energy substrate provision. To gain an understanding of what could be responsible for the exaggerated changes seen in AICAR-treated TAC animals we first investigated established hypertrophic markers and pathways in the heart.

The fetal gene program is considered a “classic” marker of trophic response in the heart with alteration in load [380-385]. Therefore we determined whether these genes were altered by AICAR treatment. Because ejection fraction and cardiac output were further decreased with AICAR in animals with TAC, we wondered whether expression of contractile proteins was altered with AMPK activation. The heart switches expression of contractile genes during hypertrophy: α MHC decreases and β MHC increases in the mouse. We found this to be the case with TAC, regardless of treatment. While AICAR treatment increased α MHC, its expression was decreased to the same degree with hypertrophy as was the saline treated group (**Figure 4.8.A.**). β MHC expression was increased with TAC but further increased with AICAR treatment suggesting a greater shift to slow twitch myosin expression (in the rodent) which may contribute to decreased cardiac function (**Figure 4.8.B.**).

A



B

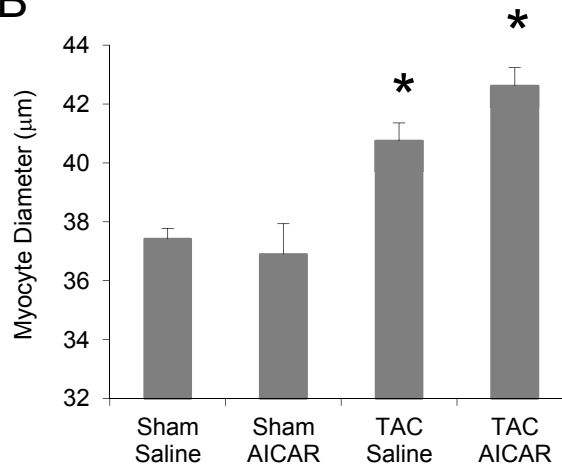


Figure 4.6. Synergistic effects of TAC and AICAR on cardiac phenotype.

(A) Representative images from cross sections of mouse hearts in response to AICAR and/or TAC. Hearts were collected, prepared, and stained using hematoxylin and eosin (H&E) stain as described in section 2.2.6.4. "Histology and Immunohistochemistry. Scale bars = 25µm. (B) Cardiomyocyte diameters were measured as described in section 2.2.6.4. "Histology and Immunohistochemistry. * $P < 0.01$ versus respective Sham group, † $P < 0.01$ versus Sham saline.

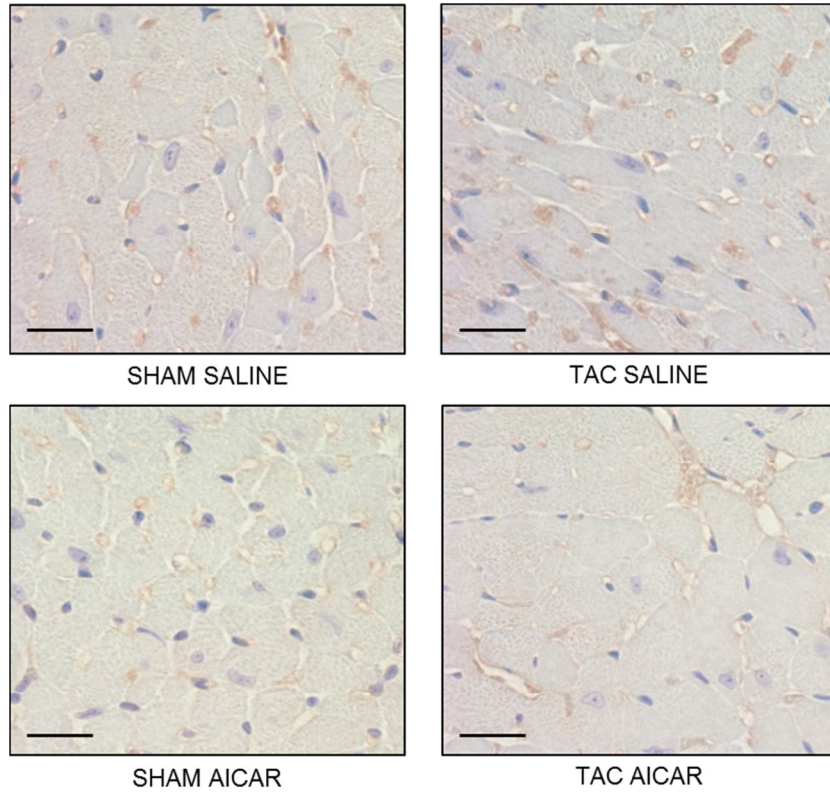
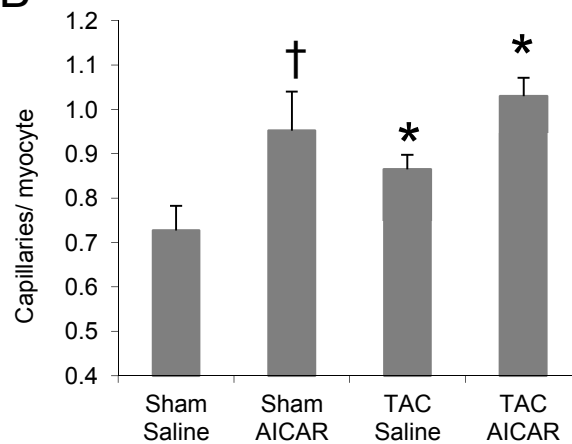
A**B**

Figure 4.7. Regulation of microvasculature in response to hypertrophy.

(A) Representative images from cross sections of mouse hearts in response to AICAR and/ or TAC. Hearts were collected, prepared, and stained with an antibody to CD31 as described in section 2.2.6.4. "Histology and Immunohistochemistry. Scale bars = 25 μ m. (B) The number of capillaries and cardiomyocytes were counted per field and plotted as a ratio. * $P < 0.01$ versus respective Sham group, † $P < 0.01$ versus Sham saline.

Atrial natriuretic factor (ANF), an early response gene was also further increased with AICAR in animals with TAC (**Figure 4.8.C.**).

In addition to structural changes, the heart metabolically adapts to pressure overload by switching its substrate utilization from reliance on fatty acids to reliance on glucose for ATP production. This is another hallmark of the fetal cardiac phenotype. Glucose uptake is regulated by GLUT1 and GLUT4, the main glucose transporters in the heart. GLUT1 is expressed in the adult heart and is not affected by hypertrophy. While translocation of glucose transporters to the membrane is regulated by AMPK, GLUT1 expression has recently been shown to be regulated by AMPK as well [386]. GLUT1 expression was increased with AICAR treatment, which was preserved with TAC, as shown in **Figure 4.8.C.** During hypertrophy GLUT4 expression is decreased; however, GLUT4 is also regulated by AMPK. AICAR treatment increased GLUT4 expression, as shown in Chapter 3. Furthermore, AICAR increased GLUT4 expression even in the hearts of TAC animals (**Figure 4.8.D.**). These data demonstrate that AICAR has a synergistic effect on fetal gene expression with TAC.

AMPK is known to regulate transcription of several groups of genes, one of which is involved in protein degradation. Indeed, AMPK activation in sham animals increased Atrogin-1 and MuRF1 expression, as previously discussed in Chapter 3. The expression of both ubiquitin ligases has also been shown to be increased in hypertrophy [199]. As with the expression of genes investigated thus far, both Atrogin-1 and MuRF1 expression were further increased with TAC upon stimulation with AICAR (**Figure 4.9.A. and B.**). Although pulse-chase analysis *in vivo* was not performed, I measured proteasome activity as a determinant of proteasome-mediated protein degradation. In the previous chapter I demonstrated that protein degradation in cardiomyocytes was increased with AICAR and decreased with Bortezomib, a proteasome inhibitor (**Figure 3.11.**). Consistent with these results, proteasome activity was significantly increased hearts with chronic AICAR treatment (**Figure 4.8.C.**). It has already been reported that proteasome activity is increased in the hypertrophied heart [125], which I also observed; however, AICAR treatment did not enhance proteasome activity in hearts from TAC animals (**Figure 4.8.C.**).

AMPK also regulates the expression of genes involved in autophagy. We found this to be the case in our experiments as well. AICAR increased the expression of Beclin, Atg5, and LC3 (**Figure 4.10.A-C**). Beclin, Atg 5, and Atg 12 expression was increased after TAC and further increased with AICAR treatment (**Figure 4.10.A, B, and D**). These results imply that AMPK activation regulates protein degradation in the heart, even during hypertrophy.

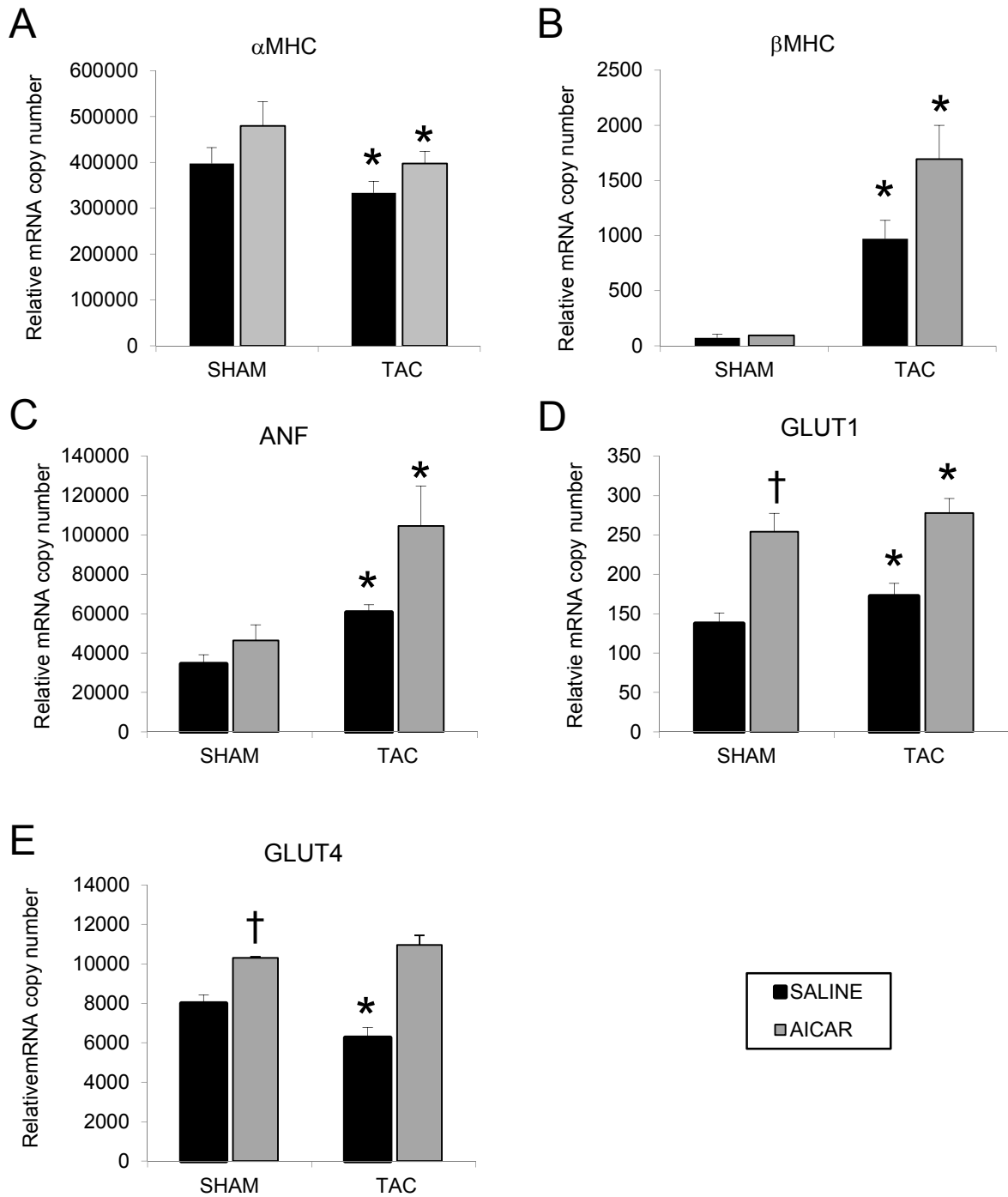


Figure 4.8. Reactivation of the fetal gene program during hypertrophy.

(A) α -Myosin Heavy Chain (α MHC), (B) β - Myosin Heavy Chain (β MHC), (C) Atrial nateuretic factor (ANF), (D) Glucose transporter 1 (GLUT1), and (E) GLUT4 gene expression in response to AICAR and/or TAC. * $P < 0.01$ versus respective Sham group, † $P < 0.01$ versus Sham saline.

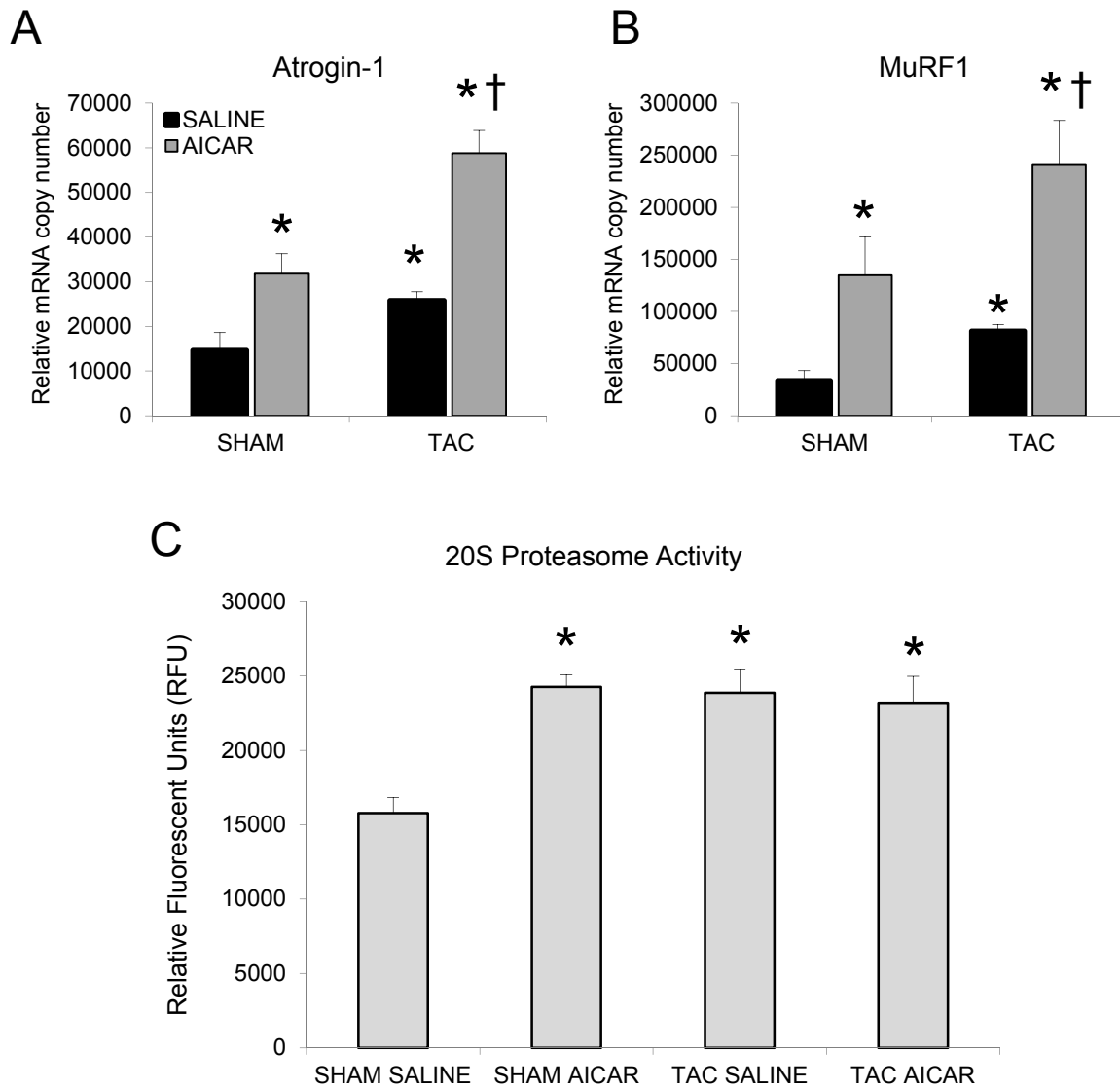


Figure 4.9. Regulation of the ubiquitin proteasome system in response to hypertrophy.

(A) Atrogin-1 and (B) MuRF1 gene expression in response to AICAR and/or TAC. (B) Proteasome activity (20S) in response to AICAR and/or TAC. The proteasome activity assay was performed as described in 2.2.7.4. "Proteasome Activity Assay". * $P < 0.01$ versus respective Sham group, † $P < 0.01$ versus respective treatment group.

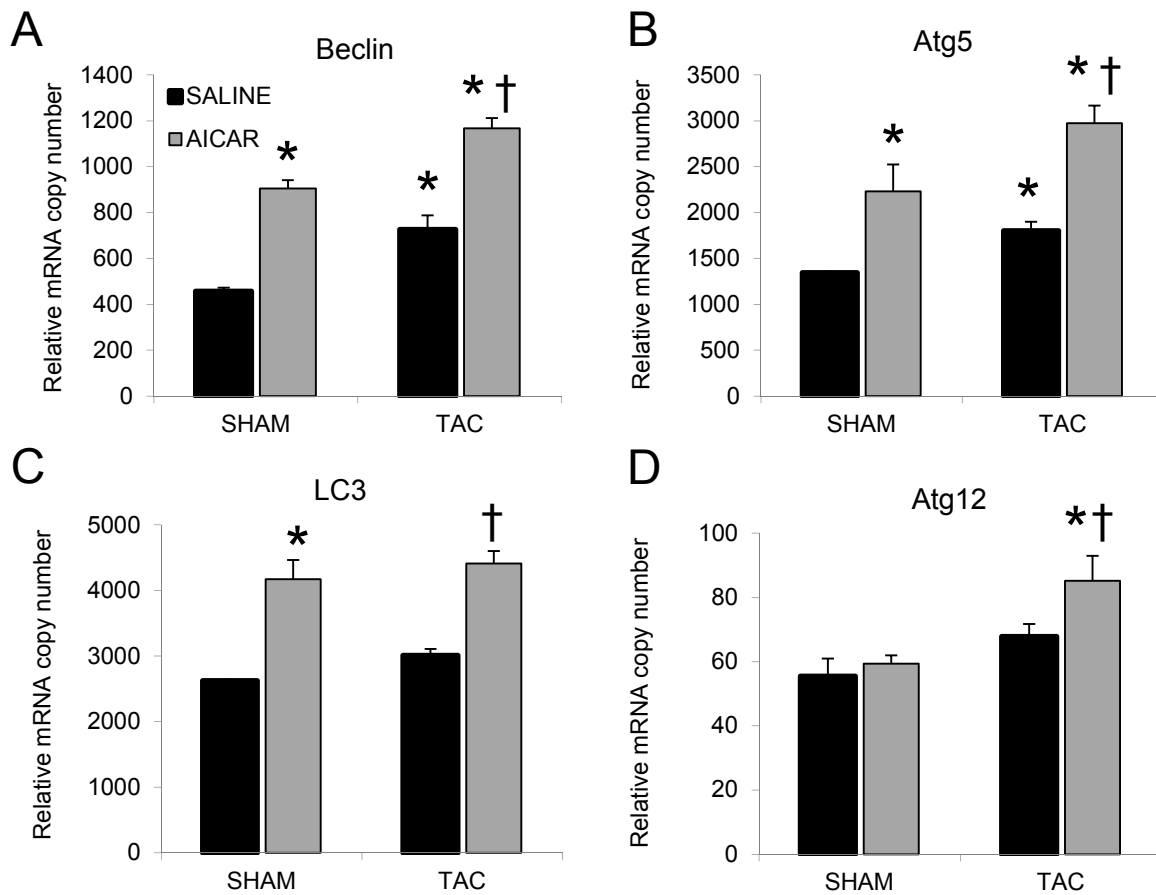


Figure 4.10. Regulation of autophagy genes in response to hypertrophy.

(A) Beclin, (B) Autophagy gene 5 (Atg5), (C) Light Chain 3 (LC3), (D) Autophagy gene 12 (Atg12) gene expression in response to AICAR and/or TAC. * $P < 0.01$ versus respective Sham groups, † $P < 0.01$ versus respective treatment group.

Although we initially thought that enhanced protein degradation would be a protective mechanism in hypertrophy, our data suggest otherwise.

To investigate further the mechanism by which AICAR mediates cardiac dysfunction we examined signaling pathways known to regulate hypertrophy. mTOR is phosphorylated in response to TAC, thus activating protein synthesis. AMPK is a known inhibitor of the mTOR signaling pathway. Activation of AMPK abolishes signaling through mTOR during hypertrophy (**Figure 4.11.**). The AKT signaling pathway is also a prominent hypertrophic pathway. Although AKT and AMPK seem to regulate each other, their interaction is still unclear. Our data presented here is not clean-cut either. AMPK, in the sham operated group, appears to slightly activate AKT; however, AMPK activation with TAC may decrease AKT phosphorylation. In any case, AKT is activated during hypertrophy (**Figure 4.11.**). AMPK, as previously shown, is increased in response to TAC and AICAR; however, there is not an additive effect of AICAR and TAC on AMPK. Acetyl-CoA carboxylase (ACC) is also phosphorylated in response to AMPK activation, whether the stimulus was AICAR or TAC (**Figure 4.11.**).

Collectively, our data show that chronic AICAR treatment, and thus activation of AMPK is detrimental to the heart on several different levels. First, cardiac function is impaired following TAC with AICAR treatment. Although AICAR alone doesn't impair cardiac function, it causes a significant increase in lung weight, suggesting that AICAR may have systemic side effects, possibly unrelated to AMPK activation. It is also interesting to note that despite the role that AMPK plays in regulating protein degradation through autophagy and proteasome-mediated protein degradation, TAC animals responded to AICAR through an enhanced hypertrophic response. Cardiomyocyte size and the fetal gene program were increased in response to TAC but more so with AICAR treatment in addition to TAC.

Although analysis of these experiments is ongoing, and I now focus on the metabolic aspects of the AICAR with TAC, I was not able to determine metabolic derangements in the hearts of these animals, as these studies require metabolic flux measurements. It would be ideal to repeat this study, but before terminating the experiment, measure substrate oxidation by perfusing the heart in working mode. The hypertrophied heart uses preferentially glucose as substrate whereas activation of AMPK not only increases glucose uptake, but also increases fatty acid oxidation. It would be interesting to investigate the combined cardiometabolic effects in the heart in response to TAC and

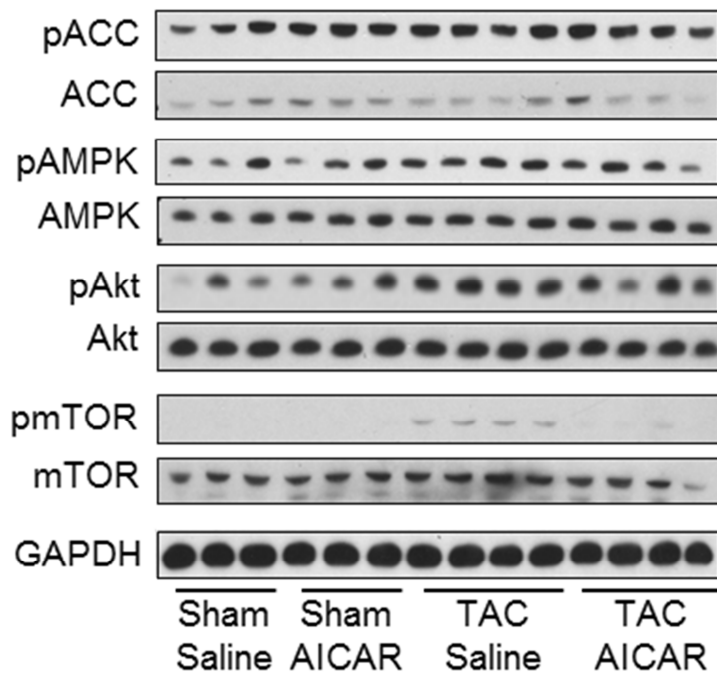


Figure 4.11. Regulation of signaling pathways during hypertrophy in response to AICAR.

Representative western blot of heart tissue in response to AICAR and/or TAC.

AICAR, as GLUT4 expression in AICAR treated TAC animals is significantly increased (**Figure 4.8.B.**).

This study is also limited by the fact that the experiment only allowed for terminal molecular changes to be investigated. Cardiac functional parameters taken throughout the course of the experiment allowed us to determine that AICAR may actually contribute to heart failure, although whether this is mediated directly through AMPK, and not a pharmacological side effect of AICAR treatment remains to be determined.

At the onset of our study, a similar report was published with results in striking contrast to what we observed [271]. In a rat model, 7 weeks of AICAR treatment (the same dose that we used) attenuated hypertrophy, as determined by echocardiographic analysis (fractional shortening and left ventricular end diastolic dimensions) and heart weight to body weight ratios. Serial echos were not taken and therefore cardiac function throughout AICAR treatment in this study is not known. A possible explanation in the drastically differing outcomes in mice compared to rats is a difference in the hypertrophy model. In the rat model, hypertrophy might develop slower than in mice, and after 7 weeks of TAC, vehicle treated rats are just beginning to show signs of severe hypertrophy. It is also interesting that after 7 weeks of TAC they found AICAR was able to normalize expression of the fetal genes ANP and BNP, and as we have shown here, decrease mTOR phosphorylation.

Along the same lines, a recent study provided evidence that ablation of $\alpha 2$ AMPK in the mouse heart deems them more susceptible to pressure-overload-induced hypertrophy [387]. Ejection fraction was significantly decreased in the knockout mice subjected to TAC. Moreover, these mice had increased myocardial fibrosis and cardiomyocyte size. Another study using the same mouse model induced short term hypertrophy by 7 days of isoproterenol (ISO) injections [306]. Consequently, AMPK $\alpha 2^{-/-}$ mice were more sensitive to ISO treatment and hypertrophied to a greater extent than WT mice. In this same study, the absence of $\alpha 2$ AMPK in the heart stimulated basal activity of p70S6 kinase, thus further highlighting the importance of AMPK in regulating protein synthesis.

It is also important to consider another activator of AMPK, the antidiabetic drug metformin. Metformin has been shown to activate AMPK indirectly by several mechanisms, although recently was shown to mediated energy charge in the liver independent of AMPK [388]. Ischemia-induced heart failure in mice can be minimized with metformin treatment, which does not occur in AMPK dominant negative Tg mice [389]. This study suggests that AMPK $\alpha 2$ is critical for metformin-mediated cardioprotection in heart failure. In support of

this hypothesis, diabetic patients with heart failure treated with metformin have a better rate of survival and fewer hospital admissions [390-393].

In conclusion, my results imply that the metabolic effects of long-term AMPK activation override AMPK's role in other cellular processes such as the regulation of protein turnover. Activation of AMPK increases insulin and non-insulin mediated glucose uptake suggesting that during hypertrophy, AICAR treated mice may suffer from excessive fuel overload, in addition to structural changes triggered by pressure overload. In a broad sense, these results give rise to the hypothesis that metabolic dysregulation may play a role in this process, although this is the topic of current investigation.

Chapter 5

CONCLUDING REMARKS AND OUTLOOK

“The game of science is, in principle, without end. He who decides one day that scientific statements do not call for any further test, and that they can be regarded as finally verified, retires from the game [394].”

~Sir Karl Popper, CH FRS FBA (1935)

The heart is a dynamic organ that adapts metabolically and structurally to various types of stress. This remodeling process is critical for survival because cardiomyocytes are terminally differentiated cells. Although there is evidence for the existence of sub-populations of cardiac progenitor cells [395], they have been suggested to generate and replace cardiomyocytes at a very low rate compared to other cell types [396]. Thus, intracellular homeostasis in the broad sense is vital for cardiomyocyte preservation and, ultimately, cardiac function.

In the preceding chapters I have provided evidence in support of the hypothesis that AMPK regulates proteasome-mediated protein degradation in the heart by regulating ubiquitin ligases. I have demonstrated that this occurs during nutrient deprivation (fasting) and also in the hypertrophied heart. Interestingly, and contrary to what I expected, fasting-induced AMPK activation and the activation of AMPK with AICAR during hypertrophy are detrimental to the heart.

The multifaceted role that AMPK plays in the cardiomyocyte makes it both an intriguing and challenging kinase to investigate. AMPK has been shown to be a transcriptional regulator and a regulator of protein synthesis, as well as protein degradation, as presented in my thesis. The metabolic function of AMPK in regulating substrate uptake and oxidation, particularly under stress, is undoubtedly the most important process that AMPK controls in the heart. This is evident by the results shown in Chapter 4. The activation of AMPK increases protein degradation during hypertrophy, while at the same time further enhancing glucose uptake (increased GLUT4 expression). Although currently under investigation, it is possible that, with chronic AMPK stimulation, and the added stress of pressure overload, glucose uptake is increased to the point of glucotoxicity, which contributes to cardiac dysfunction.

We have proposed that metabolic remodeling precedes, triggers, and sustains structural and functional remodeling of the heart [8, 272, 397] and metabolites themselves might be regulating cardiac remodeling directly. One possible mechanism is protein modification by direct metabolite interaction, such as AMP binding to AMPK, leading to AMPK activation. Another example is fatty acid regulated protein function, such as the transcriptional activation of peroxisome proliferator-activated receptor α , PPAR α [398]. Yet another example of metabolite-mediated protein modification is O-linked glycosylation. This has been shown to occur during excessive glucose uptake in the heart, resulting in enhanced transcription through modification of transcription factors [397]. Thus, in the hearts of AICAR treated TAC animals, the level of glucose metabolites could be increased,

leading to activation of detrimental processes including ER stress, in spite of the protective effects of enhanced protein degradation.

A recent study focusing on the “exercise mimetic” properties of AICAR received publicity from mainstream media due to the possibility of “exercise in a pill” [399, 400]. In this study, mice given AICAR daily for four weeks (the same dose I used in all my *in vivo* experiments) exhibited enhanced exercise endurance without exercise training. In muscle, AICAR treatment resulted in expression of an “endurance gene signature” comprised of metabolic genes. While the heart was not investigated in this study, it raises an interesting question. If AICAR-mediated AMPK activation significantly increases glucose uptake in the hypertrophied heart, and consequently increases glycolytic intermediates that can be detrimental on the heart, can these intermediates be reduced by exercise, thus preventing cardiac dysfunction?

Metabolic changes that occur in the heart during fasting, like in cardiac hypertrophy, precede any structural changes. Metabolic changes that result from fasting are complex and occur at the whole body level, organ level, and at the intracellular level as reviewed in [401]. Initially during fasting, liver glycogen stores are broken down and used for ATP generation. Once glycogen stores are depleted in the liver, proteins in the muscle are broken down and are used in the liver for gluconeogenesis. Lipolysis occurs during the later stages of fasting; fat is mobilized from adipose tissue to provide fatty acids as substrates for β -oxidation. Although numerous metabolic changes occur during fasting, I focused only on the cardiovascular changes in my *in vivo* fasting experiments (see Chapter 3).

While the heart has a limited capacity to store substrates, glycogen accumulates in the heart during fasting [402]. This is most likely a protective mechanism of the heart: it stores enough endogenous substrate for temporarily use during extreme conditions in order to maintain contractile function. I did not thoroughly investigate the metabolic changes in the heart during fasting. It would be interesting to determine if substrate uptake and utilization is differentially regulated during fasting in the absence of MuRF1. I have preliminary data suggesting that under fed conditions hearts from MuRF1^{-/-} mice show increased rates of glucose oxidation, but whether this is maintained during fasting, and whether it is detrimental to the heart during fasting is not known.

It would have also been of interest to determine how MuRF1 Tg mice respond to fasting. Because the absence of MuRF1 seems to protect the heart during fasting, I propose that increased amounts of MuRF1, higher than what occurs in WT mice in response to fasting, would be detrimental to the heart. Mitochondrial content in the heart is

increased in MuRF1 Tg mice, although there is no significant change in steady-state ATP levels [217]. Increased mitochondrial content could be caused by alterations in mitochondrial dynamics (decreased fusion or increased fission). Although I did not investigate mitochondrial changes in response to fasting, it has recently been shown that fasting decreases mitochondrial function in skeletal muscle [403]. MuRF1 might be responsible for these observations. Additionally, MuRF1-mediated degradation of the pyruvate dehydrogenase complex also suggests that MuRF1 is involved in mitochondrial regulation [209].

MuRF1 also ubiquitinates β -hydroxyisobutyrate dehydrogenase [208], an enzyme that is critical in the catabolism of valine. β -hydroxyisobutyrate dehydrogenase oxidizes 3-hydroxyisobutyric acid to methylmalonic acid semialdehyde, ultimately producing succinyl-CoA which enters the Krebs cycle [404]. Branched chain amino acids (BCAA) in the plasma decrease during conditions that lead to muscle wasting, for example during metabolic acidosis [405] and fasting. The absence of MuRF1 decreases the BCAA levels in the plasma even further [208]. These data suggest that protein degradation in the absence of MuRF1 is decreased, thus decreasing the release of BCAA into the blood stream. Furthermore, increased levels of β -hydroxyisobutyrate dehydrogenase in MuRF1^{-/-} mice suggests an increase in BCAA, and specifically valine, catabolism [208].

Another interesting observation is that hearts from MuRF1 Tg mice exhibit decreased AMPK phosphorylation at baseline [217]. The ramifications of this observation, and whether this is important during fasting, have yet to be considered. It is also not clear as to what degree fasting-induced cardiac dysfunction is mediated specifically through the AMPK-MuRF1 axis. In order to determine the contribution of AMPK-MuRF1 in fasting, MuRF1^{-/-} and MuRF1 Tg mice could be crossed with AMPK α 2^{-/-} or AMPK α 2^{DN} mice and subjected to fasting. However, it is possible that AMPK α 2^{-/-} or AMPK α 2^{DN} mice themselves may be sensitive to fasting due to the central role of AMPK in metabolic regulation in the heart during stress.

AMPK phosphorylation was decreased in the hearts of MuRF1 Tg mice, as mentioned above. This is intriguing because it raises the possibility that AMPK itself might be regulated by MuRF1. This concept is not entirely novel, because Atrogin-1, shown to be transcriptionally regulated by FOXO3A, can feed back on FOXO3A [156]. Atrogin-1 ubiquitinates FOXO3A. Consequently, ubiquitination decreases the ability of FOXO3A to be phosphorylated and thus excluded from the nucleus, and enhances its transcriptional activity [156]. It is possible that AMPK is a substrate for MuRF1 ubiquitination. Although

AMPK regulation and/or degradation by ubiquitin modification has not been thoroughly investigated, Qi et. al. demonstrated that the β -subunit of AMPK can be ubiquitinated by the ligase Cidea, thereby decreasing AMPK activity [406].

The role of Atrogin-1 in the heart during fasting was also not investigated here. Given that Atrogin-1 and MuRF1 seem to contribute equally to fasting-induced protein degradation in muscle, it seems reasonable to hypothesize that Atrogin-1 is also important in the heart during fasting. Atrogin-1 targets a different set of proteins for degradation and therefore cardiac function may not be preserved in the absence of Atrogin-1, as seen in the absence of MuRF1.

It is well established that Atrogin-1 and MuRF1 play a critical role in proteasome-mediated protein degradation in skeletal muscle and in the heart. While the UPS is an essential system regulating protein degradation, there are other systems at work as well. The calpain system and autophagy contribute to general protein degradation (see Chapter 1), whereas the degradation of misfolded proteins during protein processing through the endoplasmic reticulum (ER), known as ER-associated degradation (ERAD), is also important. These systems act together to coordinate protein quality control (PQC) in the heart to maintain cardiac protein homeostasis [119]. PQC is especially important in eliminating damaged proteins during times of cardiac stress, and can be a protective mechanism to preserve cardiac function.

While there are still many more questions than answers, it is evident that the role of protein degradation in the heart, while complex, is critical for cardiac function. I have provided strong evidence to support the hypothesis that protein turnover is metabolically regulated. Under conditions of extreme metabolic stress, AMPK is still able to regulate protein degradation. The results presented here extend the long-established concept of the “dynamic state of body constituents” set forth by Rudolph Schoenheimer in 1942 [407]. There is, I am certain, much more to come.

“What we learn from experience depends on the kind of philosophy we bring to experience [408].”

~C.S. Lewis, Author, Christian Scholar

References

1. Harvey, W. 1628. *Exercitatio Anatomica De Motu Cordis Ed Sanguinis in Animalibus*, William Fitzer, Frankfurt.
2. Roger, V. L., Go, A. S., Lloyd-Jones, D. M., Adams, R. J., Berry, J. D., Brown, T. M., Carnethon, M. R., Dai, S., de Simone, G., Ford, E. S., Fox, C. S., Fullerton, H. J., Gillespie, C., Greenlund, K. J., Hailpern, S. M., Heit, J. A., Ho, P. M., Howard, V. J., Kissela, B. M., Kittner, S. J., Lackland, D. T., Lichtman, J. H., Lisabeth, L. D., Makuc, D. M., Marcus, G. M., Marelli, A., Matchar, D. B., McDermott, M. M., Meigs, J. B., Moy, C. S., Mozaffarian, D., Mussolino, M. E., Nichol, G., Paynter, N. P., Rosamond, W. D., Sorlie, P. D., Stafford, R. S., Turan, T. N., Turner, M. B., Wong, N. D. and Wylie-Rosett, J. 2011. Heart disease and stroke statistics--2011 update: a report from the American Heart Association. *Circulation*. 123:e18-e209.
3. Rame, J. E. and Dries, D. L. 2007. Heart failure and cardiac hypertrophy. *Curr Treat Options Cardiovasc Med*. 9:289-301.
4. Marian, A. J. 2008. Genetic determinants of cardiac hypertrophy. *Curr Opin Cardiol*. 23:199-205.
5. Seidman, C. E. and Seidman, J. G. 2011. Identifying sarcomere gene mutations in hypertrophic cardiomyopathy: a personal history. *Circ Res*. 108:743-50.
6. Lips, D. J., deWindt, L. J., van Kraaij, D. J. and Doevendans, P. A. 2003. Molecular determinants of myocardial hypertrophy and failure: alternative pathways for beneficial and maladaptive hypertrophy. *Eur Heart J*. 24:883-96.
7. Sadoshima, J. and Izumo, S. 1997. The cellular and molecular response of cardiac myocytes to mechanical stress. *Annu Rev Physiol*. 59:551-71.
8. Goodwin, G. W., Taylor, C. S. and Taegtmeyer, H. 1998. Regulation of energy metabolism of the heart during acute increase in heart work. *J Biol Chem*. 273:29530-9.
9. Schonekess, B. O., Allard, M. F. and Lopaschuk, G. D. 1996. Recovery of glycolysis and oxidative metabolism during postischemic reperfusion of hypertrophied rat hearts. *Am J Physiol*. 271:H798-805.
10. Sambandam, N., Lopaschuk, G. D., Brownsey, R. W. and Allard, M. F. 2002. Energy metabolism in the hypertrophied heart. *Heart Fail Rev*. 7:161-73.
11. Taegtmeyer, H., Sen, S. and Vela, D. 2010. Return to the fetal gene program: a suggested metabolic link to gene expression in the heart. *Ann N Y Acad Sci*. 1188:191-8.
12. Hill, J. and Olson, E. 2008. Cardiac Plasticity. *N Engl J Med*. 358:1370-80.

13. Ford, L. E. 1976. Heart size. *Circ Res.* 39:297-303.
14. Dorn, G. W., 2nd, Robbins, J. and Sugden, P. H. 2003. Phenotyping hypertrophy: eschew obfuscation. *Circ Res.* 92:1171-5.
15. Braunwald, E. and Bristow, M. R. 2000. Congestive heart failure: fifty years of progress. *Circulation.* 102:IV14-23.
16. Hein, S., Arnon, E., Kostin, S., Schonburg, M., Elsasser, A., Polyakova, V., Bauer, E. P., Klovekorn, W. P. and Schaper, J. 2003. Progression from compensated hypertrophy to failure in the pressure-overloaded human heart: structural deterioration and compensatory mechanisms. *Circulation.* 107:984-91.
17. Muiesan, M. L., Salvetti, M., Rizzoni, D., Castellano, M., Donato, F. and Agabiti-Rosei, E. 1995. Association of change in left ventricular mass with prognosis during long-term antihypertensive treatment. *J Hypertens.* 13:1091-5.
18. Verdecchia, P., Schillaci, G., Borgioni, C., Ciucci, A., Gattobigio, R., Zampi, I., Reboldi, G. and Porcellati, C. 1998. Prognostic significance of serial changes in left ventricular mass in essential hypertension. *Circulation.* 97:48-54.
19. Mathew, J., Sleight, P., Lonn, E., Johnstone, D., Pogue, J., Yi, Q., Bosch, J., Sussex, B., Probstfield, J. and Yusuf, S. 2001. Reduction of cardiovascular risk by regression of electrocardiographic markers of left ventricular hypertrophy by the angiotensin-converting enzyme inhibitor ramipril. *Circulation.* 104:1615-21.
20. Fagard, R. H., Celis, H., Thijs, L. and Wouters, S. 2009. Regression of left ventricular mass by antihypertensive treatment: a meta-analysis of randomized comparative studies. *Hypertension.* 54:1084-91.
21. Frey, N. and Olson, E. N. 2003. Cardiac hypertrophy: the good, the bad, and the ugly. *Annu Rev Physiol.* 65:45-79.
22. Molkenkin, J. D. and Dorn, G. W., 2nd. 2001. Cytoplasmic signaling pathways that regulate cardiac hypertrophy. *Annu Rev Physiol.* 63:391-426.
23. Karsner, H. T., Saphir, O. and Todd, T. W. 1925. The State of the Cardiac Muscle in Hypertrophy and Atrophy. *Am J Pathol.* 1:351-372 1.
24. Russell, B., Motlagh, D. and Ashley, W. W. 2000. Form follows function: how muscle shape is regulated by work. *J Appl Physiol.* 88:1127-32.
25. Sugden, P. H. and Clerk, A. 1998. Cellular mechanisms of cardiac hypertrophy. *J Mol Med (Berl).* 76:725-46.
26. Patterson, C., Ike, C., Willis, P. W. t., Stouffer, G. A. and Willis, M. S. 2007. The bitter end: the ubiquitin-proteasome system and cardiac dysfunction. *Circulation.* 115:1456-63.

27. Banerjee, I., Fuseler, J. W., Price, R. L., Borg, T. K. and Baudino, T. A.2007. Determination of cell types and numbers during cardiac development in the neonatal and adult rat and mouse. *Am J Physiol Heart Circ Physiol.* 293:H1883-91.
28. Long, C. S., Kariya, K., Karns, L. and Simpson, P. C.1990. Trophic factors for cardiac myocytes. *J Hypertens Suppl.* 8:S219-24.
29. Baskin, K. K. and Taegtmeyer, H.2011. Taking pressure off the heart: the ins and outs of atrophic remodelling. *Cardiovasc Res.* 90:243-50.
30. Fagan, J. M., Waxman, L. and Goldberg, A. L.1987. Skeletal muscle and liver contain a soluble ATP + ubiquitin-dependent proteolytic system. *Biochem J.* 243:335-43.
31. Morgan, H. E., Rannels, D. E. and Kao, R. L.1974. Factors controlling protein turnover in heart muscle. *Circ Res.* 35 Suppl 3:22-31.
32. Jackman, R. W. and Kandarian, S. C.2004. The molecular basis of skeletal muscle atrophy. *Am J Physiol Cell Physiol.* 287:C834-43.
33. Du, J., Wang, X., Miereles, C., Bailey, J. L., Debigare, R., Zheng, B., Price, S. R. and Mitch, W. E.2004. Activation of caspase-3 is an initial step triggering accelerated muscle proteolysis in catabolic conditions. *J Clin Invest.* 113:115-23.
34. Wang, X. H., Zhang, L., Mitch, W. E., LeDoux, J. M., Hu, J. and Du, J.2010. Caspase-3 cleaves specific 19 S proteasome subunits in skeletal muscle stimulating proteasome activity. *J Biol Chem.* 285:21249-57.
35. Goll, D. E., Neti, G., Mares, S. W. and Thompson, V. F.2008. Myofibrillar protein turnover: the proteasome and the calpains. *J Anim Sci.* 86:E19-35.
36. Goll, D. E., Thompson, V. F., Li, H., Wei, W. and Cong, J.2003. The calpain system. *Physiol Rev.* 83:731-801.
37. Croall, D. E. and Ersfeld, K.2007. The calpains: modular designs and functional diversity. *Genome Biol.* 8:218.
38. Suzuki, A., Kim, K. and Ikeuchi, Y.1996. Proteolytic cleavage of connectin/titin. *Adv Biophys.* 33:53-64.
39. Raynaud, F., Fernandez, E., Coulis, G., Aubry, L., Vignon, X., Bleimling, N., Gautel, M., Benyamin, Y. and Ouali, A.2005. Calpain 1-titin interactions concentrate calpain 1 in the Z-band edges and in the N2-line region within the skeletal myofibril. *FEBS J.* 272:2578-90.
40. Dayton, W. R., Reville, W. J., Goll, D. E. and Stromer, M. H.1976. A Ca²⁺-activated protease possibly involved in myofibrillar protein turnover. Partial characterization of the purified enzyme. *Biochemistry.* 15:2159-67.

41. Pemrick, S. M. and Grebenau, R. C.1984. Qualitative analysis of skeletal myosin as substrate of Ca²⁺-activated neutral protease: comparison of filamentous and soluble, native, and L2-deficient myosin. *J Cell Biol.* 99:2297-308.
42. Duguez, S., Bartoli, M. and Richard, I.2006. Calpain 3: a key regulator of the sarcomere? *FEBS J.* 273:3427-36.
43. Mellgren, R. L.1980. Canine cardiac calcium-dependent proteases: Resolution of two forms with different requirements for calcium. *FEBS Lett.* 109:129-33.
44. Beinlich, C. J., Clark, M. G., McKee, E. E., Lins, J. A. and Morgan, H. E.1981. Neutral-alkaline proteolytic activity in rat cardiac muscle cells. *J Mol Cell Cardiol.* 13:23-36.
45. Croall, D. E. and DeMartino, G. N.1983. Purification and characterization of calcium-dependent proteases from rat heart. *J Biol Chem.* 258:5660-5.
46. Singh, R. B., Dandekar, S. P., Elimban, V., Gupta, S. K. and Dhalla, N. S.2004. Role of proteases in the pathophysiology of cardiac disease. *Mol Cell Biochem.* 263:241-56.
47. Chen, M., Won, D. J., Krajewski, S. and Gottlieb, R. A.2002. Calpain and mitochondria in ischemia/reperfusion injury. *J Biol Chem.* 277:29181-6.
48. Patterson, C., Portbury, A. L., Schisler, J. C. and Willis, M. S.2011. Tear me down: role of calpain in the development of cardiac ventricular hypertrophy. *Circ Res.* 109:453-62.
49. de Reuck, A. V. S. and Cameron, M. P., (1963) The Lysosome Concept. 1963 Ciba Foundation Symposium on Lysosomes.
50. Klionsky, D. J.2008. Autophagy revisited: a conversation with Christian de Duve. *Autophagy.* 4:740-3.
51. Ravikumar, B., Sarkar, S., Davies, J. E., Futter, M., Garcia-Arencibia, M., Green-Thompson, Z. W., Jimenez-Sanchez, M., Korolchuk, V. I., Lichtenberg, M., Luo, S., Massey, D. C., Menzies, F. M., Moreau, K., Narayanan, U., Renna, M., Siddiqi, F. H., Underwood, B. R., Winslow, A. R. and Rubinsztein, D. C.2010. Regulation of mammalian autophagy in physiology and pathophysiology. *Physiol Rev.* 90:1383-435.
52. Klionsky, D. J., Codogno, P., Cuervo, A. M., Deretic, V., Elazar, Z., Fueyo-Margareto, J., Gewirtz, D. A., Kroemer, G., Levine, B., Mizushima, N., Rubinsztein, D. C., Thumm, M. and Tooze, S. A.2010. A comprehensive glossary of autophagy-related molecules and processes. *Autophagy.* 6:

53. Yang, Z. and Klionsky, D. J.2010. Eaten alive: a history of macroautophagy. *Nat Cell Biol.* 12:814-22.
54. Mijaljica, D., Prescott, M. and Devenish, R. J.2011. Microautophagy in mammalian cells: revisiting a 40-year-old conundrum. *Autophagy.* 7:673-82.
55. Wang, K. and Klionsky, D. J.2011. Mitochondria removal by autophagy. *Autophagy.* 7:297-300.
56. Gottlieb, R. A. and Carreira, R. S.2010. Autophagy in health and disease. 5. Mitophagy as a way of life. *Am J Physiol Cell Physiol.* 299:C203-10.
57. Arias, E. and Cuervo, A. M.2011. Chaperone-mediated autophagy in protein quality control. *Curr Opin Cell Biol.* 23:184-9.
58. Danon, M. J., Oh, S. J., DiMauro, S., Manaligod, J. R., Eastwood, A., Naidu, S. and Schliselfeld, L. H.1981. Lysosomal glycogen storage disease with normal acid maltase. *Neurology.* 31:51-7.
59. Nishino, I., Fu, J., Tanji, K., Yamada, T., Shimojo, S., Koori, T., Mora, M., Riggs, J. E., Oh, S. J., Koga, Y., Sue, C. M., Yamamoto, A., Murakami, N., Shanske, S., Byrne, E., Bonilla, E., Nonaka, I., DiMauro, S. and Hirano, M.2000. Primary LAMP-2 deficiency causes X-linked vacuolar cardiomyopathy and myopathy (Danon disease). *Nature.* 406:906-10.
60. Cao, D. J., Gillette, T. G. and Hill, J. A.2009. Cardiomyocyte autophagy: remodeling, repairing, and reconstructing the heart. *Curr Hypertens Rep.* 11:406-11.
61. Nakai, A., Yamaguchi, O., Takeda, T., Higuchi, Y., Hikoso, S., Taniike, M., Omiya, S., Mizote, I., Matsumura, Y., Asahi, M., Nishida, K., Hori, M., Mizushima, N. and Otsu, K.2007. The role of autophagy in cardiomyocytes in the basal state and in response to hemodynamic stress. *Nat Med.* 13:619-24.
62. Kitsis, R. N., Peng, C. F. and Cuervo, A. M.2007. Eat your heart out. *Nat Med.* 13:539-41.
63. Gustafsson, A. B. and Gottlieb, R. A.2009. Autophagy in ischemic heart disease. *Circ Res.* 104:150-8.
64. Zhu, H., Tannous, P., Johnstone, J. L., Kong, Y., Shelton, J. M., Richardson, J. A., Le, V., Levine, B., Rothermel, B. A. and Hill, J. A.2007. Cardiac autophagy is a maladaptive response to hemodynamic stress. *J Clin Invest.* 117:1782-93.
65. Nishida, K., Yamaguchi, O. and Otsu, K.2008. Crosstalk between autophagy and apoptosis in heart disease. *Circ Res.* 103:343-51.
66. Rothermel, B. A. and Hill, J. A.2008. Autophagy in load-induced heart disease. *Circ Res.* 103:1363-9.

67. Lee, D. H. and Goldberg, A. L. 1998. Proteasome inhibitors: valuable new tools for cell biologists. *Trends Cell Biol.* 8:397-403.
68. Goldberg, A. L. and St John, A. C. 1976. Intracellular protein degradation in mammalian and bacterial cells: Part 2. *Annu Rev Biochem.* 45:747-803.
69. Etlinger, J. D. and Goldberg, A. L. 1977. A soluble ATP-dependent proteolytic system responsible for the degradation of abnormal proteins in reticulocytes. *Proc Natl Acad Sci U S A.* 74:54-8.
70. DeMartino, G. N. and Goldberg, A. L. 1979. Identification and partial purification of an ATP-stimulated alkaline protease in rat liver. *J Biol Chem.* 254:3712-5.
71. Rose, I. A., Warms, J. V. and Hershko, A. 1979. A high molecular weight protease in liver cytosol. *J Biol Chem.* 254:8135-8.
72. Hershko, A., Ciechanover, A., Heller, H., Haas, A. L. and Rose, I. A. 1980. Proposed role of ATP in protein breakdown: conjugation of protein with multiple chains of the polypeptide of ATP-dependent proteolysis. *Proc Natl Acad Sci U S A.* 77:1783-6.
73. Hershko, A., Ciechanover, A. and Rose, I. A. 1981. Identification of the active amino acid residue of the polypeptide of ATP-dependent protein breakdown. *J Biol Chem.* 256:1525-8.
74. Ciechanover, A., Heller, H., Katz-Etzion, R. and Hershko, A. 1981. Activation of the heat-stable polypeptide of the ATP-dependent proteolytic system. *Proc Natl Acad Sci U S A.* 78:761-5.
75. Hershko, A., Heller, H., Elias, S. and Ciechanover, A. 1983. Components of ubiquitin-protein ligase system. Resolution, affinity purification, and role in protein breakdown. *J Biol Chem.* 258:8206-14.
76. Hershko, A., Leshinsky, E., Ganoth, D. and Heller, H. 1984. ATP-dependent degradation of ubiquitin-protein conjugates. *Proc Natl Acad Sci U S A.* 81:1619-23.
77. Goldberg, A. L. 2005. Nobel committee tags ubiquitin for distinction. *Neuron.* 45:339-44.
78. Groettrup, M., Pelzer, C., Schmidtke, G. and Hofmann, K. 2008. Activating the ubiquitin family: UBA6 challenges the field. *Trends Biochem Sci.* 33:230-7.
79. Ye, Y. and Rape, M. 2009. Building ubiquitin chains: E2 enzymes at work. *Nat Rev Mol Cell Biol.* 10:755-64.
80. Weissman, A. M. 2001. Themes and variations on ubiquitylation. *Nat Rev Mol Cell Biol.* 2:169-78.
81. Thrower, J. S., Hoffman, L., Rechsteiner, M. and Pickart, C. M. 2000. Recognition of the polyubiquitin proteolytic signal. *EMBO J.* 19:94-102.

82. Navon, A. and Ciechanover, A.2009. The 26 S proteasome: from basic mechanisms to drug targeting. *J Biol Chem.* 284:33713-8.
83. Pelzer, C., Kassner, I., Matentzoglou, K., Singh, R. K., Wollscheid, H. P., Scheffner, M., Schmidtke, G. and Groettrup, M.2007. UBE1L2, a novel E1 enzyme specific for ubiquitin. *J Biol Chem.* 282:23010-4.
84. Jin, J., Li, X., Gygi, S. P. and Harper, J. W.2007. Dual E1 activation systems for ubiquitin differentially regulate E2 enzyme charging. *Nature.* 447:1135-8.
85. Chiu, Y. H., Sun, Q. and Chen, Z. J.2007. E1-L2 activates both ubiquitin and FAT10. *Mol Cell.* 27:1014-23.
86. McGrath, J. P., Jentsch, S. and Varshavsky, A.1991. UBA 1: an essential yeast gene encoding ubiquitin-activating enzyme. *EMBO J.* 10:227-36.
87. Kulkarni, M. and Smith, H. E.2008. E1 ubiquitin-activating enzyme UBA-1 plays multiple roles throughout *C. elegans* development. *PLoS Genet.* 4:e1000131.
88. van Wijk, S. J. and Timmers, H. T.2010. The family of ubiquitin-conjugating enzymes (E2s): deciding between life and death of proteins. *FASEB J.* 24:981-93.
89. Siepmann, T. J., Bohnsack, R. N., Tokgoz, Z., Baboshina, O. V. and Haas, A. L.2003. Protein interactions within the N-end rule ubiquitin ligation pathway. *J Biol Chem.* 278:9448-57.
90. Wenzel, D. M., Stoll, K. E. and Klevit, R. E.2011. E2s: structurally economical and functionally replete. *Biochem J.* 433:31-42.
91. Christensen, D. E. and Klevit, R. E.2009. Dynamic interactions of proteins in complex networks: identifying the complete set of interacting E2s for functional investigation of E3-dependent protein ubiquitination. *FEBS J.* 276:5381-9.
92. Eletr, Z. M., Huang, D. T., Duda, D. M., Schulman, B. A. and Kuhlman, B.2005. E2 conjugating enzymes must disengage from their E1 enzymes before E3-dependent ubiquitin and ubiquitin-like transfer. *Nat Struct Mol Biol.* 12:933-4.
93. Dikic, I. and Dotsch, V.2009. Ubiquitin linkages make a difference. *Nat Struct Mol Biol.* 16:1209-10.
94. Dikic, I., Wakatsuki, S. and Walters, K. J.2009. Ubiquitin-binding domains - from structures to functions. *Nat Rev Mol Cell Biol.* 10:659-71.
95. Hershko, A. and Ciechanover, A.1998. The ubiquitin system. *Annu Rev Biochem.* 67:425-79.
96. Nagy, V. and Dikic, I.2010. Ubiquitin ligase complexes: from substrate selectivity to conjugational specificity. *Biol Chem.* 391:163-9.

97. Tanji, K., Kamitani, T., Mori, F., Kakita, A., Takahashi, H. and Wakabayashi, K.2010. TRIM9, a novel brain-specific E3 ubiquitin ligase, is repressed in the brain of Parkinson's disease and dementia with Lewy bodies. *Neurobiol Dis.* 38:210-8.
98. Gomes, M. D., Lecker, S. H., Jagoe, R. T., Navon, A. and Goldberg, A. L.2001. Atrogin-1, a muscle-specific F-box protein highly expressed during muscle atrophy. *Proc Natl Acad Sci U S A.* 98:14440-5.
99. Bodine, S. C., Latres, E., Baumhueter, S., Lai, V. K., Nunez, L., Clarke, B. A., Poueymirou, W. T., Panaro, F. J., Na, E., Dharmarajan, K., Pan, Z. Q., Valenzuela, D. M., DeChiara, T. M., Stitt, T. N., Yancopoulos, G. D. and Glass, D. J.2001. Identification of ubiquitin ligases required for skeletal muscle atrophy. *Science.* 294:1704-8.
100. Xu, P., Duong, D. M., Seyfried, N. T., Cheng, D., Xie, Y., Robert, J., Rush, J., Hochstrasser, M., Finley, D. and Peng, J.2009. Quantitative proteomics reveals the function of unconventional ubiquitin chains in proteasomal degradation. *Cell.* 137:133-45.
101. Reyes-Turcu, F. E. and Wilkinson, K. D.2009. Polyubiquitin binding and disassembly by deubiquitinating enzymes. *Chem Rev.* 109:1495-508.
102. Reyes-Turcu, F. E., Ventii, K. H. and Wilkinson, K. D.2009. Regulation and cellular roles of ubiquitin-specific deubiquitinating enzymes. *Annu Rev Biochem.* 78:363-97.
103. Lee, M. J., Lee, B. H., Hanna, J., King, R. W. and Finley, D.2011. Trimming of ubiquitin chains by proteasome-associated deubiquitinating enzymes. *Mol Cell Proteomics.* 10:R110 003871.
104. Chen, D., Frezza, M., Schmitt, S., Kanwar, J. and Q, P. D.2011. Bortezomib as the first proteasome inhibitor anticancer drug: current status and future perspectives. *Curr Cancer Drug Targets.* 11:239-53.
105. Colland, F.2010. The therapeutic potential of deubiquitinating enzyme inhibitors. *Biochem Soc Trans.* 38:137-43.
106. Kessler, B. M. and Edelmann, M. J.2011. PTMs in conversation: activity and function of deubiquitinating enzymes regulated via post-translational modifications. *Cell Biochem Biophys.* 60:21-38.
107. Coux, O., Tanaka, K. and Goldberg, A. L.1996. Structure and functions of the 20S and 26S proteasomes. *Annu Rev Biochem.* 65:801-47.
108. Voges, D., Zwickl, P. and Baumeister, W.1999. The 26S proteasome: a molecular machine designed for controlled proteolysis. *Annu Rev Biochem.* 68:1015-68.

109. Hill, C. P., Masters, E. I. and Whitby, F. G.2002. The 11S regulators of 20S proteasome activity. *Curr Top Microbiol Immunol.* 268:73-89.
110. Savulescu, A. F. and Glickman, M. H.2011. Proteasome activator 200: the heat is on. *Mol Cell Proteomics.* 10:R110 006890.
111. Groll, M., Ditzel, L., Lowe, J., Stock, D., Bochtler, M., Bartunik, H. D. and Huber, R.1997. Structure of 20S proteasome from yeast at 2.4 Å resolution. *Nature.* 386:463-71.
112. Groll, M., Bochtler, M., Brandstetter, H., Clausen, T. and Huber, R.2005. Molecular machines for protein degradation. *ChemBiochem.* 6:222-56.
113. Gallastegui, N. and Groll, M.2010. The 26S proteasome: assembly and function of a destructive machine. *Trends Biochem Sci.* 35:634-42.
114. Li, X. and Demartino, G. N.2009. Variably modulated gating of the 26S proteasome by ATP and polyubiquitin. *Biochem J.* 421:397-404.
115. Cecarini, V., Cuccioloni, M., Mozzicafreddo, M., Bonfili, L., Angeletti, M. and Eleuteri, A. M.2011. Targeting proteasomes with natural occurring compounds in cancer treatment. *Curr Cancer Drug Targets.* 11:307-24.
116. Koga, H., Kaushik, S. and Cuervo, A. M.2011. Protein homeostasis and aging: The importance of exquisite quality control. *Ageing Res Rev.* 10:205-15.
117. Dahlmann, B.2007. Role of proteasomes in disease. *BMC Biochem.* 8 Suppl 1:S3.
118. Li, Y. F. and Wang, X.2011. The role of the proteasome in heart disease. *Biochim Biophys Acta.* 1809:141-9.
119. Wang, X. and Robbins, J.2006. Heart failure and protein quality control. *Circ Res.* 99:1315-28.
120. Powell, S. R. and Divald, A.2010. The ubiquitin-proteasome system in myocardial ischaemia and preconditioning. *Cardiovasc Res.* 85:303-11.
121. Powell, S. R., Wang, P., Katzeff, H., Shringarpure, R., Teoh, C., Khaliulin, I., Das, D. K., Davies, K. J. and Schwalb, H.2005. Oxidized and ubiquitinated proteins may predict recovery of postischemic cardiac function: essential role of the proteasome. *Antioxid Redox Signal.* 7:538-46.
122. Stansfield, W. E., Moss, N. C., Willis, M. S., Tang, R. and Selzman, C. H.2007. Proteasome inhibition attenuates infarct size and preserves cardiac function in a murine model of myocardial ischemia-reperfusion injury. *Ann Thorac Surg.* 84:120-5.
123. Divald, A., Kivity, S., Wang, P., Hochhauser, E., Roberts, B., Teichberg, S., Gomes, A. V. and Powell, S. R.2010. Myocardial ischemic preconditioning preserves

- postischemic function of the 26S proteasome through diminished oxidative damage to 19S regulatory particle subunits. *Circ Res.* 106:1829-38.
124. Li, J., Horak, K. M., Su, H., Sanbe, A., Robbins, J. and Wang, X.2011. Enhancement of proteasomal function protects against cardiac proteinopathy and ischemia/reperfusion injury in mice. *J Clin Invest.* 121:3689-700.
125. Depre, C., Wang, Q., Yan, L., Hedhli, N., Peter, P., Chen, L., Hong, C., Hittinger, L., Ghaleh, B., Sadoshima, J., Vatner, D. E., Vatner, S. F. and Madura, K.2006. Activation of the cardiac proteasome during pressure overload promotes ventricular hypertrophy. *Circulation.* 114:1821-8.
126. Drews, O., Tsukamoto, O., Liem, D., Streicher, J., Wang, Y. and Ping, P.2010. Differential regulation of proteasome function in isoproterenol-induced cardiac hypertrophy. *Circ Res.* 107:1094-101.
127. Hedhli, N., Lizano, P., Hong, C., Fritsky, L. F., Dhar, S. K., Liu, H., Tian, Y., Gao, S., Madura, K., Vatner, S. F. and Depre, C.2008. Proteasome inhibition decreases cardiac remodeling after initiation of pressure overload. *Am J Physiol Heart Circ Physiol.* 295:H1385-93.
128. Brooks, S. A.2010. Functional interactions between mRNA turnover and surveillance and the ubiquitin proteasome system. *Wiley Interdiscip Rev RNA.* 1:240-52.
129. Li, H. H., Kedar, V., Zhang, C., McDonough, H., Arya, R., Wang, D. Z. and Patterson, C.2004. Atrogin-1/muscle atrophy F-box inhibits calcineurin-dependent cardiac hypertrophy by participating in an SCF ubiquitin ligase complex. *J Clin Invest.* 114:1058-71.
130. Deshaies, R. J. and Joazeiro, A. P.2009. RING Domain E3 Ubiquitin Ligases. *Annu Rev Biochem.* 78:399-434.
131. Lecker, S. H.2003. Ubiquitin-protein ligases in muscle wasting: multiple parallel pathways? *Curr Opin Clin Nutr Metab Care.* 6:271-5.
132. Jogo, M., Shiraishi, S. and Tamura, T. A.2009. Identification of MAFbx as a myogenin-engaged F-box protein in SCF ubiquitin ligase. *FEBS Lett.* 583:2715-9.
133. Kedar, V., McDonough, H., Arya, R., Li, H. H., Rockman, H. A. and Patterson, C.2004. Muscle-specific RING finger 1 is a bona fide ubiquitin ligase that degrades cardiac troponin I. *Proc Natl Acad Sci U S A.* 101:18135-40.
134. Mrosek, M., Meier, S., Ucurum-Fotiadis, Z., von Castelmur, E., Hedbom, E., Lustig, A., Grzesiek, S., Labeit, D., Labeit, S. and Mayans, O.2008. Structural analysis of B-

- Box 2 from MuRF1: identification of a novel self-association pattern in a RING-like fold. *Biochemistry*. 47:10722-30.
135. Centner, T., Yano, J., Kimura, E., McElhinny, A. S., Pelin, K., Witt, C. C., Bang, M. L., Trombitas, K., Granzier, H., Gregorio, C. C., Sorimachi, H. and Labeit, S.2001. Identification of muscle specific ring finger proteins as potential regulators of the titin kinase domain. *J Mol Biol*. 306:717-26.
 136. Gotthardt, M., Hammer, R. E., Hubner, N., Monti, J., Witt, C. C., McNabb, M., Richardson, J. A., Granzier, H., Labeit, S. and Herz, J.2003. Conditional expression of mutant M-line titins results in cardiomyopathy with altered sarcomere structure. *J Biol Chem*. 278:6059-65.
 137. Mrosek, M., Labeit, D., Witt, S., Heerklotz, H., von Castelmur, E., Labeit, S. and Mayans, O.2007. Molecular determinants for the recruitment of the ubiquitin-ligase MuRF-1 onto M-line titin. *FASEB J*. 21:1383-92.
 138. Tintignac, L. A., Lagirand, J., Batonnet, S., Sirri, V., Leibovitch, M. P. and Leibovitch, S. A.2005. Degradation of MyoD mediated by the SCF (MAFbx) ubiquitin ligase. *J Biol Chem*. 280:2847-56.
 139. Gregorio, C. C., Perry, C. N. and McElhinny, A. S.2005. Functional properties of the titin/connectin-associated proteins, the muscle-specific RING finger proteins (MURFs), in striated muscle. *J Muscle Res Cell Motil*. 26:389-400.
 140. Spencer, J. A., Eliazer, S., Ilaria, R. L., Jr., Richardson, J. A. and Olson, E. N.2000. Regulation of microtubule dynamics and myogenic differentiation by MURF, a striated muscle RING-finger protein. *J Cell Biol*. 150:771-84.
 141. Jagoe, R. T., Lecker, S. H., Gomes, M. and Goldberg, A. L.2002. Patterns of gene expression in atrophying skeletal muscles: response to food deprivation. *Faseb J*. 16:1697-712.
 142. Satchek, J. M., Ohtsuka, A., McLary, S. C. and Goldberg, A. L.2004. IGF-I stimulates muscle growth by suppressing protein breakdown and expression of atrophy-related ubiquitin ligases, atrogin-1 and MuRF1. *Am J Physiol Endocrinol Metab*. 287:E591-601.
 143. Sandri, M., Sandri, C., Gilbert, A., Skurk, C., Calabria, E., Picard, A., Walsh, K., Schiaffino, S., Lecker, S. H. and Goldberg, A. L.2004. Foxo transcription factors induce the atrophy-related ubiquitin ligase atrogin-1 and cause skeletal muscle atrophy. *Cell*. 117:399-412.
 144. Skurk, C., Izumiya, Y., Maatz, H., Razeghi, P., Shiojima, I., Sandri, M., Sato, K., Zeng, L., Schiekofe, S., Pimentel, D., Lecker, S., Taegtmeyer, H., Goldberg, A. L.

- and Walsh, K.2005. The FOXO3a transcription factor regulates cardiac myocyte size downstream of AKT signaling. *J Biol Chem.* 280:20814-23.
145. Stitt, T. N., Drujan, D., Clarke, B. A., Panaro, F., Timofeyva, Y., Kline, W. O., Gonzalez, M., Yancopoulos, G. D. and Glass, D. J.2004. The IGF-1/PI3K/Akt pathway prevents expression of muscle atrophy-induced ubiquitin ligases by inhibiting FOXO transcription factors. *Mol Cell.* 14:395-403.
146. Maejima, Y., Zhai, P. and Sadoshima, J.2009. GSK3 β Negatively Regulates Cardiac Hypertrophy Through Activation of FoxO. *Circulation.* 120:S759 (Abstract).
147. Verhees, K. J., Schols, A. M., Kelders, M. C., Op den Kamp, C. M., van der Velden, J. L. and Langen, R. C.2011. Glycogen synthase kinase-3beta is required for the induction of skeletal muscle atrophy. *Am J Physiol Cell Physiol.* 301:C995-C1007.
148. Dehoux, M., Van Beneden, R., Pasko, N., Lause, P., Verniers, J., Underwood, L., Ketelslegers, J. M. and Thissen, J. P.2004. Role of the insulin-like growth factor I decline in the induction of atrogen-1/MAFbx during fasting and diabetes. *Endocrinology.* 145:4806-12.
149. Lee, S. W., Dai, G., Hu, Z., Wang, X., Du, J. and Mitch, W. E.2004. Regulation of muscle protein degradation: coordinated control of apoptotic and ubiquitin-proteasome systems by phosphatidylinositol 3 kinase. *J Am Soc Nephrol.* 15:1537-45.
150. Hu, Z., Lee, I. H., Wang, X., Sheng, H., Zhang, L., Du, J. and Mitch, W. E.2007. PTEN expression contributes to the regulation of muscle protein degradation in diabetes. *Diabetes.* 56:2449-56.
151. Latres, E., Amini, A. R., Amini, A. A., Griffiths, J., Martin, F. J., Wei, Y., Lin, H. C., Yancopoulos, G. D. and Glass, D. J.2005. Insulin-like growth factor-1 (IGF-1) inversely regulates atrophy-induced genes via the phosphatidylinositol 3-kinase/Akt/mammalian target of rapamycin (PI3K/Akt/mTOR) pathway. *J Biol Chem.* 280:2737-44.
152. Senf, S. M., Sandesara, P. B., Reed, S. A. and Judge, A. R.2011. p300 Acetyltransferase activity differentially regulates the localization and activity of the FOXO homologues in skeletal muscle. *Am J Physiol Cell Physiol.* 300:C1490-501.
153. Schulze, P. C., Fang, J., Kassik, K. A., Gannon, J., Cupesi, M., MacGillivray, C., Lee, R. T. and Rosenthal, N.2005. Transgenic overexpression of locally acting insulin-like growth factor-1 inhibits ubiquitin-mediated muscle atrophy in chronic left-ventricular dysfunction. *Circ Res.* 97:418-26.

154. Song, Y. H., Li, Y., Du, J., Mitch, W. E., Rosenthal, N. and Delafontaine, P.2005. Muscle-specific expression of IGF-1 blocks angiotensin II-induced skeletal muscle wasting. *J Clin Invest.* 115:451-8.
155. Li, H. H., Willis, M. S., Lockyer, P., Miller, N., McDonough, H., Glass, D. J. and Patterson, C.2007. Atrogin-1 inhibits Akt-dependent cardiac hypertrophy in mice via ubiquitin-dependent coactivation of Forkhead proteins. *J Clin Invest.* 117:3211-23.
156. Schisler, J. C., Willis, M. S. and Patterson, C.2008. You spin me round: MaFBx/Atrogin-1 feeds forward on FOXO transcription factors (like a record). *Cell Cycle.* 7:440-3.
157. McFarlane, C., Sharma, M. and Kambadur, R.2008. Myostatin is a procachectic growth factor during postnatal myogenesis. *Curr Opin Clin Nutr Metab Care.* 11:422-7.
158. McFarlane, C., Plummer, E., Thomas, M., Hennebry, A., Ashby, M., Ling, N., Smith, H., Sharma, M. and Kambadur, R.2006. Myostatin induces cachexia by activating the ubiquitin proteolytic system through an NF-kappaB-independent, FoxO1-dependent mechanism. *J Cell Physiol.* 209:501-14.
159. Morissette, M. R., Cook, S. A., Buranasombati, C., Rosenberg, M. A. and Rosenzweig, A.2009. Myostatin inhibits IGF-I-induced myotube hypertrophy through Akt. *Am J Physiol Cell Physiol.* 297:C1124-32.
160. Gilson, H., Schakman, O., Combaret, L., Lause, P., Grobet, L., Attaix, D., Ketelslegers, J. M. and Thissen, J. P.2007. Myostatin gene deletion prevents glucocorticoid-induced muscle atrophy. *Endocrinology.* 148:452-60.
161. Lokireddy, S., McFarlane, C., Ge, X., Zhang, H., Sze, S. K., Sharma, M. and Kambadur, R.2011. Myostatin Induces Degradation of Sarcomeric Proteins through a Smad3 Signaling Mechanism During Skeletal Muscle Wasting. *Mol Endocrinol.* 25:1936-49.
162. Li, Y. P., Chen, Y. and John, J.2005. TNF-alpha acts via p38 MAPK to stimulate expression of the ubiquitin ligase atrogin-1/MAFbx in skeletal muscle. *FASEB J.* 19:362-370.
163. Dehoux, M., Gobier, C., Lause, P., Bertrand, L., Ketelslegers, J. M. and Thissen, J. P.2007. IGF-I does not prevent myotube atrophy caused by proinflammatory cytokines despite activation of Akt/Foxo and GSK-3beta pathways and inhibition of atrogin-1 mRNA. *Am J Physiol Endocrinol Metab.* 292:E145-50.

164. Moylan, J. S., Smith, J. D., Chambers, M. A., McLoughlin, T. J. and Reid, M. B.2008. TNF induction of atrogin-1/MAFbx mRNA depends on Foxo4 expression but not AKT-Foxo1/3 signaling. *Am J Physiol Cell Physiol.* 295:C986-93.
165. Zhang, G., Jin, B. and Li, Y. P.2011. C/EBPbeta mediates tumour-induced ubiquitin ligase atrogin1/MAFbx upregulation and muscle wasting. *EMBO J.* 30:4323-35.
166. Adams, V., Linke, A., Wisloff, U., Doring, C., Erbs, S., Krankel, N., Witt, C. C., Labeit, S., Muller-Werdan, U., Schuler, G. and Hambrecht, R.2007. Myocardial expression of Murf-1 and MAFbx after induction of chronic heart failure: Effect on myocardial contractility. *Cardiovasc Res.* 73:120-9.
167. Adams, V., Linke, A., Gielen, S., Erbs, S., Hambrecht, R. and Schuler, G.2008. Modulation of Murf-1 and MAFbx expression in the myocardium by physical exercise training. *Eur J Cardiovasc Prev Rehabil.* 15:293-9.
168. Yamamoto, Y., Hoshino, Y., Ito, T., Nariai, T., Mohri, T., Obana, M., Hayata, N., Uozumi, Y., Maeda, M., Fujio, Y. and Azuma, J.2008. Atrogin-1 ubiquitin ligase is upregulated by doxorubicin via p38-MAP kinase in cardiac myocytes. *Cardiovasc Res.* 79:89-96.
169. Li, J. J., Zhang, T. P., Meng, Y., Du, J. and Li, H. H.2011. Stability of F-box protein atrogin-1 is regulated by p38 mitogen-activated protein kinase pathway in cardiac H9c2 cells. *Cell Physiol Biochem.* 27:463-70.
170. Frost, J. A., Xu, S., Hutchison, M. R., Marcus, S. and Cobb, M. H.1996. Actions of Rho family small G proteins and p21-activated protein kinases on mitogen-activated protein kinase family members. *Mol Cell Biol.* 16:3707-13.
171. Clavel, S., Siffroi-Fernandez, S., Coldefy, A. S., Boulukos, K., Pisani, D. F. and Derijard, B.2010. Regulation of the intracellular localization of Foxo3a by stress-activated protein kinase signaling pathways in skeletal muscle cells. *Mol Cell Biol.* 30:470-80.
172. Xie, P., Guo, S., Fan, Y., Zhang, H., Gu, D. and Li, H.2009. Atrogin-1/MAFbx enhances simulated ischemia/reperfusion-induced apoptosis in cardiomyocytes through degradation of MAPK phosphatase-1 and sustained JNK activation. *J Biol Chem.* 284:5488-96.
173. Li, H. H., Du, J., Fan, Y. N., Zhang, M. L., Liu, D. P., Li, L., Lockyer, P., Kang, E. Y., Patterson, C. and Willis, M. S.2011. The ubiquitin ligase MuRF1 protects against cardiac ischemia/reperfusion injury by its proteasome-dependent degradation of phospho-c-Jun. *Am J Pathol.* 178:1043-58.

174. Judge, A. R., Koncarevic, A., Hunter, R. B., Liou, H. C., Jackman, R. W. and Kandarian, S. C.2007. Role for I κ B α , but not c-Rel, in skeletal muscle atrophy. *Am J Physiol Cell Physiol.* 292:C372-82.
175. Cai, D., Frantz, J. D., Tawa, N. E., Jr., Melendez, P. A., Oh, B. C., Lidov, H. G., Hasselgren, P. O., Frontera, W. R., Lee, J., Glass, D. J. and Shoelson, S. E.2004. IKK β /NF- κ B activation causes severe muscle wasting in mice. *Cell.* 119:285-98.
176. Li, W., Moylan, J. S., Chambers, M. A., Smith, J. and Reid, M. B.2009. Interleukin-1 stimulates catabolism in C2C12 myotubes. *Am J Physiol Cell Physiol.* 297:C706-14.
177. Dehoux, M. J., van Beneden, R. P., Fernandez-Celemin, L., Lause, P. L. and Thissen, J. P.2003. Induction of MafBx and Murf ubiquitin ligase mRNAs in rat skeletal muscle after LPS injection. *FEBS Lett.* 544:214-7.
178. Murton, A. J., Alamdari, N., Gardiner, S. M., Constantin-Teodosiu, D., Layfield, R., Bennett, T. and Greenhaff, P. L.2009. Effects of endotoxaemia on protein metabolism in rat fast-twitch skeletal muscle and myocardium. *PLoS One.* 4:e6945.
179. Jin, B. and Li, Y. P.2007. Curcumin prevents lipopolysaccharide-induced atrogen-1/MAFbx upregulation and muscle mass loss. *J Cell Biochem.* 100:960-9.
180. Doyle, A., Zhang, G., Abdel Fattah, E. A., Eissa, N. T. and Li, Y. P.2011. Toll-like receptor 4 mediates lipopolysaccharide-induced muscle catabolism via coordinate activation of ubiquitin-proteasome and autophagy-lysosome pathways. *FASEB J.* 25:99-110.
181. Cohen, J.2002. The immunopathogenesis of sepsis. *Nature.* 420:885-91.
182. Smith, I. J., Alamdari, N., O'Neal, P., Gonnella, P., Aversa, Z. and Hasselgren, P. O.2010. Sepsis increases the expression and activity of the transcription factor Forkhead Box O 1 (FOXO1) in skeletal muscle by a glucocorticoid-dependent mechanism. *Int J Biochem Cell Biol.* 42:701-11.
183. Fareed, M. U., Evenson, A. R., Wei, W., Menconi, M., Poylin, V., Petkova, V., Pignol, B. and Hasselgren, P. O.2006. Treatment of rats with calpain inhibitors prevents sepsis-induced muscle proteolysis independent of atrogen-1/MAFbx and MuRF1 expression. *Am J Physiol Regul Integr Comp Physiol.* 290:R1589-97.
184. Molkenin, J. D. and Olson, E. N.1996. Combinatorial control of muscle development by basic helix-loop-helix and MADS-box transcription factors. *Proc Natl Acad Sci U S A.* 93:9366-73.
185. Moresi, V., Williams, A. H., Meadows, E., Flynn, J. M., Potthoff, M. J., McAnally, J., Shelton, J. M., Backs, J., Klein, W. H., Richardson, J. A., Bassel-Duby, R. and

- Olson, E. N.2010. Myogenin and class II HDACs control neurogenic muscle atrophy by inducing E3 ubiquitin ligases. *Cell*. 143:35-45.
186. Zhao, W., Wu, Y., Zhao, J., Guo, S., Bauman, W. A. and Cardozo, C. P.2005. Structure and function of the upstream promotor of the human Mafbx gene: the proximal upstream promotor modulates tissue-specificity. *J Cell Biochem*. 96:209-19.
187. Lagirand-Cantaloube, J., Cornille, K., Csibi, A., Batonnet-Pichon, S., Leibovitch, M. P. and Leibovitch, S. A.2009. Inhibition of atrogen-1/MAFbx mediated MyoD proteolysis prevents skeletal muscle atrophy in vivo. *PLoS One*. 4:e4973.
188. Jo, C., Cho, S. J. and Jo, S. A.2011. Mitogen-activated protein kinase kinase 1 (MEK1) stabilizes MyoD through direct phosphorylation at tyrosine 156 during myogenic differentiation. *J Biol Chem*. 286:18903-13.
189. Waddell, D. S., Baehr, L. M., van den Brandt, J., Johnsen, S. A., Reichardt, H. M., Furlow, J. D. and Bodine, S. C.2008. The glucocorticoid receptor and FOXO1 synergistically activate the skeletal muscle atrophy-associated MuRF1 gene. *Am J Physiol Endocrinol Metab*. 295:E785-97.
190. Clarke, B. A., Drujan, D., Willis, M. S., Murphy, L. O., Corpina, R. A., Burova, E., Rakhilin, S. V., Stitt, T. N., Patterson, C., Latres, E. and Glass, D. J.2007. The E3 Ligase MuRF1 degrades myosin heavy chain protein in dexamethasone-treated skeletal muscle. *Cell Metab*. 6:376-85.
191. Krawiec, B. J., Frost, R. A., Vary, T. C., Jefferson, L. S. and Lang, C. H.2005. Hindlimb casting decreases muscle mass in part by proteasome-dependent proteolysis but independent of protein synthesis. *Am J Physiol Endocrinol Metab*. 289:E969-80.
192. Tillis, C. C., Huang, H. W., Bi, W., Pan, S., Bruce, S. R. and Alcorn, J. L.2011. Glucocorticoid regulation of human pulmonary surfactant protein-B (SP-B) mRNA stability is independent of activated glucocorticoid receptor. *Am J Physiol Lung Cell Mol Physiol*. 300:L940-50.
193. Hanai, J., Cao, P., Tanksale, P., Imamura, S., Koshimizu, E., Zhao, J., Kishi, S., Yamashita, M., Phillips, P. S., Sukhatme, V. P. and Lecker, S. H.2007. The muscle-specific ubiquitin ligase atrogen-1/MAFbx mediates statin-induced muscle toxicity. *J Clin Invest*. 117:3940-51.
194. Cao, P., Hanai, J., Tanksale, P., Imamura, S., Sukhatme, V. P. and Lecker, S. H.2009. Statin-induced muscle damage and atrogen-1 induction is the result of a geranylgeranylation defect. *FASEB J*. 23:2844-54.

195. Small, E. M. and Olson, E. N.2011. Pervasive roles of microRNAs in cardiovascular biology. *Nature*. 469:336-42.
196. Lin, Z., Murtaza, I., Wang, K., Jiao, J., Gao, J. and Li, P. F.2009. miR-23a functions downstream of NFATc3 to regulate cardiac hypertrophy. *Proc Natl Acad Sci U S A*. 106:12103-8.
197. Wada, S., Kato, Y., Okutsu, M., Miyaki, S., Suzuki, K., Yan, Z., Schiaffino, S., Asahara, H., Ushida, T. and Akimoto, T.2011. Translational Suppression of Atrophic Regulators by MicroRNA-23a Integrates Resistance to Skeletal Muscle Atrophy. *J Biol Chem*. 286:38456-65.
198. Usui, S., Maejima, Y., Pain, J., Hong, C., Cho, J., Park, J. Y., Zablocki, D., Tian, B., Glass, D. J. and Sadoshima, J.2011. Endogenous muscle atrophy F-box mediates pressure overload-induced cardiac hypertrophy through regulation of nuclear factor-kappaB. *Circ Res*. 109:161-71.
199. Razeghi, P., Baskin, K. K., Sharma, S., Young, M. E., Stepkowski, S., Faadiel Essop, M. and Taegtmeyer, H.2006. Atrophy, hypertrophy, and hypoxemia induce transcriptional regulators of the ubiquitin proteasome system in the rat heart. *Biochem Biophys Res Commun*. 342:361-4.
200. Lagirand-Cantaloube, J., Offner, N., Csibi, A., Leibovitch, M. P., Batonnet-Pichon, S., Tintignac, L. A., Segura, C. T. and Leibovitch, S. A.2008. The initiation factor eIF3-f is a major target for atrogin1/MAFbx function in skeletal muscle atrophy. *EMBO J*. 27:1266-76.
201. Csibi, A., Leibovitch, M. P., Cornille, K., Tintignac, L. A. and Leibovitch, S. A.2009. MAFbx/Atrogin-1 controls the activity of the initiation factor eIF3-f in skeletal muscle atrophy by targeting multiple C-terminal lysines. *J Biol Chem*. 284:4413-21.
202. Csibi, A., Cornille, K., Leibovitch, M. P., Poupon, A., Tintignac, L. A., Sanchez, A. M. and Leibovitch, S. A.2010. The translation regulatory subunit eIF3f controls the kinase-dependent mTOR signaling required for muscle differentiation and hypertrophy in mouse. *PLoS One*. 5:e8994.
203. Arya, R., Kedar, V., Hwang, J. R., McDonough, H., Li, H. H., Taylor, J. and Patterson, C.2004. Muscle ring finger protein-1 inhibits PKC{epsilon} activation and prevents cardiomyocyte hypertrophy. *J Cell Biol*. 167:1147-59.
204. McElhinny, A. S., Kakinuma, K., Sorimachi, H., Labeit, S. and Gregorio, C. C.2002. Muscle-specific RING finger-1 interacts with titin to regulate sarcomeric M-line and thick filament structure and may have nuclear functions via its interaction with glucocorticoid modulatory element binding protein-1. *J Cell Biol*. 157:125-36.

205. Kim, H. T., Kim, K. P., Lledias, F., Kisselev, A. F., Scaglione, K. M., Skowyra, D., Gygi, S. P. and Goldberg, A. L.2007. Certain pairs of ubiquitin-conjugating enzymes (E2s) and ubiquitin-protein ligases (E3s) synthesize nondegradable forked ubiquitin chains containing all possible isopeptide linkages. *J Biol Chem.* 282:17375-86.
206. Witt, S. H., Granzier, H., Witt, C. C. and Labeit, S.2005. MURF-1 and MURF-2 target a specific subset of myofibrillar proteins redundantly: towards understanding MURF-dependent muscle ubiquitination. *J Mol Biol.* 350:713-22.
207. Zhao, T. J., Yan, Y. B., Liu, Y. and Zhou, H. M.2007. The generation of the oxidized form of creatine kinase is a negative regulation on muscle creatine kinase. *J Biol Chem.* 282:12022-9.
208. Koyama, S., Hata, S., Witt, C. C., Ono, Y., Lerche, S., Ojima, K., Chiba, T., Doi, N., Kitamura, F., Tanaka, K., Abe, K., Witt, S. H., Rybin, V., Gasch, A., Franz, T., Labeit, S. and Sorimachi, H.2008. Muscle RING-finger protein-1 (MuRF1) as a connector of muscle energy metabolism and protein synthesis. *J Mol Biol.* 376:1224-36.
209. Hirner, S., Krohne, C., Schuster, A., Hoffmann, S., Witt, S., Erber, R., Sticht, C., Gasch, A., Labeit, S. and Labeit, D.2008. MuRF1-dependent regulation of systemic carbohydrate metabolism as revealed from transgenic mouse studies. *J Mol Biol.* 379:666-77.
210. Cohen, S., Brault, J. J., Gygi, S. P., Glass, D. J., Valenzuela, D. M., Gartner, C., Latres, E. and Goldberg, A. L.2009. During muscle atrophy, thick, but not thin, filament components are degraded by MuRF1-dependent ubiquitylation. *J Cell Biol.* 185:1083-95.
211. Polge, C., Heng, A. E., Jarzaguat, M., Ventadour, S., Claustre, A., Combaret, L., Bechet, D., Matondo, M., Uttenweiler-Joseph, S., Monsarrat, B., Attaix, D. and Taillandier, D.2011. Muscle actin is polyubiquitinated in vitro and in vivo and targeted for breakdown by the E3 ligase MuRF1. *FASEB J.* 25:3790-802.
212. Moriscot, A. S., Baptista, I. L., Bogomolovas, J., Witt, C., Hirner, S., Granzier, H. and Labeit, S.2010. MuRF1 is a muscle fiber-type II associated factor and together with MuRF2 regulates type-II fiber tropicity and maintenance. *J Struct Biol.* 170:344-53.
213. Fielitz, J., Kim, M. S., Shelton, J. M., Latif, S., Spencer, J. A., Glass, D. J., Richardson, J. A., Bassel-Duby, R. and Olson, E. N.2007. Myosin accumulation and striated muscle myopathy result from the loss of muscle RING finger 1 and 3. *J Clin Invest.* 117:2486-95.

214. Willis, M. S., Ike, C., Li, L., Wang, D. Z., Glass, D. J. and Patterson, C.2007. Muscle ring finger 1, but not muscle ring finger 2, regulates cardiac hypertrophy in vivo. *Circ Res.* 100:456-9.
215. Willis, M. S., Rojas, M., Li, L., Selzman, C. H., Tang, R. H., Stansfield, W. E., Rodriguez, J. E., Glass, D. J. and Patterson, C.2009. Muscle ring finger 1 mediates cardiac atrophy in vivo. *Am J Physiol Heart Circ Physiol.* 296:H997-H1006.
216. Hwee, D. T., Gomes, A. V. and Bodine, S. C.2011. Cardiac proteasome activity in muscle ring finger-1 null mice at rest and following synthetic glucocorticoid treatment. *Am J Physiol Endocrinol Metab.* 301:E967-77.
217. Willis, M. S., Schisler, J. C., Li, L., Rodriguez, J. E., Hilliard, E. G., Charles, P. C. and Patterson, C.2009. Cardiac muscle ring finger-1 increases susceptibility to heart failure in vivo. *Circ Res.* 105:80-8.
218. Mearini, G., Gedicke, C., Schlossarek, S., Witt, C. C., Kramer, E., Cao, P., Gomes, M. D., Lecker, S. H., Labeit, S., Willis, M. S., Eschenhagen, T. and Carrier, L.2010. Atrogin-1 and MuRF1 regulate cardiac MyBP-C levels via different mechanisms. *Cardiovasc Res.* 85:357-66.
219. Nakao, R., Hirasaka, K., Goto, J., Ishidoh, K., Yamada, C., Ohno, A., Okumura, Y., Nonaka, I., Yasutomo, K., Baldwin, K. M., Kominami, E., Higashibata, A., Nagano, K., Tanaka, K., Yasui, N., Mills, E. M., Takeda, S. and Nikawa, T.2009. Ubiquitin ligase Cbl-b is a negative regulator for insulin-like growth factor 1 signaling during muscle atrophy caused by unloading. *Mol Cell Biol.* 29:4798-811.
220. Taegtmeyer, H., Hems, R. and Krebs, H. A.1980. Utilization of energy-providing substrates in the isolated working rat heart. *Biochem J.* 186:701-11.
221. Taegtmeyer, H.1985. Carbohydrate interconversions and energy production. *Circulation.* 72:IV1-8.
222. Bing, R. J.1955. The metabolism of the heart. *Trans Am Coll Cardiol.* 5:8-14.
223. Hardie, D. G. and Carling, D.1997. The AMP-activated protein kinase--fuel gauge of the mammalian cell? *Eur J Biochem.* 246:259-73.
224. Hardie, D. G., Hawley, S. A. and Scott, J. W.2006. AMP-activated protein kinase--development of the energy sensor concept. *J Physiol.* 574:7-15.
225. Oakhill, J. S., Scott, J. W. and Kemp, B. E.2009. Structure and function of AMP-activated protein kinase. *Acta Physiol (Oxf).* 196:3-14.
226. Verhoeven, A. J., Woods, A., Brennan, C. H., Hawley, S. A., Hardie, D. G., Scott, J., Beri, R. K. and Carling, D.1995. The AMP-activated protein kinase gene is highly

- expressed in rat skeletal muscle. Alternative splicing and tissue distribution of the mRNA. *Eur J Biochem.* 228:236-43.
227. Stapleton, D., Mitchelhill, K. I., Gao, G., Widmer, J., Michell, B. J., Teh, T., House, C. M., Fernandez, C. S., Cox, T., Witters, L. A. and Kemp, B. E.1996. Mammalian AMP-activated protein kinase subfamily. *J Biol Chem.* 271:611-4.
228. Chen, Z., Heierhorst, J., Mann, R. J., Mitchelhill, K. I., Michell, B. J., Witters, L. A., Lynch, G. S., Kemp, B. E. and Stapleton, D.1999. Expression of the AMP-activated protein kinase beta1 and beta2 subunits in skeletal muscle. *FEBS Lett.* 460:343-8.
229. Thornton, C., Snowden, M. A. and Carling, D.1998. Identification of a novel AMP-activated protein kinase beta subunit isoform that is highly expressed in skeletal muscle. *J Biol Chem.* 273:12443-50.
230. Li, J., Coven, D. L., Miller, E. J., Hu, X., Young, M. E., Carling, D., Sinusas, A. J. and Young, L. H.2006. Activation of AMPK alpha- and gamma-isoform complexes in the intact ischemic rat heart. *Am J Physiol Heart Circ Physiol.* 291:H1927-34.
231. Cheung, P. C., Salt, I. P., Davies, S. P., Hardie, D. G. and Carling, D.2000. Characterization of AMP-activated protein kinase gamma-subunit isoforms and their role in AMP binding. *Biochem J.* 346 Pt 3:659-69.
232. Hardie, D. G.2007. AMP-activated/SNF1 protein kinases: conserved guardians of cellular energy. *Nat Rev Mol Cell Biol.* 8:774-85.
233. Kemp, B. E., Oakhill, J. S. and Scott, J. W.2007. AMPK structure and regulation from three angles. *Structure.* 15:1161-3.
234. Xiao, B., Heath, R., Saiu, P., Leiper, F. C., Leone, P., Jing, C., Walker, P. A., Haire, L., Eccleston, J. F., Davis, C. T., Martin, S. R., Carling, D. and Gamblin, S. J.2007. Structural basis for AMP binding to mammalian AMP-activated protein kinase. *Nature.* 449:496-500.
235. Xiao, B., Sanders, M. J., Underwood, E., Heath, R., Mayer, F. V., Carmena, D., Jing, C., Walker, P. A., Eccleston, J. F., Haire, L. F., Saiu, P., Howell, S. A., Aasland, R., Martin, S. R., Carling, D. and Gamblin, S. J.2011. Structure of mammalian AMPK and its regulation by ADP. *Nature.* 472:230-3.
236. Woods, A., Vertommen, D., Neumann, D., Turk, R., Bayliss, J., Schlattner, U., Wallimann, T., Carling, D. and Rider, M. H.2003. Identification of phosphorylation sites in AMP-activated protein kinase (AMPK) for upstream AMPK kinases and study of their roles by site-directed mutagenesis. *J Biol Chem.* 278:28434-42.

237. Vincent, O., Townley, R., Kuchin, S. and Carlson, M.2001. Subcellular localization of the Snf1 kinase is regulated by specific beta subunits and a novel glucose signaling mechanism. *Genes Dev.* 15:1104-14.
238. Steinberg, G. R. and Kemp, B. E.2009. AMPK in Health and Disease. *Physiol Rev.* 89:1025-78.
239. Atkinson, D. E.1968. The energy charge of the adenylate pool as a regulatory parameter. Interaction with feedback modifiers. *Biochemistry.* 7:4030-4.
240. Yeh, L. A., Lee, K. H. and Kim, K. H.1980. Regulation of rat liver acetyl-CoA carboxylase. Regulation of phosphorylation and inactivation of acetyl-CoA carboxylase by the adenylate energy charge. *J Biol Chem.* 255:2308-14.
241. Munday, M. R., Campbell, D. G., Carling, D. and Hardie, D. G.1988. Identification by amino acid sequencing of three major regulatory phosphorylation sites on rat acetyl-CoA carboxylase. *Eur J Biochem.* 175:331-8.
242. McBride, A., Ghilagaber, S., Nikolaev, A. and Hardie, D. G.2009. The glycogen-binding domain on the AMPK beta subunit allows the kinase to act as a glycogen sensor. *Cell Metab.* 9:23-34.
243. Warden, S. M., Richardson, C., O'Donnell, J., Jr., Stapleton, D., Kemp, B. E. and Witters, L. A.2001. Post-translational modifications of the beta-1 subunit of AMP-activated protein kinase affect enzyme activity and cellular localization. *Biochem J.* 354:275-83.
244. Hawley, S. A., Davison, M., Woods, A., Davies, S. P., Beri, R. K., Carling, D. and Hardie, D. G.1996. Characterization of the AMP-activated protein kinase kinase from rat liver and identification of threonine 172 as the major site at which it phosphorylates AMP-activated protein kinase. *J Biol Chem.* 271:27879-87.
245. Pang, T., Xiong, B., Li, J. Y., Qiu, B. Y., Jin, G. Z., Shen, J. K. and Li, J.2007. Conserved alpha-helix acts as autoinhibitory sequence in AMP-activated protein kinase alpha subunits. *J Biol Chem.* 282:495-506.
246. Davies, S. P., Helps, N. R., Cohen, P. T. and Hardie, D. G.1995. 5'-AMP inhibits dephosphorylation, as well as promoting phosphorylation, of the AMP-activated protein kinase. Studies using bacterially expressed human protein phosphatase-2C alpha and native bovine protein phosphatase-2AC. *FEBS Lett.* 377:421-5.
247. Hawley, S. A., Boudeau, J., Reid, J. L., Mustard, K. J., Udd, L., Makela, T. P., Alessi, D. R. and Hardie, D. G.2003. Complexes between the LKB1 tumor suppressor, STRAD alpha/beta and MO25 alpha/beta are upstream kinases in the AMP-activated protein kinase cascade. *J Biol.* 2:28.

248. Sakamoto, K., Zarrinpashneh, E., Budas, G. R., Pouleur, A. C., Dutta, A., Prescott, A. R., Vanoverschelde, J. L., Ashworth, A., Jovanovic, A., Alessi, D. R. and Bertrand, L.2006. Deficiency of LKB1 in heart prevents ischemia-mediated activation of AMPK α 2 but not AMPK α 1. *Am J Physiol Endocrinol Metab.* 290:E780-8.
249. Jessen, N., Koh, H. J., Folmes, C. D., Wagg, C., Fujii, N., Lofgren, B., Wolf, C. M., Berul, C. I., Hirshman, M. F., Lopaschuk, G. D. and Goodyear, L. J.2010. Ablation of LKB1 in the heart leads to energy deprivation and impaired cardiac function. *Biochim Biophys Acta.* 1802:593-600.
250. Ikeda, Y., Sato, K., Pimentel, D. R., Sam, F., Shaw, R. J., Dyck, J. R. and Walsh, K.2009. Cardiac-specific deletion of LKB1 leads to hypertrophy and dysfunction. *J Biol Chem.* 284:35839-49.
251. Hawley, S. A., Pan, D. A., Mustard, K. J., Ross, L., Bain, J., Edelman, A. M., Frenguelli, B. G. and Hardie, D. G.2005. Calmodulin-dependent protein kinase kinase-beta is an alternative upstream kinase for AMP-activated protein kinase. *Cell Metab.* 2:9-19.
252. Woods, A., Dickerson, K., Heath, R., Hong, S. P., Momcilovic, M., Johnstone, S. R., Carlson, M. and Carling, D.2005. Ca²⁺/calmodulin-dependent protein kinase kinase-beta acts upstream of AMP-activated protein kinase in mammalian cells. *Cell Metab.* 2:21-33.
253. Xie, M., Zhang, D., Dyck, J. R., Li, Y., Zhang, H., Morishima, M., Mann, D. L., Taffet, G. E., Baldini, A., Khoury, D. S. and Schneider, M. D.2006. A pivotal role for endogenous TGF-beta-activated kinase-1 in the LKB1/AMP-activated protein kinase energy-sensor pathway. *Proc Natl Acad Sci U S A.* 103:17378-83.
254. Scholz, R., Sidler, C. L., Thali, R. F., Winssinger, N., Cheung, P. C. and Neumann, D.2010. Autoactivation of transforming growth factor beta-activated kinase 1 is a sequential bimolecular process. *J Biol Chem.* 285:25753-66.
255. Dolinsky, V. W. and Dyck, J. R.2006. Role of AMP-activated protein kinase in healthy and diseased hearts. *Am J Physiol Heart Circ Physiol.* 291:H2557-69.
256. Carling, D., Clarke, P. R., Zammit, V. A. and Hardie, D. G.1989. Purification and characterization of the AMP-activated protein kinase. Copurification of acetyl-CoA carboxylase kinase and 3-hydroxy-3-methylglutaryl-CoA reductase kinase activities. *Eur J Biochem.* 186:129-36.

257. Gimeno-Alcaniz, J. V. and Sanz, P.2003. Glucose and type 2A protein phosphatase regulate the interaction between catalytic and regulatory subunits of AMP-activated protein kinase. *J Mol Biol.* 333:201-9.
258. Moore, F., Weekes, J. and Hardie, D. G.1991. Evidence that AMP triggers phosphorylation as well as direct allosteric activation of rat liver AMP-activated protein kinase. A sensitive mechanism to protect the cell against ATP depletion. *Eur J Biochem.* 199:691-7.
259. Dyck, J. R. and Lopaschuk, G. D.2006. AMPK alterations in cardiac physiology and pathology: enemy or ally? *J Physiol.* 574:95-112.
260. Kim, A. S., Miller, E. J. and Young, L. H.2009. AMP-activated protein kinase: a core signalling pathway in the heart. *Acta Physiol (Oxf).* 196:37-53.
261. Kudo, N., Barr, A. J., Barr, R. L., Desai, S. and Lopaschuk, G. D.1995. High rates of fatty acid oxidation during reperfusion of ischemic hearts are associated with a decrease in malonyl-CoA levels due to an increase in 5'-AMP-activated protein kinase inhibition of acetyl-CoA carboxylase. *J Biol Chem.* 270:17513-20.
262. Russell, R. R., 3rd, Li, J., Coven, D. L., Pypaert, M., Zechner, C., Palmeri, M., Giordano, F. J., Mu, J., Birnbaum, M. J. and Young, L. H.2004. AMP-activated protein kinase mediates ischemic glucose uptake and prevents postischemic cardiac dysfunction, apoptosis, and injury. *J Clin Invest.* 114:495-503.
263. Hopkins, T. A., Dyck, J. R. and Lopaschuk, G. D.2003. AMP-activated protein kinase regulation of fatty acid oxidation in the ischaemic heart. *Biochem Soc Trans.* 31:207-12.
264. Marsin, A. S., Bertrand, L., Rider, M. H., Deprez, J., Beauloye, C., Vincent, M. F., Van den Berghe, G., Carling, D. and Hue, L.2000. Phosphorylation and activation of heart PFK-2 by AMPK has a role in the stimulation of glycolysis during ischaemia. *Curr Biol.* 10:1247-55.
265. Russell, R. R., 3rd, Bergeron, R., Shulman, G. I. and Young, L. H.1999. Translocation of myocardial GLUT-4 and increased glucose uptake through activation of AMPK by AICAR. *Am J Physiol.* 277:H643-9.
266. Lopaschuk, G. D.2008. AMP-activated protein kinase control of energy metabolism in the ischemic heart. *Int J Obes (Lond).* 32 Suppl 4:S29-35.
267. Liu, B., Clanachan, A. S., Schulz, R. and Lopaschuk, G. D.1996. Cardiac efficiency is improved after ischemia by altering both the source and fate of protons. *Circ Res.* 79:940-8.

268. Tian, R., Musi, N., D'Agostino, J., Hirshman, M. F. and Goodyear, L. J.2001. Increased adenosine monophosphate-activated protein kinase activity in rat hearts with pressure-overload hypertrophy. *Circulation*. 104:1664-9.
269. Allard, M. F., Parsons, H. L., Saeedi, R., Wambolt, R. B. and Brownsey, R.2007. AMPK and metabolic adaptation by the heart to pressure overload. *Am J Physiol Heart Circ Physiol*. 292:H140-8.
270. Chan, A. Y., Soltys, C. L., Young, M. E., Proud, C. G. and Dyck, J. R.2004. Activation of AMP-activated protein kinase inhibits protein synthesis associated with hypertrophy in the cardiac myocyte. *J Biol Chem*. 279:32771-9.
271. Li, H. L., Yin, R., Chen, D., Liu, D., Wang, D., Yang, Q. and Dong, Y. G.2007. Long-term activation of adenosine monophosphate-activated protein kinase attenuates pressure-overload-induced cardiac hypertrophy. *J Cell Biochem*. 100:1086-99.
272. Taegtmeyer, H., Golfman, L., Sharma, S., Razeghi, P. and van Arsdall, M.2004. Linking gene expression to function: metabolic flexibility in the normal and diseased heart. *Ann N Y Acad Sci*. 1015:202-13.
273. Wang, X., Li, W., Williams, M., Terada, N., Alessi, D. R. and Proud, C. G.2001. Regulation of elongation factor 2 kinase by p90(RSK1) and p70 S6 kinase. *EMBO J*. 20:4370-9.
274. Tee, A. R., Fingar, D. C., Manning, B. D., Kwiatkowski, D. J., Cantley, L. C. and Blenis, J.2002. Tuberous sclerosis complex-1 and -2 gene products function together to inhibit mammalian target of rapamycin (mTOR)-mediated downstream signaling. *Proc Natl Acad Sci U S A*. 99:13571-6.
275. Wang, Z., Wilson, W. A., Fujino, M. A. and Roach, P. J.2001. Antagonistic controls of autophagy and glycogen accumulation by Snf1p, the yeast homolog of AMP-activated protein kinase, and the cyclin-dependent kinase Pho85p. *Mol Cell Biol*. 21:5742-52.
276. Wilson, W. A., Wang, Z. and Roach, P. J.2002. Systematic identification of the genes affecting glycogen storage in the yeast *Saccharomyces cerevisiae*: implication of the vacuole as a determinant of glycogen level. *Mol Cell Proteomics*. 1:232-42.
277. Meley, D., Bauvy, C., Houben-Weerts, J. H., Dubbelhuis, P. F., Helmond, M. T., Codogno, P. and Meijer, A. J.2006. AMP-activated protein kinase and the regulation of autophagic proteolysis. *J Biol Chem*. 281:34870-9.
278. Liang, J., Shao, S. H., Xu, Z. X., Hennessy, B., Ding, Z., Larrea, M., Kondo, S., Dumont, D. J., Gutterman, J. U., Walker, C. L., Slingerland, J. M. and Mills, G.

- B.2007. The energy sensing LKB1-AMPK pathway regulates p27(kip1) phosphorylation mediating the decision to enter autophagy or apoptosis. *Nat Cell Biol.* 9:218-24.
279. Matsui, Y., Takagi, H., Qu, X., Abdellatif, M., Sakoda, H., Asano, T., Levine, B. and Sadoshima, J.2007. Distinct roles of autophagy in the heart during ischemia and reperfusion: roles of AMP-activated protein kinase and Beclin 1 in mediating autophagy. *Circ Res.* 100:914-22.
280. Hardie, D. G.2011. AMP-activated protein kinase: an energy sensor that regulates all aspects of cell function. *Genes Dev.* 25:1895-908.
281. Viana, R., Aguado, C., Esteban, I., Moreno, D., Viollet, B., Knecht, E. and Sanz, P.2008. Role of AMP-activated protein kinase in autophagy and proteasome function. *Biochem Biophys Res Commun.* 369:964-8.
282. Moreno, D., Viana, R. and Sanz, P.2009. Two-hybrid analysis identifies PSMD11, a non-ATPase subunit of the proteasome, as a novel interaction partner of AMP-activated protein kinase. *Int J Biochem Cell Biol.* 41:2431-9.
283. Hardie, D. G.2011. Sensing of energy and nutrients by AMP-activated protein kinase. *Am J Clin Nutr.* 93:891S-6.
284. Leclerc, I., da Silva Xavier, G. and Rutter, G. A.2002. AMP- and stress-activated protein kinases: key regulators of glucose-dependent gene transcription in mammalian cells? *Prog Nucleic Acid Res Mol Biol.* 71:69-90.
285. Kawaguchi, T., Osatomi, K., Yamashita, H., Kabashima, T. and Uyeda, K.2002. Mechanism for fatty acid "sparing" effect on glucose-induced transcription: regulation of carbohydrate-responsive element-binding protein by AMP-activated protein kinase. *J Biol Chem.* 277:3829-35.
286. Koo, S. H., Flechner, L., Qi, L., Zhang, X., Sreaton, R. A., Jeffries, S., Hedrick, S., Xu, W., Boussouar, F., Brindle, P., Takemori, H. and Montminy, M.2005. The CREB coactivator TORC2 is a key regulator of fasting glucose metabolism. *Nature.* 437:1109-11.
287. Zhou, G., Myers, R., Li, Y., Chen, Y., Shen, X., Fenyk-Melody, J., Wu, M., Ventre, J., Doebber, T., Fujii, N., Musi, N., Hirshman, M. F., Goodyear, L. J. and Moller, D. E.2001. Role of AMP-activated protein kinase in mechanism of metformin action. *J Clin Invest.* 108:1167-74.
288. Yang, W., Hong, Y. H., Shen, X. Q., Frankowski, C., Camp, H. S. and Leff, T.2001. Regulation of transcription by AMP-activated protein kinase: phosphorylation of p300 blocks its interaction with nuclear receptors. *J Biol Chem.* 276:38341-4.

289. Stoppani, J., Hildebrandt, A. L., Sakamoto, K., Cameron-Smith, D., Goodyear, L. J. and Neuffer, P. D.2002. AMP-activated protein kinase activates transcription of the UCP3 and HKII genes in rat skeletal muscle. *Am J Physiol Endocrinol Metab.* 283:E1239-48.
290. Thomson, D. M., Herway, S. T., Fillmore, N., Kim, H., Brown, J. D., Barrow, J. R. and Winder, W. W.2008. AMP-activated protein kinase phosphorylates transcription factors of the CREB family. *J Appl Physiol.* 104:429-38.
291. Zong, H., Ren, J. M., Young, L. H., Pypaert, M., Mu, J., Birnbaum, M. J. and Shulman, G. I.2002. AMP kinase is required for mitochondrial biogenesis in skeletal muscle in response to chronic energy deprivation. *Proc Natl Acad Sci U S A.* 99:15983-7.
292. Canto, C., Gerhart-Hines, Z., Feige, J. N., Lagouge, M., Noriega, L., Milne, J. C., Elliott, P. J., Puigserver, P. and Auwerx, J.2009. AMPK regulates energy expenditure by modulating NAD⁺ metabolism and SIRT1 activity. *Nature.* 458:1056-60.
293. Zheng, D., MacLean, P. S., Pohnert, S. C., Knight, J. B., Olson, A. L., Winder, W. W. and Dohm, G. L.2001. Regulation of muscle GLUT-4 transcription by AMP-activated protein kinase. *J Appl Physiol.* 91:1073-83.
294. McGee, S. L., van Denderen, B. J., Howlett, K. F., Mollica, J., Schertzer, J. D., Kemp, B. E. and Hargreaves, M.2008. AMP-activated protein kinase regulates GLUT4 transcription by phosphorylating histone deacetylase 5. *Diabetes.* 57:860-7.
295. Bungard, D., Fuerth, B. J., Zeng, P. Y., Faubert, B., Maas, N. L., Viollet, B., Carling, D., Thompson, C. B., Jones, R. G. and Berger, S. L.2010. Signaling kinase AMPK activates stress-promoted transcription via histone H2B phosphorylation. *Science.* 329:1201-5.
296. Hardie, D. G.2010. Transcription. Targeting the core of transcription. *Science.* 329:1158-9.
297. Viollet, B., Athes, Y., Mounier, R., Guigas, B., Zarrinpashneh, E., Horman, S., Lantier, L., Hebrard, S., Devin-Leclerc, J., Beauloye, C., Foretz, M., Andreelli, F., Ventura-Clapier, R. and Bertrand, L.2009. AMPK: Lessons from transgenic and knockout animals. *Front Biosci.* 14:19-44.
298. Xing, Y., Musi, N., Fujii, N., Zou, L., Luptak, I., Hirshman, M. F., Goodyear, L. J. and Tian, R.2003. Glucose metabolism and energy homeostasis in mouse hearts overexpressing dominant negative alpha2 subunit of AMP-activated protein kinase. *J Biol Chem.* 278:28372-7.

299. Jorgensen, S. B., Viollet, B., Andreelli, F., Frosig, C., Birk, J. B., Schjerling, P., Vaulont, S., Richter, E. A. and Wojtaszewski, J. F.2004. Knockout of the alpha2 but not alpha1 5'-AMP-activated protein kinase isoform abolishes 5-aminoimidazole-4-carboxamide-1-beta-4-ribofuranosidebut not contraction-induced glucose uptake in skeletal muscle. *J Biol Chem.* 279:1070-9.
300. Viollet, B., Andreelli, F., Jorgensen, S. B., Perrin, C., Geloën, A., Flamez, D., Mu, J., Lenzner, C., Baud, O., Bennoun, M., Gomas, E., Nicolas, G., Wojtaszewski, J. F., Kahn, A., Carling, D., Schuit, F. C., Birnbaum, M. J., Richter, E. A., Burcelin, R. and Vaulont, S.2003. The AMP-activated protein kinase alpha2 catalytic subunit controls whole-body insulin sensitivity. *J Clin Invest.* 111:91-8.
301. Mu, J., Brozinick, J. T., Jr., Valladares, O., Bucan, M. and Birnbaum, M. J.2001. A role for AMP-activated protein kinase in contraction- and hypoxia-regulated glucose transport in skeletal muscle. *Mol Cell.* 7:1085-94.
302. Sidhu, J. S., Rajawat, Y. S., Rami, T. G., Gollob, M. H., Wang, Z., Yuan, R., Marian, A. J., DeMayo, F. J., Weilbacher, D., Taffet, G. E., Davies, J. K., Carling, D., Khoury, D. S. and Roberts, R.2005. Transgenic mouse model of ventricular preexcitation and atrioventricular reentrant tachycardia induced by an AMP-activated protein kinase loss-of-function mutation responsible for Wolff-Parkinson-White syndrome. *Circulation.* 111:21-9.
303. Arad, M., Moskowitz, I. P., Patel, V. V., Ahmad, F., Perez-Atayde, A. R., Sawyer, D. B., Walter, M., Li, G. H., Burgon, P. G., Maguire, C. T., Stapleton, D., Schmitt, J. P., Guo, X. X., Pizard, A., Kupersmidt, S., Roden, D. M., Berul, C. I., Seidman, C. E. and Seidman, J. G.2003. Transgenic mice overexpressing mutant PRKAG2 define the cause of Wolff-Parkinson-White syndrome in glycogen storage cardiomyopathy. *Circulation.* 107:2850-6.
304. Davies, J. K., Wells, D. J., Liu, K., Whitrow, H. R., Daniel, T. D., Grignani, R., Lygate, C. A., Schneider, J. E., Noel, G., Watkins, H. and Carling, D.2006. Characterization of the role of gamma2 R531G mutation in AMP-activated protein kinase in cardiac hypertrophy and Wolff-Parkinson-White syndrome. *Am J Physiol Heart Circ Physiol.* 290:H1942-51.
305. Arad, M., Seidman, C. E. and Seidman, J. G.2007. AMP-activated protein kinase in the heart: role during health and disease. *Circ Res.* 100:474-88.
306. Zarrinpashneh, E., Beauloye, C., Ginion, A., Pouleur, A. C., Havaux, X., Hue, L., Viollet, B., Vanoverschelde, J. L. and Bertrand, L.2008. AMPKalpha2 counteracts

- the development of cardiac hypertrophy induced by isoproterenol. *Biochem Biophys Res Commun.* 376:677-81.
307. Zarrinpashneh, E., Carjaval, K., Beauloye, C., Ginion, A., Mateo, P., Pouleur, A. C., Horman, S., Vaulont, S., Hoerter, J., Viollet, B., Hue, L., Vanoverschelde, J. L. and Bertrand, L.2006. Role of the alpha2-isoform of AMP-activated protein kinase in the metabolic response of the heart to no-flow ischemia. *Am J Physiol Heart Circ Physiol.* 291:H2875-83.
308. Hudson, E. R., Pan, D. A., James, J., Lucocq, J. M., Hawley, S. A., Green, K. A., Baba, O., Terashima, T. and Hardie, D. G.2003. A novel domain in AMP-activated protein kinase causes glycogen storage bodies similar to those seen in hereditary cardiac arrhythmias. *Curr Biol.* 13:861-6.
309. Preedy, V. R., Smith, D. M., Kearney, N. F. and Sugden, P. H.1984. Rates of protein turnover in vivo and in vitro in ventricular muscle of hearts from fed and starved rats. *Biochem J.* 222:395-400.
310. Jack, A. "An acute talent for innovation". Financial Times [London], February 1, 2009.
311. Black, J. W., Crowther, A. F., Shanks, R. G., Smith, L. H. and Dornhorst, A. C.1964. A New Adrenergic Betareceptor Antagonist. *Lancet.* 1:1080-1.
312. Naya, F. J., Wu, C., Richardson, J. A., Overbeek, P. and Olson, E. N.1999. Transcriptional activity of MEF2 during mouse embryogenesis monitored with a MEF2-dependent transgene. *Development.* 126:2045-52.
313. Kimes, B. W. and Brandt, B. L.1976. Properties of a clonal muscle cell line from rat heart. *Exp Cell Res.* 98:367-81.
314. Hescheler, J., Meyer, R., Plant, S., Krautwurst, D., Rosenthal, W. and Schultz, G.1991. Morphological, biochemical, and electrophysiological characterization of a clonal cell (H9c2) line from rat heart. *Circ Res.* 69:1476-86.
315. Wang, W., Watanabe, M., Nakamura, T., Kudo, Y. and Ochi, R.1999. Properties and expression of Ca²⁺-activated K⁺ channels in H9c2 cells derived from rat ventricle. *Am J Physiol.* 276:H1559-66.
316. Graham, F. L., Smiley, J., Russell, W. C. and Nairn, R.1977. Characteristics of a human cell line transformed by DNA from human adenovirus type 5. *J Gen Virol.* 36:59-74.
317. Hall, C. V., Jacob, P. E., Ringold, G. M. and Lee, F.1983. Expression and regulation of Escherichia coli lacZ gene fusions in mammalian cells. *J Mol Appl Genet.* 2:101-9.

318. Rockman, H. A., Ross, R. S., Harris, A. N., Knowlton, K. U., Steinhilber, M. E., Field, L. J., Ross, J., Jr. and Chien, K. R. 1991. Segregation of atrial-specific and inducible expression of an atrial natriuretic factor transgene in an in vivo murine model of cardiac hypertrophy. *Proc Natl Acad Sci U S A.* 88:8277-81.
319. Chintalgattu, V., Ai, D., Langley, R. R., Zhang, J., Bankson, J. A., Shih, T. L., Reddy, A. K., Coombes, K. R., Daher, I. N., Pati, S., Patel, S. S., Pocius, J. S., Taffet, G. E., Buja, L. M., Entman, M. L. and Khakoo, A. Y. 2010. Cardiomyocyte PDGFR-beta signaling is an essential component of the mouse cardiac response to load-induced stress. *J Clin Invest.* 120:472-84.
320. Reddy, A. K., Taffet, G. E., Li, Y. H., Lim, S. W., Pham, T. T., Pocius, J. S., Entman, M. L., Michael, L. H. and Hartley, C. J. 2005. Pulsed Doppler signal processing for use in mice: applications. *IEEE Trans Biomed Eng.* 52:1771-83.
321. Hartley, C. J., Reddy, A. K., Madala, S., Michael, L. H., Entman, M. L. and Taffet, G. E. 2008. Doppler estimation of reduced coronary flow reserve in mice with pressure overload cardiac hypertrophy. *Ultrasound Med Biol.* 34:892-901.
322. Syed, F., Diwan, A. and Hahn, H. S. 2005. Murine echocardiography: a practical approach for phenotyping genetically manipulated and surgically modeled mice. *J Am Soc Echocardiogr.* 18:982-90.
323. Rottman, J. N., Ni, G. and Brown, M. 2007. Echocardiographic evaluation of ventricular function in mice. *Echocardiography.* 24:83-9.
324. Dewald, O., Sharma, S., Adroque, J., Salazar, R., Duerr, G. D., Crapo, J. D., Entman, M. L. and Taegtmeyer, H. 2005. Downregulation of peroxisome proliferator-activated receptor-alpha gene expression in a mouse model of ischemic cardiomyopathy is dependent on reactive oxygen species and prevents lipotoxicity. *Circulation.* 112:407-15.
325. Lee, V. S. 2006. Cardiovascular MRI: Physical principles to practical protocols, Lippincott Williams & Wilkins, Philadelphia, PA.
326. Epstein, F. H. 2007. MR in mouse models of cardiac disease. *NMR Biomed.* 20:238-55.
327. Hiller, K. H., Waller, C., Haase, A. and Jakob, P. M. 2008. Magnetic resonance of mouse models of cardiac disease. *Handb Exp Pharmacol.* 245-57.
328. Kulkarni, A. C. 2008. In vivo MRI of mouse heart at 11.7 t: monitoring of stem-cell therapy for myocardial infarction and evaluation of cardiac hypertrophy. PhD thesis. The Ohio State University, Columbus.

329. Lash, L. H., Jones, D.P. 1993. *Methods in Toxicology: Mitochondrial Dysfunction*, Academic Press, San Diego, CA.
330. Perissel, B., Charbonne, F., Moalic, J. M. and Malet, P. 1980. Initial stages of trypsinized cell culture of cardiac myoblasts: ultrastructural data. *J Mol Cell Cardiol.* 12:63-75.
331. Bauer, S., Maier, S. K., Neyses, L. and Maass, A. H. 2005. Optimization of gene transfer into neonatal rat cardiomyocytes and unmasking of cytomegalovirus promoter silencing. *DNA Cell Biol.* 24:381-7.
332. O'Connell, T. D., Rodrigo, M. C. and Simpson, P. C. 2007. Isolation and culture of adult mouse cardiac myocytes. *Methods Mol Biol.* 357:271-96.
333. Molecular Research Center, Inc <http://www.mrcgene.com/tri.htm>. Accessed August 1, 2006.
334. Sambrook, J., Russell, D.W. 2001. *Molecular Cloning: A Laboratory Manual*, 3rd. Cold Spring Harbor Laboratory Press, Cold Spring Harbor, NY.
335. Bradford, M. M. 1976. A rapid and sensitive method for the quantitation of microgram quantities of protein utilizing the principle of protein-dye binding. *Anal Biochem.* 72:248-54.
336. Cserjesi, P. and Olson, E. N. 1991. Myogenin induces the myocyte-specific enhancer binding factor MEF-2 independently of other muscle-specific gene products. *Mol Cell Biol.* 11:4854-62.
337. Zhao, X. S., Gallardo, T. D., Lin, L., Schageman, J. J. and Shoheit, R. V. 2002. Transcriptional mapping and genomic analysis of the cardiac atria and ventricles. *Physiol Genomics.* 12:53-60.
338. Pereira, F. A. 2001. Whole-mount histochemical detection of beta-galactosidase activity. *Curr Protoc Mol Biol.* Chapter 14:Unit 14 14.
339. Waxman, L., Fagan, J. M. and Goldberg, A. L. 1987. Demonstration of two distinct high molecular weight proteases in rabbit reticulocytes, one of which degrades ubiquitin conjugates. *J Biol Chem.* 262:2451-7.
340. Rock, K. L., Gramm, C., Rothstein, L., Clark, K., Stein, R., Dick, L., Hwang, D. and Goldberg, A. L. 1994. Inhibitors of the proteasome block the degradation of most cell proteins and the generation of peptides presented on MHC class I molecules. *Cell.* 78:761-71.
341. O'Neill, L. P. and Turner, B. M. 1996. Immunoprecipitation of chromatin. *Methods Enzymol.* 274:189-97.

342. Collas, P.2010. The current state of chromatin immunoprecipitation. *Mol Biotechnol.* 45:87-100.
343. Crute, B. E., Seefeld, K., Gamble, J., Kemp, B. E. and Witters, L. A.1998. Functional domains of the alpha1 catalytic subunit of the AMP-activated protein kinase. *J Biol Chem.* 273:35347-54.
344. Dyck, J. R., Gao, G., Widmer, J., Stapleton, D., Fernandez, C. S., Kemp, B. E. and Witters, L. A.1996. Regulation of 5'-AMP-activated protein kinase activity by the noncatalytic beta and gamma subunits. *J Biol Chem.* 271:17798-803.
345. Green, M. and Loewenstein, P. M.2006. Human adenoviruses: propagation, purification, quantification, and storage. *Curr Protoc Microbiol.* Chapter 14:Unit 14C 1.
346. AdEasy Viral Titer Kit Instruction Manual.
<http://www.genomics.agilent.com/files/Manual/972500.pdf>. Accessed May 2, 2008.
347. BLAST: Basic Local Alignment Search Tool. <http://blast.ncbi.nlm.nih.gov/Blast.cgi>. Accessed August 1, 2006 - September 23, 2009.
348. Depre, C., Shipley, G. L., Chen, W., Han, Q., Doenst, T., Moore, M. L., Stepkowski, S., Davies, P. J. and Taegtmeyer, H.1998. Unloaded heart in vivo replicates fetal gene expression of cardiac hypertrophy. *Nat Med.* 4:1269-75.
349. Bustin, S. A.2002. Quantification of mRNA using real-time reverse transcription PCR (RT-PCR): trends and problems. *J Mol Endocrinol.* 29:23-39.
350. Bustin, S. A., Benes, V., Garson, J. A., Hellemans, J., Huggett, J., Kubista, M., Mueller, R., Nolan, T., Pfaffl, M. W., Shipley, G. L., Vandesompele, J. and Wittwer, C. T.2009. The MIQE guidelines: minimum information for publication of quantitative real-time PCR experiments. *Clin Chem.* 55:611-22.
351. Nolan, T., Hands, R. E. and Bustin, S. A.2006. Quantification of mRNA using real-time RT-PCR. *Nat Protoc.* 1:1559-82.
352. Applied Biosystems, Real-Time PCR (qPCR).
<http://www.appliedbiosystems.com/absite/us/en/home/applications-technologies/real-time-pcr.html>. Accessed August 21, 2006.
353. Morgan, H. E., Earl, D. C., Broadus, A., Wolpert, E. B., Giger, K. E. and Jefferson, L. S.1971. Regulation of protein synthesis in heart muscle. I. Effect of amino acid levels on protein synthesis. *J Biol Chem.* 246:2152-62.
354. Desmond, W., Jr. and Harary, I.1972. In vitro studies of beating heart cells in culture. XV. Myosin turnover and the effect of serum. *Arch Biochem Biophys.* 151:285-94.

355. Schoenheimer, R. and Rittenberg, D.1935. Deuterium as an Indicator in the Study of Intermediary Metabolism. *Science*. 82:156-7.
356. Zhao, J., Brault, J. J., Schild, A., Cao, P., Sandri, M., Schiaffino, S., Lecker, S. H. and Goldberg, A. L.2007. FoxO3 coordinately activates protein degradation by the autophagic/lysosomal and proteasomal pathways in atrophying muscle cells. *Cell Metab*. 6:472-83.
357. Dewey, J. 1920. Reconstruction in philosophy, Henry Holt and Co.,New York.
358. Baskin, K. K. and Taegtmeyer, H.2011. AMP-Activated Protein Kinase Regulates E3 Ligases in Rodent Heart. *Circ Res*. 109:1153-61.
359. Samarel, A. M., Parmacek, M. S., Magid, N. M., Decker, R. S. and Lesch, M.1987. Protein synthesis and degradation during starvation-induced cardiac atrophy in rabbits. *Circ Res*. 60:933-41.
360. Sabina, R. L., Patterson, D. and Holmes, E. W.1985. 5-Amino-4-imidazolecarboxamide riboside (Z-ribose) metabolism in eukaryotic cells. *J Biol Chem*. 260:6107-14.
361. Corton, J. M., Gillespie, J. G., Hawley, S. A. and Hardie, D. G.1995. 5-aminoimidazole-4-carboxamide ribonucleoside. A specific method for activating AMP-activated protein kinase in intact cells? *Eur J Biochem*. 229:558-65.
362. Witters, L. A., Kemp, B. E. and Means, A. R.2006. Chutes and Ladders: the search for protein kinases that act on AMPK. *Trends Biochem Sci*. 31:13-6.
363. Krawiec, B. J., Nystrom, G. J., Frost, R. A., Jefferson, L. S. and Lang, C. H.2007. AMP-activated protein kinase agonists increase mRNA content of the muscle-specific ubiquitin ligases MAFbx and MuRF1 in C2C12 cells. *Am J Physiol Endocrinol Metab*. 292:E1555-67.
364. Nakashima, K. and Yakabe, Y.2007. AMPK activation stimulates myofibrillar protein degradation and expression of atrophy-related ubiquitin ligases by increasing FOXO transcription factors in C2C12 myotubes. *Biosci Biotechnol Biochem*. 71:1650-6.
365. Greer, E. L., Oskoui, P. R., Banko, M. R., Maniar, J. M., Gygi, M. P., Gygi, S. P. and Brunet, A.2007. The energy sensor AMP-activated protein kinase directly regulates the mammalian FOXO3 transcription factor. *J Biol Chem*. 282:30107-19.
366. Sanchez, A. M., Csibi, A., Raibon, A., Cornille, K., Gay, S., Bernardi, H. and Candau, R.2011. AMPK promotes skeletal muscle autophagy through activation of Forkhead FoxO3a and interaction with Ulk1. *J Cell Biochem*.

367. Tong, J. F., Yan, X., Zhu, M. J. and Du, M.2009. AMP-activated protein kinase enhances the expression of muscle-specific ubiquitin ligases despite its activation of IGF-1/Akt signaling in C2C12 myotubes. *J Cell Biochem.* 108:458-68.
368. Czubryt, M. P. and Olson, E. N.2004. Balancing contractility and energy production: the role of myocyte enhancer factor 2 (MEF2) in cardiac hypertrophy. *Recent Prog Horm Res.* 59:105-24.
369. Grozinger, C. M. and Schreiber, S. L.2000. Regulation of histone deacetylase 4 and 5 and transcriptional activity by 14-3-3-dependent cellular localization. *Proc Natl Acad Sci U S A.* 97:7835-40.
370. Mitch, W. E. and Goldberg, A. L.1996. Mechanisms of muscle wasting. The role of the ubiquitin-proteasome pathway. *N Engl J Med.* 335:1897-905.
371. Sandri, M., Lin, J., Handschin, C., Yang, W., Arany, Z. P., Lecker, S. H., Goldberg, A. L. and Spiegelman, B. M.2006. PGC-1alpha protects skeletal muscle from atrophy by suppressing FoxO3 action and atrophy-specific gene transcription. *Proc Natl Acad Sci U S A.* 103:16260-5.
372. Suzuki, J., Ueno, M., Uno, M., Hirose, Y., Zenimaru, Y., Takahashi, S., Osuga, J. I., Ishibashi, S., Takahashi, M., Hirose, M., Yamada, M., Kraemer, F. B. and Miyamori, I.2009. Effects of hormone-sensitive lipase-disruption on cardiac energy metabolism in response to fasting and refeeding. *Am J Physiol Endocrinol Metab.*
373. Adrouny, G. A.1969. Differential patterns of glycogen metabolism in cardiac and skeletal muscles. *Am J Physiol.* 217:686-93.
374. Lange, S., Auerbach, D., McLoughlin, P., Perriard, E., Schafer, B. W., Perriard, J. C. and Ehler, E.2002. Subcellular targeting of metabolic enzymes to titin in heart muscle may be mediated by DRAL/FHL-2. *J Cell Sci.* 115:4925-36.
375. Flexner, A. 1930. Universities: American, English, German, Oxford University Press, New York.
376. Bolster, D. R., Crozier, S. J., Kimball, S. R. and Jefferson, L. S.2002. AMP-activated protein kinase suppresses protein synthesis in rat skeletal muscle through down-regulated mammalian target of rapamycin (mTOR) signaling. *J Biol Chem.* 277:23977-80.
377. Chan, A. Y. and Dyck, J. R.2005. Activation of AMP-activated protein kinase (AMPK) inhibits protein synthesis: a potential strategy to prevent the development of cardiac hypertrophy. *Can J Physiol Pharmacol.* 83:24-8.

378. Stuck, B. J., Lenski, M., Bohm, M. and Laufs, U.2008. Metabolic switch and hypertrophy of cardiomyocytes following treatment with angiotensin II are prevented by AMP-activated protein kinase. *J Biol Chem.* 283:32562-9.
379. Ouchi, N., Shibata, R. and Walsh, K.2005. AMP-activated protein kinase signaling stimulates VEGF expression and angiogenesis in skeletal muscle. *Circ Res.* 96:838-46.
380. Mercadier, J. J., Lompre, A. M., Wisnewsky, C., Samuel, J. L., Bercovici, J., Swynghedauw, B. and Schwartz, K.1981. Myosin isoenzyme changes in several models of rat cardiac hypertrophy. *Circ Res.* 49:525-32.
381. Izumo, S., Nadal-Ginard, B. and Mahdavi, V.1988. Protooncogene induction and reprogramming of cardiac gene expression produced by pressure overload. *Proc Natl Acad Sci U S A.* 85:339-43.
382. Izumo, S., Lompre, A. M., Matsuoka, R., Koren, G., Schwartz, K., Nadal-Ginard, B. and Mahdavi, V.1987. Myosin heavy chain messenger RNA and protein isoform transitions during cardiac hypertrophy. Interaction between hemodynamic and thyroid hormone-induced signals. *J Clin Invest.* 79:970-7.
383. Schwartz, K., de la Bastie, D., Bouveret, P., Oliviero, P., Alonso, S. and Buckingham, M.1986. Alpha-skeletal muscle actin mRNA's accumulate in hypertrophied adult rat hearts. *Circ Res.* 59:551-5.
384. Schwartz, K., Boheler, K. R., de la Bastie, D., Lompre, A. M. and Mercadier, J. J.1992. Switches in cardiac muscle gene expression as a result of pressure and volume overload. *Am J Physiol.* 262:R364-9.
385. Rajabi, M., Kassiotis, C., Razeghi, P. and Taegtmeyer, H.2007. Return to the fetal gene program protects the stressed heart: a strong hypothesis. *Heart Fail Rev.* 12:331-43.
386. Phoenix, K. N., Vumbaca, F. and Claffey, K. P.2009. Therapeutic metformin/AMPK activation promotes the angiogenic phenotype in the ERalpha negative MDA-MB-435 breast cancer model. *Breast Cancer Res Treat.* 113:101-11.
387. Zhang, P., Hu, X., Xu, X., Fassett, J., Zhu, G., Viollet, B., Xu, W., Wiczler, B., Bernlohr, D. A., Bache, R. J. and Chen, Y.2008. AMP activated protein kinase-alpha2 deficiency exacerbates pressure-overload-induced left ventricular hypertrophy and dysfunction in mice. *Hypertension.* 52:918-24.
388. Foretz, M., Hebrard, S., Leclerc, J., Zarrinpashneh, E., Soty, M., Mithieux, G., Sakamoto, K., Andreelli, F. and Viollet, B.2010. Metformin inhibits hepatic

- gluconeogenesis in mice independently of the LKB1/AMPK pathway via a decrease in hepatic energy state. *J Clin Invest.* 120:2355-69.
389. Gundewar, S., Calvert, J. W., Jha, S., Toedt-Pingel, I., Ji, S. Y., Nunez, D., Ramachandran, A., Anaya-Cisneros, M., Tian, R. and Lefer, D. J.2009. Activation of AMP-activated protein kinase by metformin improves left ventricular function and survival in heart failure. *Circ Res.* 104:403-11.
390. Johnson, J. A., Majumdar, S. R., Simpson, S. H. and Toth, E. L.2002. Decreased mortality associated with the use of metformin compared with sulfonylurea monotherapy in type 2 diabetes. *Diabetes Care.* 25:2244-2248.
391. Masoudi, F. A., Inzucchi, S. E., Wang, Y., Havranek, E. P., Foody, J. M. and Krumholz, H. M.2005. Thiazolidinediones, metformin, and outcomes in older patients with diabetes and heart failure: an observational study. *Circulation.* 111:583-90.
392. Shah, D. D., Ronarow, G. C. and Horwich, T. B.2010. Metformin therapy and outcomes in patients with advanced systolic heart failure and diabetes. *J Card Fail.* 16:200-206.
393. Aguilar, D., Chan, W., Bozkurt, B., Ramasubbu, K. and Deswal, A.2011. Metformin use and mortality in ambulatory patients with diabetes and heart failure. *Circ Heart Fail.* 4:53-58.
394. Popper, K. 1935. *The Logic of Scientific Discovery*, Verlag von Julius Springer, Vienna.
395. Anversa, P., Kajstura, J., Leri, A. and Bolli, R.2006. Life and death of cardiac stem cells: a paradigm shift in cardiac biology. *Circulation.* 113:1451-63.
396. Kajstura, J., Urbanek, K., Perl, S., Hosoda, T., Zheng, H., Ogorek, B., Ferreira-Martins, J., Goichberg, P., Rondon-Clavo, C., Sanada, F., D'Amario, D., Rota, M., Del Monte, F., Orlic, D., Tisdale, J., Leri, A. and Anversa, P.2010. Cardiomyogenesis in the adult human heart. *Circ Res.* 107:305-15.
397. Young, M. E., Yan, J., Razeghi, P., Cooksey, R. C., Guthrie, P. H., Stepkowski, S. M., McClain, D. A., Tian, R. and Taegtmeyer, H.2007. Proposed regulation of gene expression by glucose in rodent heart. *Gene Regul Syst Bio.* 1:251-62.
398. Barger, P. M. and Kelly, D. P.2000. PPAR signaling in the control of cardiac energy metabolism. *Trends Cardiovasc Med.* 10:238-45.
399. Narkar, V. A., Downes, M., Yu, R. T., Emblar, E., Wang, Y. X., Banayo, E., Mihaylova, M. M., Nelson, M. C., Zou, Y., Juguilon, H., Kang, H., Shaw, R. J. and

- Evans, R. M.2008. AMPK and PPARdelta agonists are exercise mimetics. *Cell*. 134:405-15.
400. Goodyear, L. J.2008. The exercise pill--too good to be true? *N Engl J Med*. 359:1842-4.
401. Frayn, K. N. 2010. *Metabolic Regulation: A Human Perspective*, 3rd edition, John Wiley & Sons Ltd.,Oxford.
402. Evans, G.1934. The glycogen content of the rat heart. *J Physiol*. 82:468-80.
403. Hoeks, J., van Herpen, N. A., Mensink, M., Moonen-Kornips, E., van Beurden, D., Hesselink, M. K. and Schrauwen, P.2010. Prolonged fasting identifies skeletal muscle mitochondrial dysfunction as consequence rather than cause of human insulin resistance. *Diabetes*. 59:2117-25.
404. Lehninger, A. L. 2005. *Lehninger principles of biochemistry* 4th ed W.H. Freeman,New York.
405. May, R. C., Hara, Y., Kelly, R. A., Block, K. P., Buse, M. G. and Mitch, W. E.1987. Branched-chain amino acid metabolism in rat muscle: abnormal regulation in acidosis. *Am J Physiol*. 252:E712-8.
406. Qi, J., Gong, J., Zhao, T., Zhao, J., Lam, P., Ye, J., Li, J. Z., Wu, J., Zhou, H. M. and Li, P.2008. Downregulation of AMP-activated protein kinase by Cidea-mediated ubiquitination and degradation in brown adipose tissue. *EMBO J*. 27:1537-48.
407. Schoenheimer, R. 1942. *The Dynamic State of Body Constituents*, Harvard University Press,Cambridge, MA.
408. Lewis, C. S. 1947. *MIRACLES: A Preliminary Study*, G. Bles,London.

VITA

Kedryn Kjestine Baskin was born in Albuquerque, New Mexico, the first of three daughters, to Dee and Joe Baskin. After graduating from James Madison High School in San Antonio (summa cum laude, valedictorian), she matriculated to Baylor University (Waco, TX) where she pursued her two passions: soccer and education. She earned a Bachelor of Arts with a major in Biochemistry and minor in Philosophy in December, 2002. After working as a Research Technician at M.D. Anderson Cancer Center she entered graduate school. In June of 2005, she began her dissertation work at the Graduate School of Biomedical Sciences (GSBS) at The University of Texas Health Science Center at Houston. Kedryn will be entering a postdoctoral fellowship in the spring of 2012 to further her development as a scientist in academia.